Bulletin 35
Part 4
(of 7 Parts)

THE SHOCK AND VIBRATION BULLETIN

FEBRUARY 1966

A Publication of
THE SHOCK AND VIBRATION
INFORMATION CENTER
U.S. Naval Research Laboratory, Washington, D.C.

Office of
The Director of Defense
Research and Engineering

Private STINET

Citation Format: Full Citation (1F)

Accession Number:
AD0631233
Citation Status:
Active
Citation Classification:
Unclassified
Fields and Groups:
140200 - Test Facilities, Equipment and Methods
201100 - Mechanics
Corporate Author:
NAVAL RESEARCH LAB WASHINGTON D C SHOCK AND VIBRATION INFORMATION CENTER
Unclassified Title:
(U) THE SHOCK AND VIBRATION BULLETIN.
Title Classification:
Unclassified
Report Date:
Feb 1966
Media Count:
243 Page(s)
Cost:
$14.60
Report Number(s):
BULL-35-PT-4
Report Classification:
Unclassified
Supplementary Note:
Presented at Symposium on Shock, Vibration and Associated Environments (35th), New Orleans, La. 25-28 October 1965. See also AD-628 600.
Descriptors:
(U) (*SHOCK(MECHANICS), SYMPOSIA), (*VIBRATION, SYMPOSIA), INSTRUMENTATION, ACCELEROMETERS, TRANSDUCERS, SPECTRUM ANALYZERS, STRUCTURES, MATHEMATICAL ANALYSIS, DYNAMICS
Identifier Classification:
Unclassified
Abstract:
(U) Contents: Integration and double integration-a practical technique; The measurement of internal dynamics of equipment; Piezoresistive strain gage accelerometers increase spectrum of shock and vibration measurement capability; Vibration measurements using a microwave interferometer; A wideband absolute accelerometer calibrator utilizing a laser for measuring vibratory dilacements; Unpublished accelerometer characteristics; New precision calibration techniques for vibration transducers; Omnidirectional acceleration sensor; Effective use of accelerometers as calibration standards; Measurement of accelerometer transverse sensitivity; First occurrence probabilities for extreme random vibration amplitudes; Signal detection using impulse crosscorrelation; A means to

reduce random vibration analysis time; A continuous frequency constant q shock spectrum analyzer; Slope error of power spectral density measurements; The effects of phase errors upon the measurement of random processes; Utilization of a digital computer for on-line acquisition and analysis of acoustic and vibration data; A digital data recording system for structural dynamics response testing; Comparison of analog and digital methods for vibration analysis; Automatic real-time vibration spectrum analyzer system using delay line time compression techniques; The analog cross spectral density analyzer system; Transient data distortion compensation.

Abstract Classification:

Unclassified

Distribution Limitation(s):

01 - APPROVED FOR PUBLIC RELEASE

Source Code:

389004

Document Location:

DTIC AND NTIS

Bulletin 35
Part 4
(of 7 Parts)

THE SHOCK AND VIBRATION BULLETIN

FEBRUARY 1966

A Publication of
THE SHOCK AND VIBRATION
INFORMATION CENTER
U.S. Naval Research Laboratory, Washington, D.C.

The 35th Symposium on Shock, Vibration and Associated Environments was held in New Orleans, Louisiana on 25-28 October 1965. NASA Marshall Space Flight Center was host.

Office of
The Director of Defense
Research and Engineering

CONTENTS

PART 4

Instrumentation

PAPERS APPEARING IN PART 1
Part 1 - Confidential
(Titles Unclassified)

PAPERS APPEARING IN PART 2

Vibration Testing

PAPERS APPEARING IN PART 3

Structural Analysis

PAPERS APPEARING IN PART 5

Transportation

Shock and Vibration Isolation

PAPERS APPEARING IN PART 6

Shock Testing

Specification of Shock

PAPERS APPEARING IN PART 7

Prediction of Vibration Environment

Damping and Nonlinear Analysis

INSTRUMENTATION

INTEGRATION AND DOUBLE INTEGRATION— A PRACTICAL TECHNIQUE

Merval W. Oleson
U.S. Naval Research Laboratory
Washington, D.C.

Applied theory and physical experimentation are closely interdependent as the contributing elements of a developing structural dynamics technology. The potential value of structural motion analysis in the time domain has been largely unexplored and unexploited, again because of earlier experimental difficulties. In a recent series of shock evaluation tests, both the value and the feasibility of structural analysis in the time domain have been demonstrated. The approach was to measure dynamic motion with an accelerometer, and by successive integrations to produce simultaneous records of all three motion parameters, acceleration, velocity, and displacement. The results were quite striking. Simultaneous motion representations in a multi parameter format produced important interpretations of structural behavior--interpretations which were uniquely related to the format.

It is concluded that the technique which proved so valuable in this instance could be profitably adapted to other measurement situations also.

Progress in methods for the design and the construction of structures which must perform satisfactorily in a severe mechanical environment has been the result of both improved instrumentation and of a more sophisticated application of the structural dynamics. The two aspects are hardly separable. Better and more accurate measurement has led to improved mathematical models, which in turn have pointed the way toward even more pertinent data requirements. Yet, in retrospect, it appears that the advance, in an applied sense, has been more directly controlled by the prevailing measurement technology than by the available analytical tools. One need only observe the present situation with regard to mechanical impedance concepts, for a contemporary example in which the theory is waiting on the development of accurate and practical measurement techniques.

In a slightly different sense, the divergent paths which have been followed in the developing analytical treatments of shipboard and of missile mechanical environmental problems can be associated quite closely with the practical problems of suitable measuring devices. In early shipboard shock technology, the seismic velocity transducer evolved as the most practical of several devices available, primarily because it offered the best empirical correlation between peak wave shape values and shock-produced structural damage (1). Subsequent analytical treatments leading to more sophisticated physical understanding of shock phenomena and to design methods for shock resistant structures have been conditioned largely by use of the velocity parameter. With the advent of a large scale missile development effort, initial attempts were made to transfer existing shipboard shock and vibration technology, including use of the velocity transducer, to a new class of structures. However, it became apparent that the transducer was physically incompatible with the relatively flimsy missile structures, thus forcing missile experimenters into the use of less exploited acceleration transducers. Succeeding efforts to understand and interpret mechanical phenomena in terms of the acceleration parameter have produced applied analytical methods which are distinct from those developed earlier.

Recognizing that the paths of applied theory have been more or less subtly circumscribed and directed by nontheoretical instrumentation considerations, and further, that the normal cross fertilization of theory and experiment tends to perpetuate established paths, we may also recognize that our existing techniques might profit by an occasional reevaluation in terms of goals and methods. More directly to the purpose of this paper—by a reconsideration of our present experimental methods.

TIME ANALYSIS VS FREQUENCY ANALYSIS

Prior to the introduction of the "shock spectrum" concept (2), the study of mechanical shock effects was dependent upon an experimenter's interpretation of measured shock response signals, their peak values, wave shapes, recognizable oscillatory components, etc. While such an interpretation provided valuable insight into the motions of the instrumented structure, it was inadequate in other regards. Transformation of shock measurements from a time domain to a frequency domain (as a shock spectrum) offered several advantages, for example: it provided the data in a format useful to the designer, it simplified characteristically complicated time functions in a way which allowed for easier documentation, and it eliminated the subjective variable of "judgment" in signal interpretation. As a matter of fact, it is quite clear that the frequency domain presentation is an indispensable element of present shock analysis and shock design methods.

In spite of its value, however, frequency analysis by itself is also inadequate. In relieving the need for wave shape interpretation, it also removes the possibility of interpretation, and consequently, the basis for an understanding of the existing structure from which measurements have been taken. Mechanical impacting, resonance buildup and decay, dynamic distortion, and other important characteristics which are potentially recognizable from time records, are obscured when these same records are transformed to the frequency domain.

In present practice, shipboard shock response measurements are studied in both the time domain and in the frequency domain, although analysis in the time domain, with its greater demand on the investigator's judgment, is frequently abbreviated in favor of the "more sophisticated frequency analysis to follow." Studies of missile environmental measurements, on the other hand, are limited almost entirely to the frequency domain.

Without in any way attempting to depreciate the importance of frequency analysis, in either shipboard or missile environmental studies, it is the contention here that singular attention to such an analytical method has cost the loss of much valuable information.

We have developed a mathematically sophisticated, but incomplete technology; well suited to specification writing, testing, and documentation, it is inadequate to the needs of the experimental researcher who must understand and interpret real time mechanical behavior.

PARAMETER LIMITATIONS

There is, of course, no mysterious reason for our dependence on frequency analysis techniques. It is a simple fact that the larger percentage of mechanical measurements from actual structures are almost undecipherable in the time domain. Dynamic acceleration measurements from missile structures are frequently indistinguishable from electrical circuit noise (previous recognition of this similarity is partly responsible for our present use of the mathematics developed in communications theory) (3 and 4); dynamic velocity measurements are somewhat simpler, no doubt accounting for their more frequent study in the time domain, but are still characteristically complex; and the third mechanical parameter, inertial displacement, is infrequently identified or measured as a significant environmental parameter largely because it is associated with rigid body motions as distinguished from dynamic distortions.

Of the three related motion parameters: acceleration, velocity, and displacement, no one is consistently amenable to interpretation in the time domain, though each implicitly contains a total description of motion at the instrumented point. The problem is that each parameter provides a different emphasis on the frequency components of complex motion. Components which in turn tend to be associated with the motions common to correspondingly different proportions of the total structure. These components can be sorted out for orderly study by frequency analysis techniques, but only at the expense of compromising the time relationships between the components, that is, the real time motion.*

*The fact that decomposition in a complex frequency plane is mathematically unique to the real time signal is immaterial to the practical problem.

We may observe that the procedure of integrating a time function can also be viewed as a method of frequency filtering, the high frequency components being attenuated by the factor 1/frequency. However, unlike the usual frequency decomposition, time relationships in the original function are changed in a regular way, such that, for physically measured data, the integral retains a physical meaning. In particular, time records of velocity and displacement, obtained from acceleration by successive integrations, are subject to physical interpretation. Furthermore, where the representation of one motion parameter alone may present a very difficult problem in interpretation, simultaneous representations of the related parameters ease the problem substantially.

EXAMPLES OF THREE PARAMETER ANALYSIS

In the preceding paragraphs, an attempt has been made to identify two particular points; (a) that experimental techniques which ignore or depreciate mechanical motion analyses in the time domain, fail to exploit all of the information content of measured data; and (b) that mechanical motion analyses can be greatly facilitated by simultaneous presentation of the three related motion parameters: acceleration, velocity, and displacement. Perhaps these arguments can be supported most effectively by interpretive illustrations drawn from practice.

A few months ago, the Naval Research Laboratory was involved in a rather extensive series of tests intended to evaluate a newly designed shock-mitigating missile stowage system. Shock response signals taken from strain gage accelerometers on the stowed missiles were routinely integrated and double integrated during post-shot reproduction. The following examples are representative of the form in which the signals were presented, and of the interpretations which resulted.

1. Figure 1 presents the signals from three orthogonal gages attached at the same point on a missile. In each case, the direct acceleration reproduction is dominated by high frequency vibration components, which appear to be nearly the same in all axes. However, a marked difference in the important lower frequency components is immediately apparent from the velocity and displacement traces. If we observe that the slope of the velocity trace is proportional to the acceleration, it is not difficult to recognize that the instrumented point has been subjected to a greater sustained force in the upward direction than in the athwartship direction, and to substantially no sustained force in the longitudinal direction. (It is also worth noting that a form of manual frequency filtering of the acceleration-signal can be affected by averaging the velocity-signal slope over selected time intervals.)

2. The traces of Fig. 2 have been taken from a gage at the free end of a cantilevered missile. They show an increase in successive peaks of an oscillatory component, from which the presence of coupling between separate structural modes of nearly identical frequency was readily recognized. In this illustration some of the higher frequency acceleration components have been attenuated by the structure itself; the dominating modal response is reasonably apparent in all three traces.

3. Figure 3 illustrates a situation in which mechanical impacting between structural components was inferred from the acceleration and velocity traces taken together. Of the many acceleration peaks in the top trace, two in particular are seen to be coincident with abrupt velocity steps. Such a motion response is characteristic of the short duration impulsive force produced by mechanical impact.

4. Figures 4 and 5 illustrate two different instances in which instrumentation malfunction, not recognized in the direct acceleration trace, was readily identified in successive integrations. In Fig. 4, the displacement traces of four gages located at different points on the same basic structure have been replotted to a common scale. Since structural integrity was maintained throughout the test, and since the displacement indication of gage A43A was inconsistent with the rigid body motions indicated by the other three gages, it was clear that a measurement malfunction of some kind had occurred. Again in Fig. 5, the rather peculiar step seen in the velocity trace caused immediate suspicion of a gage or circuit problem; if further evidence was required, it could have been obtained by comparison of the displacement trace with those of other similarly oriented gages on the structure.

5. In Fig. 6, shock excited bending deformations of two cantilevered missiles have been plotted for the purpose of identifying their model excitations. The data points for these plots were obtained by scaling the inertial displacements (second integral) indicated by four gages mounted along the length of each missile, comparing these inertial displacements at selected times, and presenting the results as differential displacement off an axis through the missile support points.

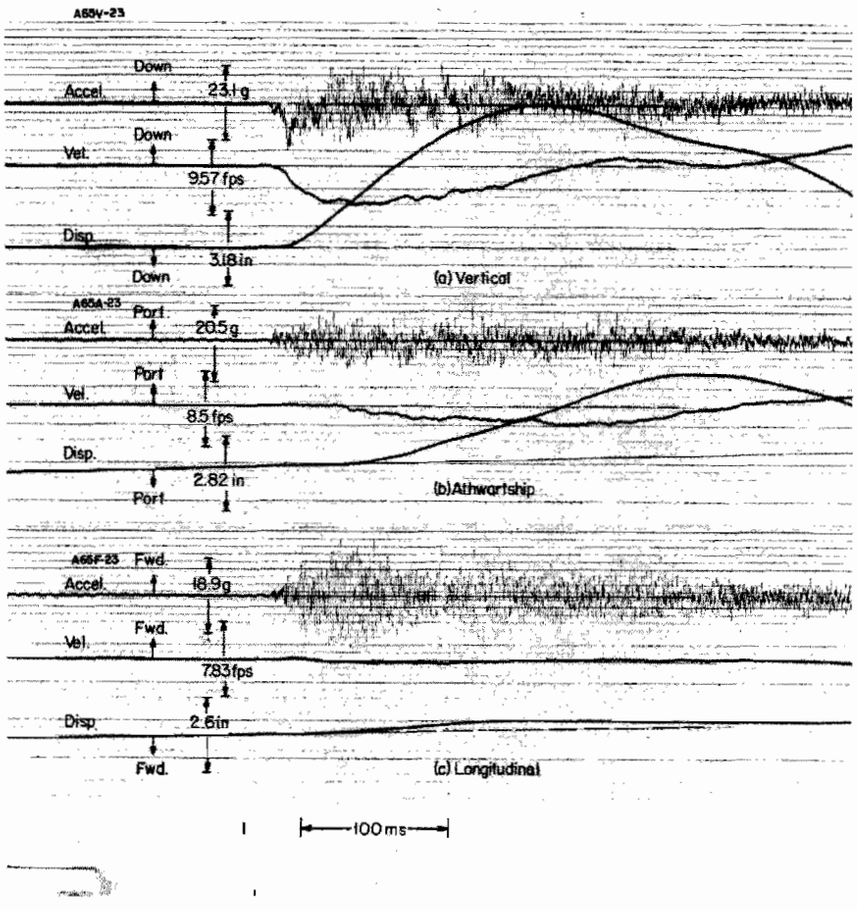

Fig. 1. Shock excited acceleration-time signals from three orthogonal gages are similar in appearance because of dominating high frequency components. The structurally significant lower frequency components, however, are dissimilar, an interpretation which is readily apparent from successive integrations of the acceleration signal.

It would be possible to extend this group of examples to considerable length. Those described have been selected as illustrative of the types of interpretation, rather than the number of instances. In each of these illustrations, the information obtained would have been wholly or partly obscured in any format other than that actually employed.

The substantial contribution of this information to the experimental problem resulted from the ability to make the interpretations and from the fact that implementation was uncomplicated. Time records in the three-parameter format could be made available comparatively soon after a test; typically, the oscillographic reproductions from some 50 installed gages were ready for study within two to four hours. As a consequence, the instrumentation, the structures under evaluation, and the test procedures were all subject to continuous improvement in the light of a concurrently accruing understanding.

It seems reasonable to conclude that the type of instrumentation, and the analytical method which was so valuable in this particular series of tests, would also be of potential value in other experimental problems.

PROBLEMS OF INSTRUMENTATION

Integration and double integration of an accelerometer signal, simple enough in concept, poses several formidable problems in practice. The fact that these problems are manageable has been demonstrated above. However, the

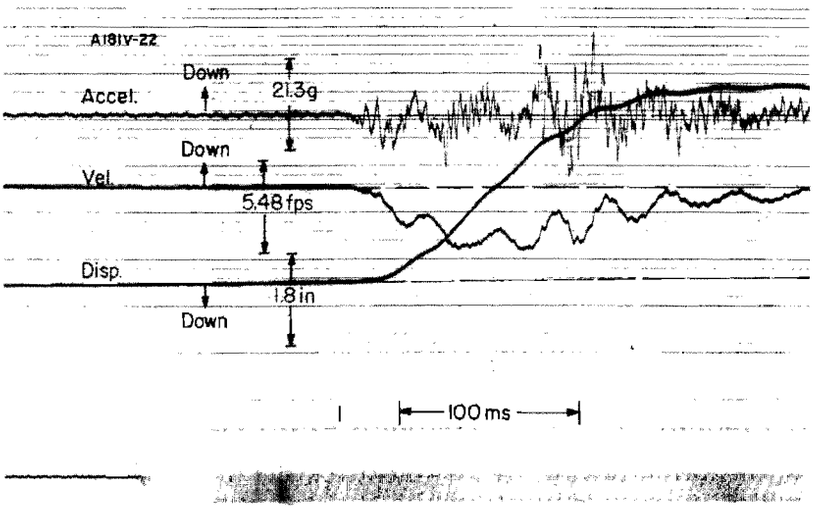

Fig. 2. Oscillatory build-up is noticeable in all three parameters, but most obvious in the velocity trace

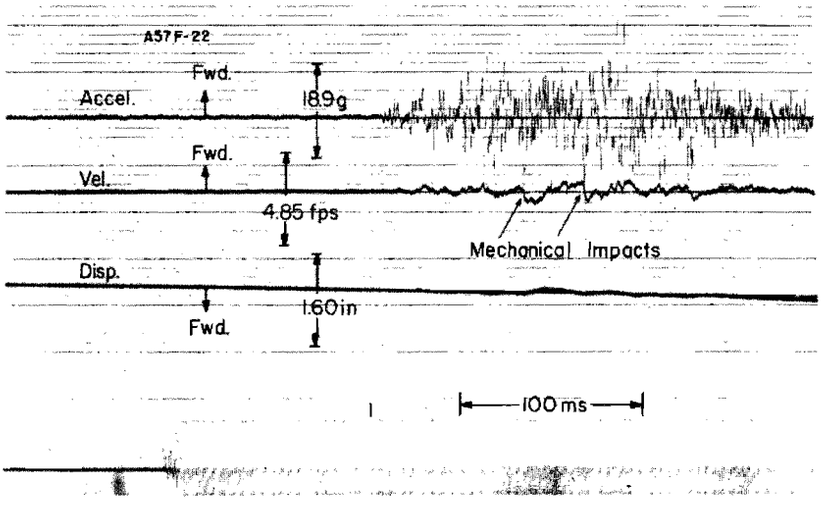

Fig. 3. Mechanical impacts are generally characterized by coincident velocity steps and acceleration spikes

specific devices developed at the Naval Research Laboratory for this purpose, while generally satisfactory, are unlikely to represent a unique implementation of the basic three-parameter approach. Given recognition of the value of such an approach as a stimulus, alternate device possibilities could no doubt be fruitfully explored.

On the other hand, many of the practical problems exist independently of specific devices, and identification of these problems is a necessary prelude to their solution. For this reason, the following remarks summarize the major difficulties encountered during development at NRL.

Basic Linearity and Stability Requirements

On many structures, particularly those rigid structures which are exposed to some form of explosive or impact loading, the

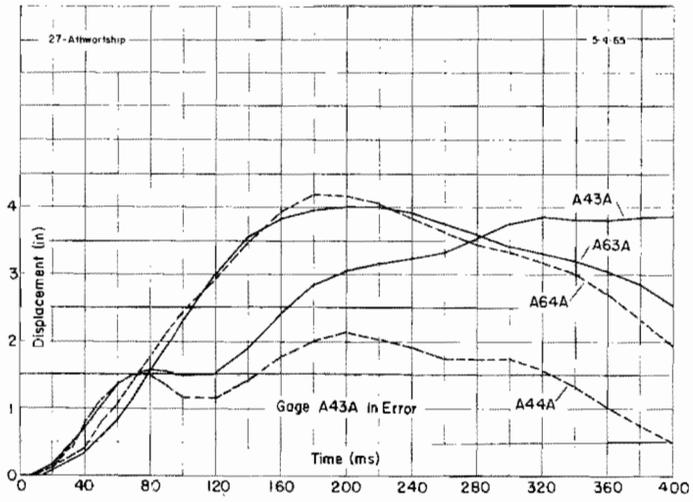

Fig. 4. The displacement traces (second integral) of four gages on the same large structure, replotted to a common scale, indicate a rigid body motion which is a combination of translation and rotation. The record of gage A43A, however, is inconsistent with this motion, indicating a gage or circuit malfunction.

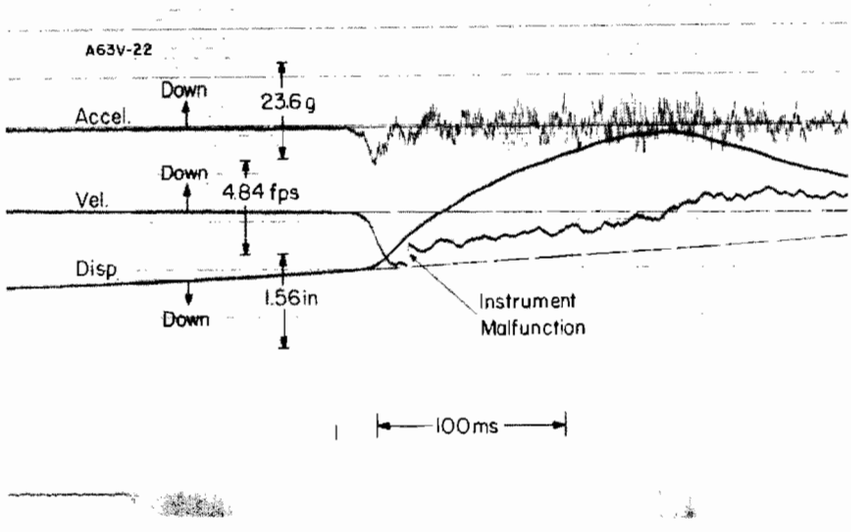

Fig. 5. The indicated abrupt velocity step is physically unlikely; it suggests a gage or circuit malfunction

dynamic range of significant acceleration signal amplitudes can easily be 60 db to 80 db; from a fraction of a g to several thousand g. To maintain velocity and displacement accuracy, the units or components of the instrumentation system which precede the actual integrating element, i.e., transducer, connected circuitry, amplifiers, etc., must be stable at the lowest signal levels, linear over the full dynamic range, and not subject to spurious nonsymmetrical noise. Simple calculations will illustrate the significance of these requirements. At low

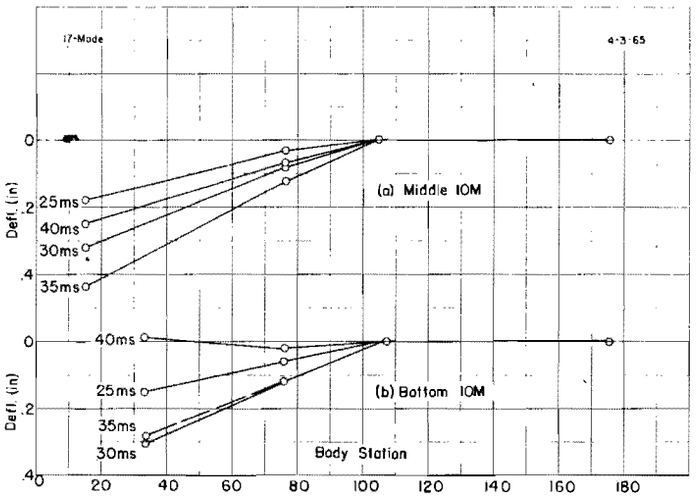

Fig. 6. Bending of two cantilevered missiles has been plotted at selected times following incidence of a shock input. Data for this presentation were obtained from the difference in displacements indicated by doubly integrated accelerometer signals.

level, a "zero shift" equivalent to 0.1 g, will, when integrated and doubly integrated for a 1/2-second interval, produce a velocity contribution of 1.6 fps and a displacement contribution of 4.8 in.; at high level, five cycles of a sinusoidal acceleration signal at 1 kc and ±1000 g, distorted by a 1 percent unilateral nonlinearity, will produce a velocity contribution of 0.8 fps within 5 ms, and a displacement contribution of 4.8 in. at the end of a 1/2-second interval. It may be noted that zero shift and nonlinearity produce distinguishable errors; the first being characterized by a velocity ramp, and the second by a velocity step. Spurious circuit noise, depending on its nature and mechanism, may introduce an error of either type.

The pertinence of this particular illustration and the significance of the indicated errors must, of course, be judged according to the circumstances of a specific instrumentation problem. The values indicated are representative of a shipboard shock measurement application. For other applications, the implied stability and linearity requirements may be more or less stringent.

Acceleration Transducer

The accelerometer, including its essential circuit accessories, is clearly a vital component. In practice, the procurement of a satisfactory gage has presented a most difficult problem. Signal anomalies, which are quite insignificant by the prevailing standards of accelerometer performance, become very apparent when integrated. On the other hand, the same prevailing standards are actually consistent with most contemporary usage, consequently there has been little commercial incentive for improved performance.

Initial attempts were made to employ piezoelectric accelerometers. In most cases where severe acceleration shocks were applied to the gage, large spurious transient pulses appeared in the integrated (velocity) signal, in spite of the fact that peak measured acceleration signals were within the gage rating. The mechanism of these anomalous signals has not been established, although their existence has been independently confirmed (5). The effect, together with the lack of low frequency response characteristic of piezoelectric gages, has prevented further use.

Strain gage accelerometers have the significant advantage of response to dc or static acceleration. When used within their ratings, some models of this gage have been quite satisfactory. However, in severe shock locations, the ±500 g to ±1000 g maximum ratings of commercially available gages are generally exceeded, resulting in nonlinear response and sometimes in damage to the gage (6).

The recently introduced piezoresistive accelerometer is electrically similar to the strain gage accelerometer, but is available in a maximum range of ±2500 g. With the addition of a

special external mount, it has been successfully employed in the most severe shock locations. Initial attempts to use this gage resulted in substantial excitation of a lightly damped internal resonance at about 35 kc (to the extent of rupture of the gage element in one instance). The external mount was subsequently developed to prevent such excitation. Serving as a low pass mechanical filter, the cutoff frequency of this mount is high enough to avoid compromising the shock signal waveform, but still well below the gage resonance frequency (7).

The same sensitivity to gage performance which has frustrated the use of many accelerometer types and models, has been turned to distinct advantage when a satisfactory model is in actual use. Faulty operation of an otherwise acceptable gage is easily recognized. In practice, calibration error, loose gages, poor circuit connections, and defective gages have all been identified and corrected as a singular result of this sensitivity.

Electronic Circuitry

Strain gage and piezoresistive accelerometers require an external excitation voltage, external balance adjustment, signal amplification, and for present purposes, signal integration. As previously remarked, the electronic accessories which precede the integrating device are subject to the same basic stability and linearity requirements as the gage itself.

In regard to the passive accessories (connecting circuitry, excitation, and balance) these requirements pose no difficulty which cannot be satisfied by good practice. In regard to the active accessories, the requirements pose somewhat greater difficulty, but are nevertheless manageable.

Piezoresistive accelerometers in the ±2500 g range, and strain gage accelerometers in the ±500 g range have transduction sensitivities of 80 μv/g to 100 μv/g. To produce a reasonable velocity sensitivity, say 50 mv/fps, the effective integration coefficient must be in the order of 2×10^4. This coefficient is not necessarily identical with a required amplifier gain, since most integrating devices have an intrinsic coefficient which may vary over wide limits, but for practical purposes it does imply the necessity of a high gain electronic amplifier either as a separate system component, or as part of the integrating circuit. Stability and linearity requirements may be conveniently referred to the previously cited example by noting that a 10 μv drift at the input of the amplifier is the equivalent of 0.1 g, and that a 1000 g acceleration peak will produce 100 mv at the input.

Manufacturers' specifications on commerically available amplifiers which are of instrumentation quality indicate that low frequency noise and drift (with respect to the amplifier input) can be held within 1 to 5 μv peak-to-peak and that linearity can be maintained within 0.1 percent over an 80 db dynamic range. In practice, one might expect some degradation of the optimum, but it is nonetheless clear that the required amplifier performance is attainable in present practice.

Symmetrical high frequency noise components introduced by the electronic circuitry are deemphasized by the subsequent integration and are thus of limited significance. However, by the same virtue, low frequency noise components (also referred to in terms of drift or stability) become increasingly important. Actually, true integration would require perfect circuit stability (an obvious impossibility in practice) since anything less would ultimately integrate to produce an out-of-range output voltage. Thus, it is evident that practical considerations impose some limiting condition on the time interval over which an accurate signal integration may be obtained.

A combined amplifier/integrator circuit capable of satisfying the conditions above has been developed over a period of several years at NRL (8). Basically, the circuit consists of a very stable voltage-controlled oscillator supplying a series of fixed charge increments to an integrating capacitor. The long time average of the capacitor voltage is held at zero by a feedback loop, which, in turn, imposes a second order low frequency cutoff on the integrated output signal.

Error in the indicated integral, introduced by this cutoff, is a function of the signal waveshape and of the cutoff frequency; in practice it is negligible within some definable short time interval, and subject to correction over longer time intervals (9).

The same amplifier/integrator circuitry which was developed for the purpose of converting an acceleration signal to its first integral has been employed in cascade to obtain both the first and second integrals.

Without attempting to either exaggerate or depreciate the development problems, results to date have been achieved with very modest manpower allocations. It is reasonable to assume

that present techniques and devices would profit by a more broadly based effort, including further transducer development, and the investigation of alternate circuit possibilities.

SUMMARY AND CONCLUSIONS

The arguments propounded in this paper are not new or especially novel. Motion-time records have actually been studied from the very beginning of our technology; distinctive characteristics of the three motion parameters have been remarked about many times in the literature (10), and the possibilities of transformation between the three parameters have been identified and occasionally implemented (11). Under these conditions, it may seem somewhat unnecessary to rehash the well established points at such length.

There are, however, two reasons why it has seemed desirable:

1. Current literature, which reflects a widespread recognition of the engineering value of motion analysis in the frequency domain, indicates little interest in, or appreciation of, the complementary value of motion analysis in the time domain.

2. Possibly by virtue of this same lack of interest, those few documented attempts which have been made to implement motion-time analyses in a usable form have been unsuccessful, impractical, or when successful have gone unrecognized to any significant degree.

The point was made earlier that existing practices tend to perpetuate themselves to the exclusion of alternate possibilities. In the presence of a widely accepted technique, there is little incentive for exploring alternates.

However, analyses in the time domain and in the frequency domain are not, in the applied sense, optional alternatives, but are valuable complements. From the same measured data, the two analytical methods provide access to different types of information. The singular advantages of analysis in a time domain have been emphasized here, not in an effort to depreciate frequency analysis, but rather to oppose an existing implied depreciation of the former, and to suggest that the real basis of this depreciation can be traced to instrumentation limitations which are presently amenable to solution.

REFERENCES

1. J. P. Walsh, "A Review of the Report on the Cameron Trials," Shock and Vibration Bulletin No. 4, July 1947

2. J. P. Walsh and R. E. Blake, "The Equivalent Static Accelerations of Shock Motions," NRL Report F3302, June 1948; also published in Proc. SESA VI (No. 2) : 150 (1948); also, M. A. Biot, Trans ASCE 106;1385 (1941)

3. Fundamentals of Guided Missile Packaging, Chapter 5. "The Meaning of Random Vibration in Field and Simulation," Edited by E. Klein, DOD Publication RD 219/3, July 1955

4. C. T. Morrow and R. B. Muchmore, "Shortcomings of Present Methods of Measuring and Simulating Vibration Environments," Shock and Vibration Bulletin, No. 21, November 1953

5. "Zero Shift in Piezoelectric Transducers," Panel Session, Shock and Vibration Bulletin No. 29, Part IV, June 1961

6. M. W. Oleson, "Calibration Study of SFNSY Floating Shock Platform, Part I - Operations and Instrumentation," NRL Report 6069, March 1964

7. E. Judd, "Development of Shock Measuring Instrumentation," Report of NRL Progress, February 1965, p. 30

8. M. W. Oelson, "Compatible Transistorized Integrator," Report of NRL Progress, February 1964, p. 22

9. S. Gendler and M. W. Oleson, "Shock Instrumentation Development (Correction of Integrated Records)," Report of NRL Progress, September 1965, pp. 22-26

10. I. Vigness, "Introductory Remarks on Shock Instrumentation," The Shock and Vibration Bulletin, No. 6, November 1947, p. 91

11. E. H. Copeland, T. E. Smart, and J. Arnold, "Acquisition, Reduction, and Analyses of Transient Data," Shock and Vibration Bulletin No. 34, Part IV, p. 55, February 1965

Mr. Kistler (Kistler Instruments): Did you try quartz accelerometers? These should respond to very low frequencies and have no zero shift under shock. They would seem to be the natural thing to use.

Mr. Oleson: I must confess that we have not thoroughly investigated the possibilities of piezoelectric transducers. I did mention in the paper that our initial attempts involved piezoelectric transducers, and we found that they were unsatisfactory primarily because of the anomalous pulses. Since these have not been explained and since we do not know that they would actually be common to all kinds of piezoelectric transducers, it would be an unfair thing to say that piezoelectric transducers are of no value in this kind of work. I will say, however, that we have not investigated them further, and it would be very nice, as a matter of fact, if somebody would.

Mr. Zell (Picatinny Arsenal): We have utilized piezoelectric instrumentation working into very high impedance electronics; and we have obtained very consistent indications in our shock test measurements of the minus 1 g during free fall, and with negligible drift. I think it is potentially possible, in particular instances, that the piezoelectric equipment could be adapted for this. There are problems, but they can be overcome.

Mr. Oleson: What I am trying to do with this paper is to point out that some of the problems which people have considered extremely difficult from the practical point of view have been overcome in an area; what I am trying to suggest is that as a group we would do well for our technology if more people would spend more effort trying to overcome these problems, perhaps at the expense of some of the more sophisticated efforts applied along directions in which we are already producing a technology that is beyond the limits which we can use. I am thinking particularly of some of the sophisticated efforts at spectral analysis. I do not deny their value. I am simply saying that we have developed a sort of single minded attention to these things and have forgotten that we are missing a big chunk of the information which our transducers are potentially capable of supplying.

Mr. Zell: Is the circuitry that you used included in the complete format of your paper?

Mr. Oleson: Negative.

Mr. Kennard (Goddard Space Flight Center): In your present state of the art with the double integration, can you give us some quantitative idea of what the errors might be?

Mr. Oleson: There is more about that in the paper than I have given here. Actually the integrator has a second order low frequency cutoff. As soon as you look at the problem of integration you recognize that you cannot integrate to a theoretical perfection because practical devices just completely eliminate this. When we use them in cascade we have two second order low frequency cutoffs. The frequency of this cutoff is subject to adjustment with simple changes in the circuit parameters. We have worked out correction equations which will take account of these things, and depending on the particular problem, we can concern ourselves with, say, something as I did in these records less than 1/2 a second or so, or we can concern ourselves with times out to a few seconds.

Mr. Linton (USN Weapons Station): Did you use some special technique in mounting the piezoresistive bridge to eliminate spurious responses without degrading the signal that you are after?

Mr. Oleson: You are asking about the mount that goes under the piezoresistive accelerometer? Basically this is to prevent the possibility of exciting the natural resonance of the gage itself which is of the order of 35 to 40 kc. Our interest in the frequency components of shock signals is confined below 500 or perhaps 1000 cps as an upper limit. This means that we have from 1000 cps up, something of the order of 30 kc to play with in selecting the kind of mount we put under the piezoresistive gage. We used a mount which has its own resonant frequency, at about 2500 cps, and at that frequency it has a Q of 3, so that it introduces very little amplification itself. Under these conditions I think we can maintain reasonable phase linearity out to something of the order of 1000 cps which was one of the objectives of the mount design.

* * *

THE MEASUREMENT OF INTERNAL DYNAMICS OF EQUIPMENT

Charles T. Morrow
The Aerospace Corporation
Los Angeles, California

One of the limiting factors in shock and vibration technology is the measurement of dynamic properties. For large, massive open structures, there is no particular difficulty, but many of the complicated devices with which we are concerned can be awkward to investigate. Except for an incipient interest in impedance measurements, there has been little preoccupation with systematic approaches to the problem. In this paper, two techniques are discussed. One provides a quick visual picture of dynamic behavior but is qualitative in some respects. The other permits a more quantitative point-by-point investigation which can be most effective if skillfully used.

INTRODUCTION

Instrumentation for the measurement of equipment dynamics should be designed for different characteristics than instrumentation designed for measuring vibration and shock environment. Generally, the following characteristics are desirable:

1. Low loading. In typical electronic and electromechanical equipment, many functional parts are light or very flexible by comparison with structural members. Therefore, any vibration probe to be used should present extremely low mechanical impedance to the point of measurement or should be amenable to the use of experimental techniques to compensate for loading.

2. Smooth velocity response. Velocity response has a practical advantage of being usable over a wide range of frequencies and a slight theoretical advantage of compatibility with definitions of resonance involving relationship of force to velocity. Some of the virtues of velocity response can be obtained by simple electrical equalization of a displacement or acceleration responsive probe. As a practical matter, response need not be accurately flat as long as any resonance effect in the probe is broad by comparison with the resonances to be measured.

3. Applicability without extreme cutting away of equipment case or other structure. To avoid change of the characteristics to be measured, it is desirable that no access openings be necessary beyond a collection of small drilled holes. In some instances, even these perforations might have a significant effect through alteration of the properties of the air cavities.

4. Capability for instant choice of measurement point for the determination of mode shapes and related information.

Generally, the characteristics of most interest for measurement in an item of equipment as an aid in improving reliability under shock and vibration environments are, approximately in the order of importance:

1. Frequencies of resonance.

2. Q's or effective bandwidths.

3. Transfer characteristics, such as transfer impedance and transmissibilities from one point to another.

4. Excitation point, output, and other impedances.

Clearly, there is a requirement to be able to identify a resonance and to do so in such a way that the observed effects are characteristic solely of the device under investigation, or nearly so, rather than of the device plus exciting or measuring apparatus. Excitation in the region of a resonance frequency is likely to be most damaging. Furthermore, there are theorems in network theory which suggest that essentially the entire behavior at any point in a mechanical system (especially if it is linear) can be inferred from measurement at the frequencies of resonance, e.g., Foster's reactance theorem.

The measurement of vibration and shock environments and the environmental test of

equipment are commonly performed with fixed accelerometer locations, elaborate monitoring and recording equipment, sizeable teams of personnel, dispersed responsibility, and extensive coordination. The use of the same methods inadvertently, or out of habit, for measurement of equipment dynamics can add confusion and chaos to an already complicated problem.

The appropriate experimental techniques are typical of a small research laboratory in a university. It is essentially that one man be able to choose the measurement point of the moment at will, and to complete the measurement or observation without delay and without using any personnel as intermediaries. The use of fixed accelerometers is a cumbersome way of exploring hardware whose dynamics are as yet essentially unknown. The experimenter can seldom proceed to measurement points that unexpectedly become interesting without waiting for another setup. The use of multichannel recorders to record the magnitude of the accelerometer signals introduces delays in interpretation of data and can yield misleading results because of failure to discriminate between fundamental and harmonic responses of resonances. It will be shown later that the use of an appropriate hand-held probe, so connected that Lissajous figures can be observed on a cathode-ray oscilloscope, is a particularly powerful method for exploring the unknown.

THE STROBOSCOPE

The optical stroboscope is such a well known instrument for vibration analysis that there is no need to dwell on its principles of operation. Its outstanding virtues are that it provides an excellent visual and intuitive understanding of all the visible portions of a vibrating system and it does not load the device under study. Its limitations are that it is inherently amplitude responsive, and therefore not very sensitive at high frequencies or adaptable to measurement of force; it provides no ready method of compensation for any spurious influences of the vibration exciter; its is rather qualitative except for measurements of frequency; and it may require large apertures or excessive dismantling of the equipment case or other structure for access to interior parts. The last limitation can be overcome by using an X-ray stroboscope. This is a rather elaborate and special instrument, but it should be especially valuable for preliminary exploration of equipment dynamics.

We might make two additional observations before passing on to other subjects. First, it is feasible to control the stroboscope from the same periodic signal that is used in the exciter. A slow apparent vibration of the parts under study can be brought about by connecting in the channel to the stroboscope a rotating 360 degree phase shifter or equivalent device to produce a small shift in frequency. Second, with an independent periodic control signal, the stroboscope can be used to provide some feeling for response to random excitation. When it is tuned to a sharp resonance, the part under observation appears to move with a slow random vibration.

COMPENSATION FOR THE EXCITER

When an equipment resonance shows significant sensitivity to mounting conditions, there are two conditions that are particularly appropriate in principle for the measurement of the characteristics of the resonance. The first is a free or zero-impedance suspension, which is preferable if the equipment is to be mounted to a structure of relatively low mechanical impedance. The other is a rigid, or infinite-impedance mounting.

In any event, a system consisting of an item of equipment, a fixture or coupling, and a shaker armature may exhibit resonance quite different from those of the equipment under either ideal condition.

Some degree of compensation for this phenomenon may be achieved by judicious attachment of a force gage or accelerometer to produce a reference signal and by making all other measurements in terms of a comparison with this reference signal. For the moment, assume that the excitation is translational in a single direction through a single point. Then, response measurements made in terms of a ratio to a reference signal from a force gage at the excitation point, or a strain gage mounted to respond to a strain proportional to applied force, yield resonance data characteristic of a freely suspended equipment. In fact, if the various other measurements are made with velocity gages or probes, the ratios are transfer impedances, and a velocity measurement at the excitation point yields the mounting point impedance. Any influence of the shaker or coupling appears in both numerator and denominator and cancels. Alternately, response measurements made in terms of a reference signal from a velocimeter at the excitation point yield resonance data characteristic of a rigidly mounted equipment. One could, in principle, excite the equipment through an impedance measuring head and have the capability with a single setup for using either

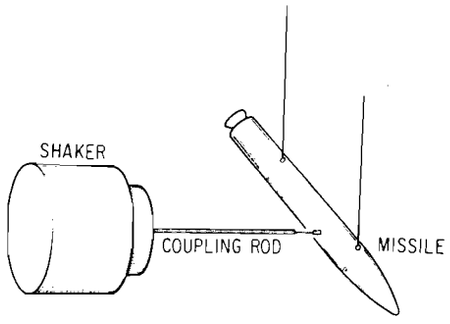

Fig. 1. Setup for measurement of lateral resonance of a small missile

type of reference signal and for getting, at the throw of a switch, a feeling for the sensitivity of any particular resonance to the mounting condition.

If we may digress briefly from measurements on equipment, consider the problem of measuring the first several lateral resonances of a small missile as in free flight. Imagine the missile suspended by wires, (Fig. 1) and a shaker exciting the missile horizontally through a coupling rod. If a strain gage is attached to a reduced section of the rod close to the excitation point, it yields a reference signal that is a measure of applied force. Measurements at other points will yield resonance data that are characteristic of free flight and qualitatively like those of a damped free-free beam.

If the airframe is highly damped, the experimenter may be surprised that he can find no nulls of motion at the nodal points. The phase swings gradually through 180 degrees rather than reversing abruptly at the nodes. Without resorting to an elaborate analysis of the system, we can make this behavior appear quite reasonable. The velocity response at the antinodes is primarily a resonance effect and nearly in phase with the applied force. The residual vibration at the nodal points is related to the acceleration of the center of gravity of the missile in response to the unbalanced force and is therefore 90 degrees out of phase.

To return to equipment, as opposed to whole missiles, the mounting of more traditional interest is the rigid mounting. As a practical matter, there are usually several mounting points on the same item, and the mounting fixture may introduce spurious effects by coupling the points together more rigidly than they may be in practice, producing some relative motion, or generating some crosstalk or rotation. For complete items of equipment, resonance analysis is merely a diagnostic tool to be used only insofar as it is helpful to the improvement of a design.

This allows the experimenter some application of engineering judgment and much compromise on precision of measurement as well as scope of exploratory investigation. Complete standardization of measurement conditions is important only for standard parts, such as vacuum tubes and relays, when results are to be published in detail.

CAPACITATIVE AND ELECTROMAGNETIC PROBES

We now turn to the problem of vibration probes. From the point of view of minimizing the loading effect, one is tempted by a capacitative probe, for which the surface surrounding a measurement point functions as one plate of a varying capacitor; or by a magnetic probe, for which the surface functions as a coupling between two magnetic poles. However, these devices have severe limitations. Access holes must be large. The probe must be at a right angle to the surface. A fixture is required because of the precise positioning that is necessary, thereby making it very inconvenient to shift from one measurement point to another.

WIRE-COUPLED PROBES

For years, vibration probes with a rod to couple mechanically from the measurement point to the sensitive element have been commercially available. They are convenient to use, can readily be moved by hand from one point to another, and can be tilted to vary the direction along which the motion is measured. Generally, they require larger access holes than we would like in the application under

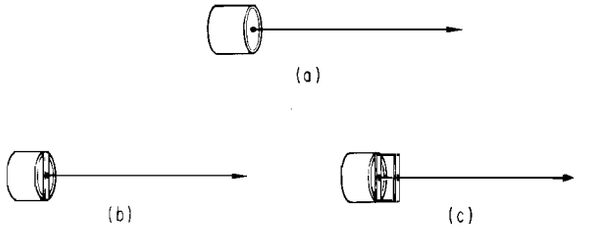

(a) WIRE SOLDERED TO DIAPHRAGM
(b) WIRE SOLDERED TO MUMETAL STRIP
(c) STRUTS AND SPRING ADDED FOR REINFORCEMENT

Fig. 2. Improvised vibration probe

discussion, and their loading effect could be reduced.

Except for observations through holes in the housing of extremely large equipment or where extreme ruggedness is required, there is no reason for the coupling rod or wire to be larger than one millimeter in diameter. One can improvise a vibration probe by soldering a wire into an axial hole in a set screw and screwing it into the base of a piezoelectric accelerometer. Perhaps a better improvization is obtained by soldering the end of the wire perpendicularly to the center of the diaphragm of a small earphone as shown in Fig. 2. The response is not quite so flat, but the loading is less.* the wire should be nonmagnetic and have a hardened, sharp point. Such a probe should be effectively held by the wire, to avoid varying the magnetic gap according to hand pressure. Sensitivity to excitation by sound can be decreased by replacing the diaphragm with a narrow mumetal strip which should be soldered at the ends. Other refinements can readily be devised to decrease sound sensitivity further, provide magnetic shielding, or make the assembly more rugged.

A probe with similar virtues can, in principle, be designed about any sensitive element that has been considered, for example, for application in a phonograph pickup cartridge. Primary considerations are low-impedance termination of the wire in the region of the sensitive element and freedom from pronounced resonance in the usable frequency range.

LISSAJOUS TECHNIQUES

Resonances that are loosely coupled to the point of measurement, or highly damped, are more evident through phase shifts than changes of amplitude with frequency. Partly for this reason, Lissajous techniques are more powerful than the observation of meters alone. The reference signal is connected to produce a horizontal deflection on a cathode-ray oscilloscope. The probe signal is connected to produce a vertical deflection. With fundamental responses of the equipment under observation, the figure on the screen is a straight line or an ellipse, which tumbles as the frequency is swept through an equipment resonance. A harmonic response is evident from a more complicated figure, such as a figure eight with one or more crossings. Resonance phenomena that are entirely in the exciter merely inflate or deflate the figure without changing its shape.

With a little practice, the experimenter can develop an ability to interpret the Lissajous figure to the extent necessary to obtain from it conveniently any required measurements of magnitude ratio, or phase, on a prominent resonance to moderate accuracy. It may be convenient to install a ganged pair of attenuators so that both channels to the oscilloscope can be changed the same amount whenever it is desired to adjust the horizontal deflection to a standard length prior to a measurement. Then an overlay for phase determination can be held against the screen.*

By locating the two half-power points, or two frequencies more or less symmetrically located about a resonance, and involving a relative phase shift of 90 degrees, one should obtain enough information to estimate the Q.

COMPENSATION FOR LOADING

Even with a probe designed for minimal mechanical impedance at the tip, there may be parts, such as small resistors, so light and flexible that they may be loaded by the probe. Generally, measurements of frequency and Q may be obtained by touching the probe tip close to a nearby nodal point (e.g. on a lead wire close to the lug) rather than to a point of maximum motion. The question as to which moving mass is most closely associated with the resonance under observation can be settled, provided there is some additional access, by touching a short rod or dummy probe to the mass with the intent of loading it and observing the effect on the signal. In fact, if a second, live probe is used, an estimate of the loaded motion of the mass can be obtained, which can be corrected by the loading measured with the first probe.

MEASUREMENTS ON VACUUM TUBES

The probe cannot be used on the interior of a vacuum tube without breaking the seal. While admission of air may affect the Q of a resonance,

*For calibration techniques see Charles T. Morrow, "Reciprocity Calibration of Vibration Probes," J. Acous. Soc. Am. 20 826(1948), also Horace M. Trent, "The Absolute Calibration of Electromechanical Pickups," J. of App. Mech. 15 49(1948)

*For an elliptical pattern, the ratio of the intercept on the horizontal axis to the peak horizontal deflection yields the sine of the phase angle.

it is unlikely to shift the frequency very much. After examination of a vacuum tube with the probe, one or more similar tubes with the seal intact can be connected as audio amplifiers and shaken on an exciter while on operation. The output signals may by themselves not readily indicate what in the interior is vibrating but should permit observation of Q's and of variability of resonance from one tube to another of the same type. Correlation of the results of the two experiments should yield a good understanding of the dynamical properties.

MEASUREMENTS ON MOCKUPS

So far we have discussed measurements in terms of completed equipment where diagnostic techniques may be important, for example, after a failure in an environmental test. We should emphasize, however, that the same measurement techniques can be even more useful if applied to dynamic mockups, or exploratory partial assemblies at an earlier stage as an assistance to the design process. If the equipment is not completely assembled, an occasional impedance measurement may be desirable as an aid in predicting problems caused by the addition of parts. In many instances, an impedance head can be used. An approximate measurement can also be obtained by fastening weight to the probe wire sufficient to produce appreciable loading and of known impedance in the frequency region of interest. The impedance to be measured is given by the ratio of the force on the weight to the change in velocity induced. The force on the weight is given by its impedance times the loaded velocity.

CONCLUSIONS

A particular style of vibration probe, in conjunction with one fixed force gage or accelerometer to supply a reference signal, and used with a Lissajous figure technique, has been shown to be particularly promising for measurement of equipment resonances. For application to design, or diagnosis of deficiencies after a failure, extreme precision is usually not necessary. The measurements to be performed on a particular setup should be performed by a single experimenter, who should have direct access to all controls, cathode-ray oscilloscopes and other readout instrumentation, and be able to touch the probe readily to any point whose motion comes to be of interest.

Should the acoustic properties of the cavities within an equipment be of potential concern, they can be explored with similar techniques with almost the same setup. Access holes can be threaded so that all but the one momentarily in use can be closed by set screws, or rubber or plastic plugs. A standard type of acoustic probe for measuring sound pressures in cavities is made by fastening over the diaphragm of a capacitor microphone a metal cap into which is soldered the end of a slender tube a millimeter or two in diameter. Rubber or plastic can be used to make a seal between the probe tube and the walls of the access hole through which it is inserted.

The measurement of equipment resonances as an aid to the improvement of reliability has undoubtedly been on the increase. Yet, little has been reported on the techniques used, and few data on standard parts or structures have been published. I hope that this paper will help to stimulate more interest in both aspects.

DISCUSSION

Mr. Tustin (Tustin Institute of Technology): What frequency accuracy do most people feel they need when determining resonances?

Dr. Morrow: I think generally most people want the highest accuracy whether they can use it or not. I think we should keep in mind that it makes a little difference whether we are trying to get measurements to explore some very subtle effect, where the accuracy of the frequency is important, or whether we are going to publish the data (and I wish people would publish data on resonances of characteristic things which they use every day), or whether we are just trying to make some measurements to help in working out a design. If we are trying to work out a design then one of the important things is to make sure we do not have a coincidence of resonances along the way. Assuming that we have a little bit of latitude to play around with by changing stiffness and mass, etc., we do not need to have frequencies measured real accurately to avoid coincidence. If we wanted to make sure they coincided it would be necessary to measure with greater precision.

Mr. Matthews (USN Missile Center): Can you give us some indications of whether these probes are effective in investigating nonlinear phenomena, or do you use them in that way at all?

Dr. Morrow: I have not used them primarily for this purpose. I think they would be effective, but if we are trying to work out a design I would say that nonlinear phenomena are a secondary

consideration. It can be very bothersome in some respects, once you have a piece assembled, if you did not design it correctly; but I do not think this is the first thing to look at for purposes of design.

Mr. Kennard (Goddard Space Flight Center): You mentioned the x-ray stroboscope and you seem to have some reservations as to its practical use. Would you want to go into that any further?

Dr. Morrow: The stroboscope is essentially an amplitude responsive device which gives it some limitations at the higher frequencies. Furthermore, you do not have a convenient way, as far as I know, of comparing what you see with any reference signal. In other words, what you have to look at is the overall effect of the exciter plus the equipment under observation, and you cannot isolate the two entirely. Also, you have no way of observing phase effects readily unless somebody wants to exercise a little ingenuity; so that some of the techniques that can be used with a probe are not available. On the other hand, it should give one a very good and quick intuitive feel for what happens inside a piece of equipment, and it would be especially useful in demonstrating to people that things do vibrate, if they do not think this happens. It should be very valuable at the beginning, but there are a lot of things that one might like to measure which it will not do very well.

* * *

PIEZORESISTIVE STRAIN GAGE ACCELEROMETERS INCREASE SPECTRUM OF SHOCK AND VIBRATION MEASUREMENT CAPABILITY

W. E. Wall
Endevco Corporation
Pasadena, California

The general acceptance of piezoresistive strain gage transducers, in particular accelerometers, suggests a look at the place of these accelerometers, suggests a look at the place of these accelerometers in the "period-of-interest" spectrum of shock and vibration measurement. This period of interest spectrum concerns the measurement of constant acceleration with superimposed high frequency vibration or long duration shock pulses. The spectrum is defined and used to compare three types of shock measuring transducers: wire wound strain gage, piezoelectric, and piezoresistive strain gage. A typical piezoresistive strain gage accelerometer is examined in detail for application, performance and user test results. A brief examination of possible future expansion of the spectrum concludes the presentation.

INTRODUCTION

A recent review of instrumentation handbooks, revealed one volume on engineering measurements (1), vintage 1948, which, while revealing a wealth of information on the measurement of time, temperature, pressure, etc., was devoide of any reference to devices for the direct measurement of displacement, velocity, or acceleration. While the development of the mathematical theory for analyzing shock pulses began to solidify in the early nineteen forties, it was not until after World War II that instrumentation to measure these shock effects began to appear. Some of these devices were developed for the transportation industry; for example, to monitor cargo shocks in trucks, railroad cars, and aircraft. Most of the postwar development seems to have been brought on by the need for blast shock measurements on ships structures, aircraft buffeting and landing shocks, and other use or abuse loads to the new weapon systems. Each new requirement brought about a need for higher natural frequencies; greater sensitivities, and higher ranges.

The most recent development in this line is the piezoresistive strain gage accelerometer. The advent of piezoresistive strain gages, with their inherently high gage factors (eight to one-hundred times that of the conventional wire wound gages) has allowed the design of accelerometers with high sensitivities, high natural frequencies and low frequency response down to dc. Strain elements such as these have brought about a minor revolution in the measurement of pressure, force, acceleration, displacement, and temperature.

Piezoresistive strain gage accelerometers have been under development since about 1960. The following presentation will examine one specific design, discuss its place in the "period-of-interest" spectrum and the future expansion of the spectrum through design improvements.

BRIEF HISTORY

The original need for inertial or displacement information was handled by the sensing elements available to the designer. The potentiometer, the linear variable differential transformer, and the magnetic pickoff were all quite suitable for the steady state and low frequency test and control instruments specified at that time. The allowance for shock response in structures was usually handled by theoretical means such as proposed by Frankland (2), in the forties. As both the structures and their environments became more complex and severe, three major fields advanced along with the requirements. These were static and flight load determinations utilizing strain gages, environmental testing as a necessary requirement, and

solid-state physics. The first brought about a vast understanding of strain measurement and strain gages, possibly due to the amazing number of test points per aircraft and number of aircraft tested. The second brought about the development of shaker type test equipment and the auxiliary monitoring equipment necessary to control and monitor them. These resulted in today's piezoelectric accelerometers and inductive velocity sensors. The third resulted in a spin-off, namely the definition of the piezoresistive effect present in many of the new electronic materials.

The first two devices to emerge were the wire wound strain gage accelerometer and the piezoelectric accelerometer. The first device had two of the essential elements, the ability to sense steady state conditions and infinite resolution. The second device was also capable of infinite resolution and, because of the nature of its construction, high natural frequencies and high signal levels. These devices had several weaknesses, too. The wire wound strain gage devices, due to their relatively large displacements,had low natural frequencies and correspondingly low frequency response even with reasonable damping. The piezoelectric accelerometer, although capable of generating essentially steady state signals, was required to operate into signal conditioning equipment with low frequency rolloff to filter out extraneous thermal effects.

The use of the semiconductor strain gage, with its gage factor one to two orders of magnitude greater than that of the wire or foil gages, allowed the design of an accelerometer combining the desirable features of both devices and eliminating many of the undesirable ones.

PERFORMANCE

Obviously, the solid-state strain gage accelerometer has not eliminated the need for all other accelerometers any more than the equivalent pressure transducer has affected the alternative designs of that discipline. Therefore, a means to examine the place of these instruments as tools in the measurement of transient acceleration, was needed.

The three parameters considered to be most important for such measurements were (a) sensitivity, (b) high frequency response, and (c) low frequency response. The sensitivities of various devices can be looked at directly. No weighting of the sensitivity figure of any accelerometer is necessary, as few, if any, transducers in existence today are blessed with too much signal. High frequency response, although becoming increasingly harder to obtain, is also essentially a linear improvement. A unit which is flat to 2000 Hz is essentially twice as good as a device which is flat to 1000 Hz. Thus, no adjustment of this figure is necessary. The use of damping to extend the response of any of these devices is taken into account and the use of ±5% response error is used to define flatness. (The use of a lower figure such as ±2% does not affect the relative merit of any one design to another.) The last parameter to be examined is the low frequency capability of these devices. The low frequency rolloff of all devices is also considered to be ±5%. This limit is taken for the signal conditioning equipment used with piezoelectrics, and is required to remove extraneous signals such as pyroelectric effects. As both strain gage accelerometer designs have low frequency response to zero Hz (steady state or direct current), the use of zero (frequency response) or infinity (period) would rapidly eliminate the utility of any comparison to the piezoelectric accelerometers. It was decided to use an algebraic expression which approached some finite limit asymptotically to compare low frequency response. The relation used is:

$$L.F.R. = \frac{T}{10 + T}$$

where T = period (in seconds) of lowest frequency response and 10 a relatively weighted constant. The limit of the expression is 1 when T approaches infinity.

Thus, the resulting figure of merit for measuring shock pulses becomes:

$$Fm = S \times (H.F.R.) \times (L.F.R.)$$

where

S = full scale sensitivity

H.F.R. = limit of high frequency response (±5% amplitude distortion)

L.F.R. = adjusted figure for low frequency response.

The advertised, or catalog sheet, performances of approximately 60 accelerometers were examined as a typical sample. (A problem existed here of too much data rather than not enough, so a certain amount of selectivity was used.) The plotted curves represent the maximum performance of each type of transducer. Lower figures of merit which exist for each are due undoubtedly

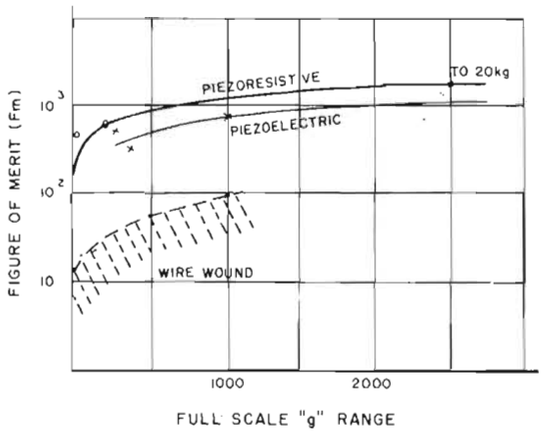

Fig. 1. Period-of-interest, typical accelerometers

to the influence of some other design restraint. The figures of merit (Fm) are plotted against the full scale acceleration range noted by the manufacturer (see Fig. 1).

The wire wound strain gage transducers can be seen to have excellent low acceleration utility along with their steady state capability. Two envelopes are noted. The maximum one being the result of optimum damping, the minimum one allowing for a maximum excursion in damping due to temperature effects. The piezoelectric and piezoresistive transducers being essentially undamped (less than 0.05 of critical damping) are not affected by viscosity changes.

The piezoresistive and piezoelectric transducers reflect approximately equal performance except in three areas (a) maximum accelerations, (b) minimum acceleration, and (c) the ability to measure long duration shock pulses.

To indicate the restrictions necessary when examining accelerometer performance reference is made to an article by L. B. Wilner in The Review of Scientific Instruments (3). Using the energy methods of Stein, he compares the measurement of steady state harmonic input signals. It is deduced that the transition frequency from the most sensitive strain gages to the most sensitive piezoelectric is in the 1000 Hz range.

The piezoresistive strain gage accelerometer has a wide application and requires no new technology on the part of the using agency. The device utilizes the Wheatstone bridge, requiring the selection of power supply and recording equipment only on the basis of the input parameters. These units are operated at reasonable strain levels (500 to 1000 microinches per inch) and can withstand overloads on the order of three times full scale. The use of sensing elements with gage factors on the order of 120 to 200, result in designs combining high sensitivities with high natural frequency.

A unit for use in long duration, high shock pulse measurement is the ENDEVCO Model 2261 shown in Fig. 2. This unit has a specified range of 2500 g's and a full scale sensitivity of 250 mv (at 10 volts dc excitation). A natural frequency of 30,000 Hz nominal allows it to operate flat to above 6000 Hz.

To indicate better the performance of piezoresistive strain gage accelerometers, the following comparison is made. Consider two accelerometers, each having the same natural frequency, operating under reasonably severe thermal conditions. Figure 3 shows the response of each to a long duration pulse with a steep front ramp. Input: An idealized ramp function of long duration. Curve (1) depicts the theoretical response of a piezoresistive accelerometer with a high resonant frequency. Curve (2) shows the response of a high resonance, underdamped system with inadequate low frequency response. Curve (3) is typical for a 0.6 damped, low resonant frequency, wire wound strain gage accelerometer.

Note that for the initial period of the shock, the performance of the instruments is essentially identical. As the long pulse continues, the piezoelectric transducer exhibits characteristic droop due to the low frequency rolloff of the signal conditioning equipment. When the shock pulse ends, there is the characteristic undershoot due to the same phenomenon. Also note the response of an equivalent strain gage accelerometer with 0.64 of critical damping.

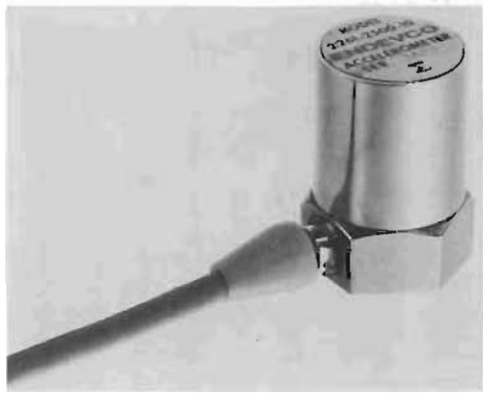

Fig. 2. Piezoresistive strain gage accelerometer

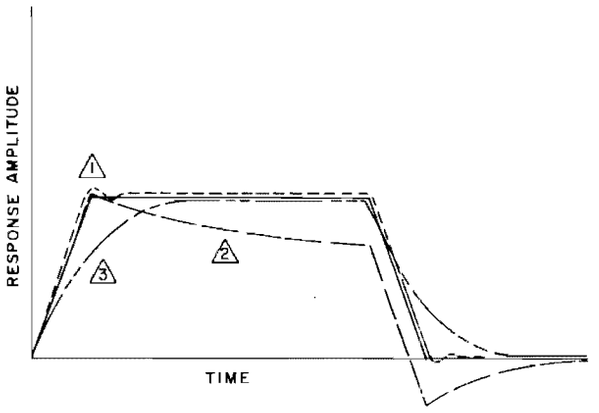

Fig. 3. Theoretical response, typical accelerometers Ref. (4)

TYPICAL APPLICATIONS

Recently the 2500 g range piezoresistive strain gage accelerometer has been used for some rather severe applications. Some of these are:

1. To record the impact shock profile of a projectile in order to determine consistency of surface penetrated.

2. Flight test data on high performance missiles having severe natural environments. Determination of boost separation shock loads superimposed on high, thrust induced, steady state accelerations.

3. Extraction and impact shock data for airborne drop tests. The continuous recording of acceleration and shock phenomena on air-dropped or high speed ground extraction of pallet mounted cargoes.

4. Ground test recording of shock and vibration on high performance rocket motors. (In one instance this included the extraction of data from a spinning motor case through slip rings.)

5. Monitoring test parameters on large hydraulic shakers, with low output impedance for use with computerized data analysis, at very low frequencies.

6. Non-military applications such as collision shocks in automotive safety testing and design load verification for a jack-hammer.

FUTURE EXPANSION

The available configurations of piezoresistive strain gage accelerometers are by no means complete. The spectrum of testing capability needs to be expanded further. There is a need for expansion of the ranges available. Low ranges are necessary for inertial data and higher ranges are available for external shock testing; for example, close in data on explosions. Eventually these units should be available, in approximately the same envelope with higher signal levels (0 - 5 volts perhaps) and capable of operating from relatively raw power supplies.

CONCLUSION

No new instrumentation concept has ever eliminated the need for already existing designs. Transducers utilizing piezoresistive strain gage sensing elements, in particular the accelerometers, have expanded and supplemented the envelope of available information. In the area of shock and vibration this appears to be a reasonable expansion of the envelope in the realm of long pulse duration. As the users need expand so has the suppliers ability to meet their requirements.

REFERENCES

1. H. Diederichs and W. C. Andrae, Experimental Mechanical Engineering Vol. 1, Engineering Instruments, John Wiley & Sons

2. J. M. Frankland, "Effects of Impact on Simple Elastic Structures", Experimental Stress Analysis, 1947 (approximate)

3. L. B. Wilner, "Sensitivity Comparison of Transduction Mechanisms", Rev. Sci. Instr. 36: 693-695 (1965)

4. D. E. Lovelace, "Development and Applications of a Piezoresistive Strain Gage Accelerometer", J. Env. Sci. 7:16 (1964)

Mr. Beline (The Boeing Co.): Have you attempted to use these at lower frequencies and at cryogenic temperatures? If so, with what results?

Mr. Wall: We have not tested them cryogenically yet. We are still attempting to produce a standard unit; but that particular doped gage does not operate well at cryogenic temperatures, and it is very difficult to compensate in that range.

* * *

VIBRATION MEASUREMENTS USING A MICROWAVE INTERFEROMETER

C. F. Augustine and J. E. Ebert
Weinschel Engineering
Gaithersburg, Maryland

Vibration amplitudes as low as a fraction of a microinch at frequencies from dc to 20 kc were measured using a noncontacting microwave interferometer. A 35 Gc signal was used for sensing. For targets that could be placed very near the portable sensing head, the sensing element was an open ended miniature coaxial cable. For more distant targets up to one foot away, the sensing head was attached to an elliptical antenna. This antenna focused the microwave energy to a diameter of about 0.15 inches on the target surface. Remote sensing, provided by the elliptical antenna, is particularly important if the target is in an oven, or vacuum, or is otherwise inaccessible.

Operating on the interferometer principle, changes in the phase of the reflected 35 Gc signal were detected and displayed either on a meter or an oscilloscope. Because the detection circuit was almost completely insensitive to the magnitude of the reflection, the instrument was usable on either dielectric or metallic targets. The detected output signal is nearly linear even for amplitudes of 0.05 in. Absolute calibrations were obtained using as a standard a calibrated micrometer-driven phase shifter attached to one arm of the microwave phase bridge. A calibration technique was developed that could be used to determine the peak-to-peak displacement of each harmonic in a complex vibration.

BACKGROUND

The optical interferometer is well recognized as the standard for measuring short distances and displacements. However, it does have limitations, particularly from a practical applications point of view. Alignments are very critical, the target surface must be a very good optical reflector, and the light interference pattern used as the readout cannot be readily converted to an electrical signal analogous to displacement. These limitations, particularly in regard to readout, severely restrict the use of the optical interferometer for shock and vibration measurement.

During recent years, reliable high quality millimeter wave components have been developed and are generally available. These developments are very recent in comparison with the century or so that optical interferometers have been used. In spite of this, it can be stated that the microwave technology that can be applied to interferometers is now superior to optical technology, since optical technology does not include such components as directional couplers, coherent amplifiers, phase sensitive detectors, and ferrite circulators. These components are of great value in interferometer applications.

Along with the components, special antennas have been developed to focus microwave beams on a remote target. Beam diameters between 0.1 and 0.2 of an inch at a distance of about 1 foot from the antenna are typical. These antennas and components permit the fabrication of microwave interferometers that are especially useful in shock and vibration analysis. Alignment is not critical and the target may be any surface that reflects even a small amount of microwave energy. Very high resolutions are possible and an electrical output proportional to displacement is readily obtained. The remote sensing feature provided by the antennas is useful when observing targets that may be in a special environment, such as a furnace or vacuum chamber.

In the following sections, the simplest form of microwave interferometer will be described and its limitation pointed out. Methods of overcoming

these limitations are revealed by describing a practical interferometer operating at 35 Gc that has been constructed and tested. Some significant test results will be given and various possible applications described. The complete instrument in a typical test setup is shown in Fig. 1. The sensing head and elliptical antenna are mounted on a seismic stand to measure spindle out-of-roundness.

BASIC PRINCIPLES

The operating principle of the microwave interferometer is analogous to its optical counterpart. A microwave signal from a monochromatic source is divided between a reference and measurement arm. The target position affects the length of the measurement arm, whereas, the length of the reference arm remains fixed. Both arms terminate in a phase comparator that yields an output proportional to length differences between the two arms.

A block diagram of a basic microwave interferometer is shown in Fig. 2. It consists of five components: A klystron that generates a microwave signal, directional couplers, an antenna, a calibrated phase shifter, and a phase comparator. The components are connected electrically through appropriate lengths of waveguide. The phase comparator output can be altered by either the calibrated phase shifter or the target position. The electrical output of the phase comparator as a function of this phase difference is shown in Fig. 3. It is essentially a sinusoid having a period equivalent to 360 degrees change of the phase shifter or a one-half wavelength displacement of the target. At 35 Gc, a half-wavelength corresponds to a displacement in air of about 0.17 in. The linear portion of the sinusoid, near the zero crossover, is equivalent to a displacement of about 0.05 in. Accurate oscilloscope presentations of vibrating targets can therefore be obtained over this linear region. The phase shifter may be calibrated from fundamental principles and is used to accurately determine target displacement.

THE COMPLETE INTERFEROMETER

The basic interferometer serves to illustrate the general principles. To obtain the practical interferometer, a great deal of attention must be paid to the features influencing accuracy, resolution, and stability. The primary considerations are klystron frequency stability, mechanical stability of the microwave assembly, and electrical signal to noise ratio in the phase comparator and phase shifter calibration. Figure 4 is a block diagram of a complete interferometer in which these factors are considered.

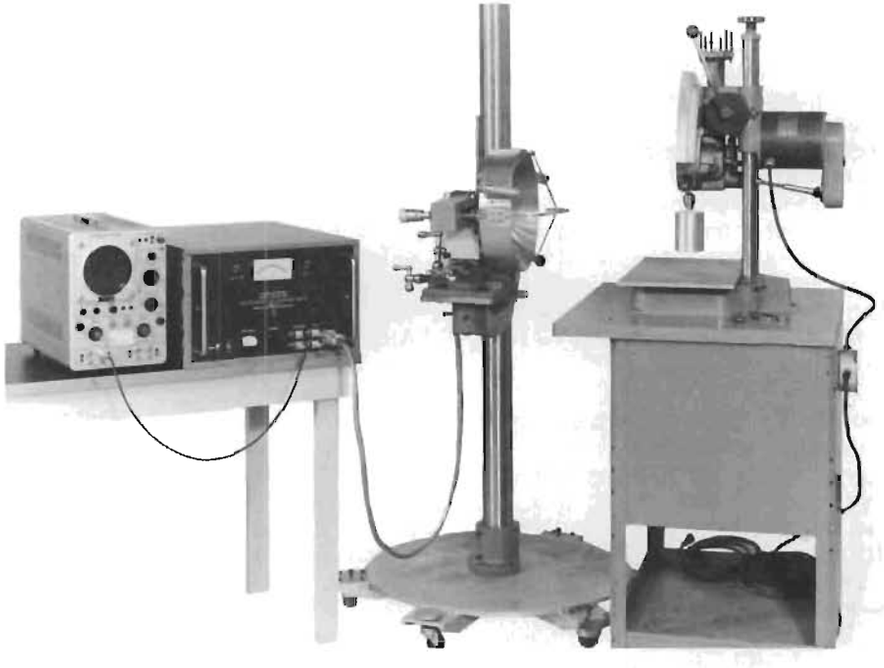

Fig. 1. Interferometer in a typical measuring setup

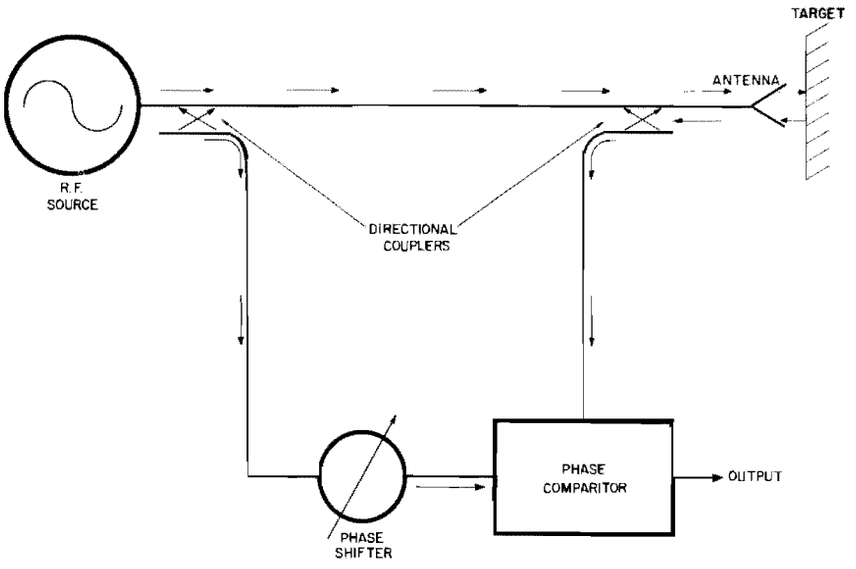

Fig. 2. Basic microwave interferometer

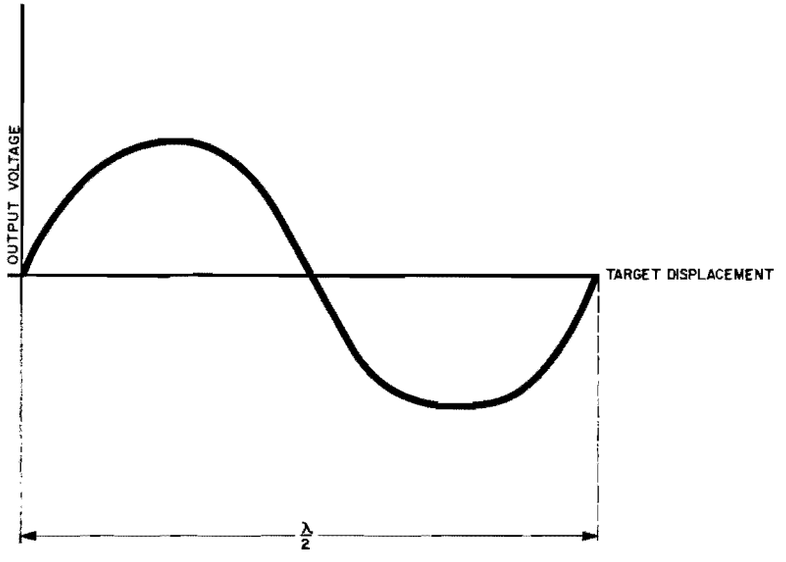

Fig. 3. Phase comparator output

Frequency stability is achieved by electronically sweeping the klystron frequency across the resonant frequency of a transmission cavity. This is done at a 100 kc rate. The input to the first hybrid junction is therefore a series of 100 kc pulses. The frequency spectrum of the pulses is almost entirely governed by the very stable characteristics obtainable from the transmission cavity.

The first hybrid junction divides the signal equally between the reference and measurement arms. The antenna is placed on one port of a ferrite circulator in the measurement arm. In the reference arm, a movable short circuit that serves as the phase shifter is placed on the corresponding circulator port. The circulators direct the incoming signal towards the antenna or short circuit. Signals reflected back into the

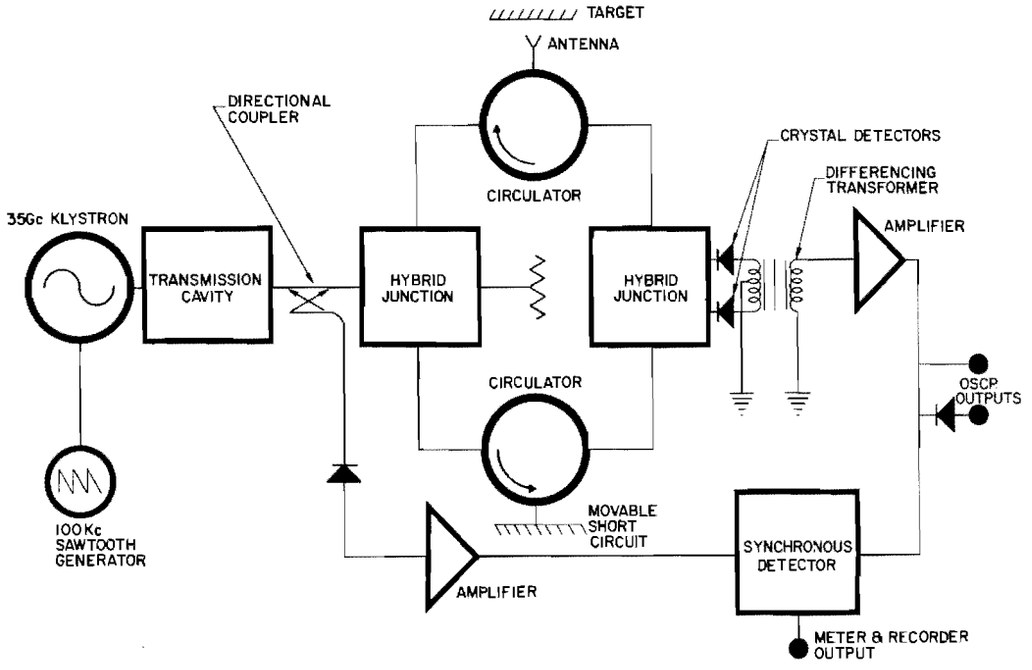

Fig. 4. Complete microwave interferometer

circulators from the target or short circuit are directed into two isolated ports of a second hybrid junction. Crystal video detectors are attached to the two remaining isolated hybrid junction ports. This second hybrid junction and the crystal detectors act as the phase comparator.

The performance of the phase comparator is explained analytically in Appendix A. For the purpose of understanding the instrument, it may be considered as a simple sum and difference device with the output of one crystal detector being the vector sum of the two rf inputs while the other output is the vector difference. The transformer network forms the difference between these two crystal outputs which is proportional to the cosine of the angle between them. If the phase shifter is set so that this angle is near 90 degrees, the cosine is almost zero and very nearly proportional to the difference between the angle and 90 degrees. Therefore, the output will change in an essentially linear manner with small target displacements. The linearity is good over a range of about 0.050 in. The phase shifter can be continuously reset to accommodate larger displacements.

Synchronous detection is used to obtain the best possible stability and resolution when the target position is changing at a slow rate. The synchronous detector output is used to operate a meter or chart recorder. Two oscilloscope outputs are available when the target motion is too rapid for a meter or recorder. One output is the 100 kc carrier. This carrier contains the modulation envelope that would be superimposed by a vibrating target. It is used in conjunction with the phase shifter to calibrate the peak-to-peak displacement of the vibrating target. The second oscilloscope output is the rectifier 100 kc envelope that is an accurate electrical analog of the target displacement.

An analysis of the electrical factors, mainly klystron stability and crystal detector noise, that limit resolution is given in Appendix B. This analysis indicates that when small detection bandwidths are used, displacements less than a microinch can be resolved before electrical noise becomes dominating. This has been verified experimentally.

A complete interferometer is shown in Fig. 5. The electronics module on the right contains all power supplies, synchronous detectors, amplifiers, etc. Microwave components are housed in a separate sensing head. These components are fabricated from a solid block of metal. The very rigid mechanical assembly obtained in this way greatly reduces drift and mechanical noise that would occur if conventional waveguide assembly techniques were used. In Fig. 5 the sensing head is shown attached to a special elliptical antenna used for distant targets.

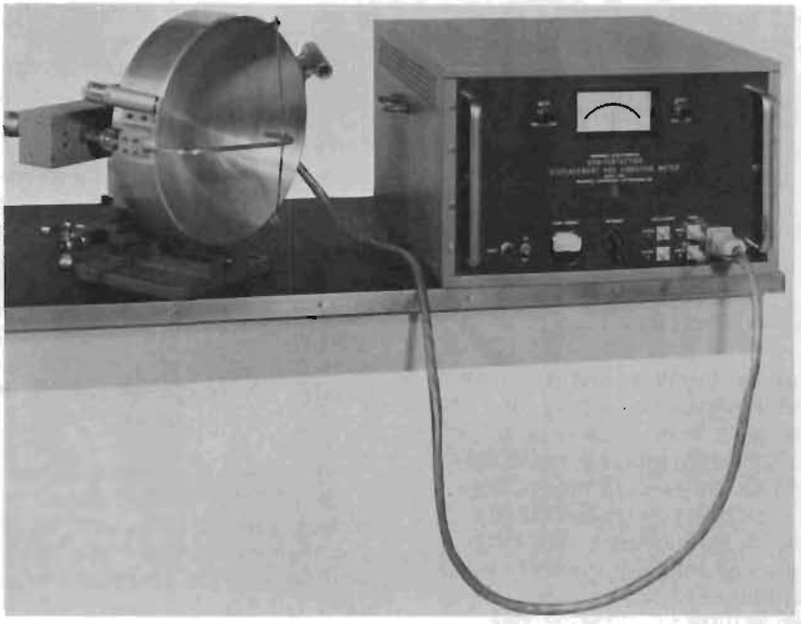

Fig. 5. Complete instrument equipped with elliptical antenna

ANTENNA CONSIDERATIONS

The antenna, Fig. 5, has an elliptically contoured reflecting surface. This type of antenna is particularly well suited for general use with the instrument. The elliptical surface collimates a narrow beam down to a diameter of about 0.15 in. at a distance of about 12 in. from the surface. The length of the collimated region is about 3 in. The target is placed in the collimated region perpendicular to the beam.

The elliptical surface of the unit has a 12-in. focal length which optimizes parameters in regard to path loss, beam diameter, and the physical size of the surface. However, special elliptical surfaces may be constructed to increase the focal length up to several feet and increase the collimated region up to about 8 in. When this is done, however, the diameter of the collimated beam is increased by a factor of 2 or more.

Figure 6 shows a capacitance pickup probe that can be used in place of the elliptical antenna for special applications. This probe is attached to the output port of the sensing head and is especially useful when extremely high resolutions are desired over a total displacement range not exceeding 0.003 in. The probe is nonradiating. It is basically a transducer from waveguide to semirigid coaxial transmission line. The sensing tip is just the open circuited end of the transmission line. Target surfaces placed near this tip add capacitance to the otherwise open circuit. This added

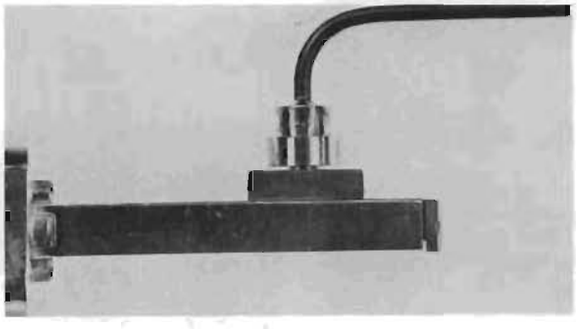

Fig. 6. High resolution capacitance probe

capacitance causes a rapid change in the angle of the reflection coefficient and alters the interferometer output. When the interferometer is used with the capacitance probe, the resolution is increased by about a factor of 30 over that obtainable with the elliptical antenna. The effective spot diameter of the probe is between 0.020 and 0.040 in. Resolutions of tenths of microinches can be obtained with the probe.

APPLICATIONS AND TEST RESULTS

Applications for the interferometer can be broadly categorized into those involving long term displacements, as might be the case in measuring expansion coefficients; or rapid displacements as might be the case in measuring shock or vibration. Stability tests indicated a residual inherent noise as indicated on a chart recorder of about plus or minus 5 microinches. The detection bandwidth used for this test was 0.2 cps. Long term stability tests were performed in a temperature controlled chamber with the elliptical antenna aimed at a fixed target. These tests indicated that the stability over several hours of elapsed time was about 15 microinches. This excellent long-term stability indicates that the instrument should be useful in measuring temperature expansion coefficients and other gradual dimensional changes.

The total detection bandwidth of the instrument is from dc to 20 kc. In any given measuring situation, most of the residual noise will be concentrated below about 20 cps. When the target is vibrating at relatively high rates, band pass filters can be inserted between the interferometer output and the oscilloscope to restrict the bandwidth and eliminate noise. Figures 7 and 8 are photographs of oscilloscope traces of a 2000 cps, 100 microinch, sinusoidal displacement using the elliptical antenna. The displacement was produced by the piston of a shaker at the National Bureau of Standards Vibration Laboratory previously calibrated by National Bureau of Standards as 100 microinches. In Fig. 7 the detection bandwidth was entirely open from dc to 20 kc. A considerable portion of the noise and smear on the trace was due to the inevitable low frequency motion of the stand supporting the antenna and sensing head.

Figure 8 illustrates the effect of restricting the bandwidth. A band pass filter was used to restrict the detection band to 2000 cps plus or minus about 200 cps. The low frequency noise, particularly that generated by motion of the stand was eliminated.

When suitable filtering is used, periodic displacements on the order of several microinches can be resolved using the elliptical antenna.

As indicated previously, much higher resolutions are possible with the capacitance pickup. Figure 9 shows a 4 microinch displacement at 2 kc of an NBS transducer using a band pass filter and the capacitance probe. The trace is essentially free of electrical noise. The 4 microinch displacement was the smallest displacement that could be accurately calibrated by NBS. To obtain the trace shown in

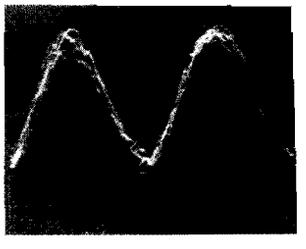

Fig. 7. A 100 microinch displacement at 2 kc with the full 20 kc detection bandwidth using the elliptical antenna

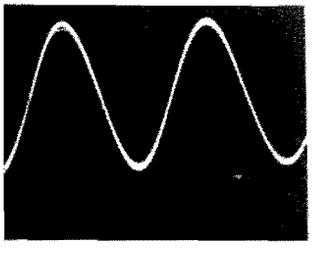

Fig. 8. A 100 microinch displacement with restricted detection bandwidth using elliptical antenna

Fig. 9. A 4 microinch displacement with restricted detection bandwidth using capacitance pickup

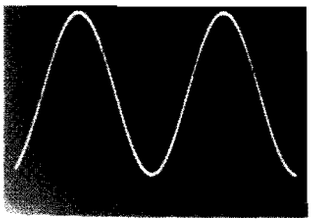

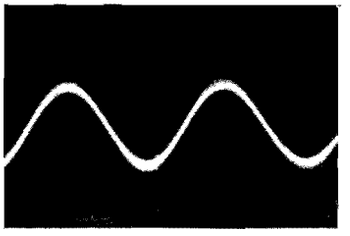

Fig. 10. An estimated 0.4 microinch displacement with restricted bandwidth using capacitance pickup

Fig. 10, the transducer voltage required for a 4 microinch displacement was divided by 10 to produce a displacement that should be about 0.4 microinches. Figure 10 indicates that resolutions on the order of tenths of a microinch are possible with the capacitance probe.

Apart from shock and vibration studies and measuring slow dimensional changes, there are a variety of other potential applications for the microwave interferometer. There is experimental evidence indicating that very small capacitance probes may be used to provide a noncontacting method of measuring surface finish. The interferometer is also useful in measuring the thickness of dielectric materials. Under certain circumstances, internal flaws in dielectric materials can be detected. The thickness of thin dielectric coatings on metallic surfaces can also be measured.

Appendix A

ANALYSIS OF THE HYBRID JUNCTION

The hybrid junction, in combination with the crystal detector ports, functions as a phase comparator, i.e., an output voltage is derived that is related to the distance d. This comes about in the following way:

If $\bar{E}_1$ and $\bar{E}_2$ represent the Reference and Measurement Arm input signals, then, as a result of the transfer characteristic of the hybrid junction, the signal inputs to the crystal detectors are:

$$\bar{E}_3 = \sqrt{\frac{2}{2}}\,(\bar{E}_2 + j\,\bar{E}_1) \qquad \text{(A-1)}$$

and

$$\bar{E}_4 = \sqrt{\frac{2}{2}}\,(\bar{E}_1 + j\,\bar{E}_2) \qquad \text{(A-2)}$$

with magnitudes equal to

$$|E_3| = \sqrt{\frac{2}{2}}\,\sqrt{(E_1 - E_2)^2 + 2E_1E_2(1 + \sin\theta)} \qquad \text{(A-3)}$$

$$|E_4| = \sqrt{\frac{2}{2}}\,\sqrt{(E_1 - E_2)^2 + 2E_1E_2(1 - \sin\theta)} \qquad \text{(A-4)}$$

where $\theta = 4\pi d/\lambda$ and λ is the free space wavelength of the microwave signal. These signals are detected by crystal detectors having square law characteristics and subtracted in a combining network. The final output signal then takes the form of

$$e_o = 2k\,E_1E_2\,\sin\frac{4\pi d}{\lambda} \qquad \text{(A-5)}$$

where k is a second order variable that is a function of signal level and detector characteristics. The output voltage is then essentially a sinusoid. A full cycle of the sinusoid is equivalent to a target displacement of 0.17 in. at 35 Gc, and the peak-to-peak voltage swing occurs during a displacement of 0.085 in.

Appendix B

RESOLUTION AND STABILITY ANALYSIS

Minimum resolution, i.e., the smallest possible discernible target displacement, is determined by klystron noise, crystal detector noise, and mechanical stability. The effect of noise can be analyzed as follows.

As shown in Appendix A, the phase detector output may be expressed as

$$E_o = E_s \sin \frac{4\pi d}{\lambda} \qquad \text{(B-1)}$$

where E_s is the peak signal voltage. In general, the operating point should be set at the steepest part of the output versus displacement characteristic, i.e., around the null condition. Then small incremental changes in distance, Δd, are related to output voltage changes, ΔE, with sufficient accuracy by

$$\Delta E_o = \frac{E_s\, 4\pi}{\lambda} \Delta d \,. \qquad \text{(B-2)}$$

To find the apparent displacement caused by crystal noise, let $\Delta E_o = E_n$, and rearranging equation (B-2)

$$\Delta d = \frac{\lambda E_n}{4\pi E_s} \,. \qquad \text{(B-3)}$$

The signal to noise ratio at the crystals is now found from the relation

$$\frac{E_s}{E_n} = \frac{P_s M}{\sqrt{4k\,TB}} \qquad \text{(B-4)}$$

where P_s is the signal power incident on the crystal, M is the detector crystal figure of merit, (units of amperes watts^{-1} ohm$^{1/2}$) and kTB is the product of Boltzman's constant, temperature and bandwidth. From Eqs. (B-3) and (B-4) the apparent displacement due to noise is:

$$\Delta d = \frac{\lambda}{4\pi} \frac{(4kTB)^{1/2}}{MP_s} \,. \qquad \text{(B-5)}$$

A graph relating the parameters of Eq. (B-5) is shown in Fig. B-1. A figure of merit equal to 40 was chosen as typical for the crystal detector. The signal power is at least 10^{-4} watts. The graph shows the theoretical limit of resolution capability as far as electrical noise is concerned.

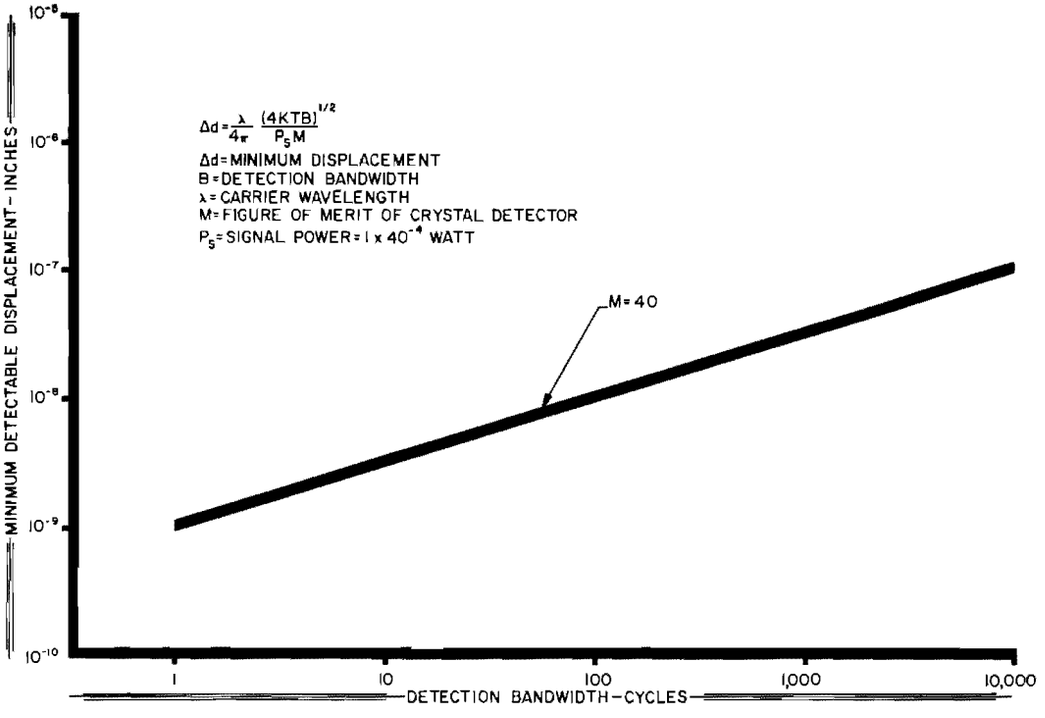

Fig. B-1. Resolution limited by crystal noise

It is important to point out that Eq. (B-5) assumes that the crystal generates white noise. This is not the case for frequencies below about 80 kc. At low frequency the noise has a $1/f$ characteristic and will be larger than the value assumed in Eq. (B-4). The system utilizes 100 kc modulation rates to avoid the increased low frequency noise.

For the purpose at hand, klystron noise can be divided into amplitude modulated and frequency modulated components. The overall effect of klystron amplitude modulation is not severe because of the balanced arrangement of the phase detector. If the two crystal detectors are well matched, the effects of amplitude modulation of a high quality klystron oscillator is not a limiting factor.

Incidental frequency modulation is important when the total path length of the Reference Arm differs from that of the Measurement Arm. The phase difference and the phase detector output, will then be frequency dependent. To obtain the magnitude of this effect, assume that the waveguide sections of the two arms are identical and the total path length difference is d, the distance between the antenna and target. The equation relating the pertinent variables is:

$$\Delta w = \frac{\Delta \beta c}{d} \qquad \text{(B-6)}$$

where Δw is the change in klystron frequency, c is the propagation velocity, and β is a specific change in phase angle.

At 35 Gc the significant constant is 89 kc per microinch per cm, i.e., if d is equal to 1 cm, the klystron frequency must change 89 kc to cause the phase detector output to give a voltage change equivalent to 1 microinch of motion. In the present system, the largest expected value for d will be about 43 cm when the far field antenna is used. This means that the long term stability of the klystron must be approximately 1 part in 10^6 to maintain the interferometer stability better than 10 microinches. Measurements have shown that the cavity stabilization technique produces the required frequency stability.

DISCUSSION

Dr. Morrow (Aerospace Corp.): Might there be any virtue in doppler techniques to improve the resolution at the high end of the spectrum?

Mr. Augustine: I think we have all the resolution we can use. The wavelength is about 4/10th of an inch. If you go through many many cycles of this you could generate a true doppler frequency that would be indicative of velocity, but in general we like to stay on the linear portion of this sinusoid.

Voice: First, have you measured the effects of temperature on your target; and second, do you intend to market the equipment?

Mr. Augustine: We made long term stability tests in a very well controlled environment. Over a period of several hours, using the elliptical antenna to look at a fixed target, we felt that our long term stability was of the order of 10 microinches. We cannot be sure of this because the devices that we were using to monitor our equipment were not absolute by any means, but these devices drifted the same way our equipment did over a period of several hours. Yes, the equipment is available commercially.

* * *

A WIDEBAND ABSOLUTE ACCELEROMETER CALIBRATOR UTILIZING A LASER FOR MEASURING VIBRATORY DISPLACEMENTS

Robert B. Davis
Naval Air Test Center
Patuxent River, Maryland

An absolute accelerometer calibrator utilizing a laser as the standard reference has been developed. The calibrator consists of a laser photodiode and appropriate electronic readout equipment, and is easy to operate with a direct digital readout for displacements greater than one-half of a wavelength. The present resolution of the prototype calibrator is one-tenth of a wavelength. This paper reports the progress on the development from its inception in March, 1965. Future development is directed toward measuring displacement with a resolution of one-hundreth of a wavelength. The results of this development are discussed in this paper.

INTRODUCTION

Several procedures now exist for calibrating the sensitivity and frequency response of vibration transducers. The current absolute calibration procedures include the reciprocity method and the interferometer, fringe method. These methods, while accurate, are difficult and time-consuming to perform. A secondary, standard comparison method is used by most laboratories for accelerometer calibrations. This method is reasonably accurate (National Bureau of Standard (NBS) error plus induced error), simple, and is the least time consuming. The undesirable features of this calibration are:

1. It is not an absolute calibration.

2. The calibration is limited to the NBS frequency and amplitude calibration range.

3. There are uncertainties in induced error.

The induced error includes: (a) accelerometer damage or change since the latest NBS calibration, and (b) erroneous output due to accelerometer case sensitivity, different magnetic or acoustic fields, etc. The ideal solution to the calibration problem would be to have an absolute calibrator for each user.

The Naval Air Test Center (NATC), under foundational research funding, is developing a Laser accelerometer calibrator to provide an absolute calibration. This calibrator is being designed for a shaker frequency range from above 0 cps to greater than 10,000 cps, and vibration amplitudes from 0 to greater than 100 g.

THEORY AND OPERATION

The calibrator consists of a continuous-wave, helium-neon gas laser, a linear polarizer, a quarter-wave plate, a transmissive, bidirectional photodiode, a front surface mirror, and appropriate electronic readout equipment (shown in block diagram form in Fig. 1).

The shaker, low distortion oscillator, power amplifier, and accelerometer readout electronics (oscilloscope and vacuum tube voltmeter) are commonly used, and require no further explanation.

The unique parts, the laser and the photodiode, do require further consideration, before the operation of the system is explained (see Fig. 2). The gaseous laser was selected as the distance reference because of its stable wavelength (6328.0 ± 0.1Å, depending on atmospheric pressure) and temperal coherence, also, because the laser has a uniphase wavefront, small beam divergence and operated single mode. These properties are required for proper operation of the calibrator.

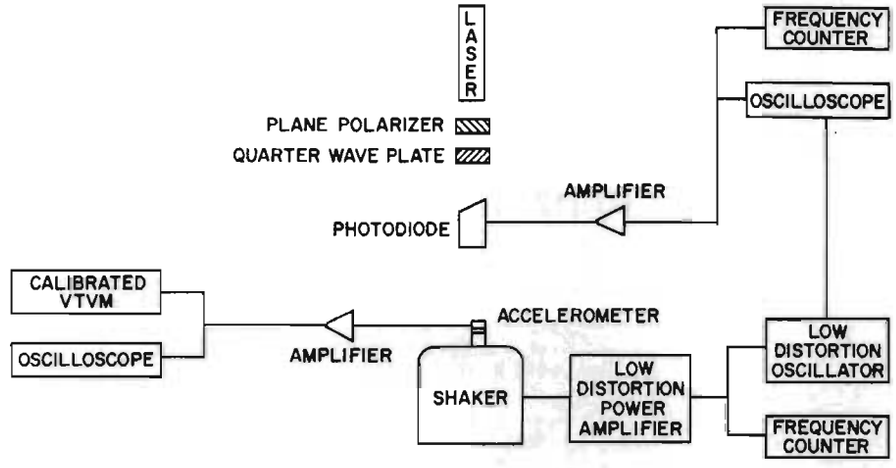

Fig. 1. Block diagram of laser accelerometer calibrator

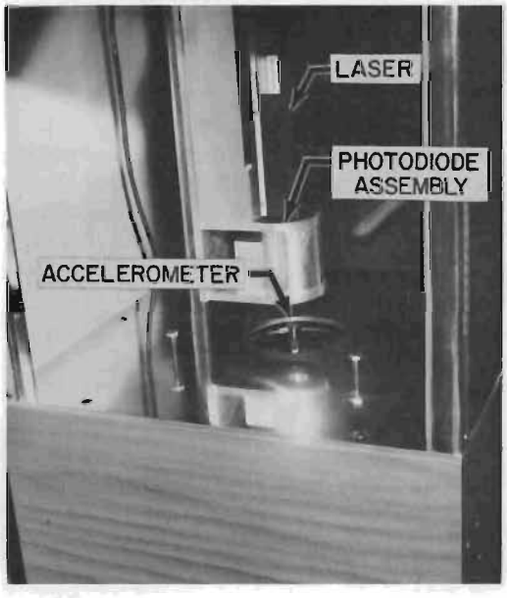

Fig. 2. Laser and photodiode assembly

A special photodiode tube was designed by the Naval Air Test Center, because no similar tube was commercially available. The photo-tube allows light to pass through the tube because its S-20 photocathode is 35 percent light-transmissive, and the anode is ring-shaped (see Fig. 3). In operation, the laser light passes through the tube, and is reflected back to the photocathode surface for light-interference measurements.

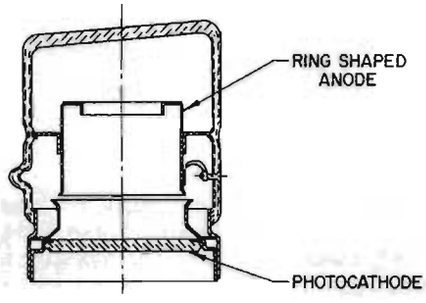

Fig. 3. Bidirectional transmissive photodiode

BIDIRECTIONAL TRANSMISSIVE PHOTODIODE

One minor problem with this calibrator was the internal reverberating light reflections between the laser, the photodiode, and the vibrating surface. A Plane polarizer and a quarter-wave plate were placed between the laser and the photodiode, to reduce these internal light reflections. Also, the photodiode was designed with one end at an angle of approximately 5 degrees, to further reduce reflections.

The operation of the calibrator (properly aligned) can be described as follows:

The low divergent light beam is emitted from the laser, and passes through the polarizer, the quarter-wave plate, and the photodiode, to the sinusoidally vibrating accelerometer. Here the light is reflected back to the

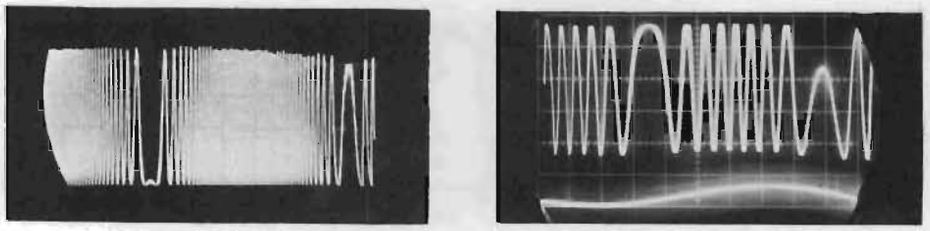

Fig. 4. Oscilloscope presentation of photodiode output, showing complete and partial beat cycles traversed; (a) 47.50 beat cycles or 27.75 wavelengths of accelerometer displacement, (b) 7.72 beat cycles or 3.86 wavelengths of accelerometer displacement

photocathode; however, as the accelerometer is vibrated, the frequency of the reflected light is Doppler-shifted, because of the continually increasing and decreasing light path length. The Doppler-shifted and emitted light waves, both having uniphase wavefronts, are superimposed at the photocathode.

A light of varying intensity results because of the constructive and destructive light wave interference between the doppler-shifted and the emitted light. The modulated light is then monitored by the photodiode as a maximum output, when the two interfering waves are in phase, and as a minimum output, when they are 180 degrees out of phase, (or one cycle (beat) for each wavelength of light traversed).

Each beat, cycle-monitored by the photodiode, represents a one-half wavelength displacement by the accelerometer, because light must travel to and from the vibrating surface. The beat cycles are counted by an electronic counter, as events per shaker cycle, to give a digital readout of the peak-to-peak vibratory displacement in wavelengths.

The photodiode output is also displayed on an oscilloscope for greater displacement resolution, by monitoring the complete and partial beat cycles traversed by the vibrating accelerometer (see Fig. 4). The partial beats occur when the shaker stroke reverses direction and, hence, reverses the light interference cycle. These complete and partial beat cycles (wavelengths) are then counted on the oscilloscope for peak-to-peak, accelerometer displacement.

PROTOTYPE CONSTRUCTION

A prototype system was constructed, as shown in Fig. 5. This construction is straight

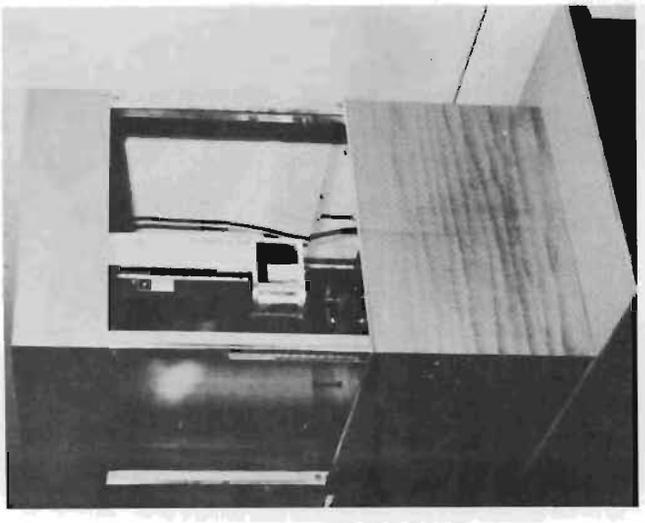

Fig. 5. Prototype accelerometer calibrator

forward, with the exception of the isolation mountings. To minimize the error caused by the extraneous movement between the laser photodiode section and the shaker section, the masses of the two sections were made equal, and were suspended on aircraft inner tubes of the same pressure (interconnected). This gave the same natural frequency (3 cps) to each section.

ERROR ANALYSIS

The various errors which occur in a sensitivity and frequency response calibration using the laser calibrator include:

1. Shaker cross motion error.
2. Shaker distortion error.
3. Accelerometer amplifier gain error.
4. Accelerometer voltmeter error.
5. Environmental effects error.

Present work includes an error analysis of the Laser accelerometer calibration system.

PLANNED FUTURE DEVELOPMENT

The present resolution of the laser calibrator is approximately one-tenth wavelength for displacement greater than one-half wavelength. Current efforts include achieving measurements of vibratory displacements with a resolution of one-hundreth wavelength. Attempts to measure subwavelength displacements are being directed toward measuring nulls as predicted by the Bessel functions. Minor consideration is also being given to measuring the subwavelength signal phase, or phase modulation, over several cycles, as an indication of the vibratory displacement.

ACKNOWLEDGMENTS

The author wishes to acknowledge the valuable contributions and efforts of the co-designers, R. J. Jordan and R. N. Phillips, in the successful development of the laser accelerometer calibrator.

* * *

UNPUBLISHED ACCELEROMETER CHARACTERISTICS

Boris Mangolds
Astro-Electronics Division
Radio Corporation of America
Princeton, New Jersey

Accelerometer sensitivity to non-vibratory environments other than those generally known was evident during a study conducted by the Astro-Electronics Division (AED) of RCA to investigate vibration data errors. The major areas of concern were determined to be base-strain sensitivity and temperature-transient sensitivity. Studies were initiated to establish the extent of vibration-data error caused by these inherent accelerometer characteristics. This paper describes the test methods used during these studies, the results obtained, and the conclusions and recommendations drawn from the results.

INTRODUCTION

During a study conducted by the Astro-Electronics Division (AED) of RCA to investigate vibration data errors resulting from application factors introduced by accelerometer handling and mounting (1), it was noticed that some transducers showed evidence of sensitivity to non-vibratory environments other than those generally known (other than, e.g., torque, cable loading, crossmotion, etc.).

Preliminary tests established of the unpublished accelerometer characteristics base-strain sensitivity and temperature-transient sensitivity seemed to be the most deleterious to AED data integrity. The primary purpose of this paper is to illustrate the importance and magnitude of these properties.

In a follow-up effort, all accelerometers in stock at AED and some interesting new models were surveyed for these influences with the following objectives:

1. Compiling a graded list as a function of the magnitude of these characteristics, to aid in selecting an accelerometer model from stock for a specific test application.

2. Comparing the results obtained from such surveys with results obtained under actual test conditions, to arrive at a concept of their practical importance.

Since the studies were conducted only for AED needs, and the results apply only to accelerometers in AED stock, or those made available to AED by the vendors specifically for the purpose of these surveys, the position of a particular model on the graded list serves only to characterize a particular accelerometer, and is not presented for the purpose of disqualifying particular vendors in general.

In the comparisons shown in Figs. 3 and 10, where a serial number is given after a listed model, only one accelerometer was available for the survey. In all other cases, the quantity of units tested per model varies between three and thirty.

CHARGE AMPLIFIERS

Charge amplifiers, because of their capability to eliminate the shunting influence of cables, are now being highly recommended as a means to conserve signal strength. However, with their advantages highly publicized, the facts are often forgotton that the accelerometer stock one has accumulated over the years of voltage-amplifier reign probably consists only of "voltage accelerometers." The ideal thing to do now would be to change to charge accelerometers, but the change-over to the new amplifier system is expensive, and one cannot normally afford to discard his old accelerometer stock, particularly when there are no direct replacements available for the subminiature models (where the use of a charge amplifier is most justified).

Therefore, the troublesome question arises, "Are there any new detrimental effects possible due to a combination of voltage accelerometers and charge amplifiers, a combination created by practical needs?"

Fig. 1. Instrumentation used for base strain sensitivity measurements

BASE-STRAIN SENSITIVITY

When the mounting surface of an accelerometer is forced to follow the bending of an object on which it is mounted, certain accelerometer models produce signals proportional to the bending stress, even if there are no vibrations in the direction of the sensitive axis of the transducer.

The survey reveals two important facts:

1. Some accelerometers produce additional, unbelievably high, output signals as a direct result of base-strain sensitivity.

2. There is a wide difference in these outputs among the individual accelerometer models for the same environmental test condition.

The test method used at AED for this survey was adopted from the ISA Standard RP37.2, para. 6.6. A steel beam (as shown in Fig. 1), 5 ft long, 3 in. wide, and 0.5 in. thick, was clamped at one end, so that the free length was 57 in. The natural frequency of the steel beam was approximately 5 cps. Four strain gages were bonded to the beam adjacent to the accelerometer mounting area (two each, top and bottom, about 1.5 in. from the edge of the clamp), and their output was fed through strain-gage conditioning equipment to one channel (the reference channel) of a two-channel Brush recorder. The output of the accelerometer under test was standardized in an Unholtz-Dickie Dial-A-Gain amplifier, and recorded on the second channel of the recorder which was calibrated directly on g(pk).

The free end of the cantilevered beam was manually deflected, and then allowed to vibrate freely. The recorder showed the output of the accelerometer adjacent to a slowly decaying strain reference trace. The outputs of different accelerometer models in g(pk), at the instant when the strain in the surface of the beam was 250×10^{-6} in./in., were used to compare their sensitivity to such stresses.

Under these conditions, the radius of curvature of the beam is 1000 in., and the displacement at the accelerometer mounting is approximately 0.001 in., which at 5 cps is equivalent to 0.003 g. This value should be subtracted from the recorder reading, but since it is so small in comparison to the output due to strain, it can be neglected for most accelerometers. A typical record of accelerometer output versus base strain is shown in Fig. 2. The results of the survey are shown in Fig. 3.

Fig. 2. Typical record of accelerometer output vs base strain

From a practical point of view, the exact output of a highly strain-sensitive accelerometer is immaterial, if there are other models available which, under the same test conditions, show practically no strain sensitivity. Fortunately, progress and competition have provided us with a wide choice; however, the existence of such a property, and particularly its magnitude, can not be ignored if accurate vibration data are desired.

Apparently, this property has been known to exist for quite some time. For example, Paragraph 3.1.3.7 of ASA Z24.21, "American Standard Method for Specifying the Characteristics of Pickups for Shock and Vibration Measurements" (1957), states, "Where applicable, the error in the pickup due to bending of the pickup case should be given." This document also suggests the beam method for obtaining the data. That was the case in 1957. A survey of the data sheets for accelerometers in use today shows no values at all regarding strain sensitivity, with the exception of those provided by Wilcoxon Research.

The detection of strain sensitivity in a "well-run" calibration laboratory is not very likely, unless one is alerted to its existence. To "run a laboratory well" means, unfortunately, to purposely create a gap between the practical conditions of an average vibration test in the environmental facility and the "pure" atmosphere of a calibration service. It means that precautions have been taken to avoid, among other things, surface deformations of the calibrating surface. Alerting test engineers to the importance of these surface strains is one of the main purposes of this paper; a wider distribution of ISA Standard RP37.2 should accomplish the same effect.

Is this property "applicable?" A practical example will illustrate best the practical magnitude of possible interference.

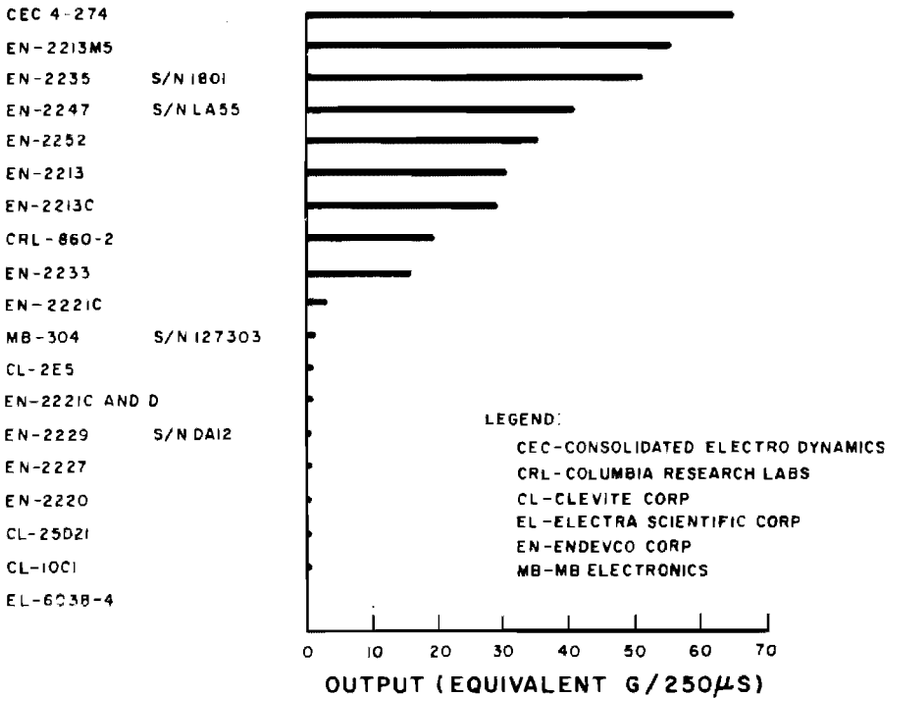

Fig. 3. Survey of accelerometer base-strain sensitivity

Figure 4(a) shows an accelerometer mounted directly on a calibration shaker (Unholtz-Dickie Mod. 106) and Fig. 4(b) the same accelerometer remounted on a simulated fixture on the same shaker. The simulated fixture is an aluminum disc, 3 in. in diameter and 0.5 in. thick, attached to the shaker with four bolts.

Figure 5 shows the frequency response curve (a), plotted for the directly mounted accelerometer, or, "pure" condition. Figure 5 also shows the response curve (b), plotted for the disc-mounted accelerometer. In both cases, the same accelerometer was used. We see that instead of the expected rolloff at lower frequencies, we have an increased output; for example, the difference at 8 cps is +20 percent. It seems that a value for the base-strain sensitivity in the data sheet of this accelerometer is certainly called for. Figure 5 (c) and (d) curves, shows the "pure" and "strained" results, taken under the same conditions as the results shown in the (a) and (b) curves, for another accelerometer. We see that at the low frequencies, it makes practically no difference whether this accelerometer is mounted on the disc, or directly on the shaker.

What can be done, short of discarding such sensitive accelerometers, especially if one has inherited a good supply?

Since the base surface of an accelerometer must follow the flexing of the test surface, in order to produce an output, the severity of interference increases with tighter coupling. The effect of decoupling was investigated by performing beam-method tests in which the following mounting techniques were used, each representing actual practices:

1. A non-insulated stud, Endevco Mod. 2981, dry.

2. A non-insulated stud, Endevco Mod. 2981, with an oil film.

3. An insulated stud, Endevco Mod. 2980M4.

4. An insulated stud, Endevco Mod. 2986B.

5. A non-insulated cementable stud, Endevco Mod. 2988.

6. Cementing directly with Locktite 404.

7. Cementing with a 1-mil fiberglass layer.

8. Cementing on an 0.5-in. aluminum cube (representing triax mounting).

The results are shown in Fig. 6

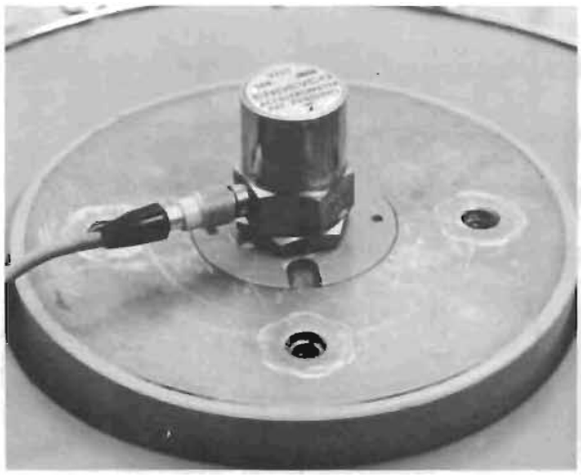

Fig. 4(a). Mounting used to obtain comparative response curves with base-strain interference (no stress)

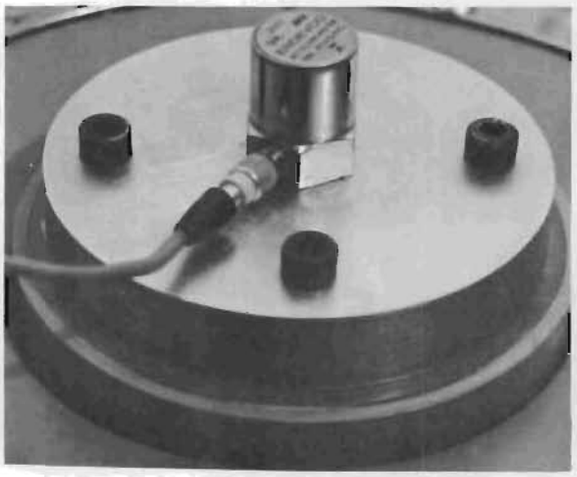

Fig. 4(b). Mounting used to obtain comparative response curves with base-strain interference (stressed)

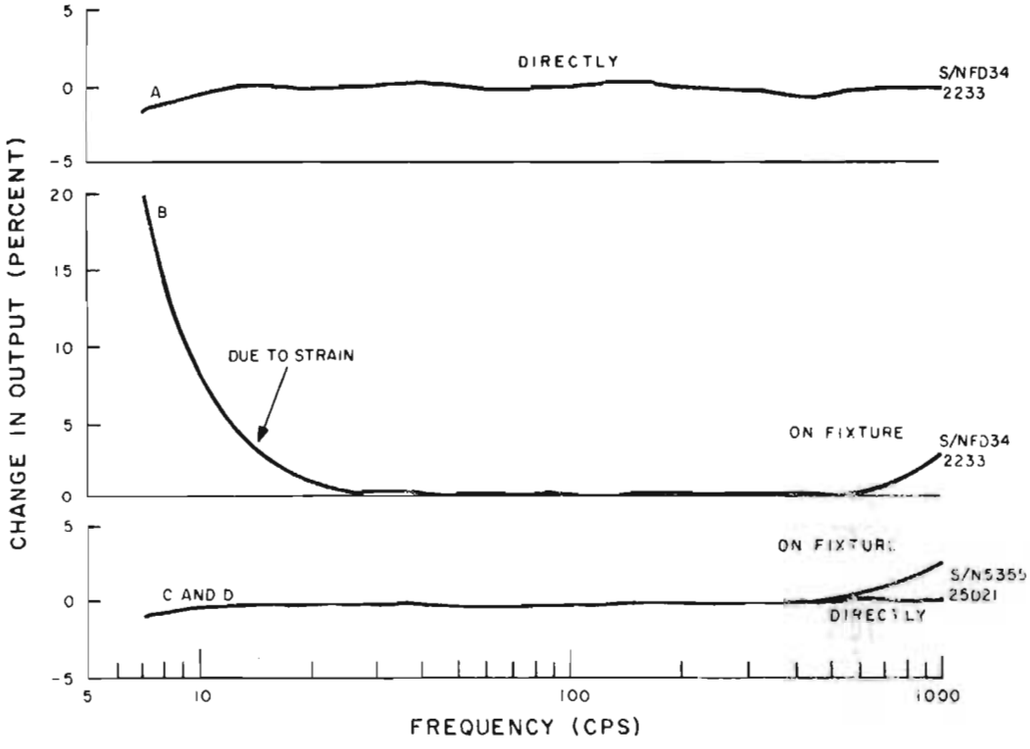

Fig. 5. Changes in accelerometer output due to bending mounting surfaces

Obviously, the worst conditions are the directly-cemented and directly-bolted ones, which seems rather logical. The results of the comparison suggest possible remedial steps, although the best solution would be to use accelerometers which simply are not strain sensitive, because most other solutions affect the frequency curve at the high-frequency end.

Figure 7 shows the three basic accelerometer construction methods: (a) compression, (b) bender, and (c) shear. As revealed in the

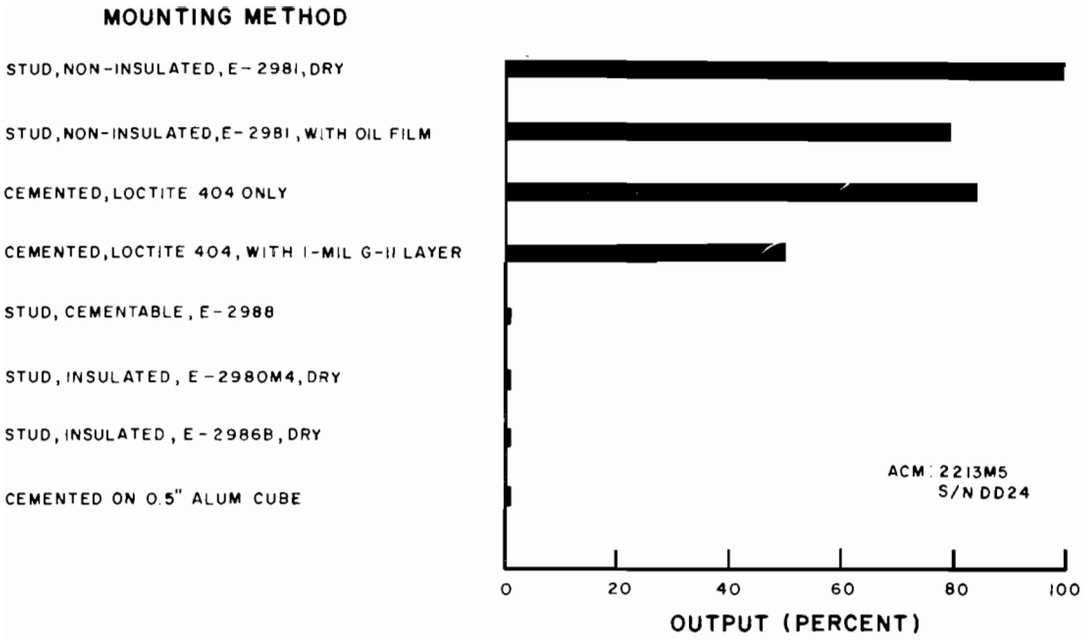

Fig. 6. Changes in base-strain output, for a given accelerometer, as the mounting method is changed

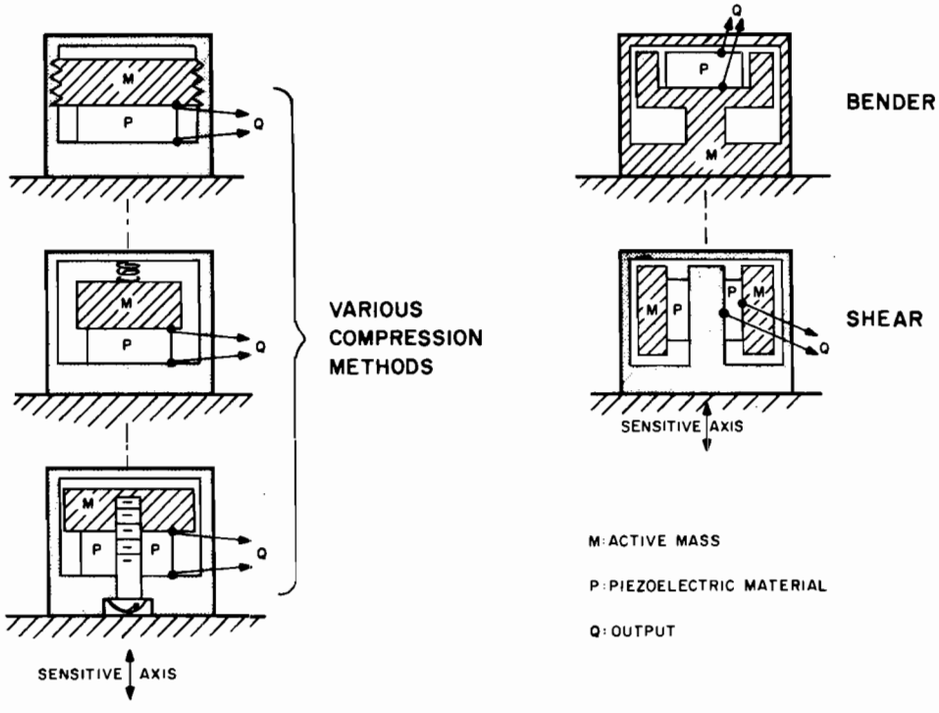

Fig. 7. Basic methods of accelerometer construction

illustrations, the active elements in both the compression and bender construction methods are more sensitive to bending stresses, while those in the shear construction method are least sensitive. Fig. 3, the graded list for accelerometer base-strain sensitivity, confirms these findings.

TEMPERATURE-TRANSIENT SENSITIVITY

Figure 8 illustrates, in a simplified manner, some basic relations between temperature and charge.

It is well known that the sensitivity of an accelerometer changes with ambient temperature. This might be due to a number of factors, such as changes in the piezo-electric sensitivity of the material, the increase of electrical conductivity, or the increase in dielectric constant which peaks at the Curie temperature, causing loss of polarization (or ferroelectric property), which, in turn, causes the accelerometer to cease operating as a piezoelectric device.

It is not as well known that the pyroelectricity of ferroelectrics (the generation of a charge attributed directly to temperature) can easily create potentials of several hundred volts, which are sufficient to change the polarization of some ferroelectrics, i.e., the sensitivity of the accelerometer. In addition, the dc shift created by the additional charge in the accelerometer can raise havoc with the associated instrumentation (such as driving amplifiers to saturation, and confusing filters and integrators, if the acceleration signal is being converted to velocity or displacement information).

The severity of interference of a pyroelectrically created charge depends on its magnitude, which, in turn, depends on the time constant of the cable and amplifier input circuitry. The practical significance of this is apparent in the precautions to be taken in certain cases, such as when testing for changes in accelerometer sensitivity, or capacitance, as a function of temperature; an accelerometer should not be left electrically unloaded while undergoing temperature changes in an environmental chamber.

Figure 8 also shows that heat can indirectly affect the output of an accelerometer, by causing mechanical stresses and displacements through the thermal expansion of accelerometer structural elements. This indirect influence can be comparable in magnitude to that of the

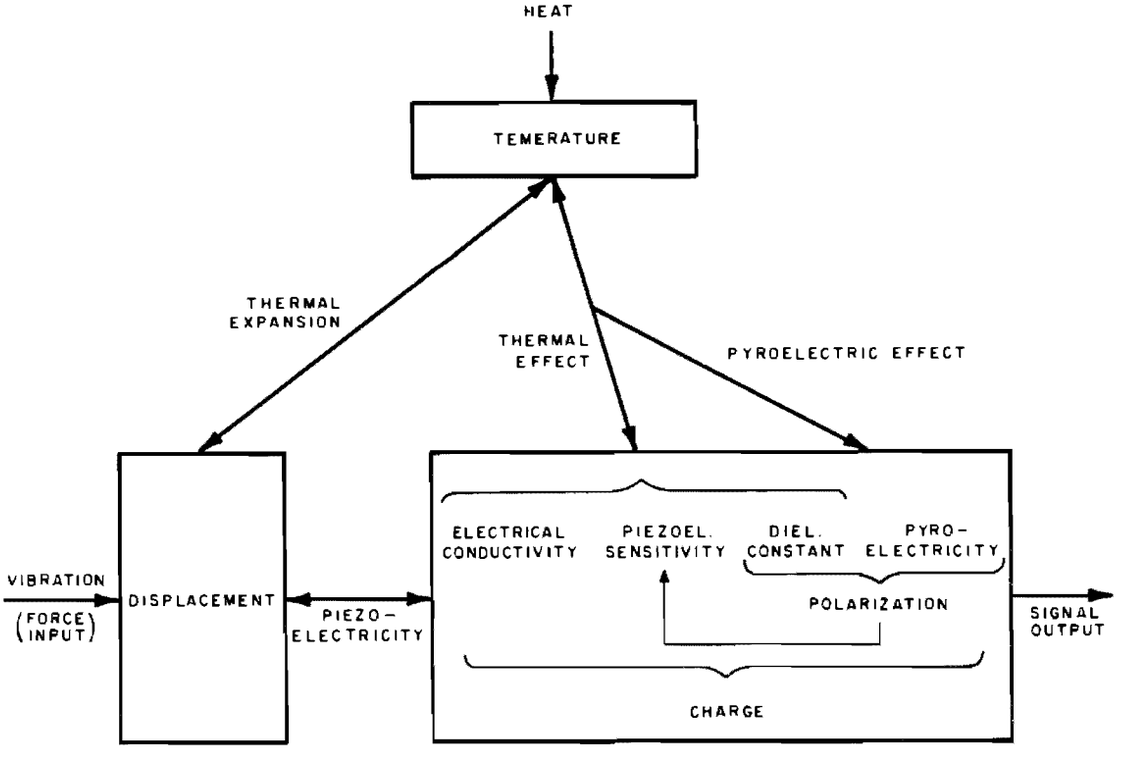

Fig. 8. Effect of temperature on accelerometer output

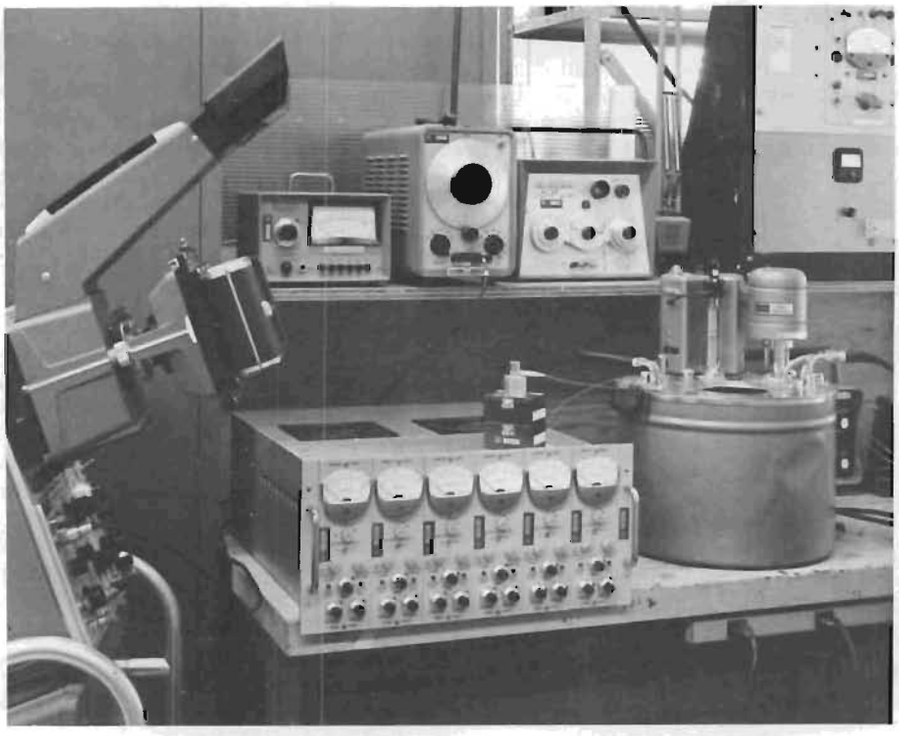

Fig. 9. Instrumentation used for measurements of accelerometer sensitivity to temperature transients

direct (pyroelectric) approach. The user is generally not interested in the individual heat effects on his particular accelerometer, but only in the total results. Therefore, all these variations are usually combined by the user into one neat term, and referred to simply as the "pyroelectric effect."

Manufacturer's data sheets provide no quantitative guidance (except for a recent data sheet by Clevite), in spite of ASA's wistful suggestion in 1957 that "where applicable, the transient response due to a sudden increase of 50° F in ambient temperature should be shown." when specifying the characteristics of pickups. No practical method was suggested. Here again, the preceding words "where applicable" might have left the door open.

In order to determine whether attention to a pyroelectric effect is of value or not, another survey was made. After consulting all standards available in this field, including the latest one still in the proposal stage (3rd draft of ASA S2-W-41, "Selection of Calibration Methods, Ranges and Limits ..." etc.), it was found that ISA was the only society recognizing the need for a uniform test method. Figure 9 shows the instrumentation recommended by Paragraph 6.8 of ISA Standard RP37.2.

The accelerometer under test was mounted on a 1-in. aluminum cube, and connected to a Dial-A-Gain amplifier (a voltage amplifier) with a 10-ft cable. This defines the time constant of the accelerometer load. The amplifier gain was readjusted for each model to produce the same output voltage per g, which was observed on an oscilloscope and photographed with a Polaroid camera. The transducer was quickly, but gently, immersed in water which was 50° F above room temperature, and the resultant peaks were converted to equivalent g(pk). A summary of the results obtained is shown in Fig. 10, where the models are listed in order of peak response.

Since the response is so high in some accelerometers, small variations in method, such as differences in speed of immersion, can be ignored. The response is also a definite function of temperature, and is not due to immersion shock. The magnitude of a possible shock or vibration component can be determined by immersing the same assembly in room temperature water. This becomes important, however, only with accelerometers which are almost insensitive to temperature transient, because a larger gain must be used to show anything at all.

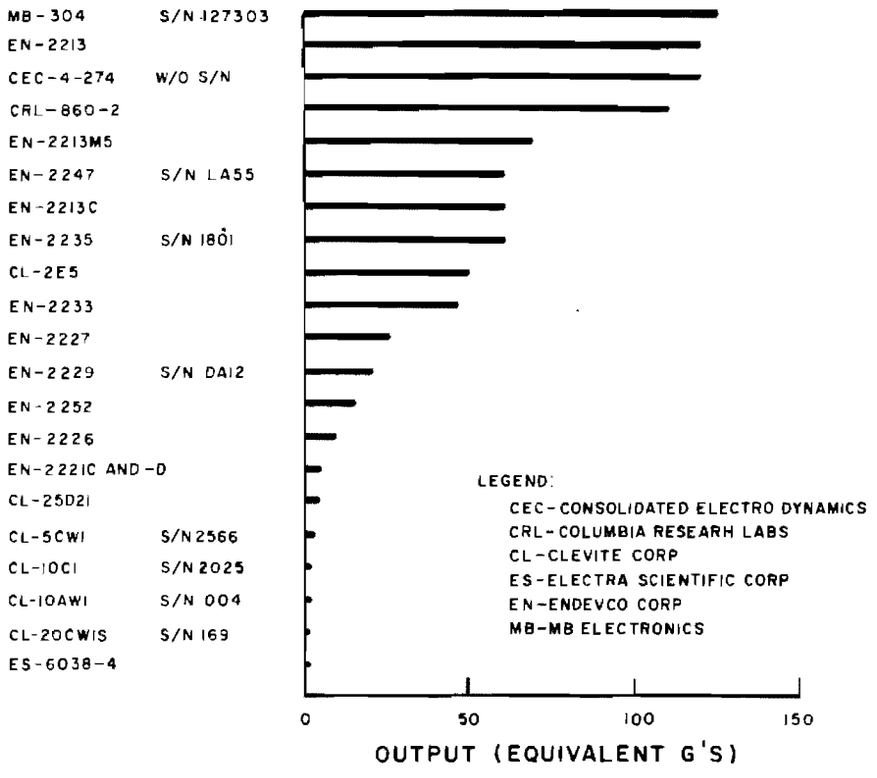

Fig. 10. Accelerometer sensitivity to temperature transients

From a practical point of view, it makes no difference whether the peak is 100 or 110 equivalent g's, if there are accelerometers with substantially lower response.

It seems unlikely that an accelerometer will experience any actual environmental testing which involves immersion in hot water. Therefore, to correlate these results with more practical conditions, some additional tests were made. For example, by use of the same instrumentation, and less bath, accelerometers from both extremes of the list shown in Fig. 10 were placed on a bench under ambient light conditions, and a 150-w light bulb was turned on at a distance of 4 ft. Figure 11 shows one of the results, which establishes a sufficient correlation between the initial graded listing for temperature transient sensitivity and the meaning of the words "where applicable."

Practically, the conditions which might cause interference in outputs from accelerometers sensitive to pyroelectric effect could be any sudden breeze (such as the opening of a door), the turning-on of lights, the sudden flow of temperature-control liquids in nearby lines, the breeze created by a drop during shock testing, etc.

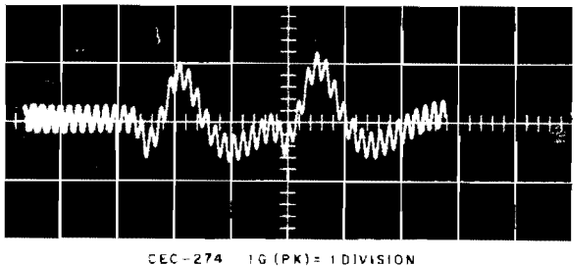

Fig. 11. Disturbance caused by Pyroelectric effect, superimposed on 1g(pk) vibration

The situation could be improved by thermally insulating the accelerometer, for example, wrapping it with masking tape, but this is not recommended. One could afford it only if the accelerometer is not case-sensitive. A surprising number are case-sensitive. Again, the best solution is to use a better model.

All previously described work was performed with voltage amplifiers. To determine whether there is a difference when regular voltage accelerometers are used with the new charge amplifiers, the pyroelectric tests were

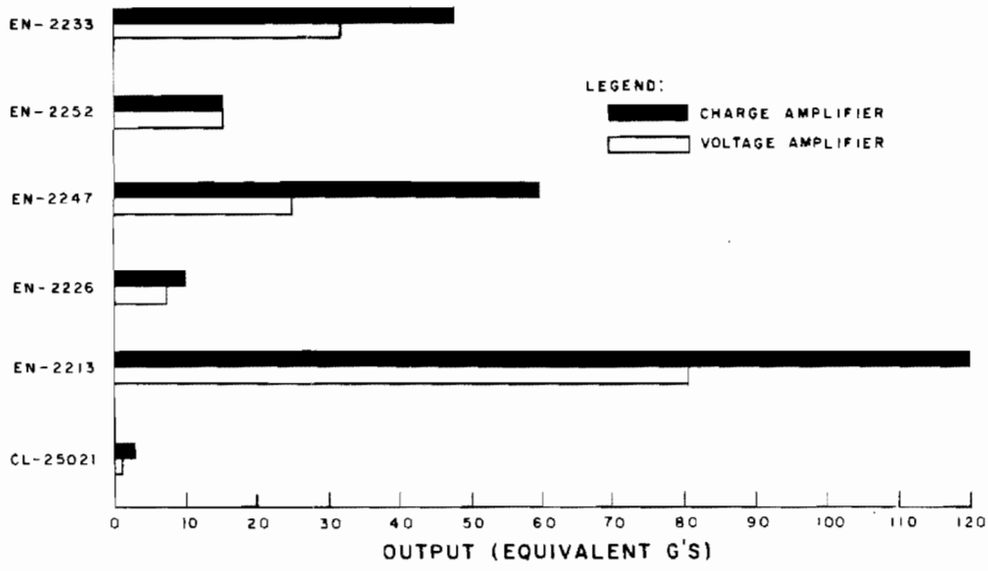

Fig. 12. Comparison of response to temperature transients (charge amplifiers vs voltage amplifiers)

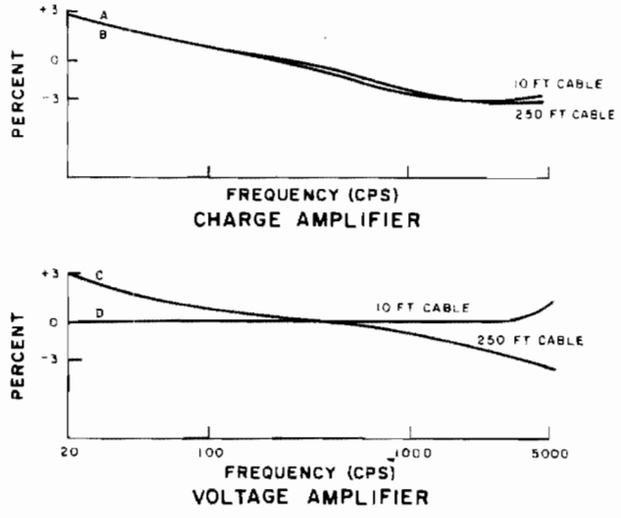

Fig. 13. Change in frequency-response slope (charge amplifier vs voltage amplifier)

repeated for some models. The results are shown in Fig. 12.

COMPATIBILITY

In conclusion, a word of caution is given concerning compatibility between charge amplifiers and voltage accelerometers. As shown in Fig. 13, the frequency-response curve of a Clevite 25D21 (a voltage accelerometer) was plotted under various load conditions at a fixed (room) temperature. Whether the accelerometer was connected to a charge amplifier with a 10-ft (300PF) cable (curve a), or a 250-ft (7500 Pf) cable (curve b), the results were practically the same, as expected. The accelerometer sensitivity, when compared at any given frequency, did not change, and, over the range of 20-5000 cps, both curves had a slope of +3 percent at 20 cps against -3 percent at 5 kc, when normalized at 200 cps. When a

voltage amplifier was substituted, the slope of the 250-ft cable frequency-response curve was very similar to the charge amplifier curves, but with a 10-ft cable (curve d) it was practically flat.

An accelerometer-amplifier combination using a voltage accelerometer with a charge amplifier thus produces a frequency-response curve which can have a slope different from that of a combination using the same voltage accelerometer with a voltage amplifier. The practical aspect of this is that, when forced to use such combinations, one should not simply derive an "equivalent" change-sensitivity value from the standard equation, $S_q = S_v \times C$, for the accelerometer from its voltage-sensitivity value. This approach is not necessarily applicable to the full frequency range, and is therefore not "equivalent." Instead, an actual calibration of each combination should be performed.

CONCLUSION AND RECOMMENDATION

The survey conducted at AED to study the effects of base-strain sensitivity and temperature transient sensitivity on accelerometer performance revealed the definite need for more data from the accelerometer suppliers. The user should not be penalized by being forced to procure transducers with insufficient data, or with characteristics unknown to him, only to discover later that he must conduct a program of evaluation to pinpoint these characteristics. This is not only time-consuming but costly and unjustifiable.

Therefore, it is recommended that the accelerometer suppliers, because of their unique qualifications, update their data sheets to include information concerning base-strain sensitivity, temperature-transient sensitivity, and any other properties heretofore unpublished which may be of considerable value to the accelerometer users.

REFERENCES

1. B. Mangolds "Effect of Mounting-Variables on Accelerometer Performance," Shock & Vibration Bulletin No. 33, Part III (Mar. 1964) p. 1
2. Guide for Specifications and Tests for Piezoelectric Acceleration Transducers for Aerospace Testing, ISA Recommended Practice RP37.2 (1964)
3. ASA Standard Z24.21, para 3.13.1

DISCUSSION

Mr. Zell (Picatinny Arsenal): What was the actual significance of the presentation in the last slide, showing the voltage sensitivity responses of a voltage accelerometer and of a charge accelerometer?

Mr. Mangolds: If you have a stock of voltage accelerometers, and use them with charge amplifiers, you must change your accelerometer voltage sensitivity figure, which is supposed to apply over the frequency that it was calibrated for, to an equivalent charge sensitivity figure. This is normally done with a simple equation; but what I wanted to show is that this does not apply to the full frequency range because there you have a change of slope.

Mr. Zell: Do you have any opinion as to the mechanism that is involved here?

Mr. Mangolds: In my opinion, it is just in the loading effect of the charge amplifier. The charge amplifier looks like a large capacitor to our voltage accelerometer.

Mr. Zell: Do you feel that if the actual measurement of capacitance were done in circuit, as a dynamic capacitance measurement, that the loading effect of the charge amplifier would apply?

Mr. Mangolds: I do not know. I have not tried it. It probably would help, but the best thing of course is to make a response curve with a charge amplifier when calibrating the accelerometer.

Mr. Zell: When you say a voltage accelerometer, do you mean a voltage accelerometer for which the sensitivity had been furnished in terms of voltage?

Mr. Mangolds: No. I mean a voltage accelerometer before it has been changed to compensate for temperature change, and by other tricks that the manufacturers do on it before they call them charge accelerometers. If you put a charge accelerometer with a charge amplifier, you will not have the slope. It will be straight.

Mr. Rhodes (Endevco Corp.): Regarding the frequency response one obtains when using accelerometers with either a voltage amplifier or a charge amplifier, it depends on whether or not q equals ce. This fundamental relationship still holds, but the data you showed relate to the fact that c, with certain piezoelectric materials, is not constant with frequency. As a result, we at the moment are reporting capacitance on our calibration data at frequencies of 50 hertz as well as 1000 hertz, and both were taken in the process of manufacture. The one impact of the matter of the frequency response is that, although with a charge amplifier there is a characteristic decrease in sensitivity with frequency until it picks up again due to the resonance frequency, it is the same for both short and long lengths of cable, whereas they are different with the voltage device as you showed. In the general area of thermal transients and base sensitivity, the net results of your very fine data is to show that shear accelerometers are far superior to compression accelerometers, in general, in these two areas. This, as well as other details concerning these effects, are covered in the paper that Dr. Bouche presented last April at the IES. The main reason that manufacturers did not adopt the ASA's suggestions of many years ago is that a good test method which all manufacturers and all buyers would use was not settled upon until the ISA document was released.

Mr. Mangolds: Thank you for that part where we are in agreement, but as far as the ASA is concerned, I would like to comment further. When we were looking for help in the selection of a method for pyroelectric tests we also considered an ASA document which is not published yet, but which has been circulated several times through industry for comments. It is not official yet but there was no mention of a method to test for pyroelectric effects. So it seems that if this document is going to be published, unless they have made a change recently, it will not contain a good method either. I do not say that I particularly like to dip accelerometers in hot water, but this was the best way that we could do it and be accepted by critical audiences such as we have here.

* * *

NEW PRECISION CALIBRATION TECHNIQUES FOR VIBRATION TRANSDUCERS

Walter P. Kistler
Kistler Instrument Corporation
Clarence, New York

Vibration calibration has not kept pace with the calibration advances of other instrumentation. This condition is due to both the limitations of most commercial accelerometers and to the difficulty in producing an exact vibration input to a vibration transducer for calibration comparison. New techniques (which have been developed and tested over a period of years) are offered to advance the state-of-the art of vibration calibration. Rather than basing an accelerometer calibration on a vibration input, a high precision static method is used—similar to the calibration method used for pressure gages. The calibration value obtained is transferred to a quartz accelerometer. This transfer standard has its sensing element inverted under its top surface. Its element connects directly to the element of any commercial accelerometer. The reference accelerometer is vibrated; the outputs of both instruments are compared, thus, calibrating the unknown accelerometer. The vibration is used only as a means of generating a signal--it need not be purely sinusoidal nor need its amplitude or frequency be precisely known. Results of this method correlate closely with those obtained from the Static Loading Method, Impact-Force Shock Calibration and Servo Accelerometer Calibration.

Vibration measurement, under the impetus of environmental testing, has gained great significance within the past ten years. Unfortunately, the development in depth of this art has not kept pace with its general expansion. This seems to be a perplexing statement in the light of the fact that most large companies have standards labs able to calibrate instruments like precision pressure gages, digital voltmeters, etc., to a precision of several digits. Yet, vibration measurements can be made with an accuracy of only a few percent. Even standard vibration pickups, used as the final reference and carefully calibrated by NBS, are only guaranteed to ± one percent.

The 'reason' and the 'remedy' for the condition described in the preceding, are the subjects of this paper.

The instruments most generally used for vibration measurement are piezo-electric accelerometers which offer the advantage of good high frequency response, small size and reasonable price. However, these instruments have the disadvantage of limited frequency range in their operation; they are only usable from 10 cycles to 10 kc. Furthermore, they do not respond to a static effect like a steady state acceleration—which explains why the more complex form of acceleration effect, a vibration, has to be used for their calibration. But vibratory motion is difficult to accurately define because it depends not only on frequency and amplitude but also upon possible distortion of the wave shape by cross-acceleration, etc.

Current calibration methods subject the transducer to a vibration of a certain amplitude and frequency (usually produced by a shake table). The amplitude and frequency are measured as accurately as practicable, and the peak acceleration is computed from the basic relationship:

$$a = \omega^2 A .$$

From the peak acceleration, other values like rms or average acceleration can, of course, be readily computed—always assuming perfect sinusoidal motion. These values are then compared with the peak, rms or average electric signal generated by the transducer, thus determining its calibration value.

For people experienced in this art it is readily evident why such a method is limited to

an accuracy of one or two percent at the very best. At low frequencies it is nearly impossible to obtain pure sinusoidal motion. At higher frequencies displacements become very small, of the order of a few thousandths of an inch, requiring displacement measurements down to microinches in order to get better than one percent accuracy for this value alone. Many further sources of error plague this procedure, such as spurious signals resulting from bending of the mounting base (which induces stresses in the instrument) and cross accelerations which may generate sizeable signals. In addition, vibrations of cable and connector can generate appreciable noise signal.

It is felt that the techniques described in this paper will advance the state-of-the-art of accelerometer calibration. These techniques, developed and thoroughly tested over a period of years, can be summarized as follows:

Rather than basing the accelerometer calibration on a vibration input (which is difficult to generate in pure form and even more difficult to measure accurately), a high precision static method is used—similar to the calibration method used for a pressure gage, voltmeter or any type of dc instrument. The calibration value is then transferred from this "Reference Standard" over a "Transfer Standard" onto the instrument being calibrated. To effect this transfer, two instruments are subjected to the same vibration and their outputs are compared. The vibration is only used as a means of generating a signal; it need not be purely sinusoidal nor need its amplitude or frequency be precisely known.

The first of these "static" techniques is the Static Loading Method. This approach uses a quartz accelerometer featuring near-dc response. Quartz has the advantage of high stability, very low thermal sensitivity, near perfect linearity and high frequency response. Because of its high electrical insulation and the absence of any pyroelectric effect, quartz transducers can be used for short-term static measurements. Time constants of the order of several days can be easily attained.

The accelerometer element, attached to its base but without its housing, is mounted on the test fixture as shown in Fig. 1 (a cross-section of an assembled unit is shown in Fig. 2). Certified weights are placed on the platform—applying a well defined force while eliminating lateral motion. The element, coupled to a charge amplifier adjusted to a unity transfer characteristic, yields a signal proportional to the applied force. When the applied force is

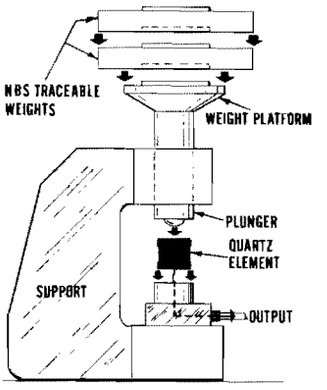

Fig. 1. Static loading calibration

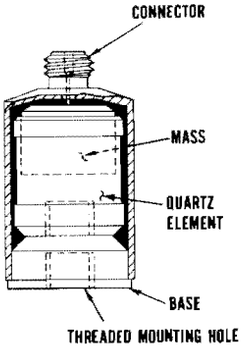

Fig. 2. Quartz accelerometer

divided by the seismic mass of the accelerometer (determined on an analytical balance before assembly), the equivalent static acceleration is computed in g's.

Weights can easily be applied to produce equivalent acceleration-levels to several thousand g's. This calibration can be repeated many times (applying weights in different sequences) to achieve a good indication of linearity, repeatability, resolution, aging, temperature effects, and so forth. An acceptable instrument will show a resolution and repeatability of well within 0.1 percent. Linearity values will, in general, lie between 0.1 percent and 0.5 percent.

The static loading method provides excellent data on the accelerometer's performance: especially its linearity and response to high g-levels. However, it is not recommended for absolute calibration. The application of weights on the seismic mass induces stresses which are not identical to those experienced when the accelerometer is subjected to actual acceleration. These different stresses may result in a very slight change in the response of the sensing

element. Nevertheless, this method is still capable of yielding absolute calibration values better than 1 percent.

The second new technique, Impact-Force Shock Calibration, involves two complete and separate systems (Fig. 3). An accelerometer riding a falling carriage impacts against a force transducer target (statically calibrated with NBS traceable weights). The sensitivity of the force transducer divided by the total weight of the objects impacting against it is "dialed" on its associated charge amplifier. Thus, the reading on its associated peak indicator is a measure of the peak deceleration experienced by the accelerometer and carriage (force divided by mass equals g's of acceleration). Under repeated shocks, the amplitude of the acceleration signal is adjusted until it equals the force/mass signal amplitude. Finally, the

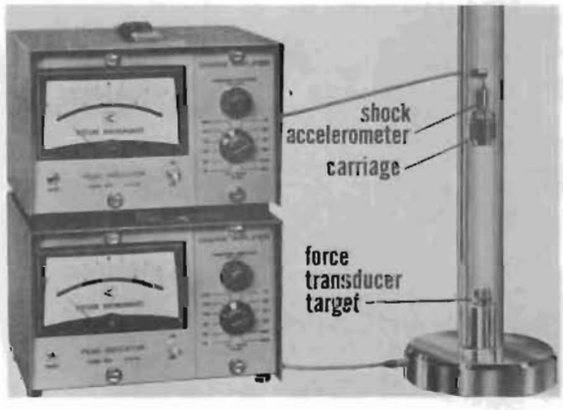

Fig. 3. Impact-force shock calibrator

accelerometer sensitivity appears on the precision dial of its associated charge amplifier.

The application of certified weights to the target transducer produces a charge output which in turn permits static calibration. Overall calibration accuracy of such a unit is between 0.5 and 1 percent—with consideration given to possible errors from side mounting, mounting distortion, etc.

Although the Impact-Force Method furnishes an absolute calibration of only one or two percent (at present), it provides valuable performance data on linearity and repeatability under shock conditions. (The use of a dual-trace storage oscilloscope verifies the moment-to-moment coincidence of the acceleration and force/mass signals—see Fig. 4). Moreover, dynamic, high g-level calibration is easily accomplished with this technique.

The last, and most precise technique, involves vibration comparison with a statically calibrated, force-balance servo accelerometer.

High precision servo accelerometers have been used for many years in inertial guidance systems and in other applications requiring the utmost in performance. These instruments are usually calibrated on a precision optical tilt table with a resolution of the order of one second of arc. Calibration is effected by direct reference to earth's gravitational field, thus making the instrument a primary standard. Stability and resolution of a good servo accelerometer are of the order of several micro-g's (or, better than one part in a hundred thousand). Linearity is normally better than 0.01 percent.

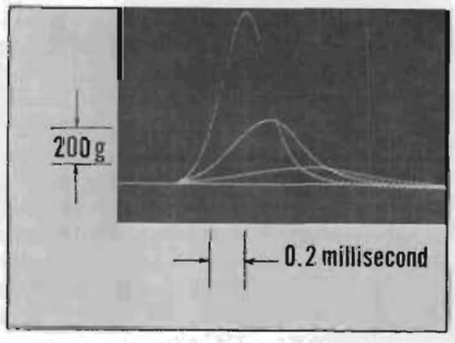

Fig. 4. Acceleration and force/mass oscilloscope traces superimposed at different g-levels

Such an instrument would therefore seem to be the ideal primary acceleration standard. Servo accelerometers, however, have not been utilized for accelerometer calibration in the past for the following reason: a normal servo accelerometer is merely a low frequency, dc type instrument with a frequency response flat to only a few cycles per second. This is well below the operating range of a standard ceramic accelerometer.

Two recent developments have now changed this picture completely. The first is the advent of miniature, rugged, high frequency servo accelerometers with resonant frequencies of several thousand cycles. The frequency response of such units can be made flat well within 1 percent up to 100 cps or more. At 10 cps the deviation from true static response is 0.1 percent.

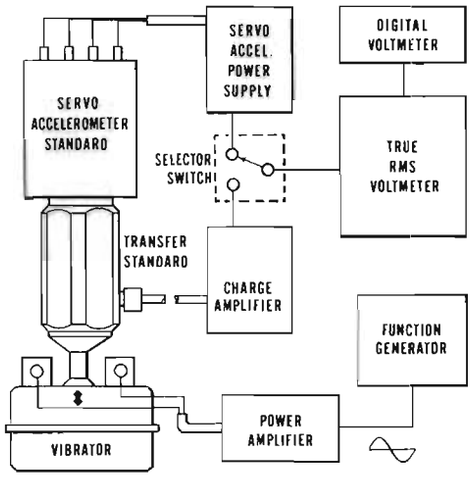

Fig. 5. Calibration of transfer standard via servo accelerometer

The second important development in vibration calibration is the use of quartz accelerometers as transfer standards. Since the frequency response of a quartz instrument is flat down to practically dc, there is a wide overlap in the frequency response of the two units so that they can be compared easily. Figure 5 shows a typical arrangement for calibration transfer from the primary standard servo accelerometer to the test unit. It uses any commercial shake table to which the transfer standard is rigidly mounted. In order to be able to exploit the range below about 10 or 20 cps, however, a special, large amplitude, low frequency shake table has to be used.

Vibration comparison of the quartz accelerometer with the servo accelerometer yields an absolute calibration value that is good to about 0.1 percent. The principal limitation of this method is the nature of the servo accelerometer: comparison is limited to relatively low amplitudes and low frequencies. Outside the ranges of from 0 to 20 g's and from 0 to 50 cps, frequency and amplitude errors from the servo accelerometer begin to be noticeable.

Fig. 6. Precision back-to-back vibration calibrator

The application of the techniques described thus far yields an accelerometer reference standard. The Static Loading Method gives an equivalent high g-level calibration, but at zero cycles per second. The Impact-Force Method gives relatively high g-level calibration for equivalent frequencies of about one thousand cps (equivalent frequencies of about 12,000 cps can be obtained with special techniques). Finally, the servo accelerometer provides an especially precise calibration at low levels of frequency and amplitude.

The focal point now becomes the actual transfer of the calibration values obtained from the described static methods to the transfer standard and then to any commercial piezoelectric vibration transducer.

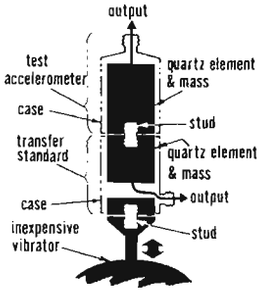

Fig. 7. Precision back-to-back calibration of piezoelectric accelerometers

A typical system for laboratory calibration is illustrated in Fig. 6. It consists of an inexpensive shake table to drive the quartz transfer standard and an electronics accessory box containing the associated charge amplifiers, ac meter and a selector switch. The transfer standard is a high quality quartz accelerometer selected for low transverse sensitivity. It consists of a sensing element (seismic mass plus quartz stack) inverted under the top end of a very sturdy cylindrical housing with heavy walls and heavy rugged end plates (Fig. 7). The sensing element is mounted on the upper end plate where the standard or test unit will be mounted so that close mechanical coupling is achieved.

One charge amplifier is permanently connected to the transfer standard. Except for the "on-off" switch, there are no controls on the panel because the amplifier characteristics have been carefully tailored and adjusted to fit the transfer unit used (they should not be

changed!). The output of the system is set to 10.00 mv/g over its entire useful amplitude and frequency range. The second charge amplifier features a range selector switch and a ten-turn calibration potentiometers with a three digit dial. The output of this unit is adjusted to match the signal from the transfer standard. The output of either charge amplifier can be connected to the ac meter by means of the selector switch.

The quartz transfer unit can now be calibrated in amplitude and frequency by use of the following procedure:

1. Amplitude Verification: The primary standard, a miniature servo accelerometer, is carefully mounted on top of the transfer standard (Fig. 5). Its output, which has been adjusted to 10.00 mv/g on a precision tilt table, is connected to the selector switch in place of the output of the second charge amplifier. A vibration of any suitable frequency and amplitude is applied. The outputs of primary standard and transfer standard are compared by alternately switching to the meter and comparing the readings, or by operating in a differential mode. The transfer charge amplifier is adjusted permanently after the difference between the outputs is reduced to zero. By mounting a statically calibrated quartz unit in place of the servo unit, the amplitude linearity of the transfer standard over any desired range can be checked (the range is limited only by the capability of the shaker). Linearity and stability should prove consistent within 0.1 percent over the entire amplitude range if a high quality unit is used as the transfer standard.

2. Frequency Response Verification: Because of the high stability and excellent resolution of the quartz standard, the aforementioned method allows precision adjustment of the transfer standard of the order of 0.1 percent. It can only be done, however, for rather low frequencies (10 to 50 cps). For higher frequencies, the resonance of the quartz accelerometer increases the signal output. At 10 kc, for instance, an overshoot error of about 6-1/4 percent must be expected. At one kc, however, this error is only one one hundredth of this value, and the accelerometer can be considered correct within its 0.1 percent specification.

There is no way of measuring the frequency deviation for higher frequencies. In order to check for any possible "bump" on the frequency curve, an accelerometer of different dimensions with substantially higher or lower resonant frequency is mounted on the transfer standard. The outputs of the two units over the complete frequency range are then carefully compared. Any minor resonance of either accelerometer will show up very conspicuously as a sudden deviation between the two outputs. Normally, a filter network designed and tested to compensate for the frequency deviation of the transfer standard is incorporated into its associated charge amplifier, thus limiting frequency deviation to approximately 1 percent over the entire range—up to 10 kc.

Having calibrated the transfer standard, routine calibration proceeds like the standard back to back technique. The test accelerometer is mounted on top of the transfer standard or working unit (as shown in Fig. 6). Its output is connected to the second charge amplifier and the vibrator is activated. By turning the calibrate dial, the two outputs can easily be made equal or their difference reduced to zero as indicated on the ac meter. The calibration factor of the unknown accelerometer unit can now be read in absolute units, picocoulombs/g.

It is not easy to give a good estimate of the combined error band for the techniques described. The major sources of error derive from: the quality of the accelerometers used, their stability, linearity and hysteresis, the side sensitivity, and the strain sensitivity. Accuracy will also depend on the noise quality of the cable used, on the tightness of the connector, and upon the method used to suspend the cables from the vibrating accelerometers. Also, failure to lap mating accelerometer surfaces (then applying a thin film of silicone grease) and to apply the recommended mounting torque will degrade calibration accuracy.

The collective experience of the Kistler Instrument Corporation indicates that a careful operator, calibrating a high quality quartz accelerometer, using the best cables available today, and applying great care in mounting the accelerometer and in running the cable, can achieve consistent and repeated calibration in the order

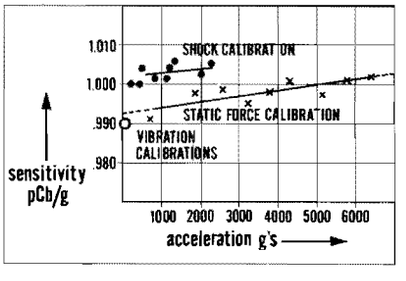

Fig. 8. Calibration correlation

of 0.1 percent with the technique described. Under such conditions, the absolute value obtained for the accelerometer sensitivity should be well within 1 percent in the lower and medium frequency range to, perhaps, 2,000 cps.

Under ideal laboratory conditions, the Impact-Force, Static Loading and combined vibration calibration techniques have been applied to a single unit providing a correlation deviation of less than 0.8 percent. Figure 8 graphically illustrates the results. This remarkable correlation strengthens our confidence in the static techniques described in this paper and increases our desire to see a wider use of these techniques so as to be better able to evaluate their performance and capabilities.

* * *

OMNIDIRECTIONAL ACCELERATION SENSOR

A. J. Buschman, Jr.
Harry Diamond Laboratories
Washington, D. C.

An acceleration sensor that is independent of the direction of the acceleration vector has been developed for NASA for use in selection of a site for a manned lunar landing. This is accomplished by employing a tri-axial accelerometer and a computer whose output is the square root of the sum of the squares of three orthogonal, acceleration-time signatures. The circuitry operates from a 20-v power supply drawing 10 ma and has a dynamic range of 1000. The tri-axial accelerometer, computer, power supply, and telemetry can be packaged in a 3-in. diameter sphere.

INTRODUCTION

Accurate information on the surface structure of the earth's moon for use in designing lunar landing vehicles and site selection can be obtained by analyzing the acceleration-time (a-t) history of an impacting projectile. Comparison of a-t signatures with those obtained experimentally on known earth materials will provide valuable information. A controlled lunar impact would be complex and expensive; therefore, methods have been sought to obtain an omnidirectional acceleration sensor to be employed in a free-fall trajectory. Harry Diamond Laboratories (HDL), under Defense Purchase Request L-31,945 with the Langley Research Center of NASA, is developing the omnidirectional acceleration sensor.

References (1), (2), and (3) present several methods considered in detail as potential omnidirectional acceleration sensors capable of fulfilling the following requirements:

1. Shock: 40 to 40,000 g.

2. Frequency Response: Half sine pulse from 250-μs to 250-ms duration.

3. Accuracy: ±5 percent from 40 to 4000 g; ±10 percent from 4000 to 40,000 g.

4. Size: Complete package including sensor, power supply, and telemetry to be contained in a 3 in. sphere; 2 in. maximum for sensor.

5. Power Supply: 20 v, 10 ma for sensor.

This paper presents the more significant portions of the method that computes the square root of the sum of the squares (SRSS) of three orthogonal, unidirectional, accelerometer a-t signatures. In this way the instantaneous magnitude of the resultant is obtained, producing an acceleration sensor free of directional sensitivity. The design of the total circuitry employed and the data obtained are presented in Ref. (3).

COMPUTER SYSTEM

Figures 1 and 2 show block and schematic diagrams of the complete computer. The system is basically simple, and can be set up to perform satisfactorily in the laboratory with only the resistor computer portion, provided low impedance sources of sufficient amplitude are available to drive the computer. The system becomes more complex in this application due to both the nature of the triaxial accelerometer, which is a high impedance charge generator with bidirectional response, and the dynamic range of 1000, from 4 mv to 4 v.

The high impedance amplifier is a unity-gain impedance matching circuit, capable of driving the rectifier. The rectifier satisfies the resistor computer requirement that inputs be of like polarity over the range of 4 mv to 4 v. The emitter follower provides impedance matching to the peak follower. The output of the resistor computer consists of three signals, the largest of which is proportional to the SRSS, and must be selected from the others. This is

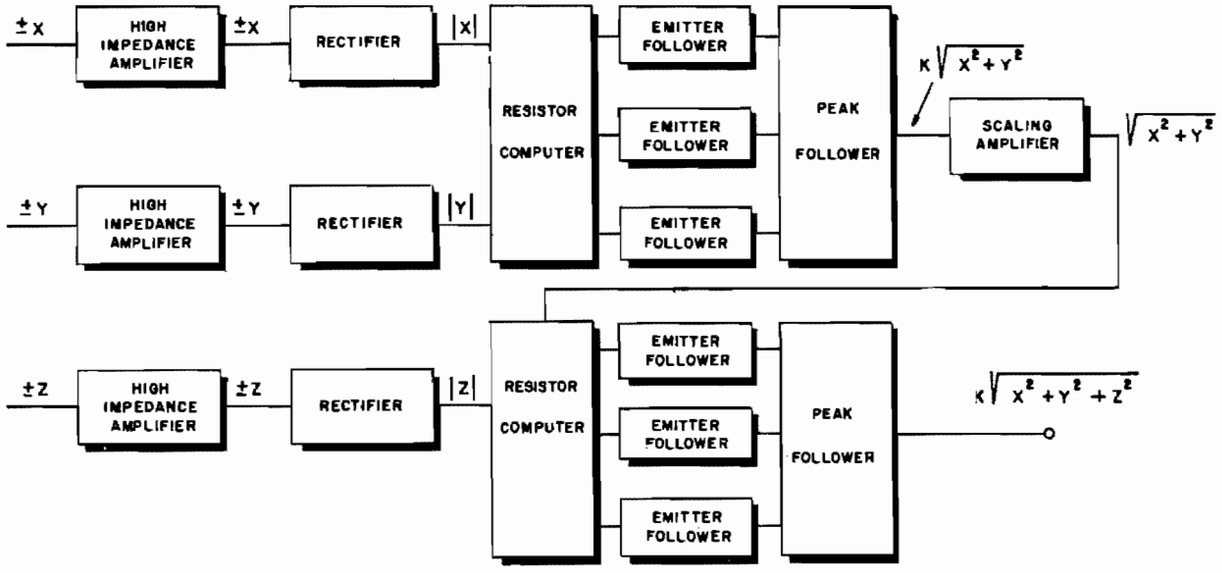

Fig. 1. Block diagram of SRSS computer system

accomplished by the peak follower down to 4 mv. The scaling amplifier has a gain capable of removing the proportionality constant introduced by the resistor computer, so that its output is the SRSS of two of the input a-t signatures. The process is repeated to obtain the resultant of the three a-t signatures.

Ryan (2) presents a resistor computer capable of obtaining the resultant of three inputs directly. This system, however, results in slightly lower accuracy for a given number of computer components.

RESISTOR COMPUTER

The heart of the SRSS computer, as presented in Fig. 1, is the resistor computer, which was first presented by Stern and Lerner (4) and extended by Ryan (2) to include three inputs. The resistor computer is a piecewise-linear passive network requiring no power supply, being driven by the input signals.

The square of the resultant of two orthogonal unknowns is

$$z^2 = x^2 + y^2 .$$

Geometrically, this is a right circular cone with its apex angle of 45 degrees at the origin. This cone can be approximated by an n-sided, inscribed pyramid. The desired accuracy can be obtained by increasing n to any reasonable value.

Consider the intersection of the cone and inscribed pyramid with the plane $z = a$. This is a circle with an inscribed regular polygon. Since the apex angle of the cone is 45 degrees, the radius of this circle is equal to the distance above the origin in the xy plane; $r = a$. For the present, consider only this circle and inscribed polygon with n sides. For the computer in this application, $n = 12$. To simplify the derivation, only the first quadrant will be considered. In this case there are three sides of the polygon, representing the first quadrant. These planes can be represented by

$$a_k = h_{xk} X + h_{yk} Y ; \qquad k = 1, 2, 3 .$$

The coefficients of X and Y necessary to represent the planes are derived by Ryan (2) and Stern and Lerner (4), and are shown to be

$$h_{xk} = \cos \frac{\pi}{n} (2k - 1) ,$$

$$h_{yk} = \sin \frac{\pi}{n} (2k - 1) .$$

Substituting into the expression for the planes yields

$$a_k = \cos \frac{\pi}{n} (2k - 1) X + \sin \frac{\pi}{n} (2k - 1) Y , \qquad k = 1, 2, 3 .$$

These linear relationships can be realized by simple resistor networks; the derivation is included by Ryan in Ref. (2).

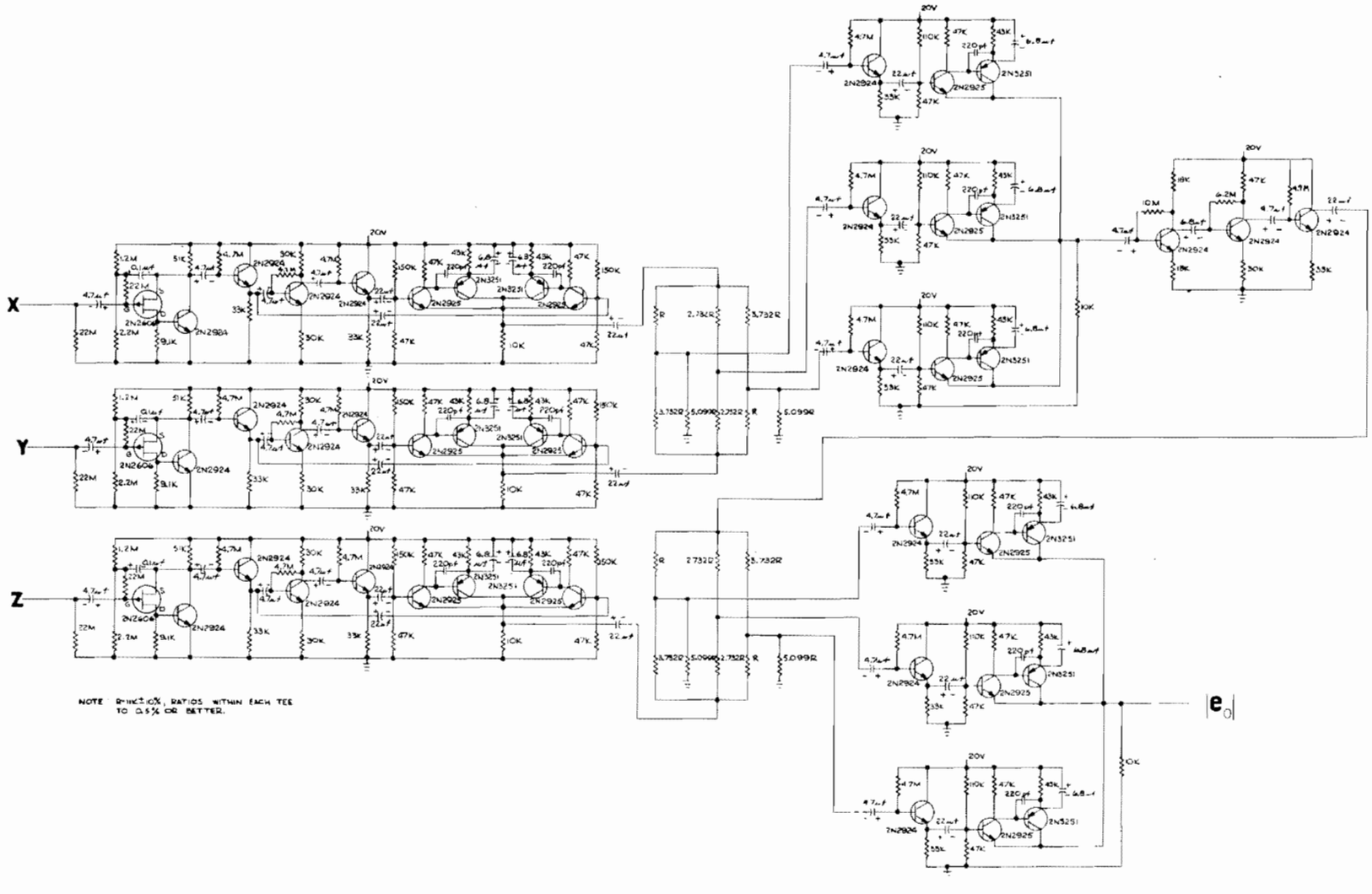

Fig. 2. Schematic diagram of SRSS computer system

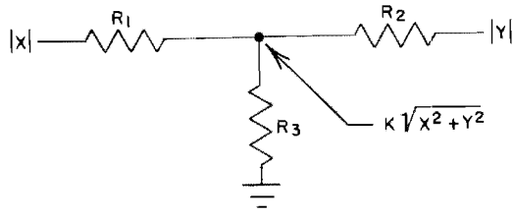

Fig. 3. Linear resistive network for two inputs

Figure 3 presents the resistor network capable of providing a_k at the junction of the three resistors, when the resistances are in the correct ratio determined by the coefficients of X and Y in the equation representating a_k. They are:

$$R_1 = \frac{\cos\frac{\pi}{n}}{\cos\frac{\pi}{n}(2k-1)}R,$$

$$R_2 = \frac{\cos\frac{\pi}{n}}{\sin\frac{\pi}{n}(2k-1)}R,$$

$$R_3 = \frac{\cos\frac{\pi}{n}}{\sqrt{2}-\cos\frac{\pi}{n}(2k-1)-\sin\frac{\pi}{n}(2k-1)}R.$$

The function of R_3 is to adjust the loss incurred through resistive network addition to a convenient value. In the network considered here, representing three planes in the first quadrant, this value is $2^{-1/2}$. The scaling amplifier employed has a gain of $2^{1/2}$, restoring the output to the correct value.

Since there are three planes representing the first quadrant, three networks in parallel are required, as shown in Fig. 4. The values of R_α, R_β, and R_γ are selected to present the desired input impedance required by the signal sources. There will be three outputs from this network, a_α, a_β, a_γ. It can be visualized geometrically that the plane containing the correct output will always be higher than the others, since the pyramid is inscribed in a concave upwards cone. Therefore, the correct output will be greater than the others. This can be verified readily by inserting values for X and Y into the equations presented in Fig. 3.

The correct output can be selected by diodes, when signal levels are high enough to allow for the diode losses. In the SRSS system, diodes are avoided in favor of the peak follower,

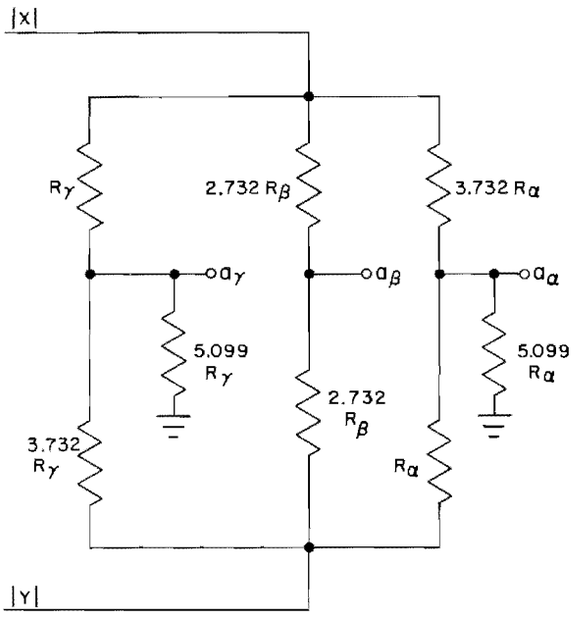

$a_\alpha = 1/\sqrt{2}\,(0.9659\,X + 0.2588\,Y)$
$a_\beta = 1/\sqrt{2}\,(0.7071\,X + 0.7071\,Y)$
$a_\gamma = 1/\sqrt{2}\,(0.2588\,X + 0.9659\,Y)$

Fig. 4. Resistor computer, schematic diagram

which is also employed in the low-level rectifier developed for this system.

LOW-LEVEL PULSE RECTIFIER

The output of the high input, low output impedance, unity-gain amplifier can be either positive or negative, depending on the orientation of the accelerometer upon impact. To supply the resistor computer with absolute values, a four-stage rectifier is employed. The first three states are conventional, consisting of an emitter follower, an inverter, and another emitter follower. In this way the signal is available in both polarities, regardless of the initial polarity. To accomplish the rectification, the positive value must be selected so that the presence of the negative value does not introduce errors. This is accomplished by a comparator circuit that selects the more positive input. This circuit has been extended to select the most positive of as many as four positive inputs.

Figure 5 presents the comparator circuit developed by Marcus, et al (3). The most significant portion of this circuit is the inclusion

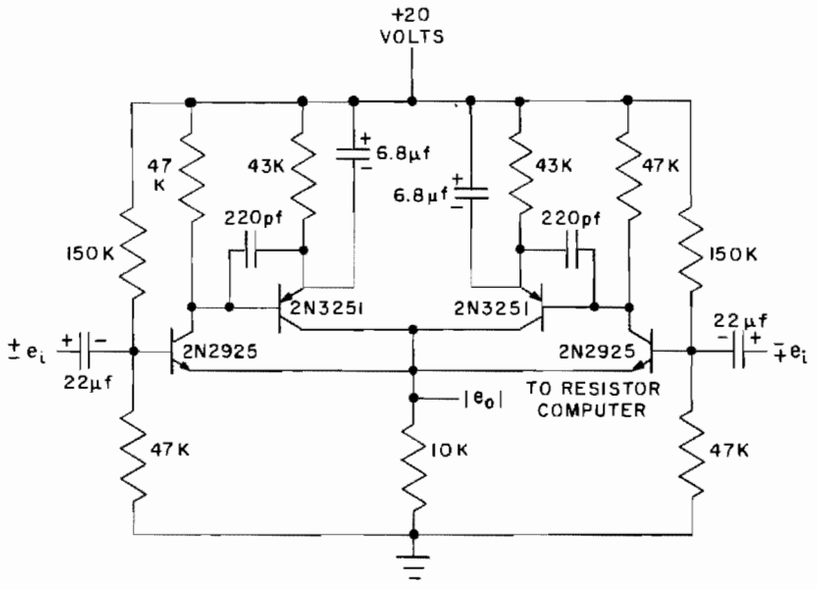

Fig. 5. Comparator, schematic diagram

of the two 2N3251 transistors. The circuit would function without errors down to approximately 40 mv without the 2N3251's. As the base current in the 2N2925 decreases below 1 μa, the base-emitter junction impedance increases rapidly. The base-emitter impedance is in series with the emitter resistor that develops the output of the circuit. Increasing base-emitter junction resistance has the effect of dividing the output between the junction impedance and the emitter resistor.

The 2N3251 serves as a current amplifier, supplementing the emitter current of the 2N2925. The collector resistor of the 2N2925 biases the 2N3251 to conduct. As current amplifiers with a beta of greater than 100, small collector current changes in the 2N2925 are compensated, keeping the quiescent base current of the 2N2925 constant during signal processing. The signal current is supplied by the 2N3251, so that the base-emitter voltage of the 2N2925 remains constant. This keeps the base-emitter junction impedance constant at a low value, compared with the 10-kohm emitter resistor for input signals down to 4 mv. The base-emitter junction impedance is kept at a low level by operating at a quiescent collector current of 100 μa. The operating point of the 2N3251 is stabilized by its emitter resistor, while current gain is increased by the bypass capacitor.

CONCLUSIONS

The resistor computer has the potential of attaining the following accuracy for a given number of resistor networks:

Network	Max deviation (%)
1	±25
2	±7.3
3	±3.4
4	±1.9
5	±1.2

Other sources of error are the frequency response of the system creating losses, which are frequency dependent and most critical at the low levels (250-ms pulse duration), and the cross axis sensitivity of the acceleration sensors. The system is currently being developed to reduce frequency dependent components by dc coupling where possible. Special accelerometers can reduce the cross axis sensitivity to a workable level. At present, component changes during shock appear to be the greatest source of spurious and erroneous signals. Components must be selected that are stable during high-energy shocks.

REFERENCES

1. A. J. Buschman, Jr., "Investigation of Four Methods of Obtaining an Omnidirectional Accelerometer—Phase I," HDL Rept. PR-65-1, February 1965

2. W. E. Ryan, "Some Methods of Approximating an Omnidirectional Accelerometer with Multiple Uniaxial Accelerometers," HDL Rept. TR-1243, May 1964

3. I. R. Marcus, J. W. Miller, Jr., and A. J. Buschman, Jr., "Circuit Realization of a Square Root Sum of Squares Computer," HDL Rept. TR-1271, January 1965

4. T. E. Stern, and R. M. Lerner, "A Circuit for the Square Root of the Sum of the Squares," Proceedings of IEEE, April 1963, Vol. 51, p. 593

* * *

EFFECTIVE USE OF ACCELEROMETERS AS CALIBRATION STANDARDS

D. R. Workman
Lockheed Missiles and Space Company
Sunnyvale, California

The paper covers in detail the methods used in obtaining maximum certainty with a conventional back-to-back calibration setup. Items discussed include: use and reduction of NBS calibration data and determination of best curve response; verification of calibration systems using electrical, resonance, and absolute determination tests; and typical calibration mounts with their associated errors. Calibration data will be shown with an analysis of the expected system certainty.

INTRODUCTION

In the field of shock and vibration measurement, the common technique for piezoelectric accelerometer calibration is the back-to-back comparison (Fig. 1). While the theory of this technique is well known, less is said regarding problems encountered in its use.

In application, ratio comparison has variables which, if uncorrected, will provide the user with erroneous data. If any degree of certainty is to be placed on measurements, the user must have a firm knowledge of system operation.

The standard used is another accelerometer system which must be calibrated by some technique to ensure its operating characteristics. While basic sensitivity is easily tested at low frequencies, overall response over the intended use range is more difficult to ascertain. Generally an accelerometer/amplifier system is periodically calibrated at the National Bureau of Standards (NBS) for this purpose. In order to use this information, techniques must be developed for valid transfers.

The calibration fixture presents its own problems. Not only does it introduce errors, but its configuration must be adaptable to all units. If adaptor blocks are used, additional uncertainties are introduced into the measurement. At the present time no universal fixture can be purchased which will test all of the configurations encountered.

These problems confront the facility which attempts to organize an effective calibration program. In most cases solutions are obtained only by research and application of trial and error technology.

This paper deals with the approach of the Primary Standards Laboratory (PSL) of Lockheed

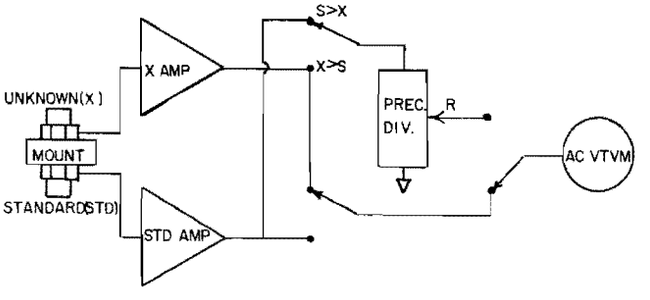

Fig. 1. Basic back-to-back calibration setup for accelerometers

Missiles & Space Co. (LMSC) to these problems and the techniques and fixtures which have evolved.

CALIBRATION REQUIREMENTS

At LMSC, approximately 1800 routine calibrations are performed each year. Due to this high workload, the only practical method for calibration is the back-to-back technique. While speed is important, the critical needs of the missile industry dictate the necessity for accuracy comparable to absolute determination methods.

Accelerometers are tested on a six-month recall basis with the following information supplied to the user:

1. Leakage resistance (megohms)

2. Capacitance (picofarads)

3. Sensitivity (Peak mv, rms, mv, Peak PCB/Peak g @ 5 peak g, 100 Hz)

4. Frequency response (% deviations 20 to 4000 Hz)

5. Dynamic linearity (% deviation 1-100 peak)

CALIBRATION SYSTEM

A picture of the PSL calibration system is shown in Fig. 2 with a block diagram in Fig. 3. From an operational standpoint, it is a conventional servo controlled vibration system with the exception of the Model G-100 Accelerometer Calibrator (2) which is a PSL design instrument.

PIEZOELECTRIC ACCELEROMETER STANDARDS

Four standard accelerometer systems are maintained to support the calibration function. The systems and their uses are:

1. Reference Standard (Ref. Std.). Endevco 2242C/2614. System periodically tested at NBS.

2. Comparison Standard (Comp. Std.). Kistler 808K2/561. Special calibration accelerometer.

3. Working Standard (Work Std.). Endevco 2242/2614. Unit installed in general purpose calibration fixture.

4. Auxilliary Standard (Aux. Std.). Endevco 2221C/2614. Adjustable standard for special tests.

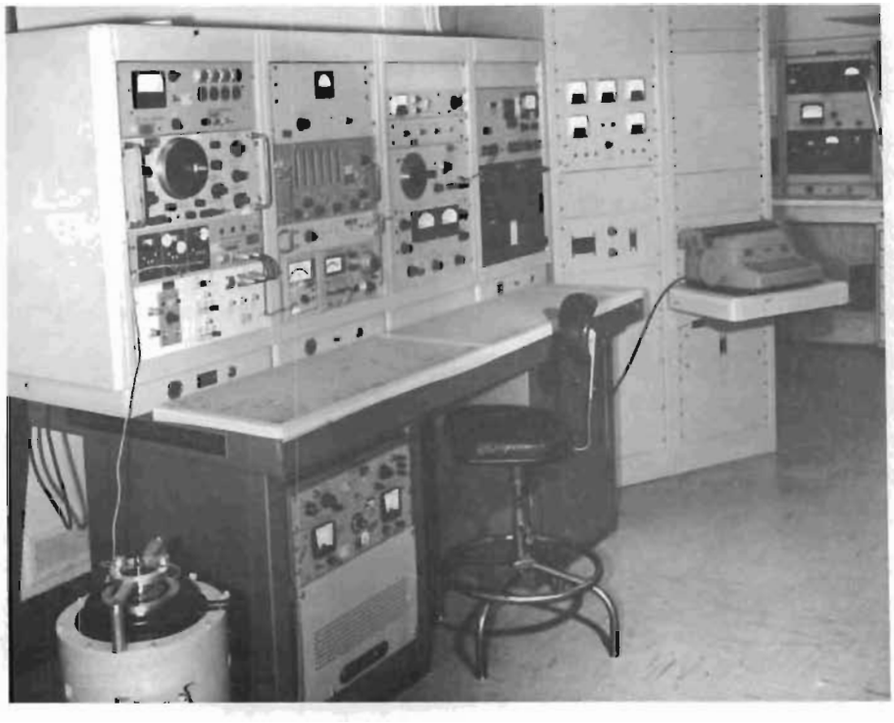

Fig. 2. PSL accelerometer calibration system

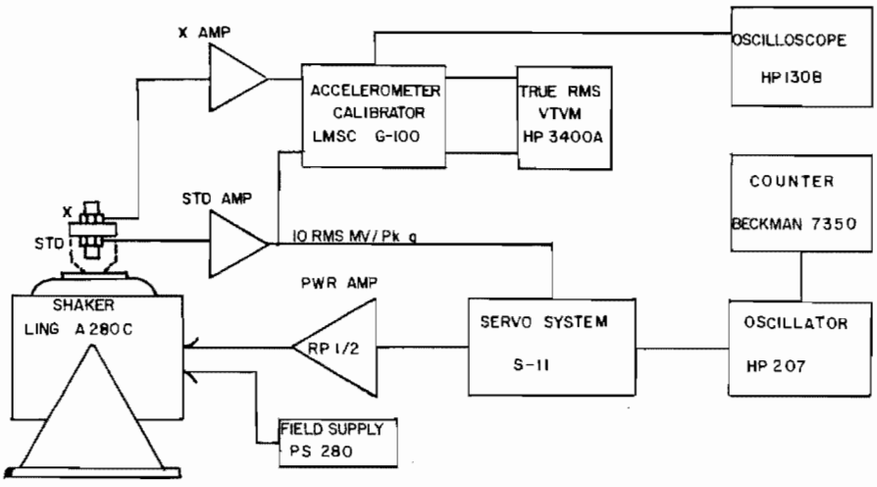

Fig. 3. Simplified block diagram of PSL accelerometer calibration system

UTILIZATION OF NBS CALIBRATION

The system calibrated by NBS is tested for absolute sensitivity over the range of 10 to 10,000 Hz at 27 frequencies with output stated in peak mv/peak g.

The calibration data are reduced to a form compatible with local test requirements, which are: basic sensitivity at 5 peak g's/100 Hz and frequency response deviations (%). Sensitivity is taken directly from the report and the response computed by the formula:

$$\Delta E \text{ std} = \left(1 - \frac{E \text{ std}}{Ef}\right) 100\% \qquad (1)$$

where

ΔE std = percent change in sensitivity at test frequency (f)

E std = sensitivity at reference frequency

Ef = sensitivity at test frequency (f)

Since data given by NBS represent the results of individual measurements, a normal scattering is indicated. For standardization purposes, it is desirable to treat this information as a curve function. The "best curve" response is determined by using a least square fit based on Eq. (1), Sec. 3.4, Ref. (1). Using data obtained with Eq. (1), best curve response is determined by the formula:

$$Rf = \left(\frac{\overline{\Delta E \text{ std}}}{\overline{f^2}}\right) f^2, \qquad (2)$$

where

Rf = best curve response at frequency (f) in percent,

$\overline{\Delta E \text{ std}}$ = mean deviation in percent,

$\overline{f^2}$ = mean test frequency squared (Hz),

f^2 = test frequency squared (Hz).

A plot of an actual NBS calibration, reduced in this manner, is shown in Fig. 4.

A form of Eq. (2) provides a convenient means of determining the indicated mounted resonant frequency (fn). Resonance can be determined by the formula:

$$fn = 10 \sqrt{\frac{\overline{f^2}}{\overline{\Delta E \text{ std}}}}. \qquad (3)$$

VERIFICATION OF NBS CALIBRATION

Because the Ref. Std. is not a passive system, it is subject to change. To maintain certainty, periodic verification tests in the following three categories are performed:

1. Electronics,
2. Frequency Response,
3. Absolute Sensitivity.

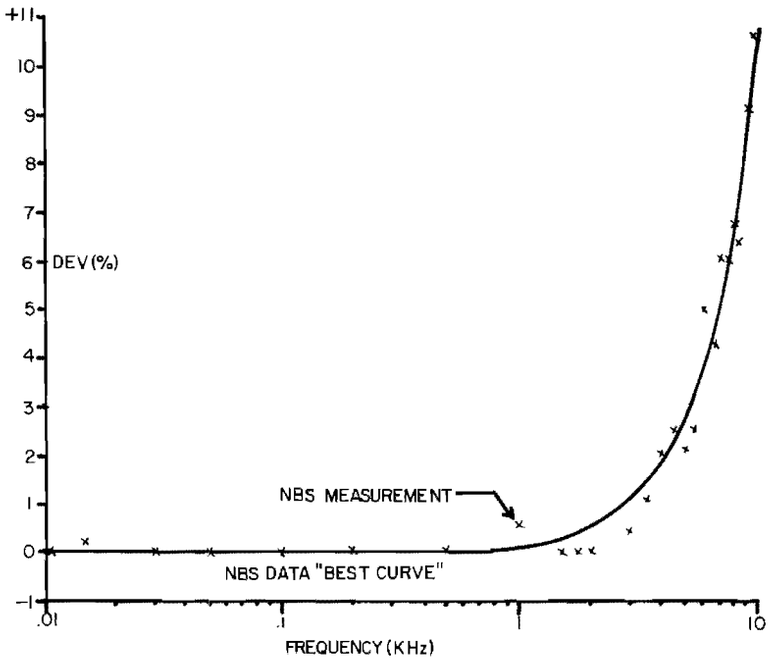

Fig. 4. Reference standard response determined from NBS data

ELECTRONICS TESTS

Tests are performed on the amplifier to determine gain and frequency response. While gain is not important from a system standpoint, knowledge of this parameter is necessary as a tie-down when a sensitivity shift occurs. The general test setup is shown in Fig. 5. Since tests are performed by PSL on a regular basis, the required circuitry has been built into an amplifier test set (LMSC Model 200) which conveniently tests the necessary functions on voltage and charge amplifiers. A picture of this instrument in an amplifier test setup is shown in Fig. 6.

Using the setup shown in Fig. 5, voltage amplifier gain at the reference frequency is determined as follows: When X = STD

$$A = R \quad (A < 1), \tag{4}$$

$$A = \frac{1}{R} \quad (A > 1), \tag{5}$$

where

A = Amplification ratio,

R = Divider indication.

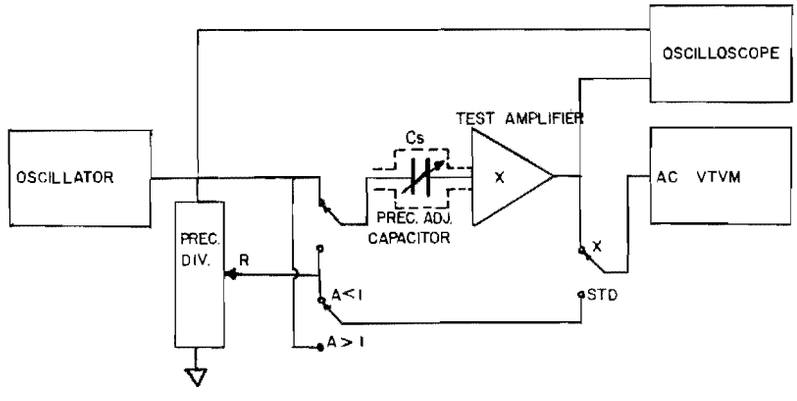

Fig. 5. Basic amplifier test setup

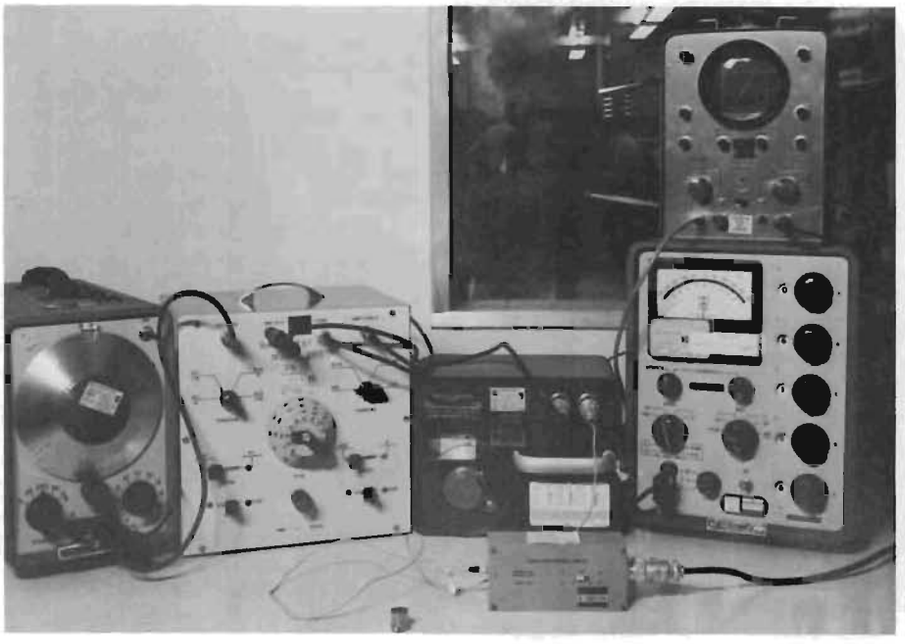

Fig. 6. Amplifier test setup

For verification, the coupling capacitance (C_S) is adjusted to the exact value of the accelerometer and the actual cable is used. Indicated gain will be lower than nominal because of the voltage divider effect between the impedance of the coupling capacitor and amplifier input plus cable. This setup simulates a charge generator with the same characteristics as the system accelerometer. This circuit is the electrical equivalent of the use system, therefore, an exact simulation of frequency response can be obtained. This is especially valuable at low frequencies where the system time constant is the primary limiting factor. Frequency response is determined as follows: When X = STD

$$\Delta Af = \left(1 - \frac{R \text{ @ } f \text{ ref}}{R \text{ @ } f \text{ test}}\right) 100\% \quad (A < 1) \qquad (6)$$

$$\Delta Af = \left(1 - \frac{R \text{ @ } f \text{ test}}{R \text{ @ } f \text{ ref}}\right) 100\% \quad (A > 1) \qquad (7)$$

where

ΔAf = amplifier response deviation (%),

$R \text{ @ } f \text{ ref}$ = divider ratio at reference frequency,

$R \text{ @ } f \text{ test}$ = divider ratio at test frequency.

An additional test for gain linearity is performed with this configuration. The PSL system is adjusted for approximately 10 rms mv/peak g, and is used from 1 to 100 peak g's. In use, the system output varies from 0.01 to 1 v rms. Using the basic output level as reference (5 peak g's = 50 rms mv) linearity is determined as follows: When X = STD

$$\Delta A = \left(1 - \frac{R \text{ @ } E \text{ ref}}{R \text{ @ } E \text{ test}}\right) 100\% \quad (A < 1) \qquad (8)$$

$$\Delta A = \left(1 - \frac{R \text{ @ } E \text{ test}}{R \text{ @ } E \text{ ref}}\right) 100\% \quad (A > 1) \qquad (9)$$

where

ΔA = change in amplifier gain (%),

$R \text{ @ } E \text{ ref}$ = divider ratio at reference output,

$R \text{ @ } E \text{ test}$ = divider ratio at test output.

ACCELEROMETER FREQUENCY RESPONSE

System low frequency response is a function of electronics, hence the predominate characteristic determining high frequency response

is the accelerometer mounted resonant frequency. Since the piezoelectric accelerometer is, by definition, a virtually undamped single-degree-of-freedom instrument, the sensitivity normally increases as frequency increases.

While PSL has the capability for absolute sensitivity determination using a Fizeau interferometer, verification tests performed in this manner would be a repeat of tests already performed at NBS. Instead of absolute measurements, the mounted resonant frequency and damping ratio are determined and the theoretical response calculated.

Two methods are used for resonance determination, the drop ball shock test, and a high frequency shaker (1 and 3).

The drop ball test is performed with an Endevco Model 2965 Shock Calibrator (Fig. 7). A steel ball is dropped on an undamped steel anvil on which the test accelerometer is mounted. The test unit will register a high initial shock pulse and then "ring" at its resonant frequency. This ringing is viewed on a storage oscilloscope and the frequency is determined from the period of one cycle.

The second method, using sinusoidal excitation, is shown in Fig. 8. The source is an oscillator-driven Endevco 2225 accelerometer with a piece of stainless steel 0.5 in. long between it and the unit under test. The 2225 has a nominal 80kHz resonance and is an ideal driver for this test. This system is simple, and it has proven to be reliable and has fewer extraneous resonances than the crystal stack or high frequency shakers which have been tested.

In operation, the oscillator frequency is adjusted until the test unit indicates maximum output on the VTVM. The oscillator frequency, as measured on the counter, is the test unit resonant frequency. The setup also provides a quick method for determining damping ratio. The procedure is:

1. With the oscillator adjusted for test unit resonance (f_n) adjust the oscillator amplitude until full scale is noted on a convenient VTVM range.

2. Without changing oscillator level, lower the oscillator frequency until 0.5 VTVM scale is noted and measure the oscillator frequency (f_y).

3. Damping ratio (C/C_c) can then be computed by the formula:

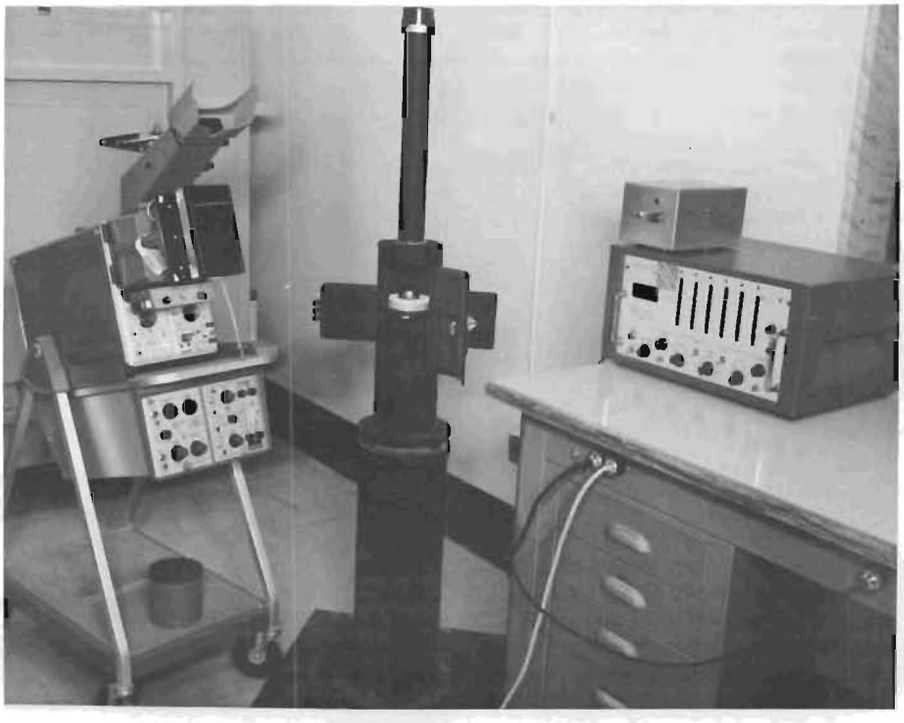

Fig. 7. Shock calibrator for determining accelerometer resonance

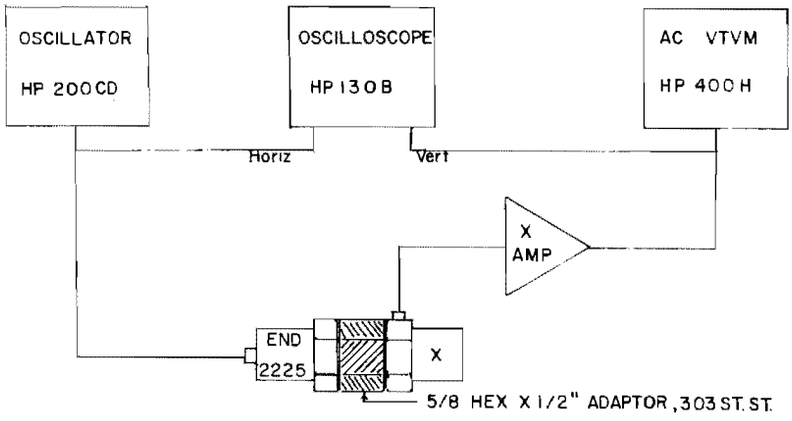

Fig. 8. Simple sinusoidal test setup for resonance determination

$$\frac{C}{Cc} = \sqrt{\frac{4(fy/fn)^2 - 1 - \sqrt{3\left[4(fy/fn)^4 - 1\right]}}{2}} \qquad (10)$$

The above equation was derived from Eqs. (10) and (11), Section 4, Ref. (1).

There are many errors in the method of determining damping ratio, the most obvious being that the applied acceleration is not constant around resonance. As the order of magnitude of the damping ratio rather than its actual value is desired, this method is more than adequate for verifying that the ratio is less than 0.1. For example, if the damping ratio is less than 0.1 and the maximum use frequency on a pickup is 0.3 of resonance, the maximum error in response calculation, ignoring damping ratio, would be less than 0.25 percent.

Agreement between shock and sinusoidal methods of determining resonance has been found to be within ±10 percent.

To determine the theoretical response from measured resonance, calculations are made from:

$$Rf = \left(\frac{(f/fn)^2}{1 - (f/fn)^2}\right) 100\%, \qquad (11)$$

where

Rf = calculated response at frequency (f) in percent,

(f/fn) = ratio of test (f) to resonant frequency (fn).

A plot of Ref. Std. response determined from electronics and resonance tests is shown in Fig. 9. A comparison between the NBS data best curve and calculated response is shown in Fig. 10a. For the purpose of comparison, the NBS curve is shown as the zero ordinate. For the intended use range of 20 to 4000 Hz, the maximum deviation between the two curves is 0.2 percent.

An additional series of verification tests are performed against the Comp. Std. system (Fig. 11). While limited in configuration, the Kistler system represents an almost perfect back-to-back comparison. Tests are performed over the range of 10 to 10,000 Hz with the results shown in Fig. 10b.

For frequencies below the normal 0.2 of resonance use range, the agreement between the various test methods is surprisingly close, the maximum deviation being less than 0.6 percent.

ABSOLUTE SENSITIVITY TESTS

One passive test, capacitance measurement, is performed on the Ref. Std. accelerometer. With the accelerometer used with a voltage amplifier, the sensitivity is directly related to its capacitance ($E = Q/C$), and any capacitance shift would directly affect the output.

Absolute sensitivity and linearity of the Ref. Std. system are determined using a high resolution microscope by the optical displacement technique. Accuracy obtained with this method is approximately ±0.5 percent. PSL is

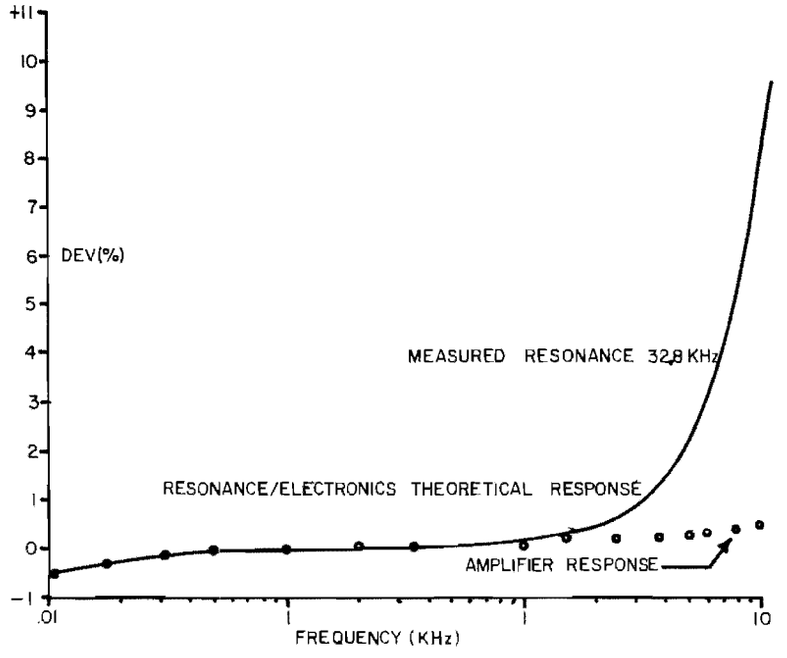

Fig. 9. Reference standard response determined by verification tests

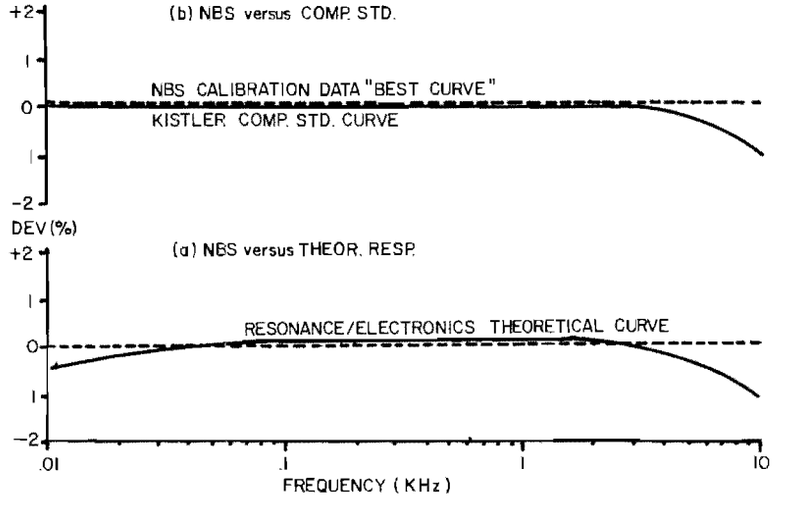

Fig. 10. Comparison of NBS calibration and verification tests

setting up to perform reciprocity calibration (4) which should provide an increased confidence level.

CALIBRATION MOUNTS

The PSL calibration mount (Fig. 12) is designed to calibrate all configuration accelerometers except tri-axial units. The mount consists of an aluminum frame which supports a thin stainless steel tie-plate. The accelerometer to be tested is mounted on a 1 oz adaptor which is connected to the top of the tie-plate. Adaptors, including blank units for glue-on, have been made for all stud configurations. Surface roughness is held to less than 63 micro inches rms and a thin film of silicone grease is used between mounting surfaces. Mounting torque for connecting the adaptors to the mount is 50

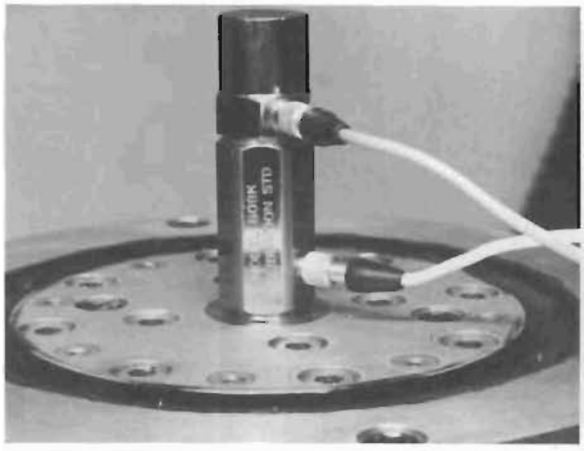

Fig. 11. Kistler accelerometer setup for comparison tests

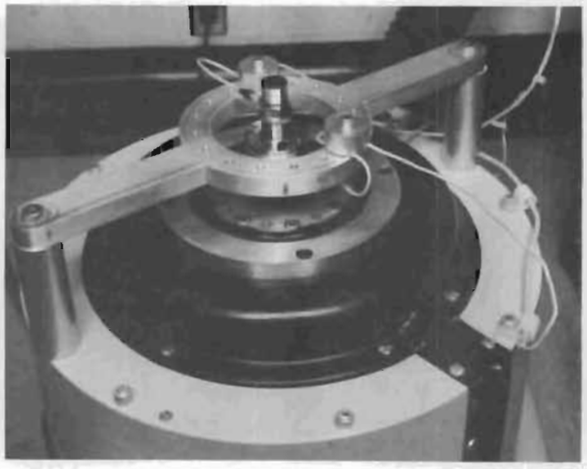

Fig. 13. PSL calibration mount and cable support frame attached to shaker

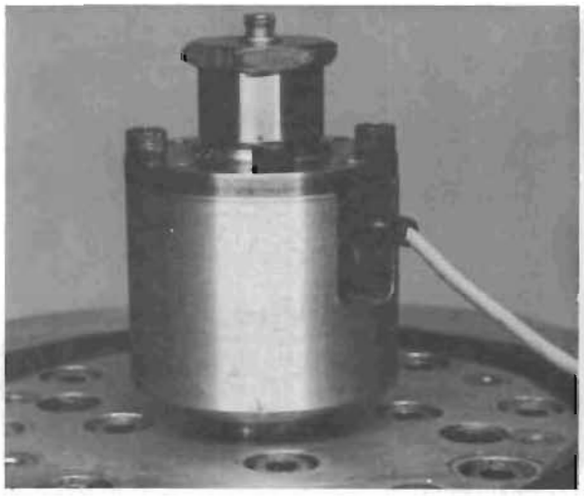

Fig. 12. PSL calibration mount

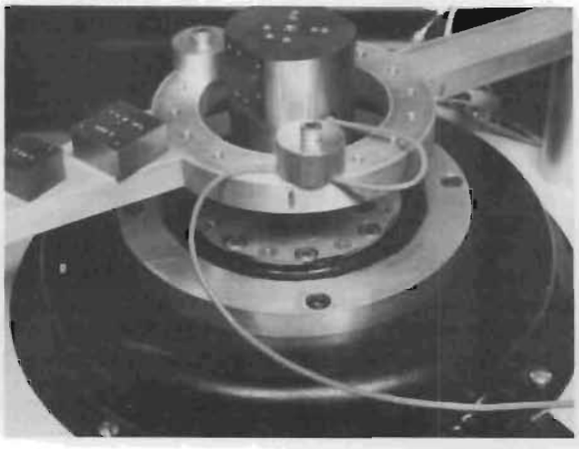

Fig. 14. Tri-axial accelerometer comparison mount

in. lbs. While this mount has the disadvantage of an extra connecting surface and added mass, its advantage is that all accelerometers are tested on an identical mount configuration.

The calibration mount, attached to the shaker, is shown in Fig. 13. The metal fixture surrounding the mount is used for cable positioning and tie-down.

Tri-axial accelerometers are tested on the mount shown in Fig. 14. This unit was designed by Endevco and made at LMSC. Additional units have been built for testing other manufacturers' accelerometers. The small metal blocks shown are used for balancing the opposite side of the mount when extra accelerometers are not available for use as counterbalances.

WORKING STANDARD CALIBRATION

To obtain a direct readout system, the Work. Std. accelerometer and amplifier are adjusted for an exact 10 rms mv/peak g sensitivity and flat response over the range of intended use. To accomplish this, the Work. Std. is installed in the comparison mount, and the Ref. Std. connected as though it were a device under test. The system is set into motion at the basic sensitivity frequency and the Work. Std. adjusted with amplifier gain until the ratio between the two indicates the NBS calibrated sensitivity.

The outputs are then compared over the frequency range, and the Work. Std. amplifier frequency response adjusted until the difference between them coincides with the best curve response. This provides a theoretically perfect calibration with a 1 oz pickup.

An effect, which is sometimes disregarded at the low basic sensitivity determination frequency, is the error caused by the standard and unknowns not having the same mass. This is commonly known as the "mass loading" error.

At basic sensitivity determination frequencies this situation is expressed by the equation:

$$\frac{Ax}{As} = \frac{ks - msw^2}{kx - mxw^2}, \qquad (12)$$

where

Ax/As = ratio of test to standard acceleration,

ks - kx = spring stiffness,

ms = standard mass,

mx = test unit mass.

The PSL mount has been evaluated for this effect with the setup shown in Fig. 15. A series of tests were run by turning the Comp. Std. upside down and adding mass to vary its case weight. The mount corrections resulting from these tests are shown in Fig. 16.

At high frequencies, errors will be encountered which will tend to indicate a premature

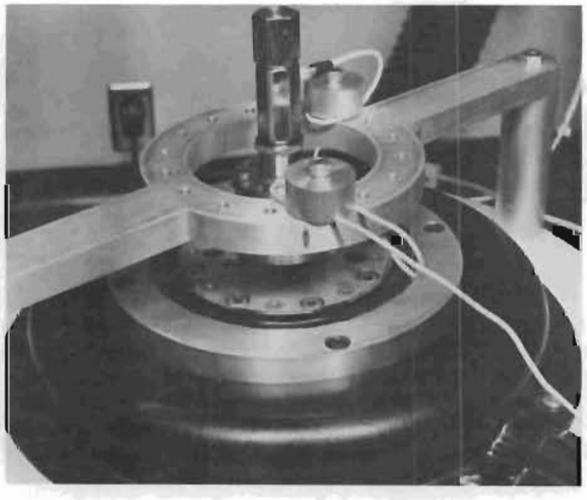

Fig. 15. Mass loading test setup

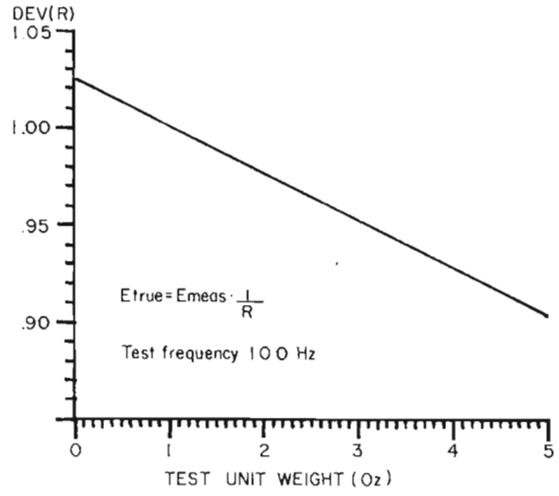

Fig. 16. PSL comparison mount loading error

rise if the test unit is heavier than the standard (4,5) or decay if the test unit is lighter. The PSL mount was evaluated for this effect using a configuration similar to that shown in Fig. 15. Results of these tests are shown in Fig. 17. The maximum error for pickups weighing from 0.5 to 2 oz was 1 percent. The mass loading errors are taken into consideration as a part of the normal calibration.

The tri-axial fixtures were adjusted and analyzed in a manner similar to that indicated for the Work. Std., with the exception that the upper frequency limit is 2 kHz.

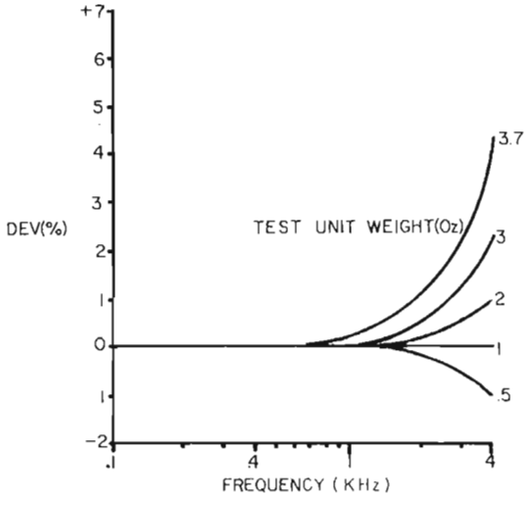

Fig. 17. PSL comparison mounting loading errors at high frequencies

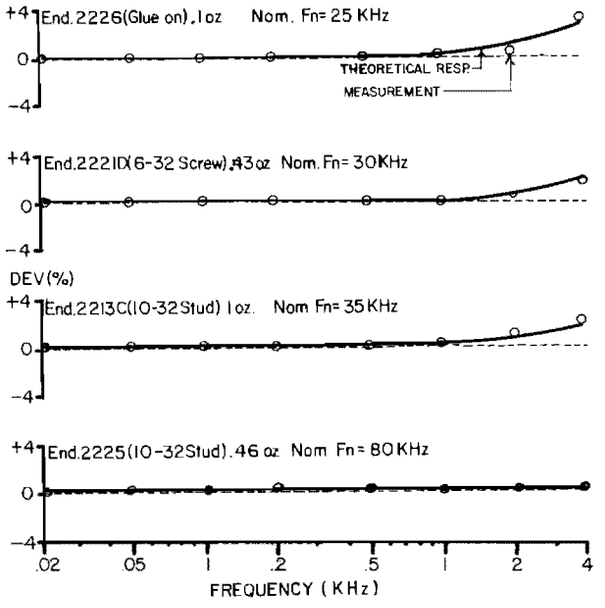

Fig. 18. Typical calibration performed with PSL/LMSC system

SYSTEM PERFORMANCE

As previously stated, a calibration system is only as good as its ability to test the various types of test units. A series of actual calibrations performed on various units is shown in Fig. 18. The curves represent the manufacturers stated theoretical response with the points representing actual measurements.

Below 100 Hz, deviations in response are predominately traceable to the cable. As PSL amplifier impedances are high, normal deviations due to system time constant are less than 0.5 percent down to 10 Hz. The cable effects fall into two general categories: cable noise and motion distortion.

The cable noise results from the mechanical distortion of the cable due to the high displacements at low frequencies. This noise is especially troublesome on low sensitivity accelerometers where it is possible for the cable to give a larger signal than the accelerometer. This effect is indicated by an apparent increase in test unit sensitivity. The normal cure for this trouble is to tie the cable to a solid frame to keep to a minimum the amount of cable undergoing motion.

The seond effect of motion distortion is often caused by the cure for the first problem, that is, the cable pulling the fixture and accelerometers under high displacements. Indication of this problem can be either an apparent increase or decrease in sensitivity depending on cable configuration.

To the best of the writer's knowledge, no presently manufactured accelerometer exhibits characteristics at low frequencies other than that determined by the system time constant. All other deviations can be traced directly to the cable and can be corrected or compensated. The best general configuration found for calibration is that shown in Fig. 13. The cable is mounted on the support frame with a loose loop to decrease lateral tension with the length of vibrating cable kept at a minimum.

Agreement on sensitivity between NBS, manufacturers, and the PSL system is generally very close. The deviations usually are less than 0.5 percent which is very good considering that most agencies claim an accuracy in the region of 1 percent.

The overall capability of the PSL system is shown in Table 1.

CONCLUSIONS

Experience has indicated that with a proper understanding of system operation and variables, it is possible to obtain a high accuracy calibration with a conventional back-to-back test configuration.

TABLE 1
Analysis of Capability of PSL/LMSC Calibration System

Measurement (Hz)	Error (%)
Work Std. transfer	
Sensitivity & linearity	
NBS calibrated Ref. Std. 2-10 g (100)	1.0
Allowable deviation	.1
Optical verification 20-100 g (100)	1.0-.5
Frequency response	
NBS calibrated Ref. Std. (10-900)/(1000-10000)	1.0/2.0
Allowable deviation	.2/.4
Calibration fixture	
"Mass loading" (100)	.2[a]
Relative motion (1000-4000)	.4[a]
System	
G-100 calibrator gain & lin. (100)/response (20-4000)	.1/.15
"X" amplifier gain & lin. (100)/response (20-4000)	.2/.2
External capacitance	.25[b]
Environmental effects (temp., acoustic, misc. in lab. controlled environment)	.25
Estimated error	
Sensitivity & linearity (100)	1.5[c]
Frequency response (20-900)	1.1[c]
(1000-4000)	2.2[c]

[a]Error shown is after correction.
[b]Estimated error based on effects of variables on 500 pf accelerometer.
[c]Determined from rms of individual errors.

The summary of this situation is evidenced by the fact that calibration data are more indicative of theoretical accelerometer operation with each successive improvement in the calibration system.

ACKNOWLEDGMENT

The writer wishes to thank D. B. Schneider and D. J. Riordan of Lockheed Missiles & Space Co. For their assistance in the preparation of this paper.

REFERENCES

1. "Calibration of Shock & Vibration Pickups," ASA Standard S2.2, 1959

2. D. R. Workman, "New Instrument for Accelerometer Calibration," Shock & Vibration Bulletin No. 34, Part 4, Feb 1965

3. R. R. Bouche, "High Frequency Response & Transient Motion Characteristics of Peizoelectric Accelerometers," ISA Paper No. 50-LA-61

4. R. R. Bouche and L. C. Ensor, "Use of Reciprocity Calibrated Accelerometers for Performing Routine Laboratory Comparison Calibrations," Shock & Vibration Bulletin No. 34, Part 4, Feb 1965

5. F. Schloss, "Inherent Limitations of Accelerometers for High Frequency Vibrations Measurements," JASA, 33, 4, 1961

6. F. Schloss, "Weight Limitations of Accelerometers for High Frequency Measurements," Wilcoxon Research Technical Bulletin No. 1, Aug 1963

* * *

MEASUREMENT OF ACCELEROMETER TRANSVERSE SENSITIVITY

D. W. Rockwell and J. D. Ramboz
Metrology Engineering Center
Bureau of Naval Weapons Representative
Pomona, California

Accelerometer transverse sensitivity is reviewed in concept, commonly used measurement methods are discussed, and new measurement techniques are proposed. Methods presently employed for the measurement of transverse sensitivity rely on the relatively pure unilateral motion available at low frequencies. Acceptable motion is difficult to achieve at higher frequencies. Because accelerometers are used at frequencies up to 10 kHz or higher, it is important that the frequency response be known throughout the range.

Several unique techniques of transverse sensitivity measurement are presented. These techniques do not depend upon the availability of pure unilateral motion, but employ methods of accounting for the vector components of the accelerometer output due to lateral motion. The proposed techniques have the advantage of not being limited to a single frequency. Preliminary tests have produced useful data at frequencies up to 2500 Hz. Future refinements in fixtures, accelerometers, and techniques should produce acceptable results at much higher frequencies. A special transducer has been fabricated with a low transverse sensitivity on a specified axis over a wide frequency range, i.e., less than 0.1 percent from 40 Hz to 1000 Hz, and less than 1 percent to 8000 Hz. The theories presented are not limited to piezoelectric accelerometers, but apply to other transducers which respond to composite vector stimuli.

INTRODUCTION

Ideally, an accelerometer should respond only to acceleration along its sensitive axis. However, in practice, accelerometers exhibit a transverse sensitivity in directions other than the sensitive axis. This transverse sensitivity contributes an output error signal which can be significant in stringent vibration specifications (1).

At present, transverse sensitivity measurements are usually performed at a single frequency in the range of 10 to 150 Hz. The measurement techniques commonly used rely on the availability of nearly pure unilateral motion in order to obtain accurate results. Vibratory motion can be generated with very small lateral components at low frequencies, but it becomes extremely difficult to generate pure motion at higher frequencies. Since accelerometers are generally used at frequencies up to 10 kHz, low frequency measurements of transverse sensitivity do not provide complete information. The effect of frequency on the transverse sensitivity response of common piezoelectric accelerometers has often been questioned (1-4), but very little data has been published (5,6).

Several new techniques for the measurement of transverse sensitivity are presented in this paper. These techniques do not depend on the availability of single degree of freedom motion, but employ methods of compensating for vector components of the accelerometer output due to lateral motion. In theory, these techniques are not restricted to single or low frequencies. Limitations and advantages of each proposed method are discussed, and preliminary data are presented for frequencies up to 2500 Hz.

A transverse compensated accelerometer has been fabricated with a controlled axis of minimum transverse sensitivity. This accelerometer is useful for the measurement of transverse motion of electrodynamic shakers, and

for the evaluation of transverse sensitivity of unknown accelerometers.

SYMBOLS

a = instantaneous acceleration

a_t = maximum value of instantaneous transverse acceleration

A_x = peak amplitude of sinusoidal acceleration on the transverse X axis

A_y = peak amplitude of sinusoidal acceleration on the transverse Y axis

A_z = peak amplitude of sinusoidal acceleration on the major Z axis

B, H, K = amplifier constants

g_s = acceleration of standard gravity

q = instantaneous charge

n_t = generalized instantaneous transducer output for transverse excitation

S_r = reference accelerometer sensitivity

S_t = maximum value of accelerometer transverse sensitivity

S_x = transverse accelerometer sensitivity in the X direction

S_y = transverse accelerometer sensitivity in the Y direction

S_z = axial accelerometer sensitivity

TAR = transverse acceleration ratio

TSR = transverse sensitivity ratio

X, Y = orthogonal coordinates denoting the transverse acceleration of a shaker, or the transverse sensitivity of an accelerometer

Z = coordinate denoting the axial acceleration of a shaker, or the sensitivity of an accelerometer

γ = phase angle of transverse sinusoidal acceleration with reference to axial acceleration

δ = mechanical angle between the true sensitive axis and the axis perpendicular to the mounting surface

θ = an arbitrary mechanical angle in the X-Y plane, which denotes the rotational displacement of the maximum lateral acceleration

ϕ = phase angle of test accelerometer sinusoidal output with respect to a reference accelerometer output

ψ = angular deviation from true perpendicularity between the mounting surface of the laterally mounted transducer and the mounting surface of the shaker.

DEFINITION AND DISCUSSION

The effect of transducer response to transverse excitation has been described and defined by most authors writing on the subject. Although all are discussing the same effect, different definitions have been employed at the authors' choice. In addition, this same effect has been identified by such names as cross-axis sensitivity, cross-talk, lateral sensitivity, transverse sensitivity, transverse sensitivity ratio, orthogonal sensitivity, and other hybrid combinations of similar terms.

In strict use of, and in agreement with, the existing definitions of transducer sensitivity, the transverse sensitivity is herein expressed in units of transducer output per unit transverse mechanical input. Hence,

$$S_t = \frac{n_t \text{ (instantaneous output)}}{a_t \text{ (instantaneous acceleration)}}, \qquad (1)$$

where S_t is the transverse sensitivity factor, n_t is the transducer output when excited with a pure transverse acceleration, a_t. (By dividing S_t by standard gravity g_s, S_t may be expressed in terms of output/g.) The transverse sensitivity ratio is defined by one of several commonly accepted descriptions. Assuming the transducer output was voltage, then the transverse sensitivity ratio would be expressed as

$$\text{TSR} = \frac{S_t \text{ (mv/unit transverse acceleration)}}{S_z \text{ (mv/unit axial acceleration)}}, \qquad (2)$$

where TSR is the transverse sensitivity ratio, and S_z is the axial sensitivity factor. From the relationship expressed by Eq. (2) above, the TSR has units of axial acceleration per

transverse acceleration. Accounting for standard gravity, the TSR may be expressed in terms of g/g. Also shown by Eq. (2), the magnitude of the TSR is independent of the parameter of transducer output, that is, voltage, charge, current, etc.

It is most common to multiply the TSR value by 100, and express the results in terms of a percentage of the axial value. This may be accomplished by simply multiplying Eq. (2) by 100, or

$$TSR\% = \frac{S_t}{S_z} \times 100 . \quad (3)$$

The TSR has also been defined in terms of an equivalent mechanical angle, δ, between the true sensitive axis and the Z axis perpendicular to the transducer's mounting surface (7). Figure 1 shows this angle δ. The TSR is numerically equal to the tangent of the angle δ, or

$$TSR = \tan \delta , \quad (4a)$$

$$\lim_{\delta \to 0} TSR = 0 . \quad (4b)$$

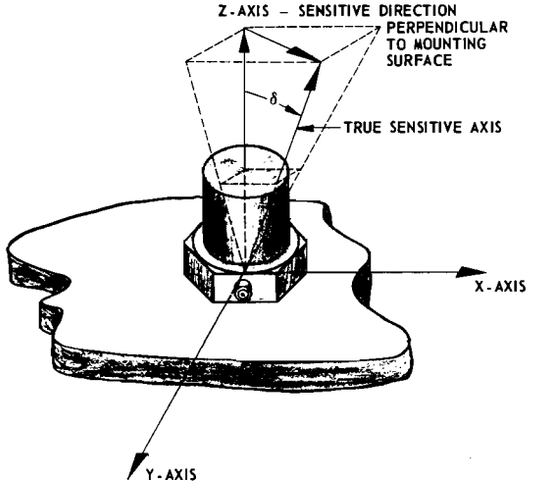

Fig. 1. The true sensitive axis and the perpendicular axis directional difference

The angle δ should ideally be zero. However, practical physical limitations do not permit the manufacturing of perfect transducers, and some small angle will always exist. In reality, δ is a composite angle resulting from several possible causes, depending on the construction of the individual transducer. A mechanical measurement of this angle is impossible to perform. It can, however, be evaluated by electro-mechanical techniques and measurements. There are very few times when this angle has to be known as such. Usually the TSR is measured and the angle determined by the relationship,

$$\delta = \tan^{-1} (TSR) . \quad (5)$$

The definition which shall be used in this paper agrees with the American Standards Association's S2.2-1959 (8) and is essentially stated as: "The transverse sensitivity ratio is the output of a pickup when oriented with its sensitive axis transverse to the direction of the input divided by the output when the sensitive axis is aligned in the direction of the same input." This has previously been expressed in Eq. (2).

CAUSES AND EFFECTS

Probably the largest single contributing factor to transverse sensitivity is the inability to align the sensitive axis perfectly with respect to a mounting surface. This is illustrated in Fig. 1 for a typical piezoelectric accelerometer. From Eq. (4) it can be determined that a defect angle, δ, of 10 milliradians (0.57 degrees) will produce a TSR of 1 percent, and likewise, an angle of 1 milliradian (0.057 degrees) will result in a TSR of 0.1 percent. For a typical piezoelectric accelerometer with a 0.5 in. diameter base, a misalignment of approximately 0.005 in. will introduce a TSR of 1 percent. For miniature "cement-on" type accelerometers having a base diameter of about 0.20 in., a 1 percent TSR would be caused by a misalignment of only 0.002 in. Therefore, assembly tolerances are very important, if the TSR is to be kept low, i.e., in the order of a few percent.

In certain transducers, the transverse sensitivity can be caused by additional defects. For example, in a compression type piezoelectric accelerometer, the lateral shear forces set up within the structure, when excited transversely, may contribute to an output. This is illustrated in Fig. 2. If a dynamic unbalance exists within the inertial mass, a transverse excitation can cause a rocking motion, which will couple into the sensitive axis of the transducing element, thus producing an undesirable output. One may think that these effects are small, and indeed they generally are, but even 1/200 the vertical force caused by such a rocking motion could generate a TSR of 0.5 percent. Other defects such as inhomogeneity of the

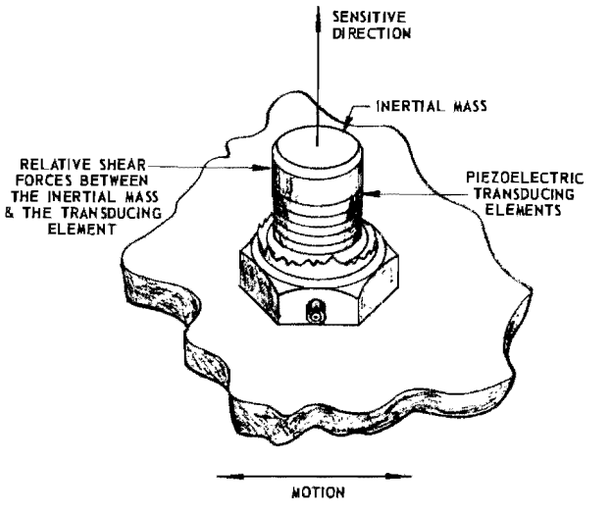

Fig. 2. A compression type accelerometer showing transverse shear force

transducing elements, dynamically unbalanced structures, lateral resonances, lateral case strains, etc., undoubtedly contribute to the total transverse defects (9).

VECTOR PROPERTIES OF MOTION AND SENSITIVITY

In order to understand the complexity of performing accurate and meaningful transverse motion measurements, the vector nature of the problem must be examined.

In the following discussion, sinusoidal motion at a single frequency is considered. Imagine a body which is free to move in two directions simultaneously. Figure 3 shows an example of two orthogonal sinusoidal motions, M and N, of different amplitudes and phase, applied to the body. At time t_o, the body begins to rotate clockwise from point p_o toward the point p_1. At time t_1, the body reaches point p_1. The process continues around the ellipse until at time t_8 and point p_8, the process begins to repeat itself.

A vector diagram of the orthogonal motions can be shown for point p_2, for example. Figure 4(a) indicates the directions and instantaneous magnitudes m and n, which define motions M and N at time t_2. This may be correlated with Fig. 3. Figure 4(b) shows the general vector diagram of the two sinusoidal motions having peak amplitudes M and N, and their vector sum of L. In vector notation,

$$\overline{M} + \overline{N} = \overline{L} . \qquad (6)$$

Expressed in terms of sinusoidal quantities,

$$M \sin (\omega t + \phi_m) + N \sin \omega t = L \sin (\omega t + \phi_\ell) . \qquad (7)$$

It is interesting and significant to note from Eq. (7) that two sinusoidal quantities of the same frequency and of different magnitudes and phase, when added, produce a third sinusoidal quantity of yet a different magnitude and phase, but of the same frequency. Several of the measurement techniques to be discussed depend upon this relationship.

In the prior example, rectilinear motion in two directions was assumed. In practice, motions occur rectilinearly in three orthogonal directions, as well as rotationally about these axes as shown by Fig. 5. The mechanical Lissajous figure which was shown by Fig. 3 will be changed when motion in the third orthogonal direction is applied. This third input will tilt the plane of the ellipse in and out of the plane of the paper.

The acceleration vectors for a sinusoidal acceleration generator (i.e., a shaker) are shown in Fig. 6.

The axial acceleration A_z is perpendicular to the table surface. Accelerations A_x and A_y are the transverse components.* Acceleration A_t is the maximum transverse acceleration at a mechanical angle θ from the X axis reference. Acceleration A_m is the maximum axial value displaced at an angle σ from the perpendicular axis.

Ideally, A_x, A_y, A_t and σ should be zero, which represents a perfect vibration exciter with respect to transverse motions.

The following relationships describe the respective vectors:

$$a_x = A_x \sin (\omega t + \theta_x) , \qquad (8a)$$

$$a_y = A_y \sin (\omega t + \theta_y) , \qquad (8b)$$

$$a_z = A_z \sin \omega t , \qquad (8c)$$

$$A_t = \sqrt{A_x^2 + A_y^2} , \qquad (9a)$$

$$A_t = A_x \sec \theta = A_y \csc \theta , \qquad (9b)$$

*These components are sometimes referred to as trunnion and cross-trunnion components, when referenced to certain electrodynamic vibration exciters.

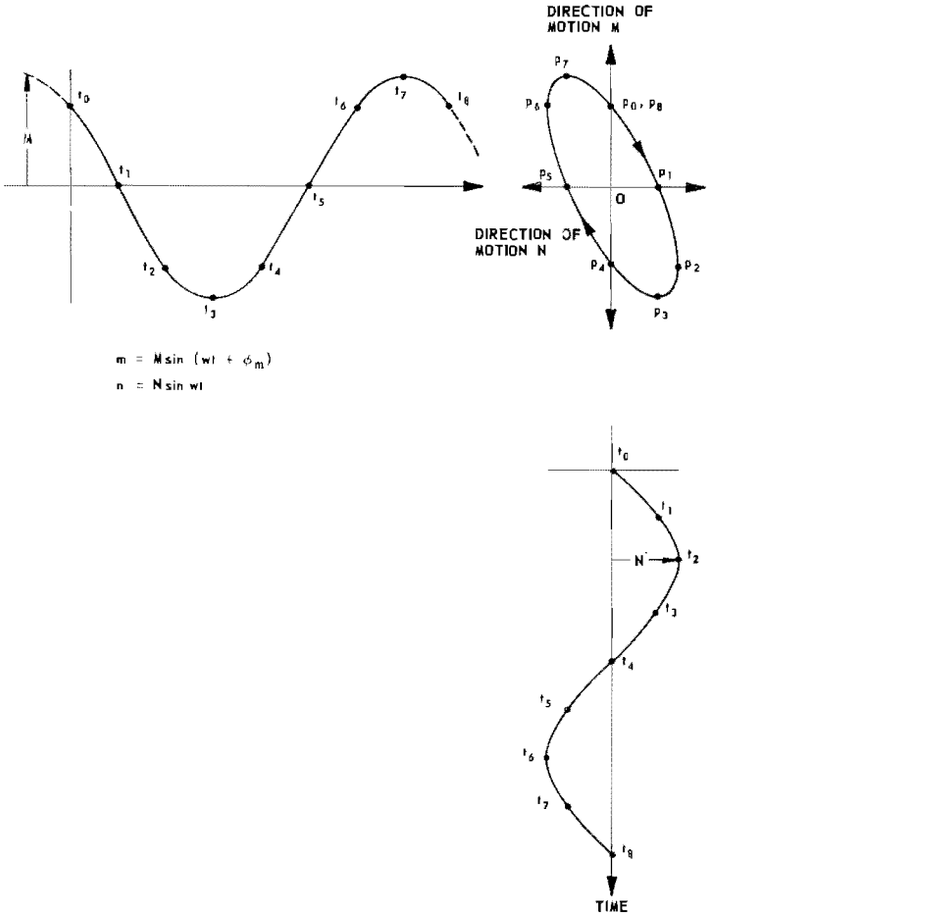

Fig. 3. Mechanical Lissajous figure generated from two orthogonal sinusoidal motions

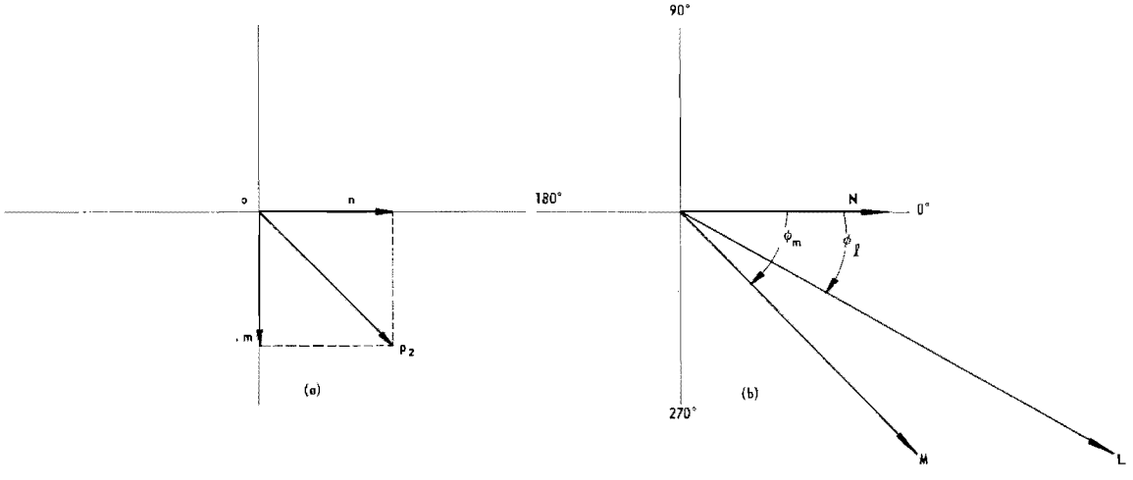

Fig. 4. Vector representation of sinusoidal quantities

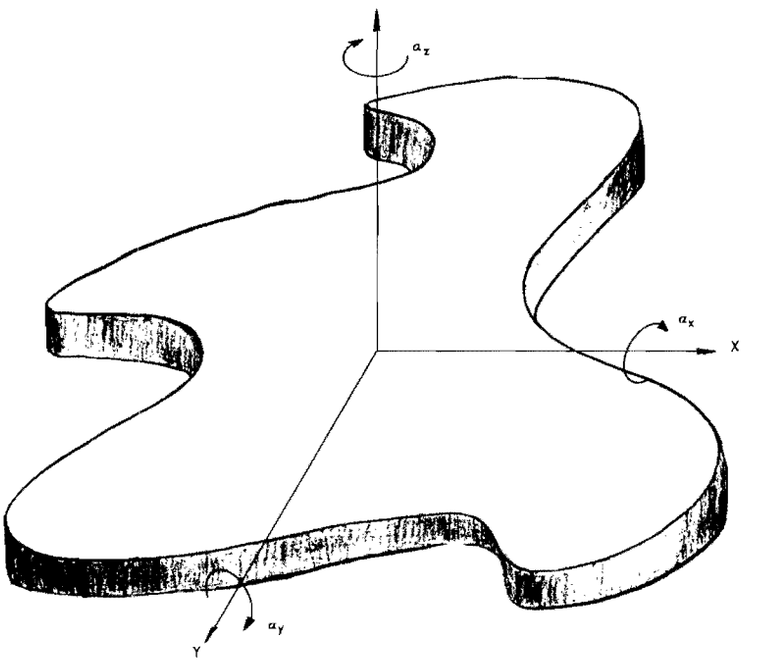

Fig. 5. The basic six degrees of freedom of a body

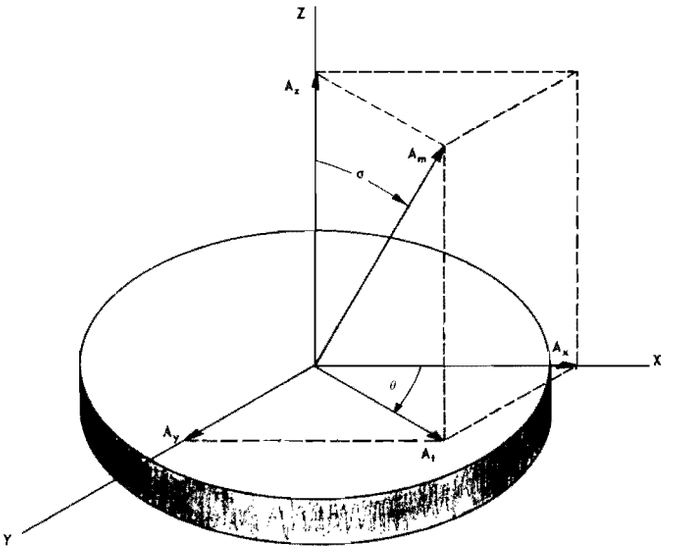

Fig. 6. Rectilinear motion vectors of a typical electrodynamic vibration exciter

$$A_m = \sqrt{A_z^2 + A_t^2} = A_z \sec \sigma . \qquad (10)$$

The transverse acceleration ratio is defined by

$$TAR = \frac{A_t}{A_z} = \tan \sigma . \qquad (11)$$

Figure 7 shows a similar group of sensitivity vectors describing the parameters of an accelerometer. The sensitivity vector S_z was previously defined as the axial or normal sensitivity factor of the accelerometer. S_x and S_y are the orthogonal components of the transverse sensitivity factor, S_t. The angle θ is the rotational angle about the Z axis between the maximum value of transverse sensitivity S_t and the X axis. The following relationships describe the vector diagram of Fig. 7:

$$S_t = \sqrt{S_x^2 + S_y^2} \qquad (12)$$

$$TSR = \frac{S_t}{S_z} = \tan \delta . \qquad (13)$$

A polar diagram of the transverse sensitivity ratio is shown in Fig. 8. The angle θ was arbitrarily chosen. Ideally, the two lobes should be symmetrical, and pass through zero orthogonally to the direction of maximum transverse output. The foregoing vector definitions and concepts will be used throughout this paper.

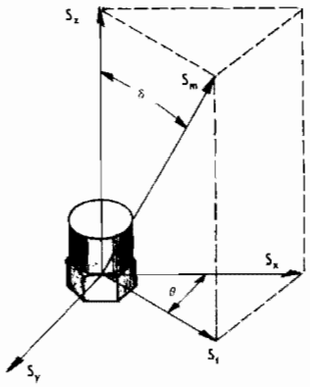

Fig. 7. Sensitivity vectors of a typical piezoelectric accelerometer

COMMON MEASUREMENT EQUIPMENT AND TECHNIQUES

A variety of techniques for the measurement of the transverse sensitivity ratio exist throughout government and industrial laboratories. All the techniques thus far examined do rely to some extent on assumptions of pure rectilinear motion in one direction only. The resulting measurement error from this assumption depends on the particular technique and the relative values and phases of the accelerometer transverse sensitivity ratio (TSR), and shaker transverse acceleration ratio (TAR).

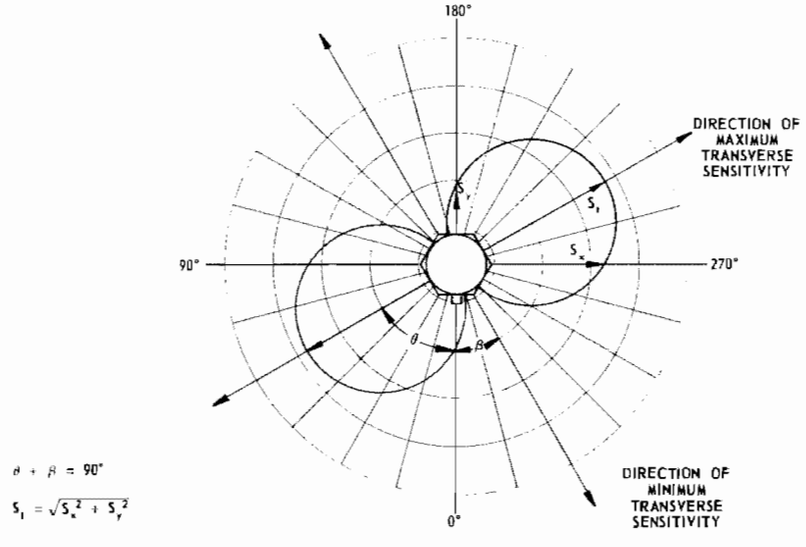

Fig. 8. Ideal polar plot of the transverse sensitivity of a piezoelectric accelerometer

Resonant Beam

A frequency may be chosen for an electrodynamic shaker where the TAR is relatively low. The shaker is then used to drive a resonant beam to enhance the purity of motion even more. Figure 9 shows a typical setup for use on a MB C-1 or C-11 shaker at about 150 Hz (2). With the accelerometers mounted as shown, the acceleration level is run up to about 5 to 10 g peak and the output of the test accelerometer measured. From this datum, an approximate value of the TSR can be obtained as previously shown by Eq. (2) or (3). The fixture has provisions for rotating the test accelerometer about its sensitive axis, thus providing information concerning the direction of the minimum and maximum TSR. This technique has the limitation of being useful only at a single frequency (i.e., beam resonance), and the assumption of pure motion can cause an error.

A sinusoid will be generated if the output is plotted while the test accelerometer is rotated, say 30 degrees, about the sensitive axis. This is shown in Fig. 10. The lower half-cycle will fold over as shown graphically by the solid line, since most instruments used to measure the output indicate magnitude only. It is common practice to take the peak-to-peak values (in this example N_{60} and N_{240}), determine the average or single peak value, and call this the transverse sensitivity ratio. As shown by Fig. 10, the "zero magnitude" line is offset from the "one-half of peak-to-peak" value line. This is the result of a component of shaker motion in the sensitive direction of the accelerometer. Figures 11 and 12 show the vector relationship for a typical measurement.

The vectors $\overline{S_y A_z}$ of Figs. 11(b) and 12(b), respectively, contain the wanted transverse component, S_y. However, these vectors are not measured in real practice, but rather measurement is made of the vector sum N_{60} and N_{240}, which also contains the components $\overline{S_z A_y}$, as illustrated. It can be appreciated that even a very small amount of transverse motion, A_y, in the direction of the accelerometer sensitive axis, S_z, can contribute significant differences between N_{60} and N_{240} (which should be equal), or any other "180 degree-pairs" of measurements. It should be emphasized and simply stated that TSR measurements involve vector quantities. If the TAR approaches the TSR in magnitude, accurate measurements cannot be obtained by scalar or magnitude measurements only. The phase relationships must be known or evaluated. It is for this reason that measurement discrepancies exist in many common techniques. Figure 13 shows a typical polar plot of the sinusoid of Fig. 10. Note that the offset of the zero-magnitude line causes the lobes to be nonsymmetrical

For the resonant beam method as shown by Fig. 9, this problem does not generally

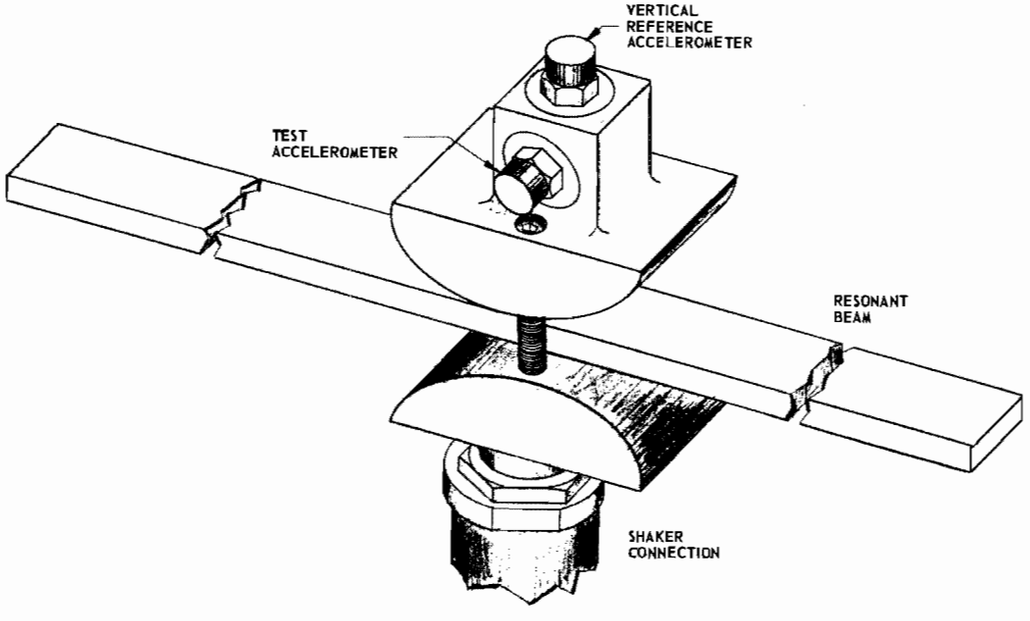

Fig. 9. A center-clamped resonant beam for improving the transverse acceleration ratio

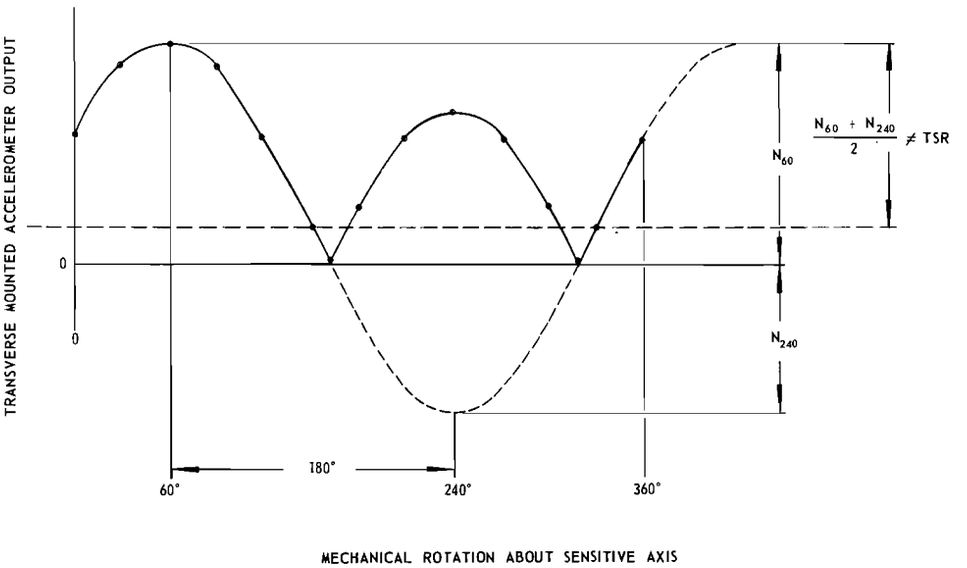

Fig. 10. Accelerometer transverse output as a function of mechanical rotation about its sensitive axis plotted in 30 degree increments

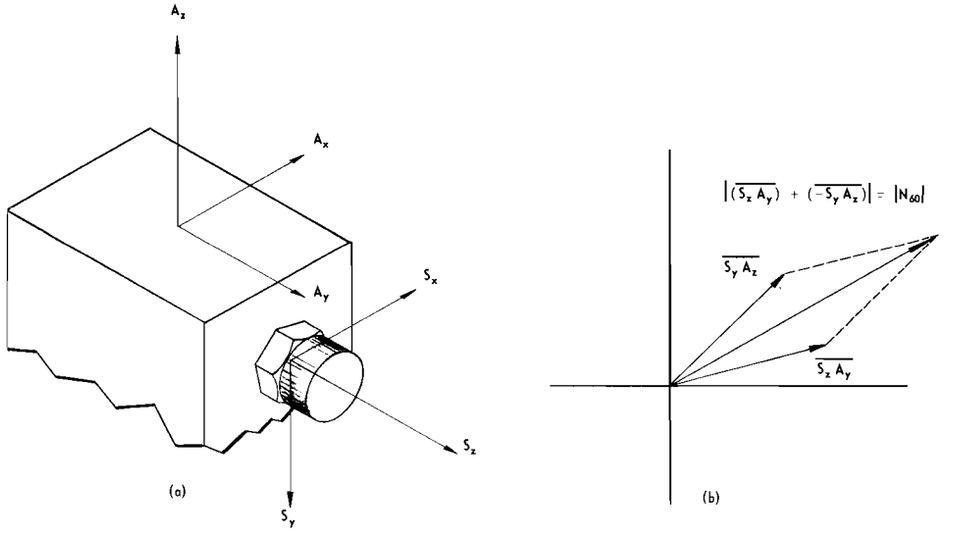

Fig. 11. Acceleration, sensitivity, and transducer output vectors for the 60 degree position

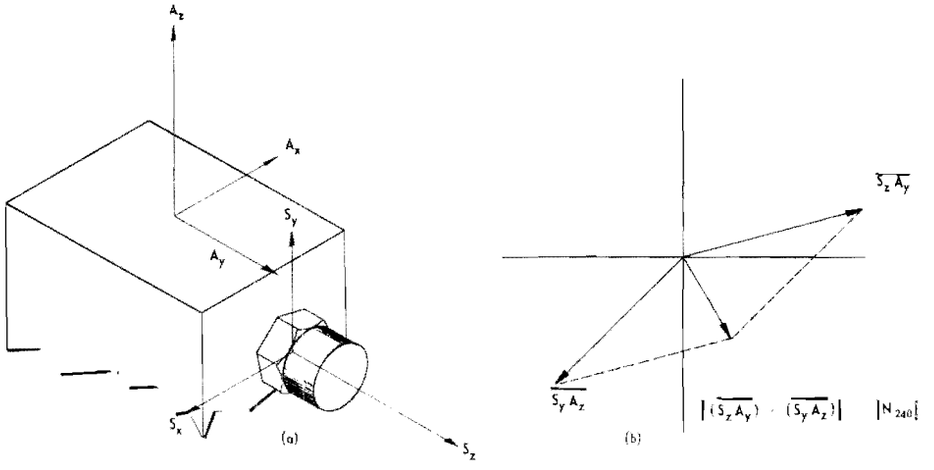

Fig. 12. Acceleration, sensitivity, and transducer output vectors for the 240 degree position

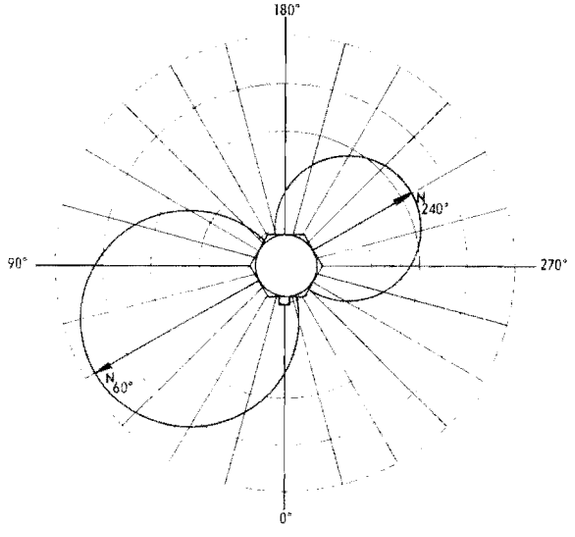

Fig. 13. Typical, but erroneous polar plot of TSR, data from Fig. 10

become significant until TSR's of less than about 3 percent are involved. This, of course, finally depends on the TAR of the shaker.

Resonant Carriage

A similar, but slightly different approach from the resonant beam technique, is that of the resonant carriage. A spring-mass system as shown by Fig. 14 is driven at its resonant frequency, typically around 90 to 100 Hz. The flexures are arranged in such a manner as to have very high compliance in the driven direction, X, moderately low in the orthogonal transverse direction, Y, and very low in the vertical axis, Z. By operating the spring-mass system at resonance, and by making the necessary adjustments, relatively pure linear motion can be obtained. The test accelerometer can be rotated about its sensitive axis by removing the screws which attach the mounting fixture to the carriage. Axial motion is measured by an accelerometer mounted in the direction of motion. This system is limited to a single operational frequency (i.e., carriage resonance), and some problems occur when transducers with extremely small TSR's (i.e., 0.25 percent or less) are tested, unless great care is taken. The measurement technique is very similar to that previously discussed concerning the resonant beam equipment, and can suffer from the same errors. It is felt that in this respect, the carriage arrangement is somewhat better, because of the ability to adjust the motion in a limited manner.

Shaker Decoupling and Lateral Inertial Equipment

Figure 15 shows a side view of an arrangement reported (3) to yield TAR's of less than 1 percent from 50 to 500 Hz, and less than 2 percent from 20 to 1000 Hz. The shaker is supported as shown, thin bars being used to help support the shaker weight. The driving rod is "necked" down to decouple lateral motions from the shaker by providing a large lateral compliance, and rather low axial compliance. The high transverse inertia of the vibrating table,

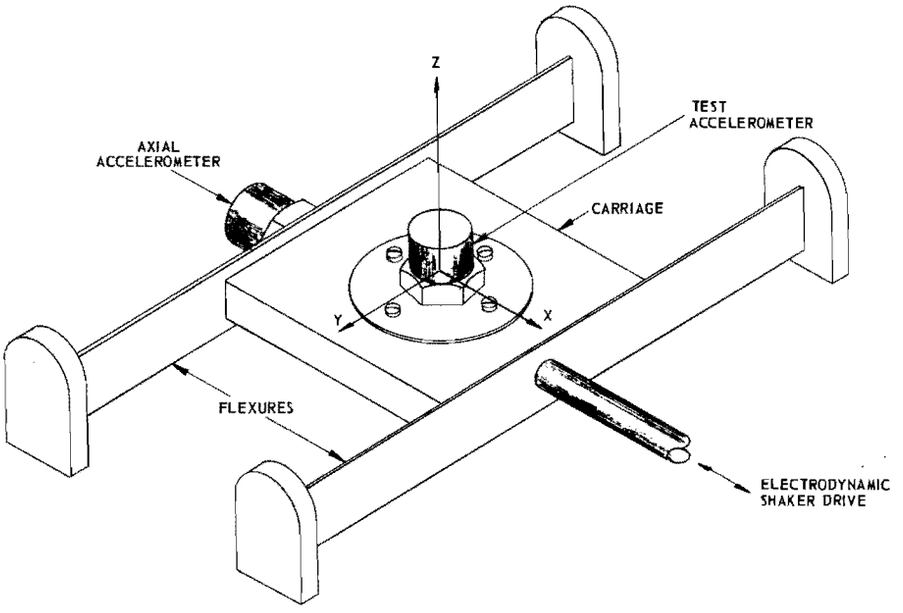

Fig. 14. Resonant carriage employed to generate nearly pure transverse motion

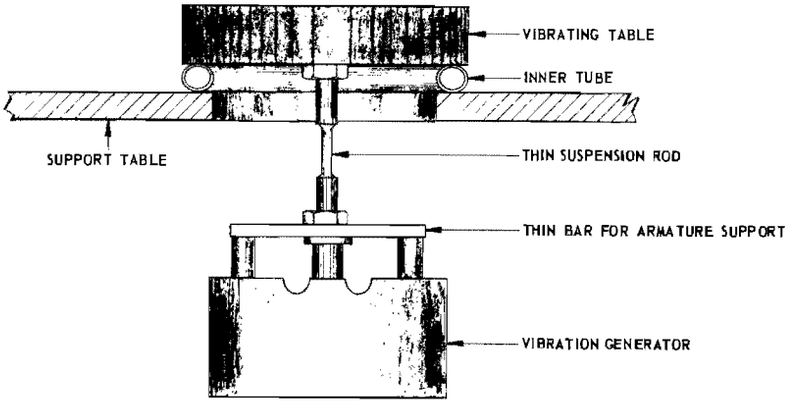

Fig. 15. Arrangement showing a decoupled vibration generator and inertial vibrator table

together with the decoupled shaker, tend to act as a mechanical filter above its spring-mass resonance (reported to be approximately 10 Hz). Other similar arrangements have been used to extend useful frequency ranges to 10 kHz.

This equipment has the advantage of not being limited to a single frequency, as were the two previously discussed schemes; however, transverse motion in the order of 1 percent or so still exists, and therefore can produce errors, if vector solutions are not employed.

Anchored Beam

Figure 16 shows an arrangement where a relatively long beam is anchored at one end, and the other driven by a small shaker. It is very stiff in the horizontal direction, yet relatively easy to drive vertically at the free end. The fact that the free end is describing an arc usually generates a negligible amount of transverse motion. For example, if the free end of an 18-in. beam were driven at 5 g peak at 100 Hz, the TAR of the rod is approximately 0.003

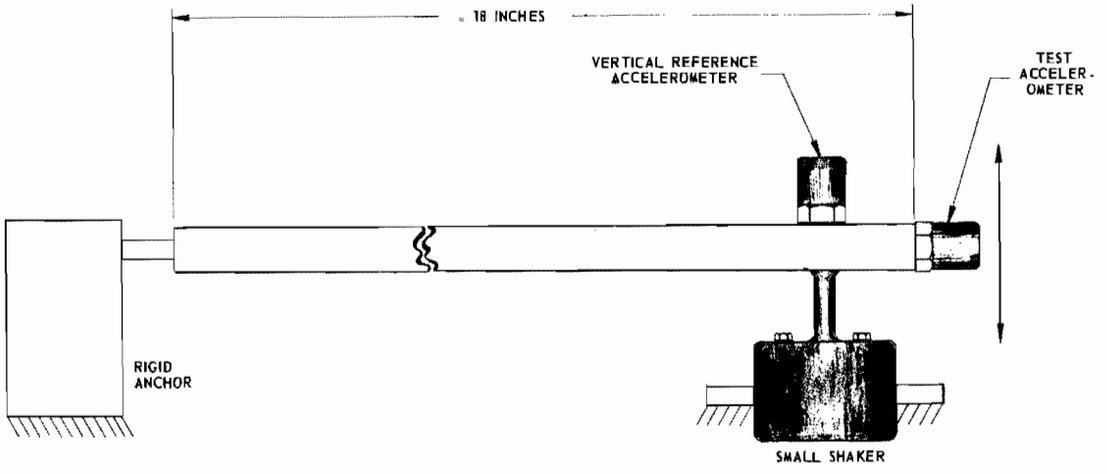

Fig. 16. Radius arm equipment used to generate transverse motion

percent. Errors due to anchor motion, machined angles, etc., will contribute more than this amount. This system can be driven at different frequencies, and like the previous equipment, does not generate ideally pure motion.

Low Frequency Long Stroke Equipment

Long-stroke low-frequency mechanical shakers may be employed to generate rather pure transverse motion (2). They generally operate at a frequency of about 11-20 Hz. The moving carriage is motor driven through an eccentric arrangement, to provide a long stroke (i.e., in the order of an inch or so). By very careful control of the guide and carriage bearings, vertical motion can be controlled to a fairly low value, typically less than about 0.2 percent. For most accelerometers to be tested which have TSR's of 2-5 percent, the effects of the shaker TAR can be neglected. A serious problem which can arise is that of cable whip, which can generate erroneous signals due to the cable noise itself and accelerometer case coupled effects. It has been found that many common accelerometers yield very significant outputs due to these two effects, sometimes 2 or 3 times the actual TSR. This system also is limited to a low and usually single frequency.

VECTOR MEASUREMENT METHODS

The following sections discuss several methods of measuring accelerometer transverse sensitivity which account for impure motion. In all cases, vector solutions are employed.

Phase Magnitude Technique with Axial Rotation

This technique makes use of one set of amplitude and phase measurement data for each of two transducer mounting positions. The two positions differ in that one position of the accelerometer is rotated 180 degrees about its sensitive axis with respect to the other. This technique has some advantages and some disadvantages over the end-to-end rotation technique which will be discussed following this section.

With the test accelerometer mounted in the first position, as shown in Fig. 17(a) (the second position is shown in Fig. 17(b)) and the fixture vibrated at a frequency of $\omega/2\pi$, the output voltage (through a charge amplifier gain H_t) is expressed by Eq. (14). The output of the reference accelerometer is expressed by Eq. (15).

$$v_{o1} = H_t \left[S_z A_x \sin(\omega t + \gamma_x) - S_x A_z \sin \omega t + S_y A_y \sin(\omega t + \gamma_y) \right], \quad (14)$$

$$v_r = H_r \left[S_r A_z \sin(\omega t + \gamma_z) \right]. \quad (15)$$

The angle γ_z in Eq. (15) is generally zero. It is convenient, however, to use the more general case, which could exist if there is a phase difference between the two transducers.

The instrumentation of Fig. 18 is utilized to measure the amplitudes of v_{o1} and v_r and the phase angle (ϕ_1) between the sinusoidal outputs. The voltage vectors are shown in Fig. 19(a), where the magnitudes and phase angles are arbitrarily chosen.

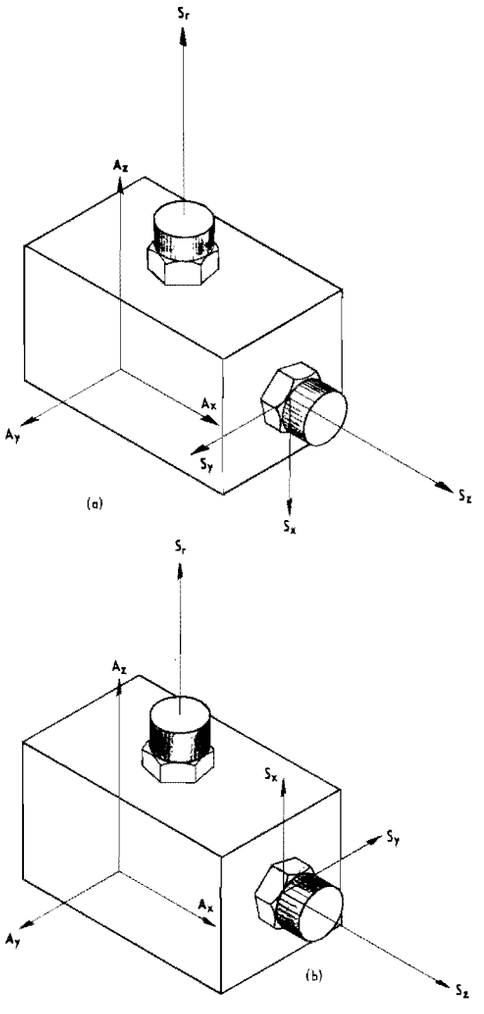

Fig. 17. Phase magnitude technique with axial rotation, (a) position 1, (b) position 2

The test accelerometer is then rotated 180 degrees about its sensitive axis and vibrated at the same level as before. The second position and the associated motion and sensitivity vectors are shown in Fig. 17(b). The transducer output for the second position is expressed by Eq. (16):

$$v_{o2} = H_t \left[S_z A_x \sin(\omega t + \gamma_x) + S_x A_z \sin \omega t - S_y A_y \sin(\omega t + \gamma_y) \right] . \quad (16)$$

The amplitude and phase of the test transducer output are again measured. A vector diagram of the test accelerometer output voltage v_{o2} and phase angle ϕ_2 are again arbitrarily chosen to represent a typical measurement, and are shown by Fig. 19(b).

If v_{o2} in Eq. (16) is subtracted from v_{o1}, Eq. (14), the difference is $v_{o(1-2)}$, as shown in Eq. (17).

$$v_{o(1-2)} = 2H_t \left[-S_x A_z \sin \omega t + S_y A_y \sin(\omega t + \gamma_y) \right] . \quad (17)$$

This subtraction is illustrated on the vector diagram of Fig. 20. The difference vector $V_{o(1-2)}$ can be obtained from the measured voltages and phase relationships by graphical solution, as shown in Fig. 20, or by calculation from the relationship of Eq. (18):

$$V_{o(1-2)} = \frac{1}{2}\sqrt{|V_{o1}|^2 + |V_{o2}|^2 - 2|V_{o1}||V_{o2}| \cos(\phi_2 - \phi_1)} . \quad (18)$$

Considering the two terms of Eq. (17), it is seen that the output voltage is a function of the transverse sensitivities and the major and transverse accelerations. The TSR can be calculated from Eq. (19):

$$\text{TSR} = \frac{V_{o(1-2)}}{S_z A_z H_r} . \quad (19)$$

The graphical solution as shown in Fig. 20 is generally easier than the mathematic solution of Eq. (18).

At present, only preliminary laboratory data have been obtained by use of this technique. Data obtained on an Endevco 2213M5 piezoelectric accelerometer indicated the TSR to be nearly flat up to 2500 Hz (within ±20 percent).

The test fixture is critical and must be fabricated with the accelerometer mounting surface perpendicular to the mounting surface of the shaker. Any deviation, ψ, from this perpendicularity results in an error in TSR of $\tan 2\psi$. The large fixture shown in Fig. 21 has a $\tan 2\psi$ error of 0.0003. Other fixtures are also shown.

Principal advantages of the phase magnitude technique with axial rotation are:

1. The technique is independent of frequency.

2. Motion does not have to be identical in magnitude or phase at different points in the fixture.

3. The shaker does not have to generate "pure" motion.

Principal disadvantages of this technique are:

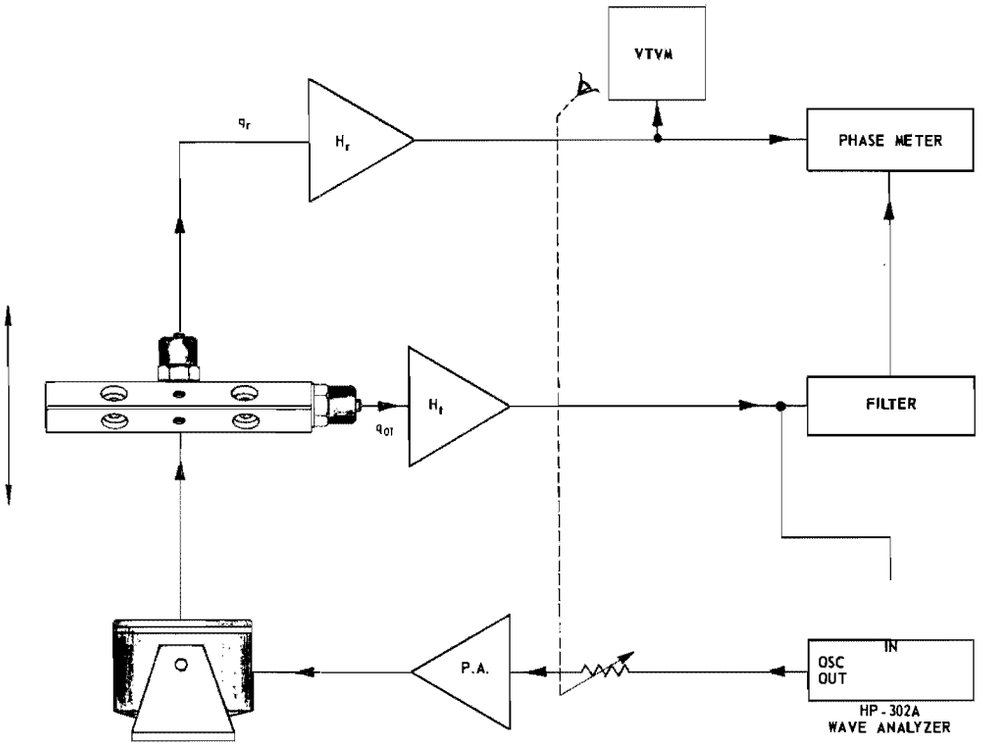

Fig. 18. Block diagram of instrumentation used with phase magnitude technique

1. Transverse motion in the third (Y) direction must be in the order of or less than 5 percent of the major axis motion Z.

2. The test fixture must have a mounting surface for the test accelerometer which is perpendicular to the shaker mounting surface within very close tolerances.

Phase Magnitude Technique with End-to-End Rotation

This technique is very similar in concept to the phase-magnitude method discussed above which used axial rotation. Two sets of measurements are required. The test accelerometer is mounted as shown in Fig. 17(a), and voltage magnitude and phase angle are measured. Next the entire test fixture is rotated 180 degrees, so that the test accelerometer is now on the left side of Fig. 17(a) in such a way that vector S_z is pointing left, S_y is pointing back, and S_x is still pointing down. The first equation for the output voltage, v_{o1}, is the same as Eq. (14), since the identical relative position and the same equipment are used. The second voltage measurement, v_{o2}, is shown by Eq. (20). When Eqs. (14) and (20) are summed, i.e., $v_{o1} + v_{o2}$, Eq. (21) results.

$$v_{o2} = H_t \left[-S_z A_x \sin(\omega t + \gamma_x) - S_x A_z \sin \omega t - S_y A_y \sin(\omega t + \gamma_y) \right], \quad (20)$$

$$v_{o(1+2)} = 2H_t \left[-S_x A_z \sin \omega t \right]. \quad (21)$$

Figures 22(a) and 22(b) show the voltage vectors where the phase and magnitudes have been arbitrarily chosen, but represent typical measurements. An algebraic solution may be obtained from Eq. (22), which is similar to Eqs. (18) and (19):

$$S_x = \frac{1}{2A_z H_t} \sqrt{|V_{o1}|^2 + |V_{o2}|^2 + 2|V_{o1}||V_{o2}| \cos(\phi_2 - \phi_1)}. \quad (22)$$

In the axial rotation method, it was necessary to assume that the output components $S_y A_y$ were small, and generally, this is valid, since the TAR (i.e., A_y/A_z) may be less than 0.05 and the TSR (i.e., S_y/S_z) may be less than 0.05; thus, the product would be less than 0.0025. This would be a worst case condition. In this

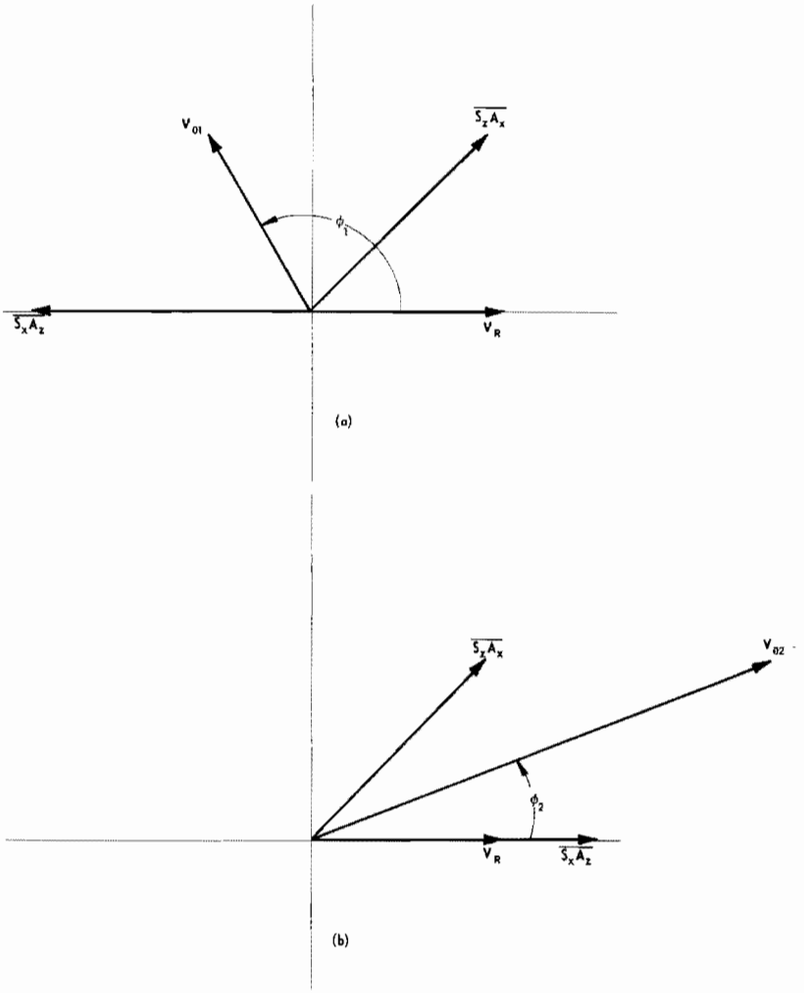

Fig. 19. Vector relationship of voltages generated in phase magnitude technique with axial rotation, (a) position 1, (b) position 2

end-to-end technique, the first measurement has a $+S_yA_y$ component, and the second has a $-S_yA_y$ term, thus assuming that A_y has not changed between measurements, this product sums to zero. This is the principal advantage of the end-to-end rotation technique; that is to say, if the shaker motion is repeatable, the Y axis motion does not enter the measurement results. Tests have shown the validity of the assumption that the shaker motion and phasing is repeatable, so long as balanced loads are employed.

Magnetic Tape Recorder Instrumentation

The two preceding techniques utilize the addition or subtraction of two sinusoidal signals obtained from the same transducer at different times for the measurement of transverse sensitivity. In the previous discussions, an operation is performed at each point by calculation or by graphical means. In theory it is possible to perform this addition or subtraction electronically with the aid of a high quality, multichannel, magnetic tape recorder.

A sinusoidal signal must first be recorded on a control channel of the magnetic tape, while the frequency is slowly swept over the desired spectrum. The control channel is then played back, and the signal used to drive the shaker while the output from the test transducer is recorded on a second channel. The accelerometer is then repositioned by rotating it either 180 degrees axially or end-to-end, depending

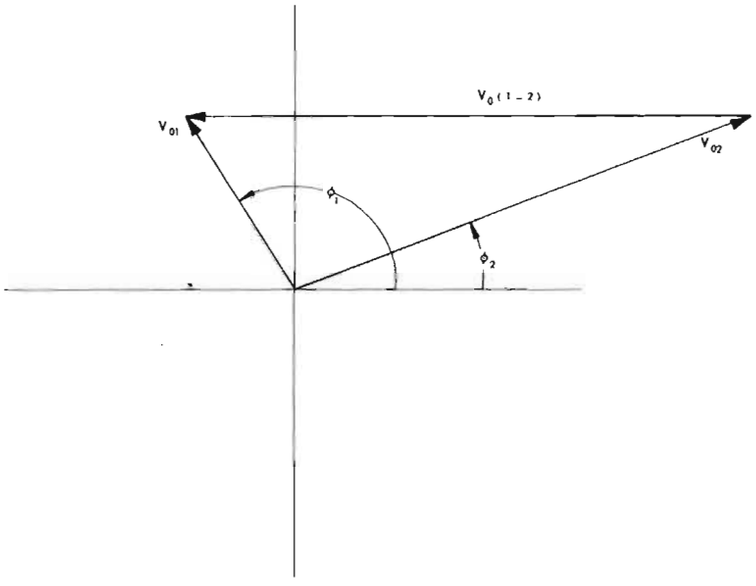

Fig. 20. Vector subtraction — graphical solution

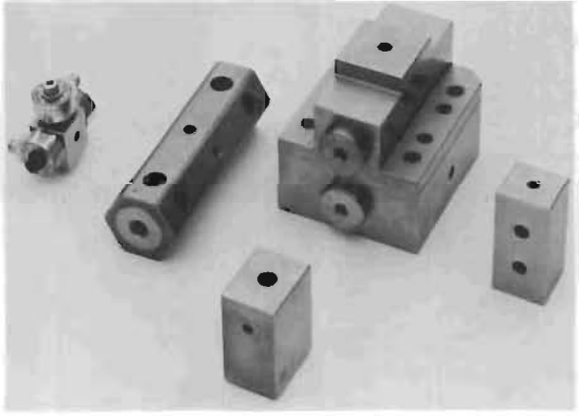

Fig. 21. Test fixtures

on which technique is used. The control channel is played back a second time and used to drive the system again, while the transducer output is recorded on a third channel. Recorder channels 2 and 3 now contain the sinusoidal outputs of the test transducer when mounted in the two positions. These outputs are phase related to the driving signal, and thus to each other. When channels 2 and 3 are played back simultaneously, the two signals can be combined electronically to produce the instantaneous sum or difference required. The result of an instantaneous difference, as required with the axial rotation technique, is a sinusoidal voltage shown by Eq. (17). Similarly, for end-to-end rotation, the instantaneous sum is represented by the sinusoidal voltage of Eq. (21). This ac voltage can be transformed by an ac to dc converter and recorded on an X-Y recorder. By adjusting the ac to dc converter gain and/or the recorder sensitivity to account for the constants and acceleration level, the output can be plotted directly in terms of transverse sensitivity versus frequency. The output can also be plotted as TSR by including the value of S_z in the constants, and adjusting the ac to dc converter gain and/or the recorder sensitivity accordingly.

This method of performing the arithmetic electronically can save a great deal of time, and provides transverse sensitivity information continuously over the entire frequency range. This analog data reduction technique is thus for only a proposed instrumentation approach, and has not been verified in the laboratory, because of lack of a suitable magnetic tape recorder. Foreseeable problems which might exist are static and dynamic skew of the record and playback heads, and repeatability of the phase relationship between the power amplifier input and the transducer output.

TRANSVERSE COMPENSATED ACCELEROMETER AND TECHNIQUE

Accelerometer

An accelerometer has been developed which has a low transverse sensitivity in a specified

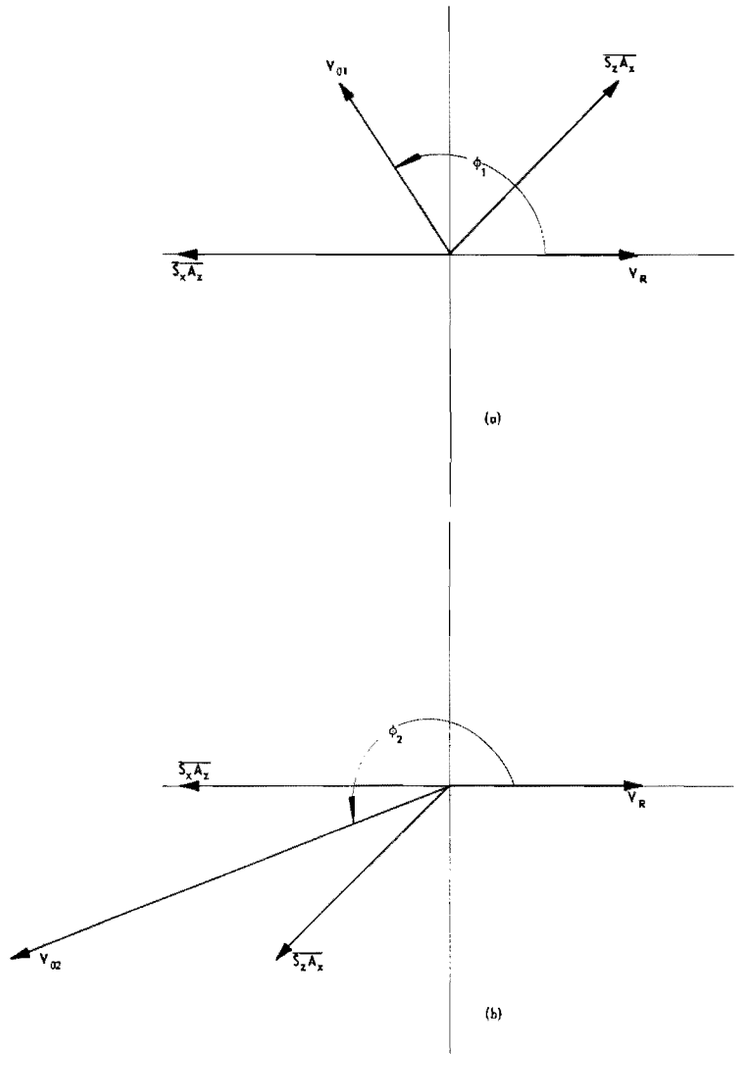

Fig. 22. Vector relationship of voltages generated in phase magnitude technique with end-to-end rotation, (a) position 1, (b) position 2

direction over the frequency range from 20 to 10,000 Hz. It is useful for the measurement of transverse motion of electrodynamic shakers, and can be employed as a tool in the measurement of the transverse sensitivity of unknown accelerometers, as discussed in the next section. The transducer was fabricated from two commercially available piezoelectric accelerometers and a precision stainless steel fixture. In principle, it utilizes the fact that the transverse sensitivity of an accelerometer is a function of the angular rotation about its sensitive axis. As such, one accelerometer is rotated so that its transverse output is equal and opposite to that of the other. The technique and theory is outlined in the four steps below:

1. Two accelerometers of the same type but with opposite axial polarities are employed.* The axial sensitivities are normalized by inserting series capacitance in the more sensitive transducer and adjusting it until both accelerometers have the same charge sensitivity. In the unit developed, the accelerometer sensitivities $S'_{z1} = S_{z2}$ within ± 0.2 percent. For the remainder of this discussion, the normalizing capacitor C_n is considered to be an integral part of accelerometer number 1, and

*Endevco Models 2221D and X2221D, the "X" designating reverse polarity. Available only on special order.

all sensitivities affected are designated with a prime (e.g., S'_{z1}) to indicate the change due to normalization.

2. The two accelerometers can be adjusted for equal sensitivity in the X-transverse direction after being mounted on the precision fixture shown in Fig. 23 (a reference accelerometer is mounted on top the block). Figure 24 shows the various components of sinusoidal acceleration and the accelerometer sensitivity vectors. The charge output of accelerometers 1 and 2 is expressed by Eqs. (23) and (24), respectively:

$$q_1 = -S'_{z1}A_z \sin \omega t + S'_{z1}A_x \sin (\omega t + \gamma_x) + S'_{y1}A_y \sin (\omega t + \gamma_y), \quad (23)$$

$$q_2 = -S_{x2}A_z \sin \omega t + S_{z2}A_x \sin (\omega t + \gamma_x) + S_{y2}A_y \sin (\omega t + \gamma_y). \quad (24)$$

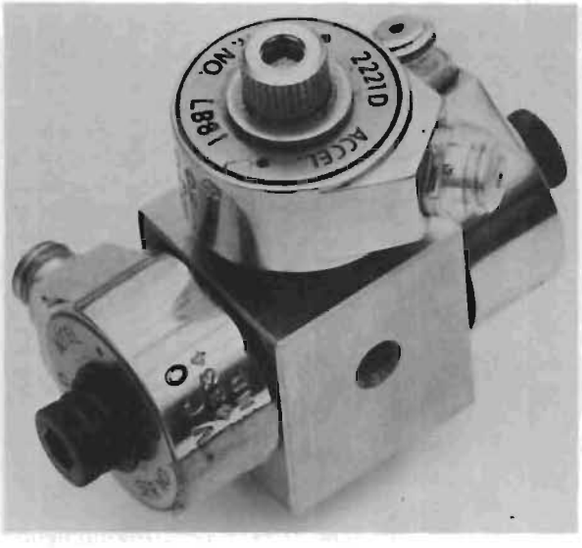

Fig. 23. Transverse compensated accelerometer, fixture, and transducers

With the accelerometers connected as shown in the block diagram of Fig. 25, the output of the differential amplifier is expressed by Eq. (25):

$$v_o = H[q_1 - q_2]. \quad (25)$$

An operating frequency should be chosen where the shaker has less than 1 percent transverse motion, so that $A_z >> A_x$ and $A_z >> A_y$.

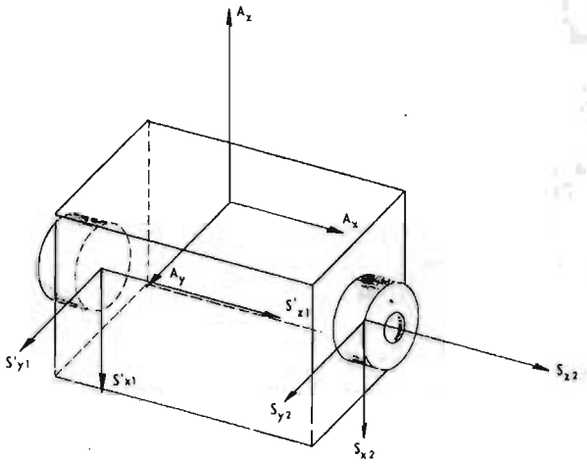

Fig. 24. Sensitivity equalization in the transverse direction

As a result of this inequality, and because $S'_{z1} = S_{z2}$ (from step (1) above), Eq. (25) can be expressed as

$$v_o \approx H\left[(S_{x2} - S'_{x1})\, A_z \sin \omega t\right]. \quad (26)$$

The X-direction sensitivities can be varied by rotating the accelerometers about their sensitive, Z, axes until the voltage monitored on the wave analyzer is minimized, at which point $S'_{x1} = S_{x2}$, as shown by Eq. (26). An intuitive understanding can be obtained from Fig. 24 by observing that if each vector of transducer number 1 is equal to the respective vectors of transducer number 2, the outputs from both transducers are equal in magnitude and phase. In practice, the equalization of all three vector pairs may not be possible, because S_y is related to S_x, as shown in Eq. (12). As mentioned above, the effect of S_y is negligible because of the low value of the product S_yA_y, so that the transducer outputs are nearly equal, regardless of the Y components, and the equalization of the S_x sensitivities may be accomplished.

3. To determine the effectiveness of the compensation and the frequency dependency of the accelerometer pair, the instrumentation shown in Fig. 25 is utilized, and the frequency slowly swept from 40 to 10,000 Hz. The results shown by the curve of Fig. 26 indicates the effectiveness of the compensation for the transducer developed. The deviation from the idealistic zero output results from a combination of Y axis motion and inequality of the two X axes and the two Z axes sensitivities over the frequency range. There are other possible contributing factors, such as angular

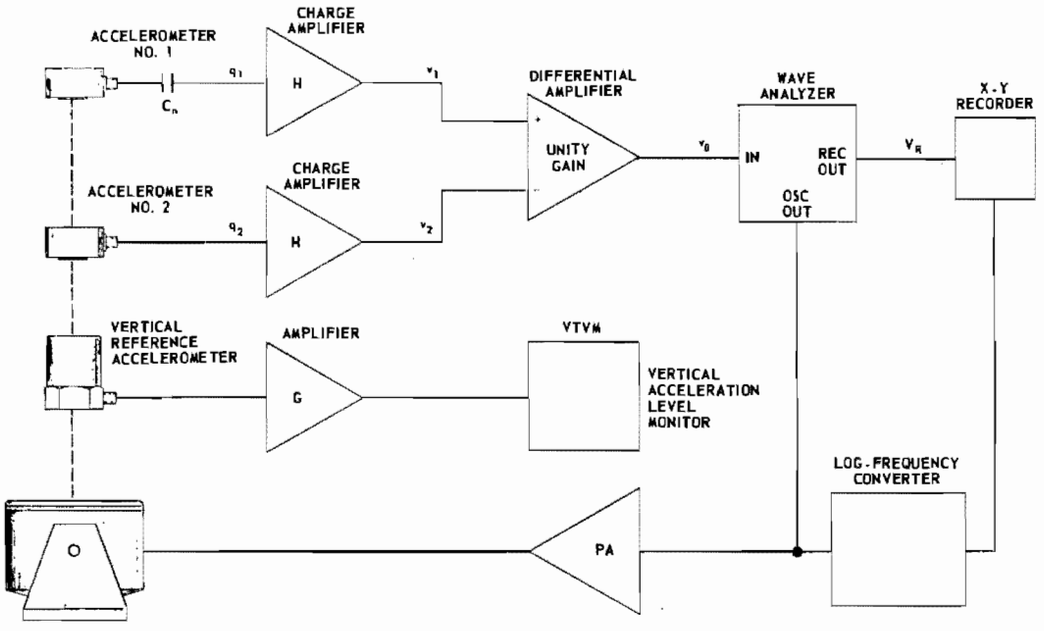

Fig. 25. Block diagram of transverse compensated accelerometer instrumentation

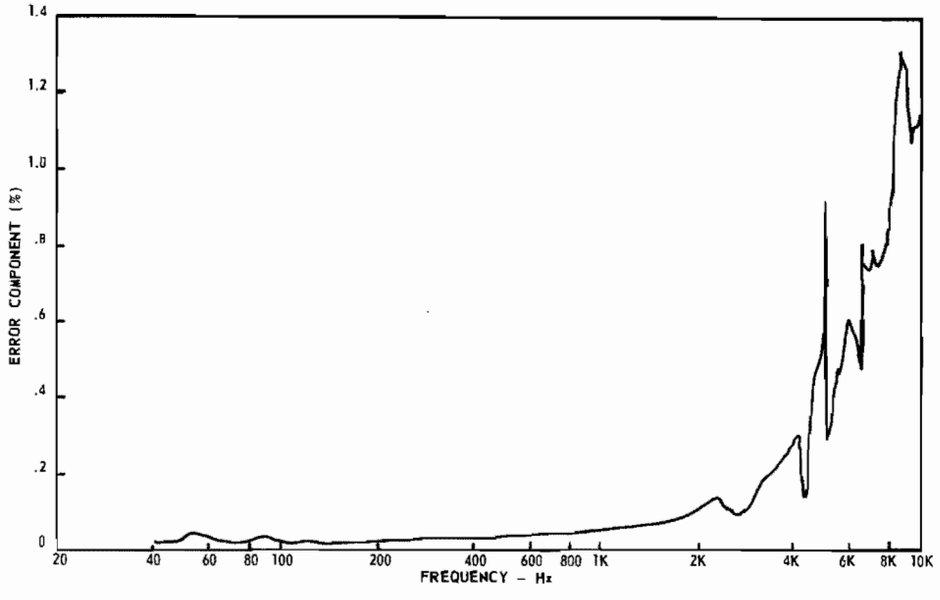

Fig. 26. Error component of transverse compensated accelerometer

accelerations and relative motion between the two accelerometers. However, in view of the relatively small error component present, the assumption that these effects are small appears valid to approximately 2 kHz.

4. To obtain a transverse compensated accelerometer, it is necessary that the sensitivity vectors be combined in a manner such that the S_z vectors add and the S_x vectors subtract or cancel. This is accomplished by rotating one of the accelerometers 180 degrees about its sensitive axis, and combining the two transducer outputs by charge summation of the parallel outputs, as illustrated in Figs. 27 and 28. The result is a transverse compensated accelerometer with sensitivities described by Eqs. (27), (28), and (29):

$$S_z = S_{z1} + S_{z2} , \quad (27)$$

$$S_x = S_{x1} - S_{x2} , \quad (28)$$

$$S_y = S_{y2} - S_{y1} . \quad (29)$$

The value of S_x in Eq. (28) deviates from zero by an error component resulting from imperfect X-axis compensation. This component consists of the error shown in Fig. 27 and an additional error which results from the 180 degree axial rotation. The magnitude of this rotational error, in terms of TSR, is equal to $\tan 2\psi$, where ψ is the angular deviation from true perpendicularity between the mounting surface of the transducer being rotated and the mounting surface of the shaker. The fixture used for the transverse compensated

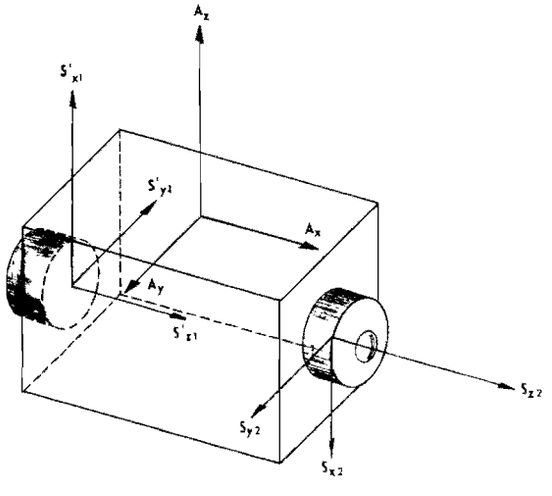

Fig. 27. Vector relationships of transverse compensated accelerometer

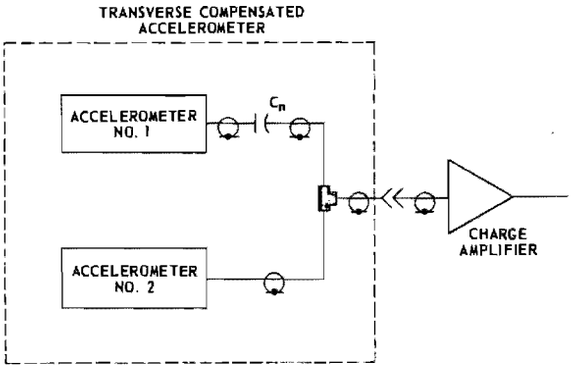

Fig. 28. Transverse compensated accelerometer charge summation

accelerometer has a ψ of approximately 0.012 degree, resulting in a $\tan 2\psi$ error in TSR of approximately 0.0004.

Combining the error component of Fig. 26 and the $\tan 2\delta$ error, the predicted TSR is

<0.001 from 40 to 1000 Hz

<0.01 from 1000 to 8000 Hz

<0.015 from 8000 to 10,000 Hz.

In an effort to confirm the predicted TSR, further testing has been initiated. A complete evaluation has not been performed, but preliminary data indicate the TSR < 0.002 from 40 to 2300 Hz. The chief advantage of the transverse compensated accelerometer is the knowledge of its frequency response over the range from 40 to 10,000 Hz, as shown by the curve of Fig. 26. This curve does not necessarily imply that the transverse sensitivity of either accelerometer is flat over the frequency range. It does, however, show that the two transducers have the same frequency response within the error component shown.

Technique

This technique requires the use of an accelerometer which has a very low transverse sensitivity over the test frequency range. The transverse compensated accelerometer discussed earlier meets the requirements, and is used to cancel that portion of the test transducer output due to unwanted shaker transverse motion. The following paragraphs describe the implementation of this technique.

The test transducer to be measured and the compensated accelerometer are mounted with

sensitive axes (S_z) aligned with the acceleration axis (a_z), and are instrumented as shown in Fig. 29. The charge amplifier outputs (v_t and v_c) can be equalized by adjusting the gains, B_t and B_c, while vibrating both accelerometers at the same level. They are adjusted until the outputs are equal, as evidenced by the differential amplifier output v_o approaching zero within the limit of system noise and relative phase difference. It is important to notice that the differential amplifier is producing an output which is the difference of the instantaneous values of the inputs v_t and v_c. For a zero output, v_t and v_c must be equal in amplitude and phase. Therefore, it is necessary that the two charge amplifiers have near equal phase characteristics over the frequency range of interest. For the equalization process, a frequency should be chosen where the transverse motion of the shaker is low (in the order of 1 percent or less). It is emphasized that the transverse motion need not be this low at all frequencies, just at the frequency of axial sensitivity equalization. Because a_z is much greater than a_x or a_y, and since $v_t = v_c$, the transducer sensitivities are related by Eq. (30),

$$S_{zt} B_t = S_{zc} B_c . \qquad (30)$$

The test and the compensating transducers are then remounted for vibration along the transverse X axis, as shown in Fig. 30. As shown, the compensated accelerometer has its sensitive axis in line with that of the test accelerometer. Since the compensated unit has practically no transverse output in its vertical direction (i.e., less than 0.1 percent), it essentially measures the shaker's lateral motion. This same motion is the source of error in the test unit. By instantaneous differencing the outputs of both transducers (as shown by Fig. 31), the shaker's lateral defect is vectorially subtracted from the output of the test accelerometer. Voltage, v_o, is proportional to the TSR of the test accelerometer. The instrumentation system of Fig. 31 can be utilized to provide an automatic plot of the vector difference output between the test transducer and the compensated accelerometer. The output v_o is shown by Eq. (31), where the sensitivity vectors have been previously defined:

$$v_o = \Big[(S_{zt} B_t - S_{zc} B_c) A_x \sin(\omega t + \gamma_x) - S_{xt} B_t A_z \sin \omega t + (S_{yt} B_t - S_{yc} B_c) A_y \sin(\omega t + \gamma_y)\Big] . \qquad (31)$$

The voltage, v_o, is proportional to the rms value of the instantaneous voltage represented by the term in the brackets. The wave analyzer is used for its very narrow band width centered about the oscillator frequency, thus minimizing noise, pick-up, distortion, etc. The equality of the equation $S_{zt}B_t = S_{zc}B_c$ eliminates the first term in the brackets of Eq. (31), and the result is shown in Eq. (32):

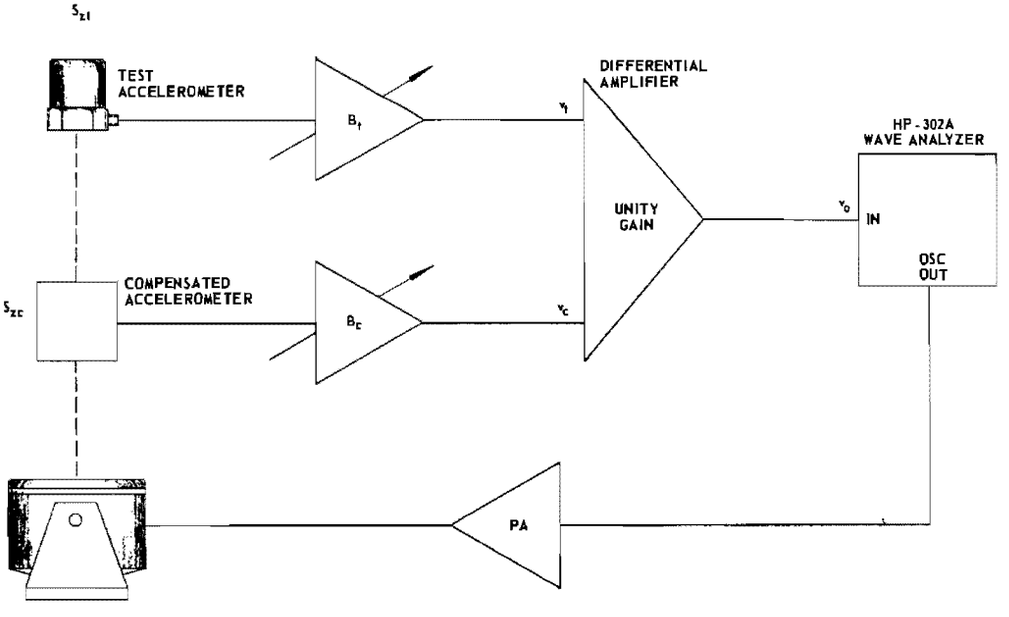

Fig. 29. Block diagram of axial sensitivity equalization instrumentation

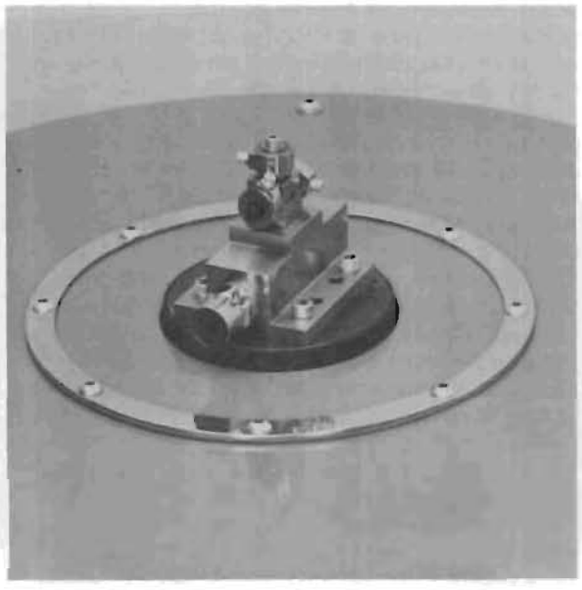

Fig. 30. Test setup using transverse compensated accelerometer

$$v_o = \left[- S_{xt} B_t A_z \sin \omega t + (S_{yt} B_t - S_{yc} B_c) A_y \sin (\omega t + \gamma_y) \right] . \quad (32)$$

For many conditions of operation, the second term in the brackets of Eq. (32) can be neglected, and the result expressed by Eq. (33):

$$v_o \approx B_t S_{xt} A_z \sin \omega t . \quad (33)$$

The assumption that this term can be neglected is valid when the transverse motion in the Y direction is insignificant. Generally speaking, the Y axis components may be neglected, if the transverse acceleration A_y is less than 10 percent of A_z. This places a restriction on the transverse motion characteristics of the shaker which is far more liberal (by about an order or two of magnitude) than that imposed by conventional methods assuming unilateral motion. Equation (34) shows that the wave analyzer output, V_w, contains the desired transverse sensitivity information S_{xt}:

$$V_w \approx K_2 B_t S_{xt} A_z . \quad (34)$$

If the transducer is vibrated at a constant known level of sinusoidal acceleration (A_z) as the frequency is swept over the range, a voltage can be plotted on an X-Y recorder which is proportional to S_{xt} (transverse sensitivity of the test transducer in the X direction). The combined constants of Eq. (34) are easily determined by a system measurement. This is most easily accomplished after the Z-axis sensitivity equalization, but while the accelerometer is still mounted with its sensitive axis aligned with the shaker axis. In this position,

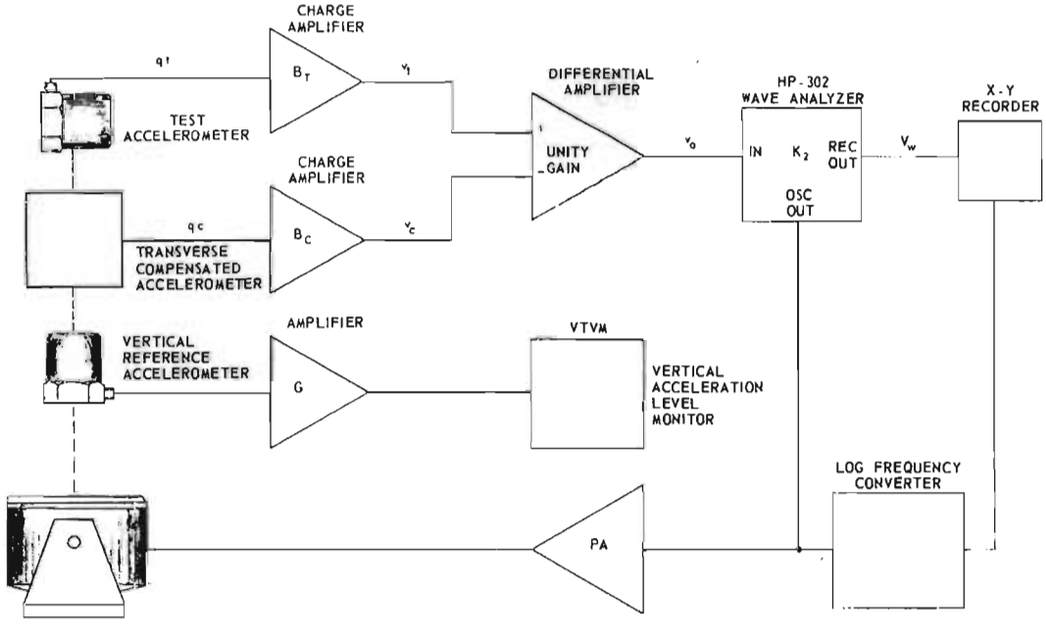

Fig. 31. Block diagram of transverse sensitivity measurement instrumentation

the circuit of Fig. 31 is utilized, but with the compensating accelerometer disconnected. The Y-axis recorder input is then expressed by Eq. (35). In accordance with common practice when performing sensitive axis measurements, the products of transverse motion and sensitivity are neglected. If the transducer is vibrated at the same acceleration level used for transverse measurement, the output voltage V_w represents 100 percent TSR.

$$V'_w = K_2 B_t S_{zt} A_z . \quad (35)$$

Dividing Eq. (34) by Eq. (35) yields the relationship in Eq. (36), which gives a voltage ratio that is equal to the TSR:

$$\frac{V_w}{V'_w} = \frac{S_{xt}}{S_{zt}} = \text{TSR} . \quad (36)$$

It should be noticed that the usually troublesome $S_z A_x$ product, discussed earlier, has been eliminated from the results. There is the restriction on the Y direction transverse motion previously mentioned; however, it is relatively liberal, and can be met by most good shakers with the exception of a few resonant points. Another assumption is that both the test and the compensating accelerometers experience the same motion. This is not necessarily true as mechanical resonances are approached, or if angular acceleration is present. The validity of this assumption depends to a great extent upon the test fixture, accelerometers, and shaker used.

As is frequently the case in vibration work, one of the major problems is the test fixture. The fixture needed for this technique has several requirements which complicate its design:

1. The fixture must provide for rotating the test accelerometer about its sensitive axis to determine the transverse sensitivity as a function of angular rotation.

2. The fixture must have an accelerometer mounting surface perpendicular to the shaker mounting surface.* Any deviations from this perpendicularity results in an error in the measured TSR equal to $\tan \psi$.

3. As a unique requirement, the fixture must provide for mounting the compensating accelerometer with its sensitive axis and transverse axis aligned with the test accelerometers respective axis.

4. The motions must be the same in magnitude and phase at both transducers. It is especially important that dynamic mass unbalance does not cause rocking motion, and that resonant frequencies be as high as possible.

The fixtures used with this experiment were previously shown in Fig. 21. Stainless steel (5144F) was used to increase resonant frequencies and minimize deformation. The maximum value of $\tan \psi$ error component for any of the fixtures is less than 0.0004. The fixtures shown produced good results up to about 1000 to 1500 Hz, above which the motion of the two transducers appears to differ. A different concept in fixturing and/or choice of accelerometers will be required for a second generation system capable of higher frequency measurements. A test fixture with an integral accelerometer might provide a partial solution. Examples of test data obtained by this technique are shown in Figs. 32(a) and 32(b). The data of Fig. 32(a) were obtained from a Clevite 2E5 compression type piezoelectric "cement on" accelerometer. The data shown in Fig. 32(b) were obtained on an Endevco 2215C compression type piezoelectric accelerometer. Above 1000 Hz, the transverse sensitivity curves rapidly become unreliable. Both of the curves have perturbations which may be attributed to angular accelerations and Y-axis transverse motion, as well as accelerometer, connector, and cable resonances. In particular, note the large changes in Fig. 32(b) at the lower frequencies. Cable effects become very significant in this region and below. Two different electrodynamic shakers were used to obtain the data shown. These results indicate that for the two accelerometers tested, the frequency response was nearly flat (i.e., ±20 percent of the "midband" TSR) from about 60 to 800 Hz.

One of the chief advantages of this technique is the ability to sweep frequency and avoid laborious and discontinuous point-by-point data. In theory, the technique is useful throughout the frequency range, providing the transverse motion is on the order of 10 percent or less. At present, test fixture and accelerometer problems have been encountered that prevent reliable test data from being taken above about 1 kHz.

SUMMARY

The basic concepts of accelerometer transverse sensitivity measurements were

*Some shakers generate motion parallel to the mounting surface, such as the ITT Model ST-100, or the MicroGee Models 702L, 728L, and 738L. If this is the case, the fixture must be parallel to the shaker's mounting surface.

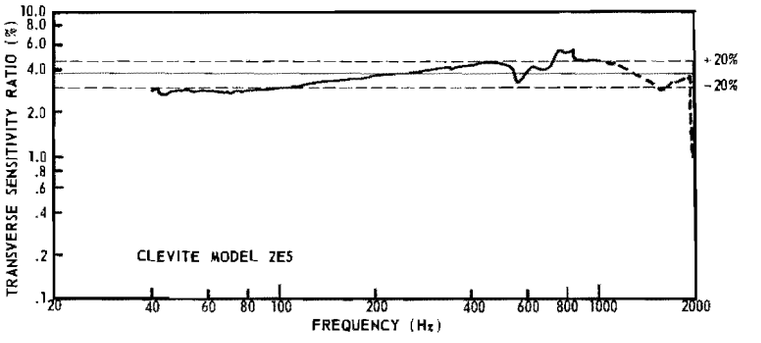

(a)

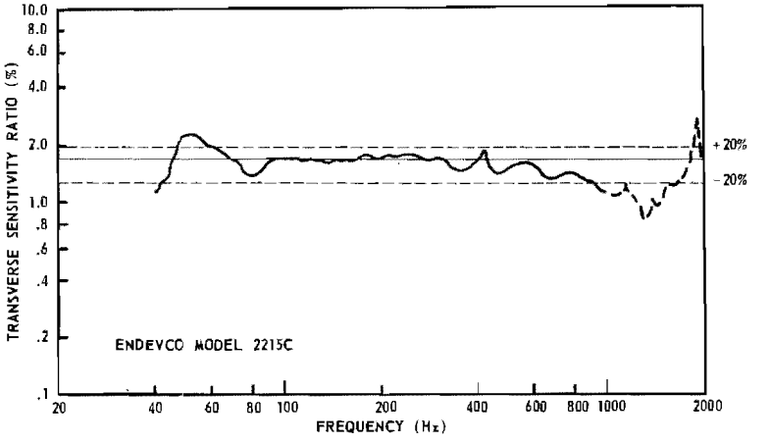

(b)

Fig. 32. Frequency response of transverse sensitivity ratio

discussed, and several techniques were presented which account for undesired components of motion. Their respective advantages, shortcomings, and frequency dependency were discussed. In all cases, where accurate measurements are required, the vector nature of the problem must be examined. In theory, the techniques are independent of frequency. However, practical electronic equipment and fixture limitations impose certain restrictions on the frequency range as a whole. Narrow band filters are required for suitable measurements because the signal level from high quality accelerometers is extremely small when vibrated transversely. Say, for example, that a transducer has an axial sensitivity of 10 mv/g, a maximum TSR of 1 percent, and the acceleration was 10 g. The maximum output voltage from the pickup (assuming pure motion) would be (10 mv/g) (10 g) (1 percent) = 1 mv.

When the transducer is rotated in such a way that the axis of maximum transverse sensitivity is not aligned with the direction of acceleration, the output varies with the cosine of the rotational angle. Thus, when the signal levels are typically less than system noise levels, it is essential that narrow band techniques be employed. This immediately limits the low frequency end, since the bandwidth of the filter becomes more the limiting factor as zero frequency is approached. At higher frequencies, the flexural stiffness, cable, connector, and fixture problems appear as limits.

Measurements as low as 14 Hz, and as high as 10 kHz, were performed; however, because of the mentioned problems (and undoubtedly more), it is felt that reliable results were obtained over a frequency range from about 40 to 2500 Hz, depending on the particular fixture,

accelerometers, cable arrangement, etc. Further refinements are expected to permit measurements at much higher frequencies.

Data taken as a function of frequency on several piezoelectric accelerometers indicate a frequency response flat to within ±20 percent as an arbitrary figure. The deviations from the ideally flat response are not all explained at this time, and are certainly insufficient to permit stating with absolute certainty that the TSR is or is not frequency dependent. It is felt, however, as the measurement confidence increases at the higher and lower frequencies, deviations will be noted.

ACKNOWLEDGMENT

The authors would like to express appreciation for the assistance of Mr. G. E. Null and Mr. C. A. Blanchard in encouraging the project and reviewing the manuscript, respectively. Also, thanks is extended to Mr. Tom Vasquez for the illustrations and to Mrs. Madeline Johnson and Mrs. Mardri Williams for the patience in typing the manuscript.

REFERENCES

1. K. R. Jackman, "Cross-Axis "G" Control in Instrument Linear Vibration," Institute of Environmental Sciences 1965 Proceedings

2. W. Tustin, "Calibration of Vibration Transducers," Metrology Engineering Center, Bureau of Naval Weapons Representative, Pomona, California, 1965, pp. 9-1 to 9-4

3. "A Method of Generating Pure Linear Motion Over an Extended Frequency Range Using Conventional Vibration Generators," Wilcoxon Research Technical Bulletin No. 6

4. J. E. Judd, "Measurement of Motion in Planes Perpendicular to High Level Vibratory Motions," Instrument Society of America Preprint Number 99-NY60, 1960

5. R. R. Bouche, "Ensuring the Accuracy of Shock and Vibration Measurements," Institute of Environmental Sciences 1965 Proceedings

6. R. Tengwall, "Cross Axis Sensitivity of Accelerometers from 10 cps to 2000 cps," Endevco Tech-Data No. 58

7. C. M. Harris and C. E. Crede, Shock and Vibration Handbook (McGraw-Hill, New York), 1961, Vol. 1, pp. 12-18 and 12-20.

8. "American Standard Method for the Calibration of Shock and Vibration Pickups," ASA S2.2-1959

9. Y. I. Iorish and K. R. Tsekhanskii, "Transverse Sensitivity in Nonaligned Piezoceramic Vibration Transducers," Izmeritel 'naya Tekhnika, No. 11, Nov. 1962

* * *

FIRST OCCURRENCE PROBABILITIES FOR EXTREME RANDOM VIBRATION AMPLITUDES

Cory L. Gray
Measurement Analysis Corporation
Los Angeles, California

The problem of a failure caused by the first occurrence of a statistically rare, extreme vibration amplitude is investigated theoretically and partially verified by experiment. Such failures might be associated with the exceedance of an ultimate strength, a preload, or an allowable deflection. Although an exact solution to the problem is unknown, equations which form theoretical bounds are presented. These equations answer the questions: How many times can a particular random vibration be sampled for specific time periods before a critical amplitude will be observed? Or, given an observation period, what is the maximum amplitude that will be reached during that time with specified probability? The theoretical results are shown to compare favorably with analog computer data for the special case of simple, mechanical oscillator response. Finally, it is shown how the analysis can be applied to practical engineering problems.

INTRODUCTION

Many engineering designs are governed by criteria specifying some critical level or amplitude which, if exceeded, will produce unacceptable results. These results might include an intolerable malfunction, or complete failure of the system. Some common examples of such critical amplitudes include: (a) the yield or ultimate strength of material, (b) the force needed to overcome a required preload, and (3) excursions of shock-mounted components which equal the allowed clearances. If the phenomenon of interest is random in nature, the design criteria must be expressed in probabilistic terms. Often in the past, this has been done by assuming a particular amplitude distribution of the phenomenon, usually Gaussian, and selecting some multiple of the standard deviation amplitude, which is statistically unlikely to occur very often. The multiple most often selected seems to be three standard deviations, or 3σ. For normally distributed data, this would amount to a critical level, occurring approximately three-tenths of one percent of the time. However, since even the first occurrence of such a critical amplitude extreme may constitute complete failure, a better way of specifying probabilities is needed. Such a specification would include the effect of time of observation of the phenomenon. This is required, as most random probability distributions imply that arbitrarily large amplitudes will be observed, if the period of observation is infinite.

As developed in this paper, the meaning of the probability-time relationship can be illustrated by the question: How many times on the average can a particular random vibration $x(t)$ be sampled for time periods T before the amplitude will be observed to equal or exceed the level $x = a$? Or, conversely: How high an amplitude (a) would be reached in time T with probability $P_T(a)$? Exact answers to these questions are unknown. It is possible, however, to establish conservative theoretical bounds on the probability, which will have practical application to engineering problems. In the following development, the only initial assumptions are that the vibration under investigation is random and stationary.

ANALYSIS OF EXTREME AMPLITUDE PROBABILITIES

The range of amplitudes to be discussed here includes only those rare extremes which are usually ignored as being too improbable. Nominally, the range extends upward from 3σ.

The first occurrence of a pre-selected amplitude (a) experienced by a random vibration $x(t)$, τ seconds after an arbitrary starting

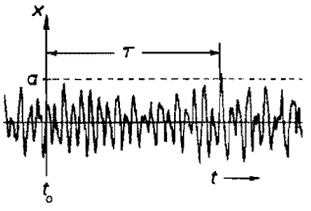

Fig. 1. First occurrence of a given vibration amplitude, following an arbitrary starting time

time t_0, is illustrated by Fig. 1. Note that $x(t)$ may exceed the amplitude (a) after the first level crossing. Thus it is not simply peak value statistics which are needed to describe this failure mechanism. It is desired to estimate the *minimum* time of observation, before $x(t)$ reaches failure amplitude. To do this, it is necessary to know the statistical distribution of the times to a first-level crossing occurrence. This information is not available in exact analytical form for the general case. Therefore, certain simplifying assumptions must be made in order to continue the analysis. First, assume that each exceedance of a given level is an independent event, which is not related to previous exceedances of that level. Then the elapsed time, τ, from an arbitrary starting time t_0 to the first exceedance of the level (a), is a random variable having an exponential, probability density function

$$p_a(\tau) = \lambda e^{-\lambda\tau} . \qquad (1)$$

This is the first crossing probability density function for a Poisson process, and is shown as the curve of Fig. 2.

If the Poisson process is accepted as a model for extreme amplitude occurrences of random vibration, then the probability that the variable $x(t)$ will equal or exceed level (a) in time T is obtained by integrating Eq. (1) from 0 to T. The resulting probability term can be expressed as $P_T(a)$ and would have the form

$$P_T(a) = 1 - e^{-\lambda T} , \qquad (2)$$

where λ in this case would be the average or expected number of crossings of the level (a) with positive slope per unit time, N_a^+.

Substituting this in Eq. (2) above,

$$P_T(a) = 1 - e^{-N_a^+ T} . \qquad (3)$$

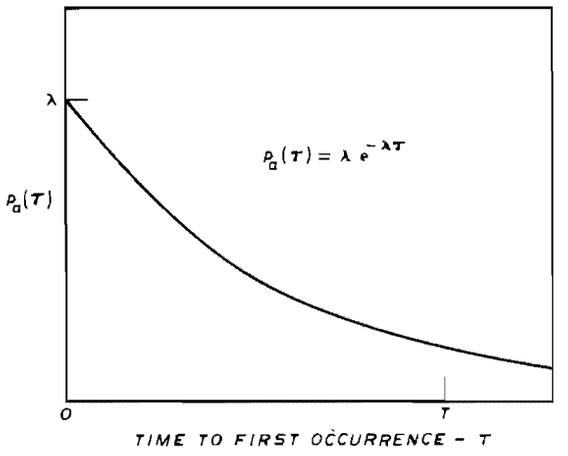

Fig. 2. Probability density function for the time to a first occurrence of x = a, based on independence of events

For small values of probability $P_T(a)$, Eq. (3) is approximated by Eq. (4),

$$P_T(a) = N_a^+ T . \qquad (4)$$

If the vibration is symmetrically distributed about zero mean, and both positive and negative extremes are included as independent events,

$$P_T(a) = 2N_a^+ T . \qquad (5)$$

The simple expression in Eq. (5) has been shown in Ref. 1 to constitute an upper bound on the probability of crossing a positive or negative extreme value (a) in time T, regardless of the assumption of independence of crossing occurrences. This is a highly significant proof, as it shows that any correlation between successive extremes will tend to decrease the probability of such extremes occurring in specific time periods. Equation (5) can then be modified to reflect this bounding condition:

$$P_T(a) \leq 2N_a^+ T , \qquad (6a)$$

$$T \geq \frac{P_T(a)}{2N_a^+} . \qquad (6b)$$

Equation (6) ignores the remote probability that $x(t)$ will be above level (a) at time t_0. This probability can be added directly to the right-hand side of Eq. (6a), if it becomes significiant. For the present analysis, however, the amplitudes being considered are extreme, and this instantaneous probability will usually

be very small compared to $N_a^+ T$. The importance of Eq. (6) is that although an exact analysis of extreme values for engineering problems may not be possible, at least some problems can be bounded.

The main difficulty in applying Eq. (6) to practical problems involves the determination of the expected number of crossings of the level (a) in unit time. N_a^+ may be evaluated either experimentally or analytically. The former method can be approached from the standpoint of two different measured quantities, both of which are difficult to obtain. The analytical method requires prior knowledge of the joint distribution of $x(t)$ and its time derivative $\dot{x}(t)$.

The value of N_a^+ can be measured directly from sampled vibration data by setting a threshold counter at various amplitude levels, and averaging the counts indicating positive level crossings having positive slope over the sample length. The obvious shortcoming of this approach is that several occurrence of the highest level of interest must actually appear in the data sample, in order to average effectively. This would normally require sample lengths which are impractically long. The same drawback applies to the measurement of another function, which can be used to derive N_a^+. This is the joint probability density of the vibration amplitude and its time derivative $p(x, \dot{x})$. By selecting the particular amplitude of interest, the conditional probability density function for the time derivative at that amplitude can be substituted in the following expression from Ref. 2, to obtain the average rate of crossing for positive amplitudes with positive slope:

$$N_a^+ = \int_0^\infty \dot{x} p(a, \dot{x})\, d\dot{x} . \qquad (7)$$

Although employing measured data to evaluate Eq. (7) may be impractical, the required probability function may be idealized with an analytical form. The only really applicable form which has been solved is for stationary Gaussian vibration with zero mean value. Therefore, an analytical approach to the evaluation of N_a^+, for most cases, requires an assumption of data normality.

The joint probability density function for a Gaussian random variable $x(t)$ and its time derivative $\dot{x}(t)$ is given in Ref. 3 as

$$p(x, \dot{x}) = \frac{1}{2\pi\sigma^2} \exp\left[-\left(\frac{x^2}{2\sigma^2} + \frac{\dot{x}^2}{2\sigma^2\,\Omega^2}\right)\right] . \qquad (8)$$

where σ is the rms value of $x(t)$ and Ω is 2π times the expected frequency with which $x(t)$ crosses zero with positive slope N_0^+. For Gaussian vibration with known power spectrum $G(f)$, Ω is given by Ref. 3 as

$$\Omega = 2\pi N_0^+ = 2\pi \left[\frac{\int_0^\infty f^2 G(f)\, df}{\int_0^\infty G(f)\, df}\right]^{1/2} = \frac{\sigma_{\dot{x}}}{\sigma} . \qquad (9)$$

The term $\sigma_{\dot{x}}$ in Eq. (9) is the rms value of the time derivative of $x(t)$. Substituting Eq. (8), with x evaluated at (a), into Eq. (7) and integrating produces

$$N_a^+ = \frac{\Omega}{2\pi} \exp\left(\frac{-a^2}{2\sigma^2}\right) . \qquad (10)$$

Substituting this in turn into Eq. (6a) gives the probability relationship

$$P_T(a) \le \frac{\Omega T}{\pi} \exp\left(\frac{-a^2}{2\sigma^2}\right) , \qquad (11)$$

which is valid for extreme amplitude of Gaussian vibration that are greater than about three times the rms value. Since x is a random variable, x/σ is also, and may be substituted in Eq. (11) to obtain

$$P_T(K) \le \frac{\Omega T}{\pi} \exp\left(\frac{-K^2}{2}\right) ; \quad K = \frac{a}{\sigma} . \qquad (12)$$

The parameter K may be called a dimensionless extreme value. Written another way, Eq. (12) states

$$\Omega T \ge \pi P_T(K) \exp\left(\frac{K^2}{2}\right) . \qquad (13)$$

Three bounding cases of Eq. (13) are plotted in Fig. 3 as K versus ΩT, with $P_T(K)$ as a parameter.

Equations (12) and (13) are both very simple, easy-to-use relationships. Having selected a time period, the upper probability of exceeding given levels can be readily calculated from Eq. (12). Conversely, for a given probability, the minimum time to reach an arbitrary level is obtainable using Eq. (13). So long as the Gaussian assumption is made, all that is required for solution of a problem is the zero crossing rate, the power spectrum of the vibration, or the rms values of $x(t)$ and its time derivative.

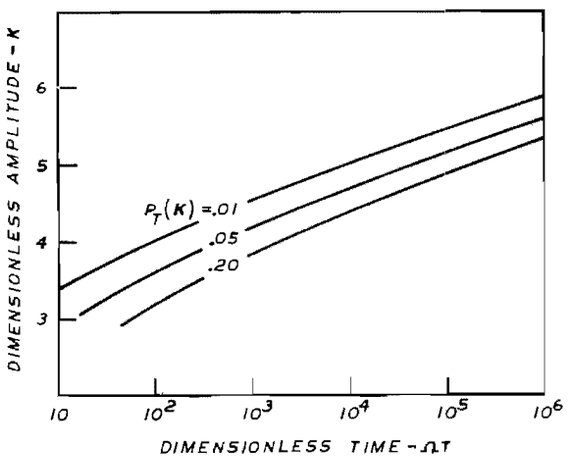

Fig. 3. Maximum amplitude likely to occur during a period of observation, with three levels of probability

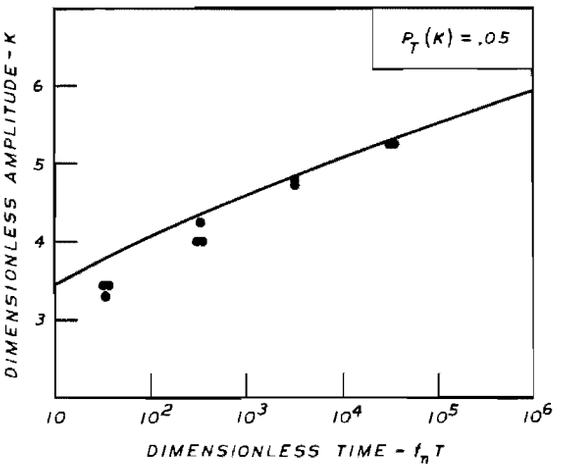

Fig. 4. Comparison of analysis and analog computed data for the case of a simple, mechanical oscillator, with 5 percent probability of exceedance

COMPARISON WITH EXPERIMENTAL RESULTS

Experimental verification of the theories presented above has been reported in Ref. 4 for the special case of a simple, mechanical oscillator. Data were obtained using an analog computer. The velocity response of a narrow band (lightly damped) mechanical oscillator analog, driven by a random forcing function, was observed for periods of time varying in duration from 0.1 to 100 sec. The resonant frequency of the oscillator, f_n, was 2000 rad/sec or 318 cps. System damping was varied over the range 1 to 10 percent of critical. The maximum positive and negative velocity amplitudes for each of 100 trials at each condition were recorded. Sample distributions of these values as multiples of the rms velocity were plotted, and mean curves were drawn through the data. Points were then taken from these mean sample distributions at various levels of probability.

In order to compare Eq. (13) to these data, it is only necessary to evaluate Ω and substitute the proper value of probability $P_T(K)$. In Eq. (9), Ω was defined as 2π times the number of zero crossings with positive slope in unit time. For a lightly damped, mechanical oscillator, the number of zero crossings with positive slope is equal to the frequency of oscillation f_n. Therefore, substituting $\Omega = 2\pi f_n$ in Eq. (13), and rearranging terms,

$$f_n T \geq \frac{1}{2} P_T(K) \exp\left(\frac{K^2}{2}\right). \qquad (14)$$

Figure 4 illustrates the desired comparison for a 5 percent probability of exceeding the dimensionless extreme amplitude K in a dimensionless time of observation $f_n T$.

The continuous curve represents the bounding condition of Eq. (14), and the data points are from the analog study. Vertical scatter in the data points reflect the influence of system damping variation, with the lowest amplitudes generally corresponding to the least damping. Two significant points are brought out by Fig. 4: (a) the Poisson assumption of independence does actually amount to a bound on the minimum observation time (or total number of cycles $f_n T$), prior to a level exceedance, and (b) as the number of cycles increases, and the value of extremes gets higher, extreme amplitude occurrences actually become independent, and the curve becomes a very good prediction tool. The data from Ref. 4 show that these general observations have held true for a wide range of system damping coefficients and exceedance probabilities.

APPLICATION

At this point, it is worthwhile to review the assumptions of the development, in order to understand its applications. The vibration environment under consideration was specified to be random and stationary. Occurrences of extreme amplitudes were assumed to be independent of similar events in either the past or future. The development was restricted to small

probabilities of exceeding any given amplitude, and both positive and negative extremes were considered to occur independently. In order to perform the analysis without measured probability data, the vibration was assumed Gaussian, and extreme amplitudes were considered to be greater than three times the rms vibration level.

These simplifying assumptions would appear to impose severe limitations on the application of extreme value, prediction techniques to practical problems. However, with good engineering judgment, some problem areas can at least be bounded. For example, vehicle vibration during the launch phase of a missile would not be considered stationary, yet it may be important to estimate the maximum probability of a given amplitude extreme. For this application, a Gaussian assumption would be reasonable, as actual deviations in amplitude distribution would usually tend toward a conservative, or lower, probability result than calculated using the Gaussian assumption. The assumption of independence of extreme amplitude occurrences would also tend toward a conservative result, as real vibration data generally exhibit a degree of time correlation between extremes. In the range below four times the rms amplitude, the grouping of extremes renders the independence assumption quite conservative, as was demonstrated by the analog computer study results of Ref. 4 shown in Fig. 4.

To obtain the necessary parameters for an analysis of the missile launch vibration problem, the short time, averaged rms vibration-time history of concern should be recorded. Then, Ω in Eq. (9) may be evaluated by making any of three measurements, (a) zero crossing count, (b) rms value of $\dot{x}(t)$, or (c) power spectrum of $x(t)$. If $\sigma_{\dot{x}}$ is used, the maximum value, likely to occur at liftoff or transonic flight, should be divided by the maximum value of σ the rms of $x(t)$. To use power spectral data, compute the time-averaged, power spectrum over a period which includes the maximum rms vibration. Absolute spectral values are not relevant to the computation of Ω, as the denominator of Eq. (9) is a normalizing factor. Treating the worst case vibration as if it were stationary, Eq. (12) or Eq. (13) can then be employed to predict extreme amplitude behavior in a highly conservative manner for this nonstationary environment.

As a numerical example, assume a spacecraft part responds at a single vibration frequency $f_n = 100$ cps. Further, assume that the maximum rms vibration during the worst part of the launch phase, lasting 5 sec, has been estimated, and a failure criterion has been established at 4.5 times this rms level. Determine the maximum probability of failure of the part.

Substituting the given parameter values into Eq. (12) with $\Omega = 2\pi(100)$,

$$P_T(4.5) \leq 2(100)\,5\,e^{-\frac{20.25}{2}}$$

$$\leq 0.036 .$$

This result indicates that on the average, failure of the part from vibration will occur on fewer than one in twenty-eight launches of the spacecraft.

REFERENCES

1. G. P. Thrall, "Extreme Values of Random Processes in Seakeeping Applications," MAC Report 307-03, prepared under contract Nonr-4305(00) for David Taylor Model Basin, August 1964
2. J. S. Bendat, "Principles and Applications of Random Noise Theory," (John Wiley and Sons, Inc., New York), 1958, p. 125
3. S. O. Rice, "Mathematical Analysis of Random Noise," in Selected Papers on Noise and Stochastic Processes, edited by N. Wax (Dover Publications, Inc.), 1954, p. 192
4. R. L. Barnoski and R. H. MacNeal, "The Peak Response of Simple Mechanical Systems to Random Excitation," CEA Project No. ES 182-6, Technical Rept. prepared by Computer Engineering Associates, Pasadena, California, for Lockheed Missiles and Space Co., Sunnyvale, California, March 1962

DISCUSSION

Mr. Burgwin (Honeywell Inc.): In a practical sense, you did not mention anything about the limitation that your test equipment would put on this. If you have a shaker that can shake so many pounds, a top limit is put on what you get in the probability. I might say though, before we get into this, that at Honeywell we have done very much the same thing that you did and

we have some experimental confirmation. I did some rapid checking and it agrees well with what you have said. In actual vibration testing, however, you are limited by the amount of power you can put into it. This, of course, is multiplied by the Q of the resonance and you are limited in the sigma that you can get, although we have seen some peaks up as high as 10 sigma in a relatively short time.

Mr. Gray: This would often be the case with acceleration because you have the opposite effect. If you have a hard spring or nonlinear excursions, this will have the opposite effect and will tend to increase the tails of the acceleration distribution. I limited what I was saying to stresses or excursions. Nonlinear effects are generally stiffening effects with higher amplitudes. This will have the tendency to limit stresses and excursions, but it will, as you say, increase the accelerations on the tails.

Mr. Burgwin: Without getting into this, we feel that the chance of getting a 3 sigma peak is fairly small. But, if you have a resonant frequency of 100 cps, you can get a 4 sigma peak as often as once a second. I think that agrees with your curve pretty closely.

Mr. Gray: That would not agree with a Gaussian distribution. You have to specify a probability.

Mr. Burgwin: Well, this comes from a probability.

Mr. Gray: Are you saying that on the average they occur about once a second?

Mr. Burgwin: Yes. This agrees with your curve quite well. Assume a particular body that has a resonant frequency of 100 cps. When you figure the probability I think you get a little less than a 4 sigma peak once a second. We have actually experienced this. On a piece of equipment that resonated at a little over 100 cps we were getting approximately a 4 sigma peak about once a second.

* * *

SIGNAL DETECTION USING IMPULSE CROSSCORRELATION

S. W. Marshall, Texas Instruments, Inc.
and
A. C. Keller, White Sands Missile Range

A system has been developed and fabricated which displays the crosscorrelation function of an arbitrary signal with a periodic signal of selectable frequency. Based on the theory that the crosscorrelation function of an extremely noisy signal with a noise-free periodic signal contains no noise, and using the sampling property of the Dirac delta function, the relation

$$\phi_{12}(\tau) = \frac{1}{T_0} \int_{-T_0/2}^{T_0/2} S(t)\ \delta(t + \tau - nT_0)\, dt$$

has been physically implemented.

Requiring a knowledge only of the fundamental frequency of the signal of interest (as obtained through autocorrelation spectrum analysis or other a priori information) the exact waveshape of any periodic signal may be recovered from a total noisy signal. Features of the system include frequency response from 2 cps to 100 kc and signal to noise enhancement of up to 53 db.

INTRODUCTION

In communication theory and many other fields involving the processing of random data, one of the classical problems has been the detection of a periodic signal masked by random noise. Many techniques have been implemented in the past to detect the desired signal including coherent integration, spectrum analysis, autocorrelation, and statistical tests for randomness. Each of these methods has one or more unique features to recommend it, such as versatility, speed, wideband spectrum information, or statistical accuracy. However, none of the aforementioned methods are capable of recovering an entire periodic waveform with complete phasing and amplitudes preserved through an efficient implementation.

Perhaps the most widely understood method of extracting a signal from noise is by autocorrelating it with itself. Although noise will be present in the final autocorrelation function, it will tend to decrease with increasing time delay between signals revealing the desired periodicity. In an analog situation, the advantages of autocorrelation are often overshadowed by the practical difficulty of developing accurate time delays between signals over a wide range of lag times. This problem is also encountered in the crosscorrelating of two arbitrary signals with each other. In the method which shall be developed below, many of the advantages of correlation techniques are preserved, including an additional advantage unique to this method, while the problem of time delay generation is transformed into a simple phase advancement.

The three topics to be presented are; the mathematical derivation of a unit impulse crosscorrelation function, the design of a system to perform the required mathematical operations, and several examples of the application of this system to extremely noisy signals.

THEORY

Crosscorrelation may be considered as a measure of the coherence of one signal with another. In communications systems dealing with periodic signals, crosscorrelation has been used to improve signal to noise ratios. The crosscorrelation function ($\phi_{12}(\tau)$) for periodic signals is defined as

$$\phi_{12}(\tau) = \frac{1}{T} \int_{-T/2}^{T/2} f_1(t)\ f_2(t + \tau)\, dt\,, \qquad (1)$$

where $f(t)$ and $g(t)$ are periodic signals of period T_0, and τ is a shift in time. It is apparent that $\phi_{12}(\tau)$ is the time average value over one period of the product $f(t) \times g(t+\tau)$. Since the time average value of a periodic function averaged over one period is the same as the time average value averaged over two, three or n periods, we can redefine the crosscorrelation function as

$$\phi_{fg}(\tau) = \lim_{T \to \infty} \frac{1}{T} \int_{-T/2}^{T/2} f(t)\, g(t+\tau)\, dt \qquad (2)$$

without changing $\phi_{fg}(\tau)$.

Equation (2) is also useful in determining whether or not two random variables $f(t)$ and $g(t)$ are related. For two independently generated random variables, crosscorrelation results in a constant which is the product of the individual mean values of the two variables. These variables are then said to be incoherent and if either one has a zero mean the crosscorrelation function is zero everywhere. If $\phi_{fg}(\tau)$ is nonzero there is then good reason to believe that $f(t)$ and $g(t)$ are related.

Since Eq. (2) is good for both periodic and random signals, it may be used to advantage when crosscorrelating a periodic signal masked in random noise with another periodic signal. Let $g(t)$ be a periodic noise-free local signal of period T_0 and let

$$f(t) = S(t) + n(T) \qquad (3)$$

where $S(t)$ is a periodic signal of period T_0 which is buried in independent noise $n(t)$. A necessary requirement is

$$\lim_{T \to \infty} \frac{1}{T} \int_{-T/2}^{T/2} n(t)dt = \text{constant}. \qquad (4)$$

For simplicity in this presentation, the constant in Eq. (4) is set equal to zero; that is the average value of the random noise superimposed on the signal is made to be zero.

$$\lim_{T \to \infty} \frac{1}{T} \int_{-T/2}^{T/2} n(t)\, dt = 0 \quad \text{or} \quad \overline{n(t)} = 0 \qquad (5)$$

where the overbar indicates average value. Equation (5) restricts $n(t)$ from having a direct current term, which is not unusual in capacitor-coupled equipment.

Combining Eqs. (2) and (3) yields

$$\begin{aligned}\phi_{fg}(\tau) &= \lim_{T \to \infty} \frac{1}{T} \int_{-T/2}^{T/2} [S(t) + n(t)]\, g(t+\tau)\, dt \\ &= \lim_{T \to \infty} \frac{1}{T} \int_{-T/2}^{T/2} S(t)\, g(t+\tau)\, dt \\ &\quad + \lim_{T \to \infty} \frac{1}{T} \int_{-T/2}^{T/2} n(t)\, g(t+\tau)\, dt \\ &= \phi_{sg}(\tau) + \phi_{ng}(\tau)\,, \end{aligned} \qquad (6)$$

$$\phi_{fg}(\tau) = \overline{S(t)\, g(t+\tau)} + \overline{n(t)\, g(t+\tau)}\,.$$

Since $n(t)$ and $g(t)$ are independent and since $\overline{n(t)} = 0$

$$\begin{aligned}\phi_{fg}(\tau) &= \overline{S(t)\, g(t+\tau)} + \overline{n(t)}\ \overline{g(t+\tau)} \\ &= \overline{S(t)\, g(t+\tau)} \end{aligned} \qquad (7)$$

or going back to the integral form:

$$\phi_{fg}(\tau) = \lim_{T \to \infty} \frac{1}{T} \int_{-T/2}^{T/2} S(t)\, g(t+\tau)\, dt\,. \qquad (8)$$

Using the definition of crosscorrelation, Eq. (8) becomes

$$\phi_{fg}(\tau) = \phi_{sg}(\tau) \quad \text{or} \quad \phi_{ng}(\tau) = 0\,. \qquad (9)$$

Equation (9) states the important result that the crosscorrelation function $\phi_{fg}(\tau)$ of a noisy signal with a noise-free reference signal contains no noise. Practically, the integrations cannot be carried on for an infinite length of time and $\phi_{ng}(\tau) \neq 0$. The usual procedure is to tolerate a certain amount of noise in $\phi_{fg}(\tau)$ in exchange for obtaining $\phi_{fg}(\tau)$ in a finite length of time. For this reason the crosscorrelation function becomes

$$\phi_{fg}(\tau) = \frac{1}{T_1} \int_{-T_{1/2}}^{T_{1/2}} f(t)\, g(t+\tau)\, dt\,, \qquad (10)$$

where T_1 is the length of time necessary for

$$\frac{1}{T_1} \int_{-T_{1/2}}^{T_{1/2}} n(t)\, g(t+\tau)\, dt$$

to become small compared with $\phi_{sg}(\tau)$.

CROSSCORRELATION USING PULSE TECHNIQUES

So far, the only requirement on $g(t)$ is that it be periodic. Now let

$$g(t+\tau) = \delta(t+\tau-nT_0), \tag{11}$$

where $\delta(t+\tau-nT_0)$ is a periodic Dirac delta function or unit impulse function. This function is defined by

$$\int_{nT_0-\tau-\epsilon}^{nT_0-\tau+\epsilon} \delta(t+\tau-nT_0)dt = 1 \quad -\epsilon < t < \epsilon \tag{12}$$
$$= 0 \quad \epsilon < t < -\epsilon.$$

Another well-known relationship for the Dirac delta function is

$$\int_{nT_0-\tau-\epsilon}^{nT_0-\tau+\epsilon} f(t)\,\delta(t+\tau-nT_0)dt = f(nT_0-\tau); \; -\epsilon < t < \epsilon \tag{13}$$
$$= 0 \quad \epsilon < t < -\epsilon.$$

The crosscorrelation of a noisy signal with a unit impulse can be found by combining Eqs. (10), (11), and (13):

$$\phi_{fg}(\tau) = \phi_{sg}(\tau) = \frac{1}{T_1}\int_{-T_1/2}^{T_1/2} S(t)\,\delta(t+\tau-nT_0)dt, \tag{14}$$

$$\phi_{fg}(\tau) = \frac{N}{T_1}\,S(nT_0-\tau); \quad N = \text{No. of pulses in } T_1.$$

Since $S(nT_0-\tau)$ is a periodic function, it may be represented by a Fourier series:

$$S(nT_0-\tau) = \sum_{m=1}^{\infty} [a_m \cos m\omega_0(nT_0-\tau) + b_m \sin m\omega_0(nT_0-\tau)], \tag{15}$$

$$S(nT_0-\tau) = \sum_{m=1}^{\infty} [a_m \cos(2\pi mn - m\omega_0\tau) + b_m \sin(2\pi mn - m\omega_0\tau)].$$

The $2\pi mn$ terms add nothing to the Fourier series since they just represent mn revolutions about the origin. Equation (15) then becomes

$$S(nT_0-\tau) = \sum_{m=1}^{\infty} [a_m \cos(-m\omega_0\tau) + b_m \sin(-m\omega_0\tau)], \tag{16}$$

but $\cos(-X) = \cos(X)$ and $\sin(-X) = -\sin(x)$ so that

$$S(nT_0-\tau) = \sum_{m=1}^{\infty} [a_m \cos(m\omega_0\tau) - b_m \sin(m\omega_0\tau)]$$

$$= \sum_{m=1}^{\infty} [a'_m \cos(m\omega_0\tau) + b'_m \sin(m\omega_0\tau)], \tag{17}$$

and finally,

$$S(nT_0-\tau) = S(\tau). \tag{18}$$

Going back to Eq. (14), the crosscorrelation becomes

$$\phi_{fg}(\tau) = \phi_{sg}(\tau) = \frac{N}{T_1}\,S(\tau); \quad N \cong \frac{T_1}{T_0}. \tag{19}$$

Equation (19) states that the crosscorrelation function for the unit impulse crosscorrelation has the same form as the original periodic signal $S(t)$, except for a slow down in time. As an example, if $S(t)$ is a square wave, $\phi_{fg}(\tau)$ is also a square wave. For crosscorrelation with functions, other than a periodic delta function, Eq. (19) does not necessarily hold.

It is important to note that by using the impulse correlation technique developed above, the entire periodic waveform is recovered from the total noisy signal. Thus, if a pulse train or any other nonsinusoidal periodic signal is present in noise it can be recovered exactly. This must be contrasted with crosscorrelation using, for instance, a sinusoid. In this case only sinusoidal (harmonic) information would be recovered since if the sampling property of the Dirac delta function is not exploited, a crosscorrelation can produce only those signals which are mutually present in both signals.

Another way of viewing the above development is as follows.

It is desired to recover a periodic waveform completely including all unknown harmonic components. To do this through crosscorrelation requires the use of a reference signal which contains all frequencies, since the complete harmonics of the periodicity are unknown and the output of the crosscorrelation process contains only those signals which are present in both functions being correlated. Fortunately the delta function qualifies as the ideal reference signal for this purpose.

EXAMPLE

Crosscorrelate $f(t) = \cos \omega_0 t + n(t)$ with $g(t) = \delta(t - nT_0)$,

$$\phi_{fg}(\tau) = \frac{1}{T_1} \int_{-T_{1/2}}^{T_{1/2}} \cos \omega_0 t \delta(t + \tau - nT_0) dt + \frac{1}{T_1} \int_{-T_{1/2}}^{T_{1/2}} n(t) \delta(t + \tau - nT_0) dt . \quad (20)$$

For T_1 large enough

$$\frac{1}{T_1} \int_{-T_{1/2}}^{T_{1/2}} n(t) \delta(t + \tau - nT_0) dt \cong 0 , \quad (21)$$

and

$$\phi_{fg}(\tau) \cong \frac{1}{T_1} \int_{-T_{1/2}}^{T_{1/2}} \cos \omega_0 t \delta(t + \tau - nT_0) dt , \quad (22)$$

$$\phi_{fg}(\tau) \cong \frac{N}{T_1} \cos \omega_0 (nT_0 - \tau)$$

or

$$\phi_{fg}(\tau) \cong \frac{N}{T_1} \cos (2\pi n - \omega_0 \tau) . \quad (23)$$

Since $2\pi n$ does not add anything and since $\cos(-X) = \cos(X)$ Eq. (23) becomes

$$\phi_{fg}(\tau) \cong \frac{N}{T_1} \cos \omega_0 \tau , \quad (24)$$

but N, which is the total number of pulses occurring in time T_1, is given by

$$N = \frac{T_1}{T_0} . \quad (25)$$

Equation (24) now becomes,

$$\phi_{fg}(\tau) \cong \frac{1}{T_0} \cos \omega_0 \tau . \quad (26)$$

It is apparent that the crosscorrelation function is indeed the same as the original signal and independent of the averaging time T_1. This example is represented in Fig. 1.

DEVELOPMENT OF THE UNIT IMPULSE CROSSCORRELATOR (UIC)

A system which will perform unit impulse crosscorrelation must be able to: (a) generate pulses approximating unit impulses at the proper repetition rate, (b) sweep these pulses past the input signal in a manner corresponding to increasing τ, (c) multiply the swept pulses by the input signal, and (4) form the time average value of this product (see Fig. 2).

Since the system under consideration is required only to extract periodicities from noise and assuming that the fundamental period (T_0) of the desired signal has been previously ascertained, the repetition rate required of the unit impulses is then uniquely determined.

The impulses are derived from a sinusoidal reference of period T_0 which is applied to a Schmitt trigger (Fig. 3). The Schmitt trigger is adjusted to provide a fast rise time positive step for each positive going zero crossover of the reference sinusoid. The step output of the Schmitt trigger is then applied simultaneously to a string of decade counters and to a dual one-shot multivibrator. The dual one-shot produces a negative 3 μsec erase pulse. The positive going trailing edge of this pulse then generates a 3 μsec sample pulse. Erase and sample pulses are applied to a sample and hold circuit (Fig. 4), the third input of which is the noisy signal under analysis.

The multiplication process is simple for unit impulse crosscorrelation. Because of the sampling property of the Dirac delta function the input signal must only be multiplied by zero or one. This is accomplished by sampling the input signal during the 3 μsec sample pulse interval. The value of the signal during the sampling interval is held in a storage capacitor until the next sampling pulse. The holding circuit eliminates the $1/T_0$ coefficient from the crosscorrelation function and produces a flat frequency response.

The cathode follower coupled output of the holding circuit is then integrated using a Philbrick P65 operational amplifier as a standard averaging circuit. This summing integrator has a discharge time constant equal to the charge time constant. A six position switch permits time constant selection of 0.01, 0.1, 0.5, 1.0, 5.0 or 10.0 sec.

The process of sweeping impulses past the input signal as a function of increasing τ is converted to one of providing linear phase variation in the UIC. Prior to sample and erase pulse generation, the reference sinusoid (R_1) is converted into 40 discrete increments in phase as follows:

R_1 is first introduced to a pair of wideband phase shifters producing two output sinusoids

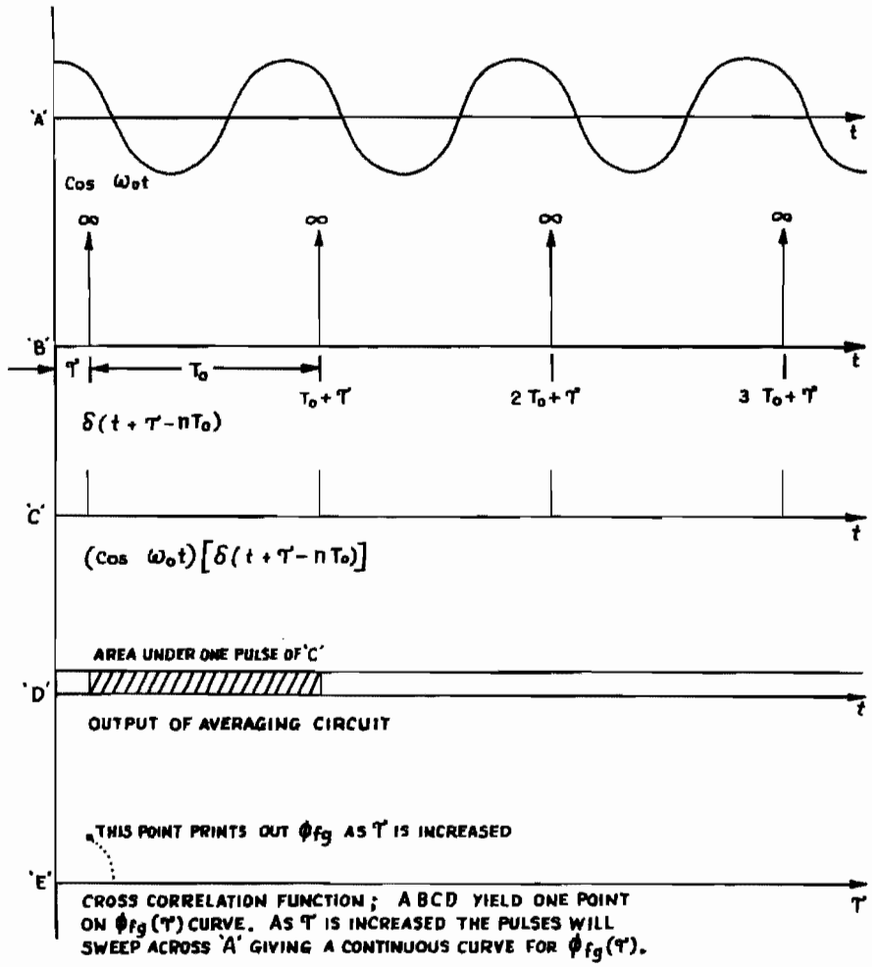

Fig. 1. Graphical interpretation of crosscorrelation using unit impulse techniques

which differ in phase by exactly 90 degrees. These 0° and 90° outputs drive two split load phase inverters which provide 0°, 90°, 180° and 270° reference outputs. The reference outputs are adjusted for equal amplitude and applied to the four quadrants respectively, of a 40 position stepping switch to which have been connected 40 one thousand ohm, 1 percent resistors (Fig. 5). This provides a rotating current in the direction of leading phase around the stepping switch. Each time the stepping switch steps, the phase of the reference output sinusoid moves ahead approximately 9° with respect to R_1. The voltage output of the stepping switch will thus vary from maximum at 0°, 90°, 180° and 270° to 0.707 maximum at 45°, 135°, 225° and 315°.

For example, the first quadrant is shown in Fig. 6. Summing voltages around the periphery yields

$$\sin \omega t = 10\ Ri + \cos \omega t\ , \tag{27}$$

$$i = \frac{1}{(10R)} (\sin \omega t - \cos \omega t)\ , \tag{28}$$

where i is the current through the resistor string. Similarly the potential of the wiper (v) is given by

$$v = \sin \omega t - n Ri\ , \tag{29}$$

where n is the number of 1 k ohm resistors from the 0° reference to an arbitrary wiper position. We then have

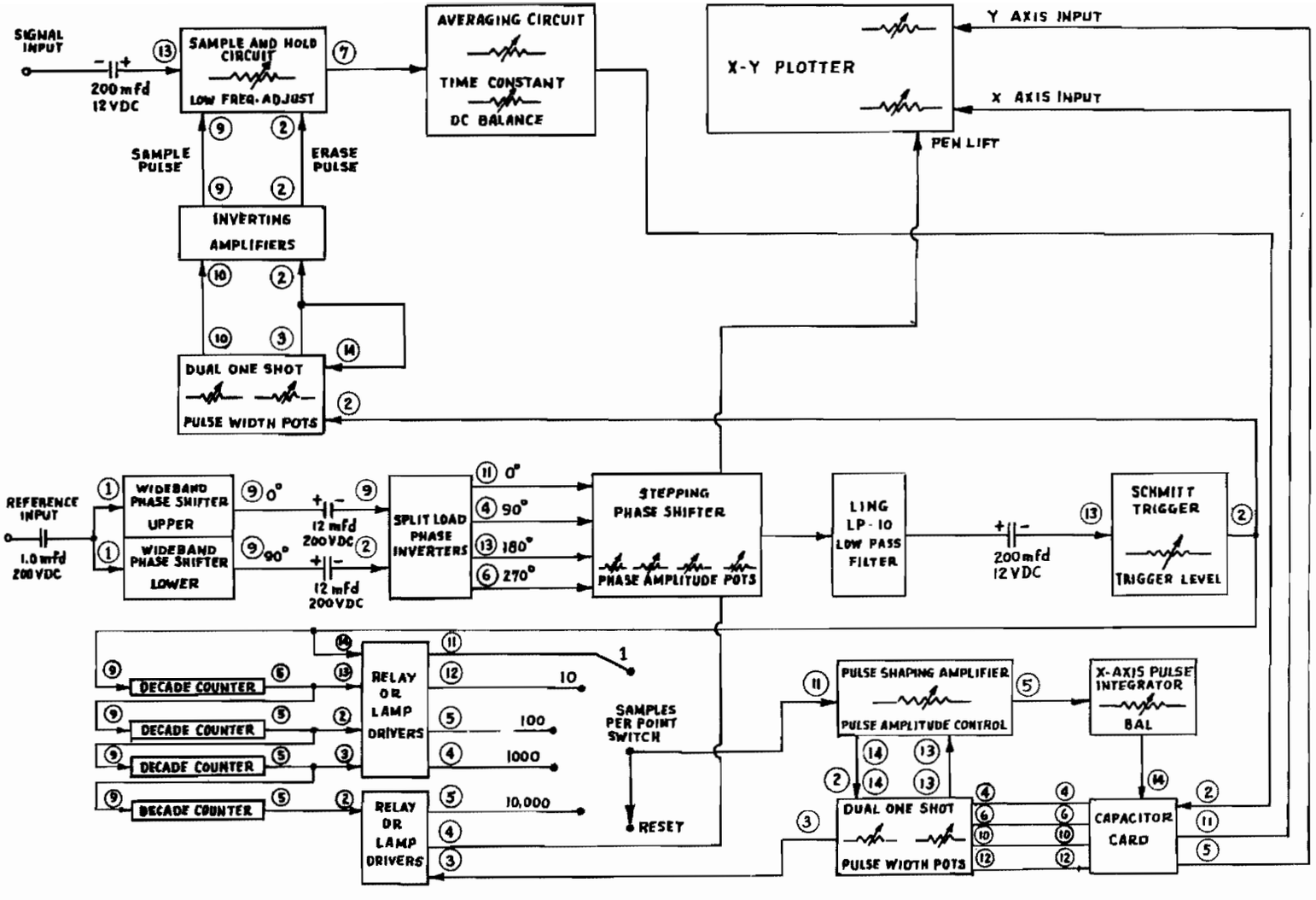

Fig. 2. Block diagram, unit impulse crosscorrelator (UIC)

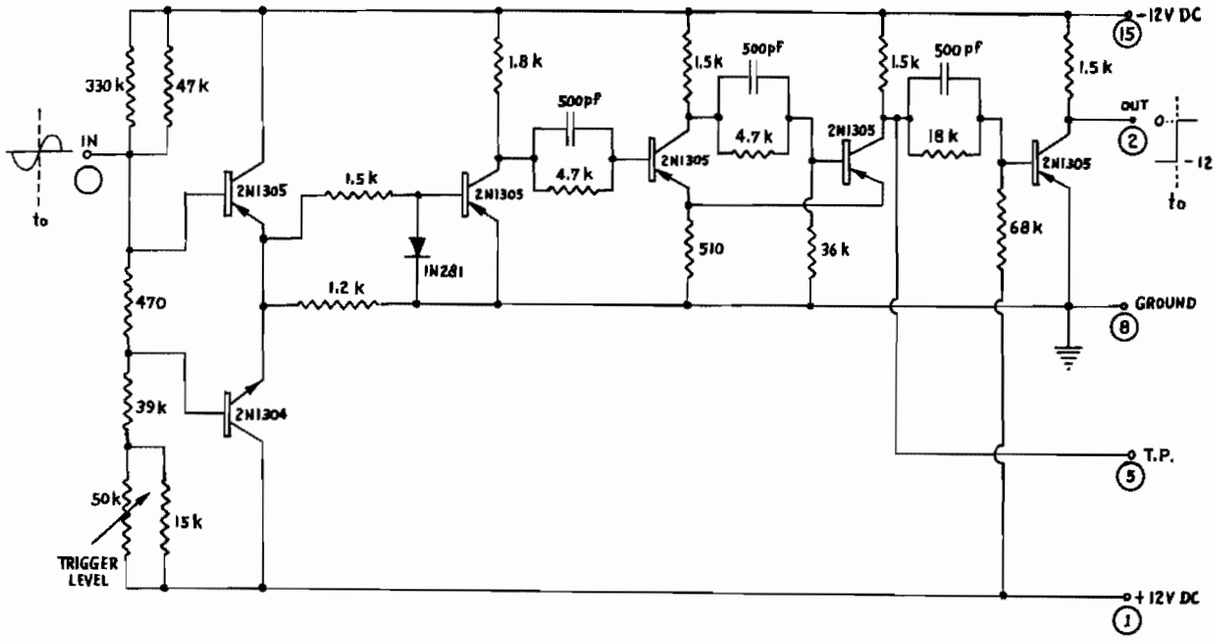

Fig. 3. Schmitt trigger

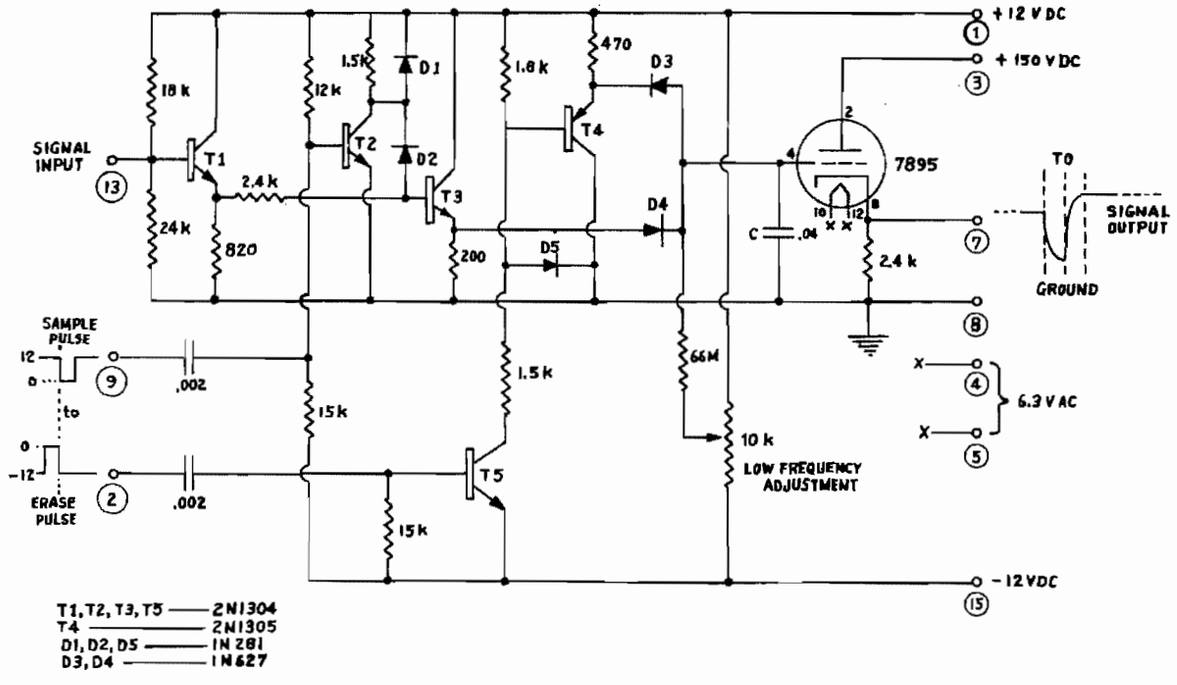

Fig. 4. Sample and hold circuit

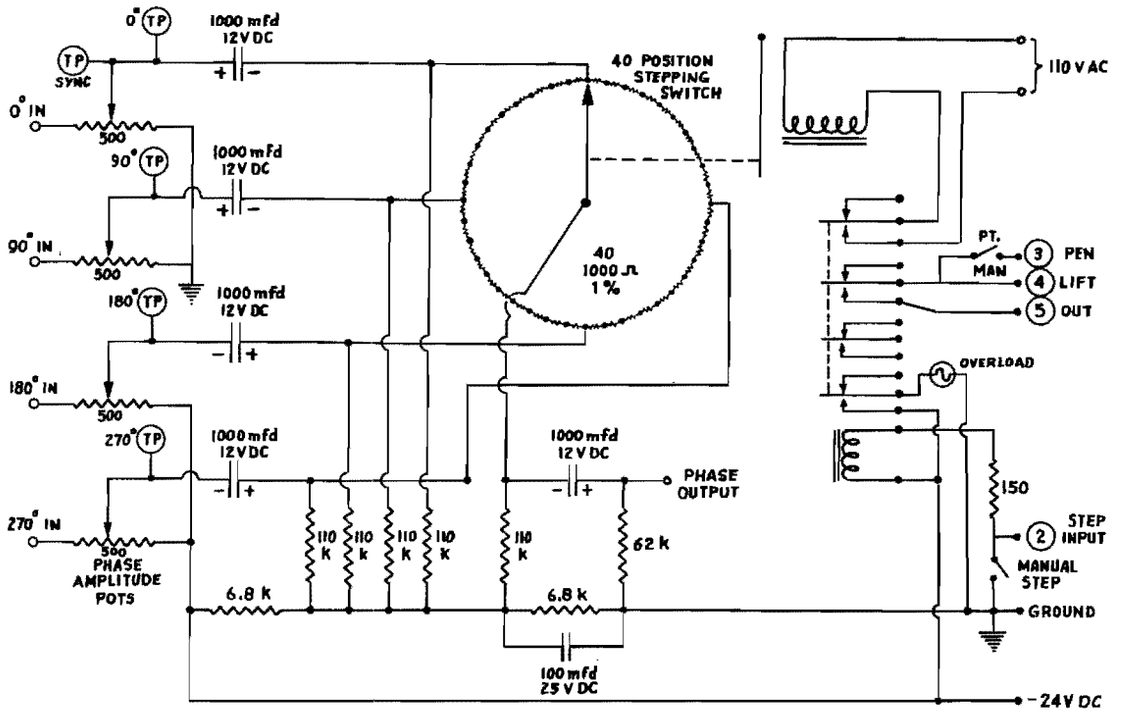

Fig. 5. Stepping phase shifter

$$v = \sin \omega t - \frac{n}{10} (\sin \omega t - \cos \omega t), \quad (30)$$

$$v = \frac{(1-n)}{10} \sin \omega t + \frac{n}{10} \cos \omega t . \quad (31)$$

From the table in Fig. 6, we may note that the maximum phase error introduced is thus approximately four percent in any given quadrant. The effective time delay resolution ($\Delta\tau$) for the stepping phase shifter is

$$\Delta\tau \cong \frac{T_0}{40} = \frac{1}{40f} , \quad (32)$$

and the stepping rate (S.R.) is

$$\text{S.R.} = \frac{F}{\text{No. of samples per point}} , \quad (33)$$

where F and T_0 are the frequency and period respectively, of the reference sinusoid.

The rate at which the stepping switch is actuated is a function of the number of samples which are to be taken and averaged at each of the 40 discrete phase points. This in turn depends on the noise to signal ratio of the data, the averaging time constant selected and the time available for analysis.

The positive going output of the Schmitt trigger which is driven by positive zero crossings of the phase shifted reference signal, is used to derive the erase and sample pulses and is also connected to a string of four decade counters. These counters are used to count up the periods of the reference signal and provide options of 1, 10, 100, 1,000 or 10,000 samples per point of phase. (It should be noted here that although 100 kc logic has been used in this system and the system has been operated to 120 kc, counting rates up to 10,000 only have been employed. Although this produces 10 plotter points per second at a 100 kc reference rate, which is extremely hard on plotters and furnishes little signal enhancement, the system is mainly intended for use below 10 kc. The simple expediency of adding one or two additional decade counters to the present configuration would assure effective enhancement at rates in excess of 100 kc.)

The selected output of the samples per point switch is then shaped and used to drive both the X-axis integrator and the stepping switch of the phase shifter. The pen-lift feature of a standard X-Y recorder has also been included in the system so that either continuous or point plotting of the recovered signal is possible.

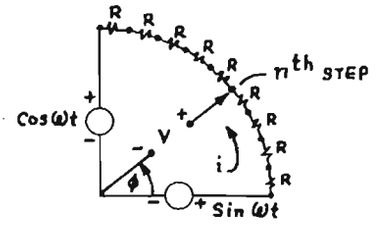

n	0	1	2	3	4	5	6	7	8	9	10
|V|	1	.903	.825	.762	.722	.707	.722	.762	.825	.903	1
ϕ ACTUAL	0°	6.3°	14.2°	23.2°	33.7°	45°	56.3°	66.7°	75.7°	83.6°	90°
ϕ THEORETICAL	0°	9°	18°	27°	36°	45°	54°	63°	72°	81°	90°

Fig. 6. Sample quadrant of phase shifter with actual and theoretical phasors developed

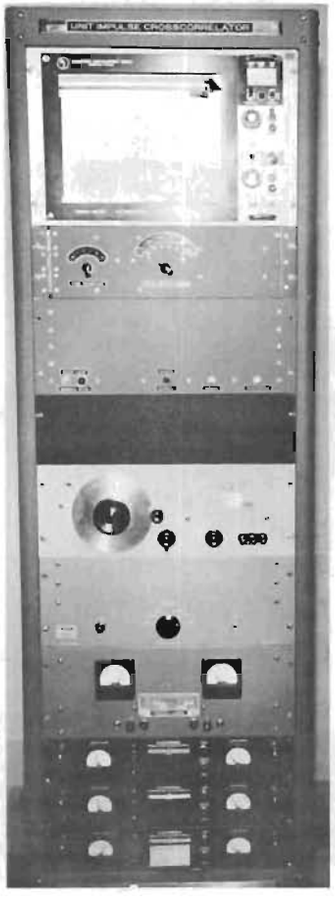

Fig. 7. Front view, UIC

The system which has been fabricated at White Sands Missile Range is shown in Figs. 7 through 10.

APPLICATION OF SYSTEM TO NOISY SIGNALS

The UIC has been applied to the detection of many types of periodicities masked by random noise. Figures 11 through 13 demonstrate the recovery of square, triangle and sine waves respectively, which were initially of a rms value 20 db below the rms value of superimposed 20 kc Gaussian noise. Figure 14 shows a sinusoid recovered from 40 db below an added noise component. The total enhancement in this case is at least 50 db. Figures 15 and 16 display fundamental and third harmonic combinations which were plotted by tuning to the fundamental component. Note that although the spectrum and autocorrelation display for each of these signals is identical, the slight change in phasing of the components produces radically different total signals which are quite conveniently detected through impulse crosscorrelation. The same third harmonic composite was then detected using impulses tuned to the third harmonic. This is displayed in Fig. 17 which indicates the selective filtering accomplished through "harmonic tuning." Here only the third harmonic has been recovered revealing another characteristic of unit impulse crosscorrelation. Namely, that all harmonics of a rate equal to or higher than the reference frequency F_0, will

Fig. 8. Control panel, UIC

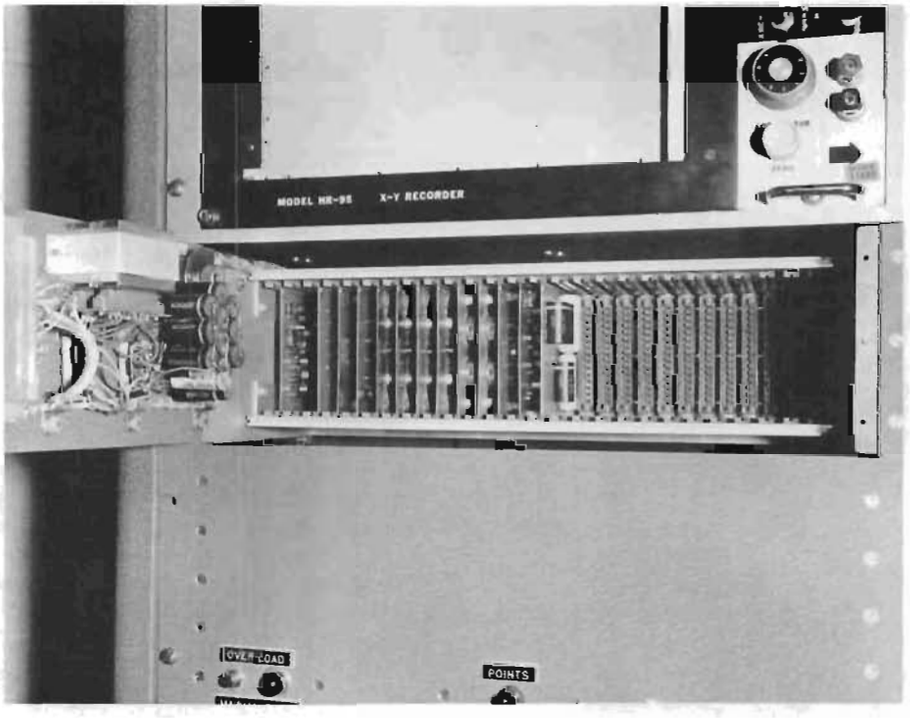

Fig. 9. Logic — front, UIC

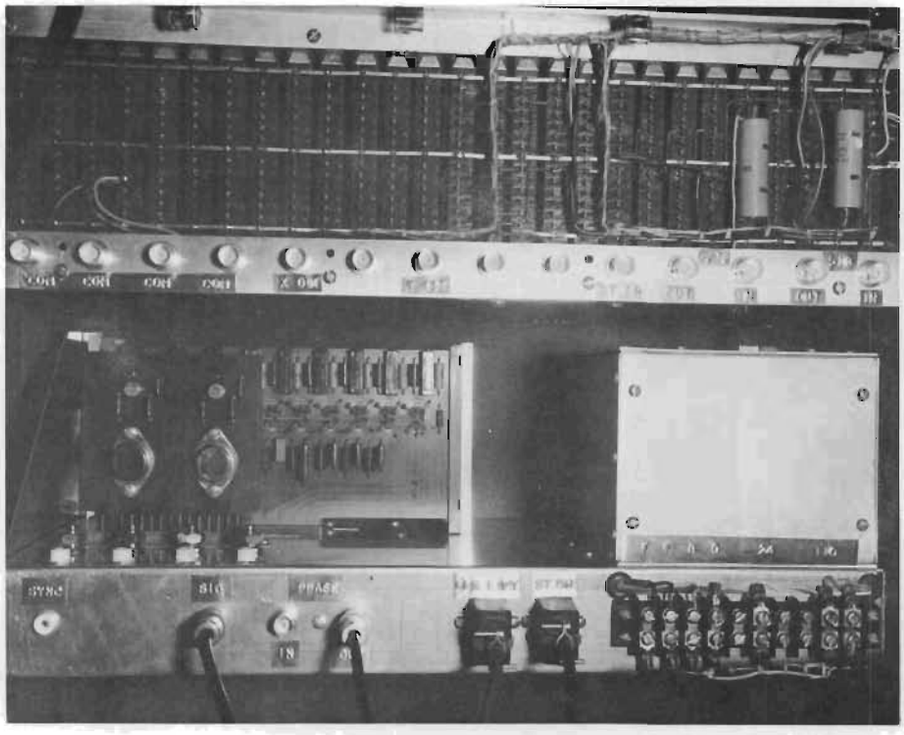

Fig. 10. Phase shifter and rear logic, UIC

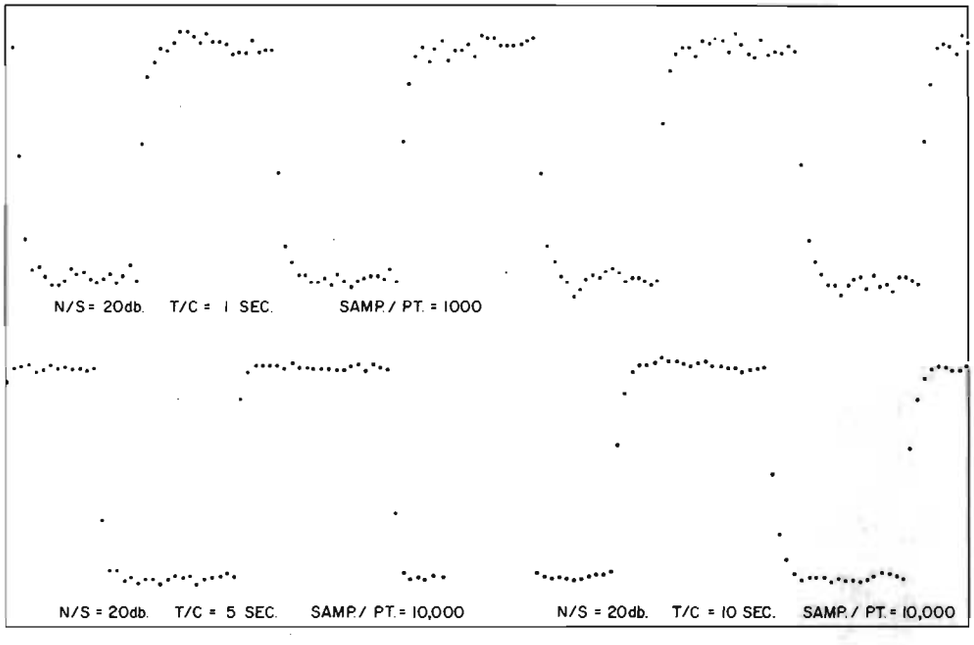

Fig. 11. Recovered square wave 20 db N/S, different time constants

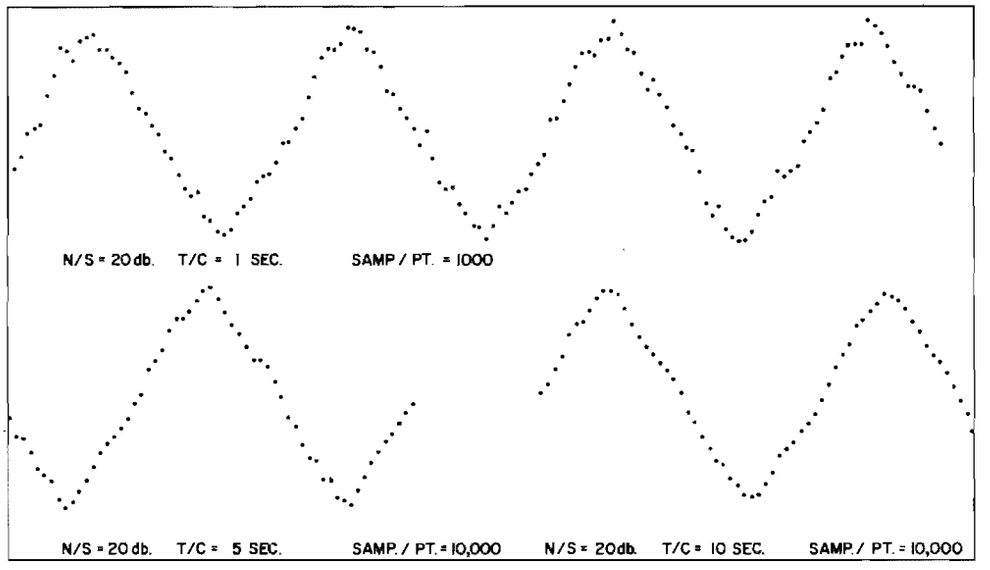

Fig. 12. Recovered triangle wave 20 db N/S, different time constants

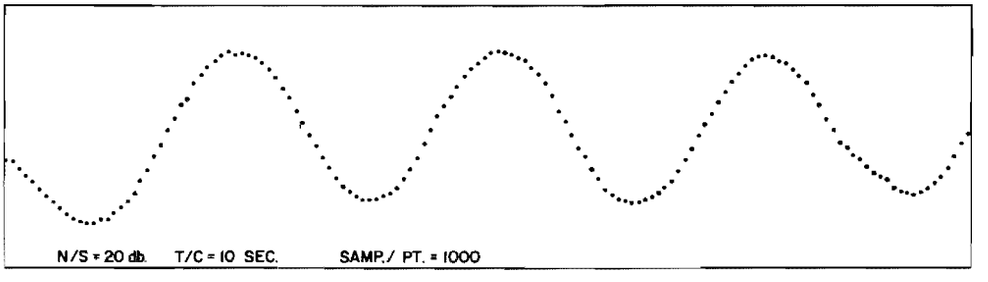

Fig. 13. Recovered sine wave 20 db N/S

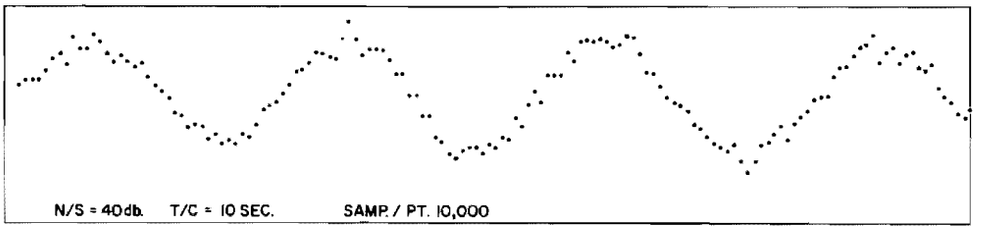

Fig. 14. Recovered sine wave 40 db N/S

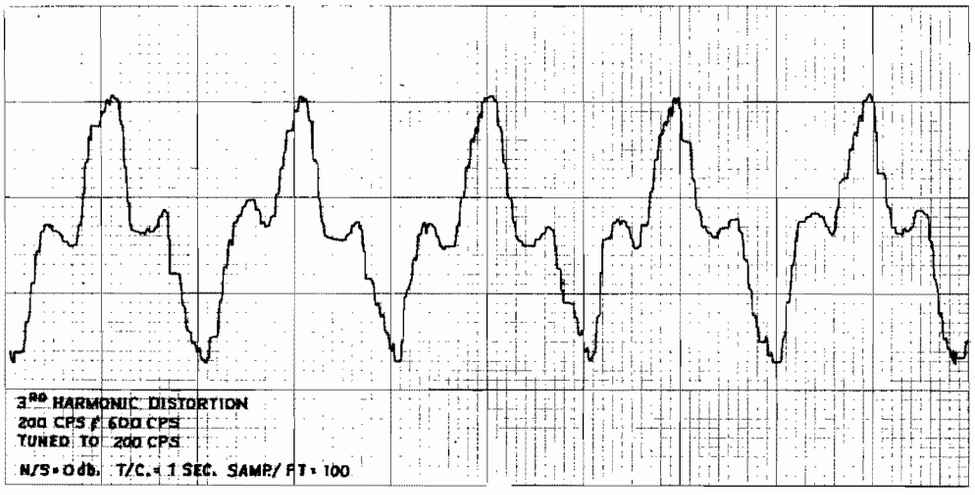

Fig. 15. Recovered third harmonic

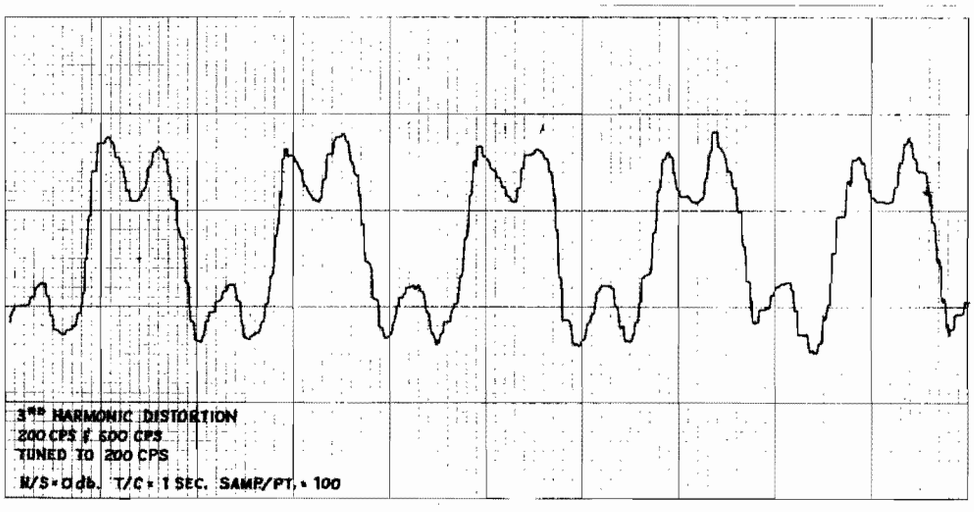

Fig. 16. Recovered third harmonic

be recovered; while all harmonics of frequency lower than F_0, will be discarded. The effective filtering accomplished through this technique is analogous to the "lock-in-bandwidth" of the system which has a selectivity of approximately 1 cps at any frequency.

Figure 18 shows the application of the UIC to an unsymmetrical pulse train. The 40 recovered points correspond to the 40 positions of the stepping phase shifter.

Finally, in Fig. 19, is shown the recovery of a 1/40 duty cycle pulse train which was initially 22 db below the rms value of superimposed noise. Note that with the UIC, since there are 40 points in phase investigated per cycle, pulse trains with duty cycles less than 1/40 would be recovered only intermittently. However, if one were willing to provide enough steps, then theoretically, any duty cycle pulse train is recoverable.

CONCLUSIONS

Based on the fact that the crosscorrelation function of an extremely noisy signal with a noise-free periodic signal contains no noise and using the sampling property of the Dirac delta function the relation

$$\phi_{12} = \frac{1}{T_0} \int_{-T_0/2}^{T_0/2} S(t)\ \delta(t + \tau - nT_0)dt$$

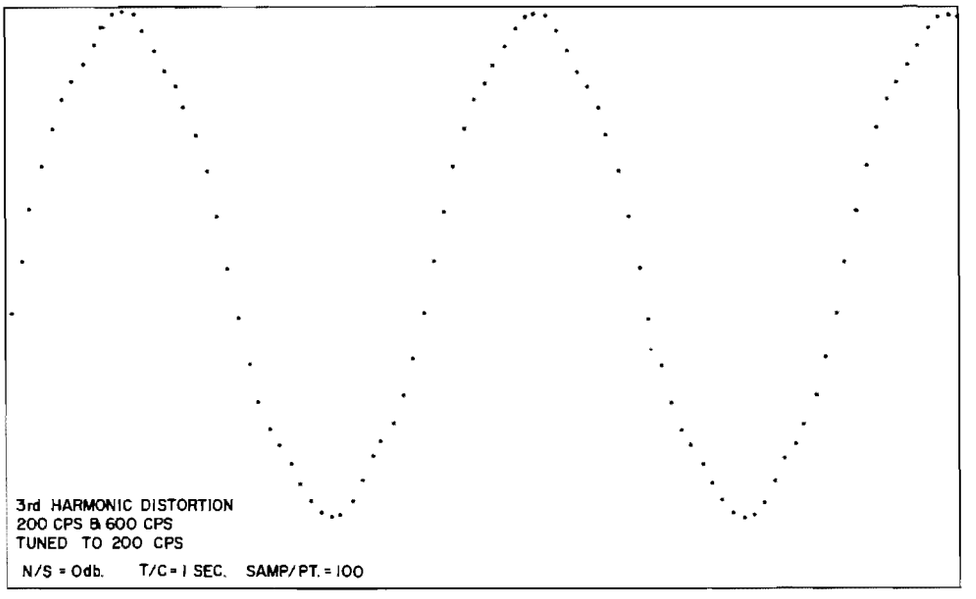

Fig. 17. Recovered fifth harmonic

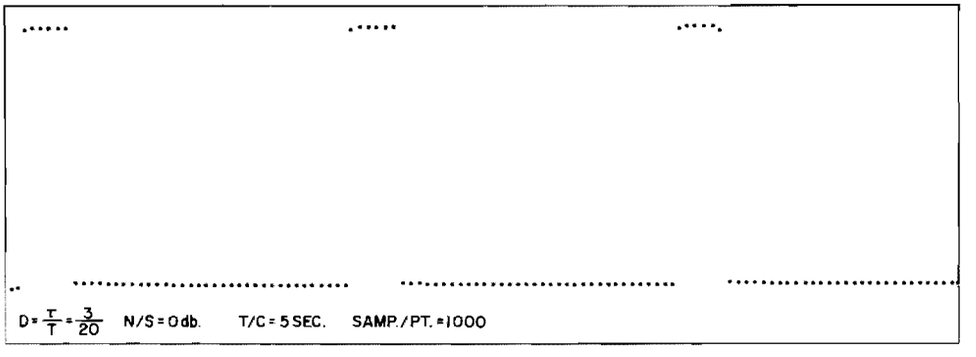

Fig. 18. Recovered pulse train duty cycle = 3/20; N/S = 0 db

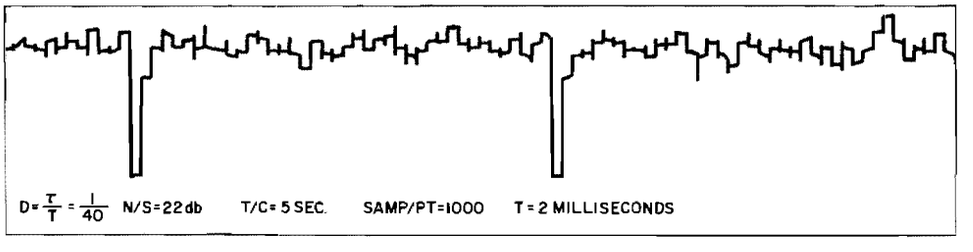

Fig. 19. Recovered pulse train duty cycle = 1/40; N/S = 22 db

has been physically implemented. It has been shown that given only the approximate spectral location of the fundamental of the periodic waveform of interest, the entire periodic waveform can be recovered for display purposes. This is in direct contrast with filtering and coherent integration where only spectrum components are recovered individually; autocorrelation where following suitable time delay generation the correlation function of the periodicity is recovered; or statistical tests where only qualitative information concerning a signal is revealed.

The system which has been designed and built to perform the mathematics involved in Eq. (1) features extremely low cost and operates from 2 cps to 100 kc with an average signal to noise enhancement of 52 db. In addition to displaying the entire periodic waveform, extremely selective high pass filtering can also be performed using the unit impulse technique.

This technique represents an extremely powerful tool for use in signal processing. The method of unit impulse crosscorrelation or variations thereof is the only technique which has been shown to date, to be capable of recovering complete periodic waveforms from an otherwise incoherent signal. In this light it is hoped that further developments in high speed sampling and commutation will only tend to increase the practical usefulness of this strong analytic concept.

BIBLIOGRAPHY

W. B. Davenport, Jr. and W. L. Root, Random Signals and Noise (McGraw-Hill Book Co., New York), 1958

F. J. Farley, Elements of Pulse Circuits (Methuen and Co., Ltd.), London, 1962

Y. W. Lee, Statistical Theory of Communication (John Wiley and Sons, Inc., New York), 1960

Y. W. Lee, T. P. Cheatham, Jr., and J. B. Wisner, "Application of Correlation Analysis to the Detection of Periodic Signals in Noise," Proceedings of the IRE, Oct. 1950, pp. 1165-1171

J. Millman and H. Taub, Pulse and Digital Circuits (McGraw-Hill Book Co., New York), 1956

DISCUSSION

Mr. Lyon (Bolt Beranek & Newman): Can you tell us what the bandwidth of the noise was on the experiment that you described at 50 db enhancement?

Mr. Keller: In the cases shown, the bandwidth of the noise implied was approximately 20 kc.

Mr. Lyon: What was the frequency of the signal?

Mr. Keller: The system has operated from 2 cycles to 120 kc, so the signal was in one of those ranges. Most of the signals I showed were approximately 5 kc in fundamental. The system has recovered 10 kc square waves exactly, with about 53 db signal to noise enhancement.

* * *

A MEANS TO REDUCE RANDOM VIBRATION ANALYSIS TIME

N. Bahringer and R. W. Lochner, Jr.
Honeywell, Inc.
St. Petersburg, Florida

This paper presents results of an investigation to evaluate several techniques by means of which appreciable time savings could be realized during the analysis of random vibration test data. These savings can be accomplished without sacrifice of statistical accuracy. The time required to perform a typical analog, sweep-type, spectrum analysis and the attendant accuracy were used as baselines for comparison.

Initial reductions of analysis time were achieved by performing step analyses by use of an analog analyzer, which provided true integration in lieu of sweep analyses that provide RC averaging. A time saving of 4 to 1 was realized.

Additional significant reductions of analysis time were achieved by manipulating tape recorder speeds. Random vibration data were recorded on magnetic tape at slow speed and played back at a faster speed. An analysis filter was selected that enabled the reduction of analysis time by a factor of 8 to 1, without loss of statistical accuracy.

A combination of the two techniques, step analysis and tape speed changing, provided reductions of analysis time on the order of 32 to 1.

INTRODUCTION

The determination of power spectral-density (PSD) information from vibration data is a time-consuming task because PSD is measured by time averaging, and these measurements must be obtained from long data sample records to be highly accurate. While time averaging makes analog analysis techniques particularly lengthy, most facilities are now using these techniques because they may be performed with relatively inexpensive equipment. Power spectral-density analysis time can be significantly reduced by utilizing high speed analog to digital converters and a digital computer. Unfortunately, such an installation is very expensive.

This paper presents the results of a study at Honeywell Aero-Florida, to investigate various means by which the time required to perform analog PSD analysis might be significantly reduced. A derivation of the PSD function, the statistical relationships involved in the measurement of this function, and the requirements for proper analysis resolution can be found in Ref. (1) and (2). No attempt will be made to derive or prove these relationships in this paper.

PROBLEM

This study was undertaken in conjunction with an inertial measurement unit development program. An inertial measurement unit (IMU), or stable platform, is the sensing unit of an inertial guidance system. Because the platform senses dynamic inputs, the dynamic response characteristics of this unit should be completely defined. The IMU was subjected to a series of random vibration test exposures, and the response at various critical locations was recorded on magnetic tape for analysis.

The basic parameters of the data acquisition/analysis problem were fixed. There were six test exposures, 30 sec duration each. Ten transducer signals were recorded during each exposure. Design analysis had indicated the presence of a resonance (f_r) between 100 cps and 150 cps, with a quality factor (Q) of approximately 12. The characteristics of this resonance were such thay they could adversely affect the performance of the IMU during exposure to vibration. Because platform resonance was of prime importance, the PSD analysis was made between 20 and 200 cps, to

accurately define the dynamic response of the IMU.

The data acquisition/analysis instrumentation at the Honeywell-Aero environmental facility included a fourteen-channel magnetic tape recorder with continuous loop capabilities, as well as record/playback functions at standard Inter-Range Instrumentation Group (IRIG) speeds between 1-7/8 ips and 60 ips. A spectrum analyzer was available with several data filters and time constants, and the capability of performing sweep analyses (RC average) or step analyses (true integration). Prior to this study and to the acquisition of the analyzer, PSD analyses were obtained from the analyzer portion of the random vibration control console, or through the use of a tracking filter, sweep oscillator, and a log converter. The console analyzer incorporated 80 fixed 25-cps bandwidth filters, which provided adequate analyses for equalization of the broad band spectrum, but provided insufficient resolution to define anything as narrow as platform resonance. Therefore, the tracking filter was used for analyses in the area of platform resonance because it had a very narrow bandwidth and good resolution. The time required to perform each analysis, however, was in excess of one and one-half hours. The following discussion presents the parameters to be considered in a PSD analysis, and illustrates the time dependence of an accurate analysis.

DISCUSSION OF ANALYSIS PARAMETERS

Bandwidth

Selection of the proper analysis bandwidth was the first consideration in establishing the analysis parameters. Proper resolution was essential for adequate definition of the shape of resonance.

The proper analysis bandwidth, B, in cps, was determined as follows (1):

$$B \leq \frac{B_r}{4}, \qquad (1)$$

where B_r is the resonance half-power bandwidth, in cps, which is defined as

$$B_r = \frac{f_r}{Q},$$

where

f_r = resonant frequency, in cps, and

Q = quality factor.

Substituting the anticipated platform values:

$$B_r = \frac{100}{12} = 8.4 \text{ cps},$$

and

$$B \leq \frac{8.4}{4} = 2.1 \text{ cps}.$$

That is to say, the maximum practical bandwidth which could be used to define the platform resonance was two cps. Therefore, a two-cps filter was used in all platform PSD analyses.

Standard Error

The second analysis parameter to be considered was that of the minimum standard error (ϵ), which is defined as (1):

$$\epsilon = \frac{1}{\sqrt{BT}}, \qquad (2)$$

where T = the record length (T_r) in seconds.

The standard error defines a confidence interval for the true value of the PSD function, based upon a measured value of PSD. As the standard error is reduced, the interval, or range, of the true PSD function decreases. Equation (2) is presented graphically in Fig. 1, and indicates that small standard errors are associated with large BT products. However, little reduction in the standard error results from selecting a BT product of more than approximately 100. The practical lower limit for the BT product is about 50, because of the exponential increase in standard error with the decreasing BT product.

By substitution of the selected values for B and T in Eq. (2), the minimum standard error was:

$$\epsilon = \frac{1}{\sqrt{BT}} = \frac{1}{\sqrt{2(30)}} = 0.13 \text{ or } 13 \text{ percent}.$$

This was compatible with instrumentation error and the intended end use of the data; however, any significant increase was deemed undesirable.

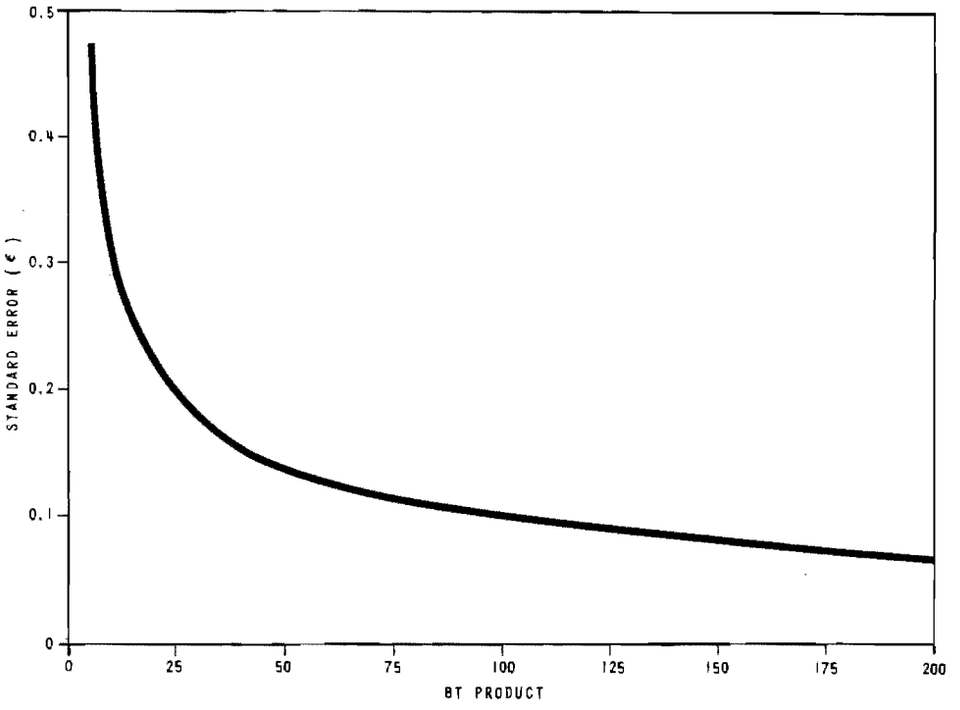

Fig. 1. Standard error versus BT product

Averaging Time Constant

The PSD function is a time-averaged function. Time averaging may be achieved by RC averaging, or by a true averaging (integration) process. The tracking filter performed a sweep analysis with RC averaging. Therefore, selection of the proper RC time constant (K) was essential to an accurate analysis.

The standard error defined by Eq. (2) can only be approached as the RC time constant of the averaging circuit approaches infinity, because an RC circuit never fully responds to an input. Thus, the standard error of a measurement obtained by RC averaging will always be greater than the minimum value indicated by Eq. (2).

This equation can be expressed as:

$$\epsilon = \frac{C_o}{\sqrt{BT_r}}, \qquad (3)$$

where

$$C_o = \frac{\left[\left(\frac{T_r}{2K}\right)\left(1 - e^{\frac{-2T_r}{K}}\right)\right]^{1/2}}{\left(1 - e^{\frac{-T_r}{K}}\right)}, \qquad (4)$$

and $K = RC$.

The coefficient, C_o, is always greater than unity and is the factor by which the standard error is increased over the minimum standard error. Values of C_o for several T_r/K ratios are presented in Table 1.

TABLE 1
Values of Coefficient for Uncertainty Expression (1)

T_r/K	C_o	T_r/K	C_o
0	1.00	3.0	1.28
0.5	1.01	4.0	1.44
1.0	1.04	5.0	1.59
2.0	1.14		

Selection of an RC time constant much larger than the record length is necessary to minimize the standard error. Values for the time constant K between T_r and $T_1/2$ will normally provide a good compromise between the inconsistent requirements of a minimum standard error and a fast analysis. When a range of 70 db is presented on an analysis plot, the difference between a plot obtained with $K = T_r$ and a plot obtained with $K = T_r/2$ could never be resolved. However, if precision analysis is required, with use of an expanded scale, the additional error could become significant. Because this difference is small, an RC time constant equal to $T_r/2$ was used for the majority of the sweep analyses conducted at Honeywell.

Once the time constant has been selected, the actual standard error can be determined, and the determination of sweep rate and analysis time is straightforward.

$$\epsilon = \frac{C_o}{\sqrt{BT_r}} = \frac{1.14}{\sqrt{2(30)}} = 0.147 \text{ or } 14.7 \text{ percent.}$$

Sweep Rate

The required sweep rate (R_s) in cps is given by (1):

$$R_s \leq \frac{B^2}{10}, \tag{5}$$

or

$$R_s \leq \frac{B}{4K} \tag{6}$$

whichever is smaller.

By substitution of the selected values for B and K, the required sweep rate was:

$$R_s \leq \frac{2}{4\left(\frac{30}{2}\right)} \leq 0.033 \text{ cps.}$$

Analysis Time

The time (T_s) in seconds, required to make a complete PSD analysis, was then (1):

$$T_s = \frac{F}{R_s}, \tag{7}$$

where F was the frequency range of the analysis in cps:

$$T_s = \frac{180}{0.033} = 5400 \text{ sec or } 90 \text{ min.}$$

The time required for all 60 analyses then was $60 \times 1.5 = 90$ hours.

Ninety hours for data analysis alone is an overwhelming requirement, and with several such tests conducted each week, the analysis time required soon exceeded the calendar time available.

From the above discussion, it is apparent that any attempt in the selection of the analysis parameters to decrease the time required for a sweep analysis would result in only a modest time savings. This time savings would also result in either an increase in the standard error, a loss of resolution, a reduction in circuit response, or a combination of these.

STEP ANALYSIS (TRUE INTEGRATION)

Time averaging by true integration was then investigated. Compared to RC averaging, it offered some definite advantages. For true integration, the integration time T_a was set equal to T_r. The bandwidth requirements for proper resolution are independent of the analysis method, of the BT product of the analysis was the same in both cases. The standard error was then given by Eq. (2), which was equivalent to the minimum standard error obtainable by an infinitely long RC averaging time constant. The sweep rate for true integration (1):

$$R_s = \frac{B}{T_a} = \frac{2}{30} = 0.0667 \text{ cps.} \tag{8}$$

This was twice the necessary RC averaging sweep rate. The required analysis time was thus reduced to 45 minutes per analysis with a slight reduction in the standard error. The reduction in standard error was certainly desirable. However, an additional reduction in analysis time was also desired.

TAPE RECORDER SPEED

The record/playback process was investigated next to determine what time savings might result from possible changes in its use. One function of the tape machine is to record the vibration data for the PSD analysis. The recorded length of tape contains the complete vibration time history. Any means which presents this data sample to the analyzer faster, without a loss in resolution or accuracy, will also reduce analysis time.

This can be accomplished by increasing the tape playback speed, which decreases the record length T_r in seconds. Referring again to Fig. 1, unless the analysis filter bandwidth is increased proportional to the tape speed increase, the standard error increases exponentially with the smaller BT product.

Considering the characteristics of the platform resonance (f_r and Q), it might appear that a serious loss in resolution would be introduced by this increase in bandwidth. The increased tape speed, however, increases the frequency spectrum of the data proportionally, preserving the original resolution of the data. This is readily apparent in the case of a direct recording of periodic data of a constant frequency. A 100-cps sine signal, played back at a speed 10 times faster than that at which it was recorded, will become a 1 Kc sine signal of the same amplitude.

The advantages of FM techniques in tape recording and playback of vibration data make it the accepted method of recording. An examination of the equation for the frequency modulated signal recorded on tape shows that the frequency spectrum of the data is increased in proportion to the increase in playback speed in the same manner as direct recording. The general equation for the FM signal can be derived and shown to be (2):

$$a = A \sin \left(2\pi F t + \frac{\Delta F}{f} \sin 2\pi f t \right) , \qquad (9)$$

where

a = analog current or voltage

A = amplitude of the carrier

F = unmodulated carrier frequency

ΔF = peak frequency deviation

f = modulation or data frequency.

A random signal, of course, is composed of many frequency components. Hence the random modulating signal can be expressed in terms of all of its frequency components in Eq. (9). While the magnitude of F, ΔF, and f are all increased in proportion to the increase in playback speed, the coefficients A and $\Delta F/f$ remain constant. The amplitude characteristics are unaffected by the speedup process. Therefore, resolution is maintained because the ratio $B_r/B \geq 4$ is unchanged.

SINGLE FREQUENCY COMPONENT EVALUATION

A simple test was conducted to evaluate the equivalence of the increased frequency spectrum analysis compared to analysis by normal methods. A one-volt 100-cps sine signal from a battery powered oscillator was analyzed "on line," and simultaneously recorded on tape at 7-1/2 ips. A five-cps filter and a 30-sec integration time (BT = 150) were used in a step spectrum analysis.

The spectrum analysis was intended to show the harmonic content of the oscillator output, the noise level of the analyzer, and distortion introduced by the analyzer. This analysis, Fig. (2a), was the basis for further comparison.

The data record was then made into a 30 sec tape loop at 7-1/2 ips, and the analysis repeated under the same conditions. A comparison of this analysis, Fig. (2b) to the "on line" analysis, demonstrates good reproduction of the data with an expected slight increase in noise level and some harmonic distortion caused by the tape record/playback process in the -60 db region.

The tape loop was then played back at 60 ips. This produced a reduction in record length T_r of 8 to 1, requiring a coresponding increase in analysis bandwidth

With the bandwidths available, the closest bandwidth ratio increase was 10 to 1. This, of course, does increase the BT product, decreasing the standard error and resolution slightly. A spectrum analysis, Fig. (2c) was obtained. Little or no change can be seen in the amplitude characteristics of the data (one volt 100 cps and its harmonics). The noise level and harmonic distortion induced by the tape recorder are still low (-50 to -60 db). Note, however, the increase in the data frequency spectrum by a factor of eight.

Obviously, the advantages of step analysis (true integration) over sweep analysis (RC averaging) would accrue regardless of the playback speed of the data sampled. Using this technique in PSD step analyses of the IMU, the required sweep rate was:

$$R_s \geq \frac{B}{T_a} \geq \frac{20}{3} \geq 6.67 \text{ cps/sec} ,$$

where B was increased from 2 to 20 cps and T_a, which was set equal to T_r, was reduced from 30 to 3 seconds.

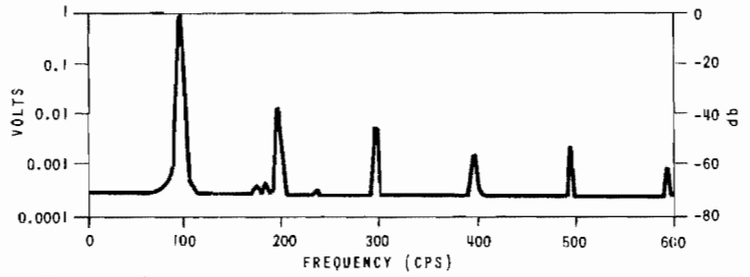

(a) "ON LINE" SPECTRUM ANALYSIS OF 1 VOLT, 100 CPS SINE SIGNAL

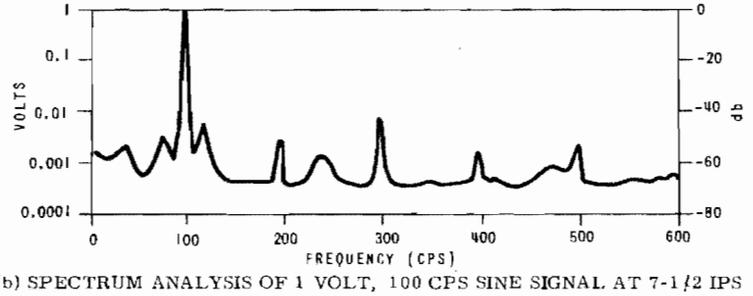

(b) SPECTRUM ANALYSIS OF 1 VOLT, 100 CPS SINE SIGNAL AT 7-1/2 IPS

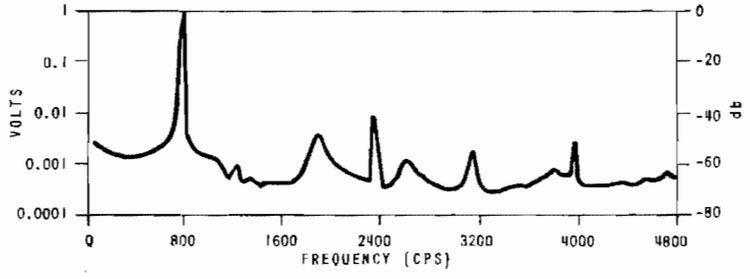

(c) SPECTRUM ANALYSIS OF 1 VOLT, 100 CPS SINE SIGNAL AT 60 IPS

Fig. 2. Sine signal spectrum analysis at various playback speeds

The analysis time,

$$T_s = \frac{F}{R_s} = \frac{1440}{6.67} = 3.6 \text{ min},$$

represents a reduction of 25 to 1 over the original requirement. A slight decrease in the standard error also resulted.

$$\epsilon = \frac{1}{\sqrt{BT}} = \frac{1}{\sqrt{20(3)}} = 0.129 \text{ or } 12.9 \text{ percent}.$$

An examination of Fig. 3 demonstrates the equivalence of the analysis by either method. The solid curve was obtained in ninety minutes by RC averaging. The points (circled for clarity) represent a step analysis of the same data sample played back at 60 ips and was obtained in 3.6 minutes.

COMMENTS AND CONCLUSIONS

There are means available to significantly reduce analog PSD analysis time requirements. Implementation of these means is not a difficult problem, and several stages of time savings are available.

One means of reducing analysis time is that of step analysis, or the use of true integration. A 4 to 1 time savings is possible when step analysis is compared to the sweep analysis with $K = T_r$. Even if the sweep time constant is reduced to a minimum acceptable value ($K = T_r/2$), a 2 to 1 time savings may be realized by using step analysis. In this case, there is also an approximate 14 percent reduction in the standard error.

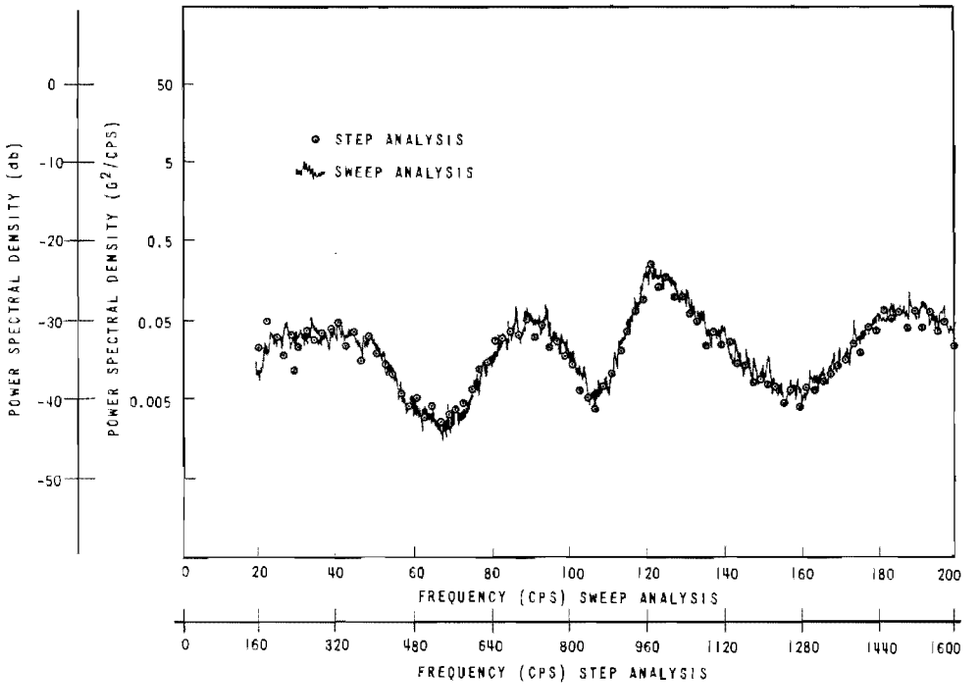

Fig. 3. Comparison of PSD analyses of IMU vibration response

However, a more significant time savings results from the tape speed change technique. The practical limitations of magnetic tape recorders maximize this ratio at 8 to 1, and 4 to 1 may be common. This time savings can be realized in either sweep or step analysis. A maximum time savings of 32 to 1 (and a slight reduction in statistical error) can be realized by using both tape speed change and step analysis techniques in place of the standard RC averaging sweep analysis.

SOME PRACTICAL CONSIDERATIONS

True Integration Versus RC Averaging

The analysis requirements of any particular program or facility determine the optimum extent to which analysis time savings can be achieved. An analyzer that will perform true integration and produce a step plot is quite expensive, compared to a simple RC averaging analyzer, because extensive logic and timing circuits are required in the step analyzer.

However, the analyzer with true integration does offer a possible 4 to 1 time savings with a slight increase in accuracy over RC analysis. It is also the only type of analyzer that can synchronize the integration start time with a particular point in the data sample. This is of particular value when the data is nonstationary.

Tape Speed Changes

The requirements of the tape recorder also make it an expensive piece of equipment required for high speed analysis. It must, of course, be capable of recording at 7-1/2 ips and reproducing at 60 ips, with the necessary frequency response. This usually means the addition of high density or extended-range signal electronics. It might appear advantageous to increase the playback speed to 120 ips for a maximum record length reduction of 16 to 1. The dynamics of the tape loop become the limiting factor at this speed, and loop length may be limited. Seven and one-half ips is the minimum possible recording speed for vibration data, even with high density signal electronics, assuming a required spectrum of 2,500 cps.

There is also a slight inconsistency or incompatibility between tape recorders and analyzers. The tape recorder speeds make possible time reductions of 2 to 1, 4 to 1, 8 to 1, etc., while the bandwidths and time intervals available in the analyzer are often multiples of decimals and decades. This results in a possible

speed increase of 8 to 1, while the normal compatible filter bandwidth ratio is 10 to 1, requiring a large range of filter bandwidths and time constants in the analyzer for optimum use of the time reduction process. The upper frequency response limit of the analyzer must also be high enough to accommodate the increased data spectrum. All of this increases the cost of the equipment. Time savings in data analysis and reduction in testing program delays can offset the cost of the necessary equipment very rapidly. If current or future testing programs require high volumes of accurate vibration data analyses, implementation of this rapid analysis method should certainly be considered.

REFERENCES

1. Bendat and Piersol, Design Considerations and Use of Analog Power Spectral Density Analyzers (Honeywell, Inc., Denver), 1964
2. Goldman, Frequency Analysis, Modulation and Noise (McGraw-Hill, New York), 1948
3. Harris and Crede, Shock and Vibration Handbook (McGraw-Hill, New York), 1961
4. "Power Spectral Density Analysis System Using a Tracking Filter," Spectral Dynamics Corporation of San Diego, July 1963

* * *

A CONTINUOUS FREQUENCY CONSTANT Q SHOCK SPECTRUM ANALYZER*

G. W. Painter and H. J. Parry
Lockheed-California Company
Burbank, California

In a previous paper (1), the authors described a method for producing complex shock transients with prescribed shock spectra. As a part of that work, it was found necessary to develop a special analyzer for quick readout of the shock spectrum. The analyzer has several unique and interesting features which make it a valuable laboratory instrument whenever shock spectra must be determined. It may be used to analyze either complex transients or classical transients such as half sine or sawtooth pulses. In particular, the analyzer can maintain constant values of Q while the frequency is continuously variable from 0 to 2000 cps. In addition, it can be used to simulate force-excited or base-excited single-degree-of-freedom systems for broadband random or sinusoidal analyses.

This paper describes the essential circuitry and design principles of the analyzer and presents typical performance data.

INTRODUCTION

Determination of shock spectra of motion transients has been accomplished by a variety of methods. These have ranged from the use of simple mechanical reed gages to analog and digital computers. Since the shock spectrum analyzer which will be described in this paper can be considered to be a special purpose analog computer, it will be useful to consider the merits of related analog shock spectrum analyzers.

There are two types of electrical analog computers which have been used for the determination of shock spectra. The first type, generally referred to as a direct analog computer, incorporates inductors, capacitors, and resistors to provide a direct simulation of the elements that comprise a base-excited single-degree-of-freedom mechanical oscillator. A second type, called an indirect analog computer, uses dc amplifiers with appropriately chosen input and feedback impedances to perform the operations of addition, integration, multiplication, and sign inversion which are required to solve the second order differential equation associated with simple mechanical oscillators.

The primary advantage of the direct analog computer is its inherent simplicity. For example, only three passive elements are required to simulate a damped resonator. Important disadvantages include:

1. Large and expensive passive elements to simulate low frequency oscillators.

2. The limited practicable simulation range of oscillator natural frequencies by using variable passive elements.

3. Purely reactive elements cannot be obtained. This results in the necessity of using active elements to provide "negative" resistance when it is required to simulate simple oscillators having low damping.

The indirect analog method is inherently more complex but has the advantage of greater flexibility. Once the operational amplifiers have been arranged to simulate a single-degree-of-freedom system, natural frequency and damping can be readily adjusted over a wide range. If the signal representing the motion transient whose shock spectrum is desired can be reproduced repeatedly, the analyzer can be

*Patent applied for.

set at any frequency within its operating range, thereby providing the shock spectrum over the frequency range of interest.

Independent changes in the natural frequency and the damping of the simulated mechanical oscillators are accomplished by adjusting at least two of the impedances in the analog computer. In particular, if one varies an impedance that changes the natural frequency, it will also be necessary to change a second impedance in order to keep the Q of the oscillator at a constant value. The necessity of making two impedance adjustments for each frequency at which the spectrum is to be evaluated can be very time consuming and makes it impracticable to automate the measurement procedure. The shock spectrum analyzer to be described has the capability of allowing the natural frequency of the simulated oscillator to be easily changed while Q remains constant. It is unique in that the impedance changes required to provide the above performance are accomplished by the adjustment of a single external control.

The following sections present a brief review of the shock spectrum concept, a discussion of the standard approach to the determination of shock spectra with an indirect analog computer, a description of a design innovation which greatly improves the efficiency of analog shock spectrum analyzers, and a discussion of the performance characteristics of an analyzer that incorporates the referenced improved design features.

THE SHOCK SPECTRUM

The shock spectrum concept is based upon the maximum motional response of the system shown in Fig. 1. A hypothetical simple oscillator whose mass, spring constant, and damping coefficient are represented by m, k and c respectively is one of an infinite set of such oscillators whose natural frequencies cover the spectrum range of interest. The transient whose shock spectrum is to be determined is represented by the motion, U, of the base. In general this excitation transient can be given as a displacement, a velocity, or an acceleration. One may be interested in a variety of types of shock spectra. These include spectra based on the absolute motion of the mass, as well as relative motion between the mass and the base. Spectra can be obtained in terms of displacement, velocity, or acceleration based upon the maximum motion of the mass: (a) during the time the excitation transients exists (primary spectra), (b) after the excitation transient has ceased (residual spectra), or (c) upon the maximum motion irrespective of when it occurs (total spectra). Furthermore, the spectrum may be based upon the response of either damped or undamped oscillators. In the following analysis, attention will be directed toward the determination of total acceleration spectra based on the response of damped oscillators (although the computer is capable of measuring any of the three types of spectra mentioned above).

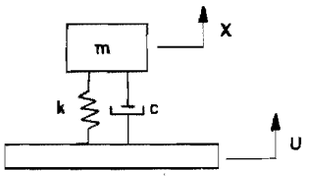

Fig. 1. Hypothetical simple oscillator

The equation of motion for the damped simple oscillator shown in Fig. 1 is:

$$m\ddot{X} + c(\dot{X} - \dot{U}) + k(X - U) = 0 , \qquad (1\text{-A})$$

or

$$\ddot{X} + \frac{c}{m}(\dot{X} - \dot{U}) + \frac{k}{m}(X - U) = 0 .$$

Let

$$c_c = 2m\omega_n ,$$

$$\omega_n^2 = \frac{k}{m} ,$$

and

$$\rho = \frac{c}{c_c} = \frac{1}{2Q} ,$$

where

c_c = critical damping coefficient,

ω_n = natural frequency,

Q = quality factor.

Therefore

$$\ddot{X} + 2\rho\omega_n(\dot{X} - \dot{U}) + \omega_n^2(X - U) = 0 , \qquad (1\text{-B})$$

$$\ddot{X} + \frac{\omega_n}{Q}(\dot{X} - \dot{U}) + \omega_n^2(X - U) = 0 . \qquad (1\text{-C})$$

Let $Z = (X - U)$ = relative displacement. Then $\ddot{X} = \ddot{Z} + \ddot{U}$, and

$$\ddot{Z} + \ddot{U} + \frac{\omega_n}{Q}\dot{Z} + \omega_n^2 Z = 0 . \qquad (1\text{-}D)$$

STANDARD AND IMPROVED METHODS FOR OBTAINING SHOCK SPECTRA ON AN ANALOG COMPUTER

In computer modeling, it is desirable to arrange Eq. (1-D) in the form

$$\ddot{Z} = -\ddot{U} - \frac{\omega_n}{Q}\dot{Z} - \omega_n^2 Z .$$

A computer block diagram for solving the above equation is shown in Fig. 2 where the operations of addition, integration, and multiplication by a constant are indicated by blocks designated A, J, and C respectively. A more detailed representation of the computer network is given in Fig. 3 which indicates the components associated with the various computer operations. The ratio of the output to input voltages for any operational amplifier having a feedback impedance, Z_f, and an input impedance, Z_i, can be shown to be $-Z_f/Z_i$. For example, if the input impedance is a resistance, R, and the feedback impedance a capacitance, C

$$e_{out} = \frac{-1}{j\omega RC} , \qquad e_{in} = -\frac{1}{RC}\int e_{in}\,dt .$$

If the input and feedback impedances are resistances

$$e_{out} = -\frac{R_f}{R_i} e_{in} .$$

Operation No. 1 in Fig. 2 accomplishes an integration of $\ddot{Z}$, an algebraic sign inversion and multiplication by the constant, $1/R_1C_1$. A second integration, sign inversion, and multiplication occurs at operation No. 2. Operation No. 3 involves a sign inversion and multiplication by a constant while at No. 4, when a simple potentiometer is used, a multiplication by a constant is accomplished without a sign change. Letting the 1/RC values at (1) and (2) be represented by A_1 and A_2 respectively and the constants at (3) and (4) by A_3 and A_4, the operations at the four locations become

$$① \frac{A_1}{j\omega} \quad ② \frac{A_2}{j\omega} \quad ③ A_3 \quad ④ A_4 .$$

By following the inner loop (1 and 3) and the outer loop (1, 2 and 4) one obtains the following equations:

$$\frac{\omega_n}{Q}\dot{Z} = \ddot{Z}\frac{A_1A_3}{j\omega} = A_1A_3\dot{Z} , \qquad (2\text{-}A)$$

$$\frac{\omega_n}{Q} = A_1A_3 , \qquad (2\text{-}B)$$

$$\omega_n^2 Z = \ddot{Z}\frac{A_1}{j\omega}\frac{A_2}{j\omega}A_4 = A_1A_2A_4Z , \qquad (3\text{-}A)$$

$$\omega_n^2 = A_1A_2A_4 . \qquad (3\text{-}B)$$

Equations 2 and 3 when combined give

$$Q^2 = \frac{A_2A_4}{A_1A_3^2} . \qquad (4)$$

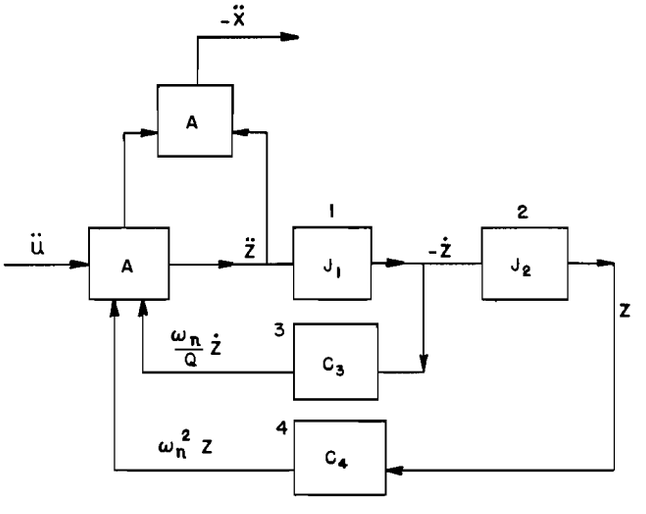

Fig. 2. Symbolic computer arrangement

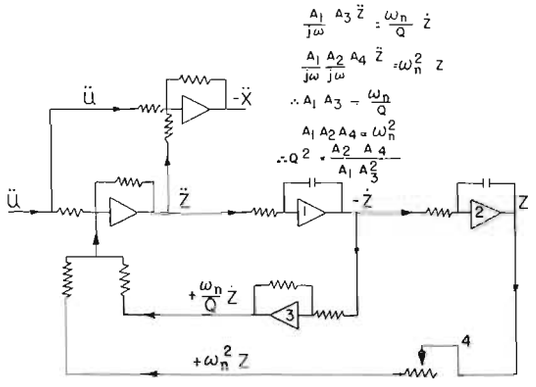

Fig. 3. Computer component arrangement

It is common practice to consider the operations at (3) and (4) to be analogous to the damping coefficient and spring rate respectively. In the determination of damped shock spectra, it is required that the Q of the simple oscillator remain constant while the natural frequency is varied. The usual procedure in obtaining shock spectra is to vary the natural frequency by changing the value of A_4. Equation (4) shows that when A_4 alone is changed, Q will also change. In the standard procedure Q is returned to the value desired by changing A_3. Equation (3-B) shows that a change in A_3 has no effect on the natural frequency, ω_n.

Equation (3-B) and Eq. (4) show that the response characteristics of the oscillator depend not only upon A_3 and A_4, but also upon A_1 and A_2. These equations indicate methods which will allow Q to remain constant as ω_n is varied. For instance, ω_n can be varied by changing A_1, A_2 and A_4 singly or in combination as is suggested by Eq. (3-B). From Eq. (4) it can be seen that if either or both of the ratios A_2/A_1 or A_4/A_1 are maintained at a constant value while A_3 remains unchanged, Q will remain constant.

The above considerations suggest methods for designing an improved shock spectrum analyzer. For example A_2/A_1 can be held to a constant value by having the variable resistances R_2 and R_1 ganged to a common shaft. An alternate, and equally suitable method for holding Q constant as ω_n is varied, is to gang R_4 and R_1 to a common shaft. A third method involves ganging variable capacitors in the integrators and varying them simultaneously so as to maintain A_2/A_1 at a constant value. In fact, any method which will allow the ratio on the right side of Eq. (4) to remain constant as ω_n is varied will provide the desired results.

PERFORMANCE CHARACTERISTICS OF SHOCK SPECTRUM ANALYZER

Two shock spectrum analyzers incorporating the design features discussed in the preceding section have been fabricated and have been in use for approximately two years. A photograph of the first analyzer constructed is shown in Fig. 4. An improved analyzer, using solid state operational amplifiers, is shown in Fig. 5.

Fig. 4. Prototype analyzer

Fig. 5. Improved analyzer using solid state circuitry

Both of the analyzers shown can perform a real time shock spectrum analysis over a frequency range of 0-2000 cps with selectable values of Q ranging from 1 to 50. Commercially available versions of the analyzer have extended the frequency range to 4000 cps by careful preservation of phase linearity.

Two methods have been used to check the accuracy of the analyzer. The first method involved the determination of the transfer function of the oscillator at various settings of natural frequency and Q. Examples of transfer functions measured with the Q control set at 10 and 50 are given in Figs. 6 and 7 respectively. It can be seen that Q remains constant within ±1 db over the frequency range of interest. The second method involved a comparison of shock spectra obtained with the analyzer and with a digital computer for the same complex transients. Two of the transients and associated

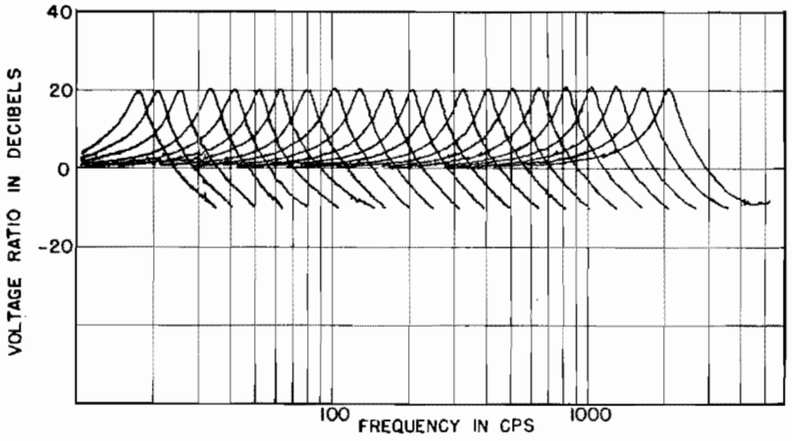

Fig. 6. Transfer function of analyzer (Q = 10)

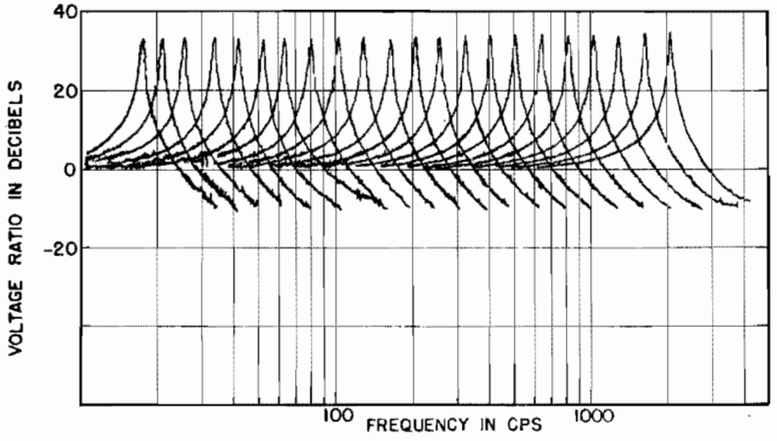

Fig. 7. Transfer function of analyzer (Q = 50)

shock spectra are shown in Fig. 8. It can be seen that the agreement between analog and digitally derived spectra is within a few percent over the frequency range explored.

SUMMARY

The use of the analyzer permits the analysis of complex shock transients in the laboratory during test setup. This allows the shock spectrum to be determined in much the same way as a random spectrum without the necessity of having to use a digital computer.

The analyzer can be used to measure the spectrum at any frequency within its operating range. This feature is particularly desirable in the analysis of complex transients whose spectral pattern can be quite jagged.

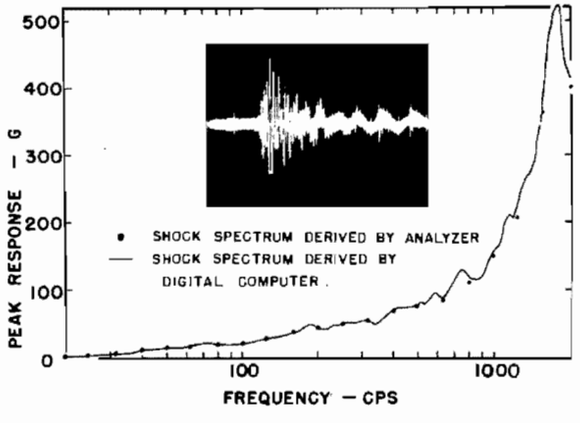

Fig. 8. Comparison of spectra obtained with the shock spectrum analyzer and a digital computer (Q = 10)

The analyzer output can be delivered either to an oscilloscope or to a peak reading voltmeter. The instrument can also be used in conjunction with an X-Y recorder, thereby allowing an automatic plotting of the shock spectrum to be obtained.

REFERENCE

1. G. W. Painter and H. J. Parry, "Simulating Flight Environment Shock on an Electrodynamic Shaker," Shock, Vibration and Associated Environments, Bulletin No. 33, Part III, March 1964, pp. 85-95

DISCUSSION

Dr. Morrow (Aerospace Corp.): Have you considered adding any extra features to this, or any additional simple manipulations so that one could obtain at least part of a Fourier spectrum at the same time? This is a little more fundamental and many people may prefer to work from this on occasion.

Mr. Painter: Yes, this could possibly be done. The main problem one runs into is that of getting an exact zero damping, or something very close to it. I believe the absolute value of the Fourier spectrum is equal to the residual, undamped spectrum. If one could have a very high Q and read the system that persists after the transient is over, this would be one way of getting the Fourier spectrum.

Mr. Zell (Picatinny Arsenal): As a commercial unit in the continuous frequency mode, do you have a direct readout of the frequency being set?

Mr. Painter: Yes, auxiliary equipment has been developed so that one can actually plot the spectrum versus frequency. There is also a peak reading voltmeter. One can use either an oscilloscope, which we used, or a peak reading voltmeter, which is somewhat more convenient for this purpose. There is a method now for obtaining an automatic plotting of the shock spectrum. One, of course, has to repeat the transient over and over again as you sweep along.

Mr. Othmer (Sandia Corp.): Had you considered nonlinear springs or damping in any of your considerations?

Mr. Painter: No. We were dealing strictly with conventional shock spectrum analysis. I believe there is a paper being given on the last day in the shock session that refers to nonlinear effects, at least as far as the synthesis procedure is concerned, and he may touch upon that.

* * *

SLOPE ERROR OF POWER SPECTRAL DENSITY MEASUREMENTS

Robert L. Gordon
Pratt and Whitney Aircraft
East Hartford, Connecticut

In analog power spectral density analyzers, the spectral density at a particular frequency is obtained by measuring the power in a bandpass filter and dividing the value obtained by the filter bandwidth. The resulting density value is assumed to be equal to the density at the filter center frequency. This density (or average power) is, in general, unequal to the actual power at the center frequency except for straight line spectral density functions. An expression for this error is developed for the case in which the true spectral density is a function of frequency raised to a power.

INTRODUCTION

In the analysis of power spectrum, an error in the maximum and minimum values of the power spectral density curve is introduced when the bandwidth of the analyzer filter is larger than the bandwidth of the response spectrum being analyzed. An expression for this error, called "blurring error," has been developed and documented by W. R. Forlifer (1). Analyzers employing bandpass filters to measure the power spectrum introduce error into the measurement of the power on the response slopes as well as the peaks and notches. Definition and evaluation of this "slope error" are the subjects of this paper.

The average value of any straight line segment of a function (plotted on Cartesian coordinates) occurs midway between the two end points. Most power spectrum analyzers employ one or more bandpass filters to measure the average value of a density function within its passband and display this value at the center frequency of the filter. This analysis is correct for straight line functions. However, it is only an approximation when the function is a curved line; i.e., $y = f(x^2)$. The difference between the true and the approximate plotted values, will be called the "slope error" and will be shown to be identical to the statistical bias of a power spectral density estimate which is given in section 4.8.2 of Ref. 2.

This article will show that although the slope error is usually less significant than the more widely used blurring error and the random process "statistical error," there are special situations in which the slope error may be more significant, namely: (1) at very low frequencies, (2) in the analysis of lightly damped structures, and (3) when using low Q filters.

DEVELOPMENT OF ERROR EXPRESSION

An idealized rectangular filter is used to develop the error term and a series approximation is made to simplify the resulting expression. Although an idealized filter is used, the results may be extended to other filters when the noise bandwidth (3) is used and the filter shape is symmetrical. Most linear physical systems may be approximated by linear differential equations of order n. Therefore, the resulting power spectral density may be sectionally represented by an equation of the following form:

$$S_a = cf^n \qquad (1)$$

where

S_a = actual power spectral density,

c = constant,

f = frequency in cps, and

n = slope of S_a on log-log coordinates [linear ordinate distance/linear abscissa distance].

The above curve of spectral density will appear on log-log paper as a straight line having a slope n, and as a power curve on linear coordinates as in Fig. 1. The filter, also shown in Fig. 1, will be defined as

$$H(f) = 0, \quad f_c - B/2 > f > f_c + B/2$$
$$H(f) = 1, \quad f_c - B/2 < f < f_c + B/2 \tag{2}$$

where

$H(f)$ = value of filter transfer function,

f_c = filter center frequency, and

B = filter bandwidth.

Knowing that the filter quality factor Q is defined as:

$$Q = \frac{f_c}{B}, \tag{5}$$

and putting

$$k = n + 1, \tag{6}$$

Eq. (4) becomes

For $k \neq 0$,

$$S_m = c f_c^{k-1} \frac{Q}{k} \left[\left(1 + \frac{1}{2Q}\right)^k - \left(1 - \frac{1}{2Q}\right)^k \right]. \tag{7}$$

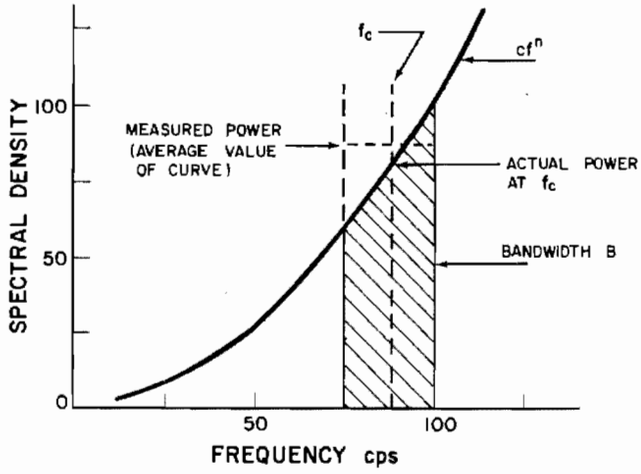

Fig. 1. Schematic of spectrum analysis process

The power spectral density is usually obtained by measuring the energy in the filter (shown as a cross-hatched area in Fig. 1) which is then divided by the bandwidth. The resulting level is then assumed to be the power spectral density at f_c. This is done mathematically as follows:

$$S_m = \frac{1}{B} \int_{f_c - B/2}^{f_c + B/2} c f^n \, df \tag{3}$$

where S_m = measured power spectral density.

For $n \neq -1$ Eq. (3) becomes

$$S_m = \frac{c}{B(n+1)} \left[\left(f_c + \frac{B}{2}\right)^{n+1} - \left(f_c - \frac{B}{2}\right)^{n+1} \right]. \tag{4}$$

Since $0 < 1/2Q < 1$ for filters with Q's greater than 1/2, the expression inside the brackets may be expanded in a power series so Eq. (7) becomes, to a first order approximation:

$$S_m \approx c f_c^{k-1} \left[1 + \frac{(k-1)(k-2)}{24Q^2} + \ldots \right], \quad k \neq 0. \tag{8}$$

Now defining an error term as follows:

$$S_e = \frac{S_m - S_a}{S_a} \tag{9}$$

where S_e = relative error in power spectral density at f_c, and using Eqs. (8) and (1), the error term is as follows:

$$S_e \approx \frac{(k-1)(k-2)}{24Q^2} + \ldots, \quad k \neq 0. \tag{10}$$

For the case where $k = 0$ $(n = -1)$ Eq. (3) is

$$S_m = \frac{1}{B} \int_{f_c - B/2}^{f_c + B/2} \frac{c}{f} \, df \, , \qquad (11)$$

which becomes

$$S_m = \frac{cQ}{f_c} \left[\ell n \left(1 + \frac{1}{2Q} \right) - \ell n \left(1 - \frac{1}{2Q} \right) \right] . \qquad (12)$$

Using a power series representation of

$$\ell n \left(1 + \frac{1}{2Q} \right)$$

Eq. (12) becomes

$$S_m \approx \frac{c}{f_c} \left[1 + \frac{1}{12Q^2} + \ldots \right] , \qquad (13)$$

and using Eq. (9), Eq. (13) becomes, to a first order approximation:

$$S_e \approx \frac{1}{12Q^2} + \ldots ,$$

which is equivalent to Eq. (10) with $k = 0$. So we may write:

$$S_e \approx \frac{(k-1)(k-2)}{24Q^2} \qquad \text{(all } k\text{)} . \qquad (14)$$

By substitution of Eq. (6) into Eq. (14), the error term is obtained in terms of the slope n, and is

$$S_e \approx \frac{n^2 - n}{24Q^2} . \qquad (15)$$

Curves of percent error versus n for three values of filter Q are shown in Fig. 2.

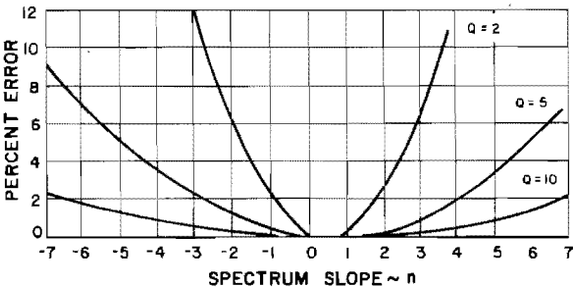

Fig. 2. Slope error for various Q filters

A slightly more useful form of Eq. (15) is obtained by substitution of Eq. (5), and is

$$S_e \approx \frac{B^2 (n^2 - n)}{24 f_c^2} . \qquad (16)$$

Curves of error versus frequency are obtained in Fig. 3 for three fixed bandwidths and a slope $n = -2$, which is commonly found in second order systems.

In section 4.8.2 of Ref. 2 an analysis of bias for a similar system (idealized rectangular filter) indicates the bias term to be

$$\left| b \left[S_x(f, T, B) \right] \right| \approx \frac{B^2}{24} \left| S_x''(f) \right| \qquad (17)$$

where

$b[\,]$ = statistical bias of term in brackets,

$E[\,]$ = expected value of quantity in brackets,

B = bandwidth of an idealized filter,

T = time in seconds,

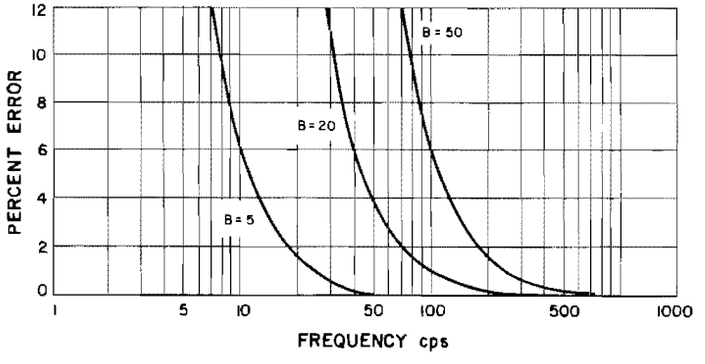

Fig. 3. Slope error for various bandwidths with slope = -2 or +3

$S_x(f)$ = actual spectral density,

f = frequency in cps, and

$S_x(f,T,B)$ = estimate of spectral density.

$$S_x''(f) = \frac{d^2[S_x(f)]}{df^2} .$$

If $S_x(f) = cf^n$ as in Eq. (1), then

$$S_x''(f) = c(n^2 - n)\ f^{n-2} . \qquad (18)$$

Using the relationships of Eq. (5) and Eq. (18), Eq. (17) becomes

$$|b[S_x(f,T,B)]| \approx cf_c^n \frac{(n^2 - n)}{24Q^2} . \qquad (19)$$

Since

$$|b[S_x(f,T,B)]| = |E[S_x(f,T,B)] - S_x(f)|, \qquad (20)$$

and

$$S_x(f) = S_a , \quad E[S_x(f,T,B)] = S_m ,$$

then

$$|b[S_x(f,T,B)]| = |S_m - S_a| . \qquad (21)$$

Thus, it is evident from Eq. (9) that the bias is equal to S_eS_a, or the absolute value of the slope error.

CONCLUSIONS

While it is evident from Fig. 2 that the slope error is small for small n and large Q and is generally much less than normal statistical and blurring errors, it is worthy to note from Fig. 3 that a significant error may be present at low frequencies for fixed bandwidth systems. If analyses of lightly damped structures are made, large positive and negative slopes are encountered near the resonant frequency and the error will be large. The error at the resonant frequency is the blurring error, described in Ref. 2, and may be avoided by observing the bandwidth criteria mentioned therein.

REFERENCES

1. W. R. Forlifer, "The Effects of Filter Bandwidths in Spectral Analysis of Random Vibration," Shock and Vibration Bulletin No. 33, Part II:273 (1964)

2. Julis S. Bendat, Loren D. Enochson, G. Harold Klein, and Allan G. Piersol, "The Application of Statistics to the Flight Vehicle Vibration Problem," ASD Technical Report 61-123, December 1961, Section 4.8.2

3. Julius S. Bendat, and Allan G. Piersol, "Design Considerations and Use of Analog Power Spectral Density Analyzers," reprint of a Technical Report by Measurement Analysis Corporation for the Honeywell Co., Denver Division.

DISCUSSION

Mr. Lessem (USA Engineer Waterways Experiment Station): Suppose you analyze data at a higher frequency than that at which it was recorded, either for purposes of saving time as was implied in an earlier paper, or for purposes of getting the data within the frequency capabilities of your analysis system, what implications are there for this low frequency error due to the bandwidth?

Mr. Gordon: As I understand it, you ask what effect a frequency translation in the analysis process will have on this type of analysis. If there is a system which heterodynes an incoming signal up to a higher frequency so that a bandpass filter, such as a crystal filter, can handle it, and if this system is viewed as a black box or a passive device, it has certain characteristics. It will only pass frequencies in the audio range, therefore when it is viewed as an end-to-end system the error would be applicable. For example, if this were a 50 cps filter centered at 100 cps, it would pass frequencies between 50 and 150 cps even though it was actually internally operating at 100 kc. This error would still be applicable for that type of instrument. Also, a time compression technique is used in which the frequency range is multiplied and a wider filter is used; the question of the resolution in the initial data range remains. For example, if with a 10 to 1 time compression and a 100 cps filter, this would be equal to a 10 cps filter in the audio range. The same type of slope error would exist.

* * *

THE EFFECTS OF PHASE ERRORS UPON THE MEASUREMENT OF RANDOM PROCESSES

Ronald D. Kelly
Measurement Analysis Corporation
Los Angeles, California

Within the past year there has been an increasing interest in the effects of phase errors on the measurement of random processes. Phase errors can occur in transducers, signal conditioners, transmission lines, telemetry units, and tape recorders. These phase errors can be either static or dynamic in nature. If measurement of certain properties of the data is to be made accurately, these errors must be confined within acceptable bounds, or compensated for in the data reduction process.

Those types of analyses that are not affected by static phase errors in the measurement system, such as ordinary power spectral density and autocorrelation analyses, are briefly treated to demonstrate why they are not affected. In addition, the inaccuracies in these analyses from dynamic phase errors are discussed.

It is the primary purpose of this paper, however, to examine those types of analyses that are affected by phase errors, such as cross-spectral density and cross-correlation. The resultant inaccuracies in the reduced data are presented for several typical kinds of phase errors, so that the phase characteristics of practical measurement systems can be quantitatively related to the accuracy of the reduced data.

INTRODUCTION

The demands placed upon environmental measurements are constantly becoming more stringent. For example, the requirements for cross-correlation and cross-spectral density measurements of environments have rapidly increased. These measurements are required to define such things as the spatial distribution, over a structure, of the dynamic pressure fluctuations from a turbulent boundary layer, the convection velocity characteristics of a turbulent flow, the energy transmission paths between two points, the frequency response functions of complicated structures, etc. It is the purpose of this paper to examine the inaccuracies resulting in cross-correlation and cross-spectral density analyses from typical phase errors in the measurement equipment.

These phase errors occur in every part of the measuring system, in the transducers, the signal conditioners, the transmission lines, the telemetry units, the tape recorders, the A/D converters, the analyzers, and the print-out devices. These phase errors can be either static or dynamic (time-varying) in character. To ensure that the environment is measured accurately, these errors must be confined to acceptable bounds, or compensated for in the data reduction process. The following discussions provide guidelines for evaluating the severity of different types of phase errors and for error compensation techniques.

ORDINARY SPECTRAL DENSITY AND AUTOCORRELATION ANALYSES

In ordinary spectral density and autocorrelation analyses, the phase errors must be split into the static and dynamic components and discussed separately. The static phase errors introduce no inaccuracies into the measurement process, while the dynamic phase errors do.

Static Phase Errors

For the first case, assume that the measuring circuit has a constant time delay error τ. This type of error is encountered in every instrument in the measuring chain, since they all

have finite bandwidths. Of course, restrictions must be placed on the frequency bandwidth over which the constant time delay approximation is valid for each individual instrument. In general, those instruments having the narrowest bandwidths will cause the greatest time delay. For example, assume that the response of the transducer can be approximated by a simple mechanical oscillator. The phase factor for this transducer can be written as (1)

$$\phi(f) = \tan^{-1}\left[\frac{2\zeta\,\frac{f}{f_n}}{1-\left(\frac{f}{f_n}\right)^2}\right], \qquad (1)$$

where

$\phi(f)$ = the phase factor,

ζ = the damping ratio,

f = the frequency in cps of the measured data, and

f_n = the undamped natural frequency in cps of the transducer.

Equation (1) can be expanded in series form:

$$\phi(f) = \left[\frac{2\zeta\,\frac{f}{f_n}}{1-\left(\frac{f}{f_n}\right)^2}\right] - \frac{1}{3}\left[\frac{2\zeta\,\frac{f}{f_n}}{1-\left(\frac{f}{f_n}\right)^2}\right]^3 + \frac{1}{5}\left[\frac{2\zeta\,\frac{f}{f_n}}{1-\left(\frac{f}{f_n}\right)^2}\right]^5 \qquad (2)$$

If the restrictions $f \le 0.1\,f_n$ and $\zeta \le 1.0$ are applied, then

$$\phi(f) \approx \frac{2\zeta f}{f_n}.$$

The time delay, τ_0, is a constant under these restrictions, since

$$\tau_0 = \frac{\phi(f)}{2\pi f} = \frac{\zeta}{\pi f_n}. \qquad (3)$$

The autocorrelation function is defined as

$$R_x(\tau) = \lim_{T\to\infty}\frac{1}{2T}\int_{-T}^{T} x(t)\,x(t+\tau)\,dt. \qquad (4)$$

Let the measured signal be

$$x^m(t) = x(t+\tau_0),$$

where τ_0 is the time delay in the measuring circuitry. The measured autocorrelation function is now

$$R_x^m(\tau) = \lim_{T\to\infty}\frac{1}{2T}\int_{-T}^{T} x^m(x)\,x^m(t+\tau)\,dt$$

$$= \lim_{T\to\infty}\frac{1}{2T}\int_{-T}^{T} x(t+\tau_0)\,x(t+\tau_0+\tau)\,dt. \qquad (5)$$

Let $u = t+\tau_0$; $du = dt$

$$R_x^m(\tau) = \lim_{T\to\infty}\frac{1}{2T}\int_{-T+\tau_0}^{T+\tau_0} x(u)\,x(u+\tau)\,du$$

$$= R_x(\tau)$$

Since the process being analyzed is stationary and ergodic, no error is introduced into the autocorrelation function by computing from $(-T+\tau_0)$ to $(T+\tau_0)$, instead of from $(-T)$ to (T). Because the ordinary spectral density is the Fourier transform (Wiener-Khintchine Theorem (2)) of the autocorrelation function, it can be seen that the constant time delay error also introduces no error in the spectral density analysis.

Next consider the case of a phase shift that is independent of frequency:

$$\phi = k, \qquad (6)$$

where k = a constant.

The true spectral density (the two-sided form being used for simplicity) is

$$S_x(f) = \lim_{T\to\infty}\frac{1}{2T}\left[\int_{-T}^{T} x(t)\,e^{-j2\pi ft}\,dt\right] \times \left[\int_{-T}^{T} x(t)\,e^{j2\pi ft}\,dt\right], \qquad (7)$$

where

$S_x(f)$ = the two-sided ordinary spectral density function, and

$x(t)$ = the data signal.

Let the measured signal be

$$x^m(t) = x(t+k/2\pi f). \qquad (8)$$

Then the measured spectral density becomes

$$S_x^m(f) = \lim_{T\to\infty} \frac{1}{2T} \left[\int_{-T}^{T} x(t + k/2\pi f)\, e^{-j2\pi ft} dt\right] \times \left[\int_{-T}^{T} x(t + k/2\pi f)\, e^{j2\pi ft}\, dt\right] . \quad (9)$$

Let

$$u = t + k/2\pi f , \qquad du = dt . \quad (10)$$

Then

$$S_x^m(f) = \lim_{T\to\infty} \frac{1}{2T} \left[\int_{-T+k/2\pi f}^{T+k/2\pi f} x(u)\, e^{-j2\pi f(u-k/2\pi f)}\, du\right] \times \left[\int_{-T+k/2\pi f}^{T+k/2\pi f} x(u)\, e^{-j2\pi f(u-k/2\pi f)}\right] du$$

$$= \lim_{T\to\infty} \frac{\exp\left(\frac{jk}{2\pi f}\right) \exp\left(\frac{-jk}{2\pi f}\right)}{2T} \times \left[\int_{-T+k/2\pi f}^{T+k/2\pi f} x(u)\, e^{-j2\pi fu}\, du\right] \times \left[\int_{-T+k/2\pi f}^{T+k/2\pi f} x(u)\, e^{-j2\pi fu} dt\right]$$

$$= S_x(f) . \quad (11)$$

Since the measured spectral density equals the true spectral density, it can also be stated through the Wiener Khintchine Theorem that a constant phase error will not cause any error in the measured autocorrelation function.

The above result can be extended to cover the general case where the phase angle becomes some arbitrary function of frequency,

$$\phi(f) = g(f) . \quad (12)$$

The substitution becomes

$$u = t + \frac{g(f)}{2\pi f} \quad \text{and} \quad du = dt . \quad (13)$$

Since the operation in Eq. (9) is essentially a narrowband filtering operation, $g(f_0)$ is a constant in the narrow frequency band about f_0. Hence, the measured spectral density equals the true spectral density. (The fact that $g(f)$ results in a new constant for each value of f does not influence the result, since a new value of $S_x^m(f)$ is computed for each value of f.) Again, this means that there will be no error in the autocorrelation function due to a static phase error.

Dynamic Phase Errors

Dynamic phase errors occur in the magnetic tape recorder from nonuniform velocity of the magnetic tape over the record and reproduce heads. Let an arbitrary function of time, $h(t)$, represent the dynamic phase error. Then the measured data has the form

$$x^m(t) = x[t + h(t)] . \quad (14)$$

The measured autocorrelation function is

$$\hat{R}_x^m(\tau) = \frac{1}{2T} \int_{-T}^{T} x^m(t)\, x^m(t+\tau)\, dt \quad (15a)$$

$$= \frac{1}{2T} \int_{-T}^{T} x[t+h(t)]\, x[t+\tau+h(t+\tau)]\, dt . \quad (15b)$$

($\hat{R}(\tau)$ represents an estimate of $R(\tau)$, the limiting value obtained as $T\to\infty$.) Because $h(t)$ is small (0.25 to 1 percent), Eq. (15b) can be approximated by letting

$$x[t + h(t)] \approx x(t)\, h(t)\, \dot{x}(t) , \quad (16)$$

$$x[t + \tau + h(t+\tau)] \approx x(t+\tau) + h(t+\tau)\, \dot{x}(t+\tau), \quad (17)$$

where only the first two terms of the Taylor series expansion are used, and the dot represents a time derivative ($\dot{x}(t) = d[x(t)]/dt$). (See Ref. (3).) Then

$$\hat{R}_x^m(\tau) \approx \frac{1}{2T} \int_{-T}^{T} [x(t) + h(t)\, \dot{x}(t)] \times [x(t+\tau) + h(t+\tau)\, \dot{x}(t+\tau)]dt$$

$$\approx \frac{1}{2T} \int_{-T}^{T} x(t)\, x(t+\tau)dt + \frac{1}{2T} \int_{-T}^{T} h(t+\tau)\, x(t)\, \dot{x}(t+\tau)dt \quad (18)$$

(Cont.)

$$+ \frac{1}{2T}\int_{-T}^{T} \dot{x}(t)\, x(t+\tau)\, h(t)\,dt$$

$$+ \frac{1}{2T}\int_{-T}^{T} \dot{x}(t)\, \dot{x}(t+\tau)\, h(t)\, h(t+\tau)\,dt. \quad (18)$$

If we repeat our measurement many times, we can find the expected value of the measured correlation function

$$R_x^m(\tau) = \left[E\, \hat{R}_x^m(\tau)\right]. \quad (19)$$

Separating out the individual components of Eq. (18), one finds

$$E\left[\frac{1}{2T}\int_{-T}^{T} x(t)\, x(t)\, x(t+\tau)dt\right] = R_x(\tau), \quad (20)$$

and since $x(t)$ and $h(t)$ are independent and stationary,

$$E\left[\frac{1}{2T}\int_{-T}^{T} x(t)\, \dot{x}(t+\tau)\, h(t+\tau)dt\right]$$

$$= \frac{R_x'(\tau)}{2T}\int_{-T}^{T} h(t+\tau)dt \quad \begin{matrix}(\text{when } h(t+\tau) \text{ is} \\ \text{deterministic})\end{matrix}$$

$$= 0 \quad (\text{when } h(t+\tau) \text{ is random with zero mean}) \quad (21)$$

where the prime denotes a derivative with respect to τ,

$$\left(R'(\tau) = \frac{d[R(\tau)]}{d\tau}\right).$$

$$E\left[\frac{1}{2T}\int_{-T}^{T} \dot{x}(t)\, x(t+\tau)\, h(t)\,dt\right]$$

$$= \frac{-R_x'(\tau)}{2T}\int_{-T-\tau}^{T-\tau} h(t-\tau)dt \quad \begin{matrix}(\text{when } h(t-\tau) \text{ is} \\ \text{deterministic})\end{matrix}$$

$$= 0 \quad (\text{when } h(t-\tau) \text{ is random with zero mean}) \quad (22)$$

$$E\left[\frac{1}{2T}\int_{-T}^{T} \dot{x}(t)\, \dot{x}(t+\tau)\, h(t)\, h(t+\tau)dt\right]$$

$$= -R_x''(\tau)\, R_h(\tau). \quad (23)$$

With a magnetic tape recorder, two types of dynamic phase errors occur from flutter. The first type of flutter is approximately sinusoidal, and results from rotational unbalances. The second type of flutter can be approximated by a white Gaussian, bandlimited, random noise. Examination of Eqs. (21) and (22), when $h(t)$ has a sinusoidal form, reveals that in taking the expected value of these equations, one would expect them to go to zero, since the phase angle of the sinusoid is an unknown random variable and is uniformly distributed about zero. Thus, for the magnetic tape recorder

$$R_x^m(\tau) \approx R_x(\tau) - R_x''(\tau)\, R_h(\tau). \quad (24)$$

Davies (4) shows that for a sinusoidal data signal modulated by one sinusoidal flutter component, when frequency modulation recording is used, the dynamic phase error is

$$h(t) = \frac{b}{2\pi f_3} \sin 2\pi f_3 t, \quad (25)$$

where

b = the peak flutter amplitude, and

f_3 = the flutter frequency.

Obviously, the lower the value of b and the higher the value of f_3, the less will the measured autocorrelation function vary from the true autocorrelation function.

To determine the effect of dynamic phase errors on the spectral density function, the Fourier transform of the measured autocorrelation function is taken:

$$S_x^m(f) = \int_{-\infty}^{\infty} R_x^m(\tau)\, e^{-j2\pi f\tau}\, d\tau$$

$$\approx \int_{-\infty}^{\infty} [R_x(\tau) - R_x''(\tau)\, R_h(\tau)]\, e^{-j2\pi f\tau}\, d\tau$$

$$\approx S_x(f) - \int_{-\infty}^{\infty} R_x''(\tau)\, R_h(\tau)\, e^{-j2\pi f\tau}\, d\tau. \quad (26)$$

Thus, the measured spectral density also has a bias error dependent upon the second derivative of the data correlation function and upon the correlation function of the dynamic phase error.

CROSS-CORRELATION AND CROSS-SPECTRAL DENSITY MEASUREMENTS

In the measurement of cross-correlation or cross-spectral density functions, both static and

dynamic phase errors contribute to inaccuracies. In the following sections, typical types of phase errors will be examined to demonstrate the inaccuracies that they cause.

Constant Time Delay Error

The true cross-correlation function is defined as

$$R_{xy}(\tau) = \lim_{T\to\infty} \frac{1}{2T} \int_{T}^{T} x(t)\, y(t+\tau)\, dt. \quad (27)$$

Let a constant time delay error, τ_0, be introduced into $y(t)$ relative to $x(t)$. This could be from using transducers with different natural frequencies, as one example,

$$y^m(t) = y(t+\tau_0). \quad (28)$$

The measured cross-correlation function becomes

$$R^m_{xy}(\tau) = \lim_{T\to\infty} \frac{1}{2T} \int_{-T}^{T} x(t)\, y(t+\tau_0+\tau)\, dt$$

$$= R_{xy}(\tau+\tau_0),$$

which means that the correlation function has been shifted along the τ axis by an amount τ_0. This error can be compensated easily if we know τ_0 accurately.

To see the effect of a constant time delay error on the cross spectrum, let us take the Fourier transform of the measured cross-correlation function

$$S^m_{xy}(f) = \int_{-\infty}^{\infty} R^m_{xy}(\tau)\, e^{-j2\pi f\tau}\, d\tau$$

$$= \int_{-\infty}^{\infty} R_{xy}(\tau+\tau_0)\, e^{-j2\pi f\tau}\, d\tau. \quad (29)$$

Making the substitution $u = \tau+\tau_0$, $du = d\tau$, one obtains

$$S^m_{xy}(f) = e^{j2\pi f\tau_0} \int_{-\infty}^{\infty} R_{xy}(u)\, e^{-j2\pi fu}\, du$$

$$= e^{j2\pi f\tau_0}\, S_{xy}(f). \quad (30)$$

The cross spectrum is frequently computed by measuring its real part (cospectrum) and imaginary part (quadspectrum), or the magnitude and phase factor of the cross spectrum

$$S_{xy}(f) = C_{xy}(f) - jQ_{xy}(f)$$

$$= |S_{xy}(f)|\, e^{j\phi_{xy}(f)}, \quad (31)$$

where

$C_{xy}(f)$ = the cospectrum,

$Q_{xy}(f)$ = the quadspectrum, and

$\phi_{xy}(f)$ = the phase factor.

It can be shown that a constant time delay phase error will result in the following measured values:

$$C^m_{xy}(f) = C_{xy}(f)\left[\cos 2\pi f\tau_0 + (\sin 2\pi f\tau_0)\left(\frac{Q_{xy}(f)}{C_{xy}(f)}\right)\right], \quad (33)$$

$$Q^m_{xy}(f) = Q_{xy}(f)\left[\cos 2\pi f\tau_0 - (\sin 2\pi f\tau_0)\left(\frac{C_{xy}(f)}{Q_{xy}(f)}\right)\right], \quad (34)$$

$$|S^m_{xy}(f)| = |S_{xy}(f)|, \quad (35)$$

$$\phi^m_{xy}(f) = \phi_{xy}(f) - 2\pi f\tau_0. \quad (36)$$

Constant Percentage Time Delay Error

A constant percentage time delay error can occur in the correlation analyzer, if the time delay mechanism or the readout is improperly calibrated. The measured value of the delayed signal is

$$y^m(t+\tau) = y(t+k\tau),$$

where k = a constant. The measured cross-correlation function with this type of phase error is

$$R^m_{xy}(\tau) = \lim_{T\to\infty} \frac{1}{2T} \int_{-T}^{T} x(t)\, y(t+k\tau)\, dt.$$

Let

$$u = k\tau \quad (37)$$

(Cont.)

$$u = \lim_{T \to \infty} \frac{1}{2T} \int_{-T}^{T} x(t)\, y(t+u)\, dt$$

$$= R_{xy}(u) = R_{xy}(k\tau) . \qquad (37)$$

The measured cross-spectral density function resulting when there is a constant percentage time delay type of error is

$$S^m_{xy}(f) = \int_{-\infty}^{\infty} R^m_{xy}(\tau)\, e^{-j2\pi f\tau}\, d\tau$$

$$= \int_{-\infty}^{\infty} R_{xy}(k\tau)\, e^{-j2\pi f\tau}\, d\tau .$$

Let

$$u = k\tau \quad \text{and} \quad du = k\,d\tau$$

$$S^m_{xy}(f) = \frac{1}{k} \int_{-\infty}^{\infty} R_{xy}(u)\, e^{-j2\pi(f/k)u}\, du$$

$$= \frac{1}{k} S_{xy}(f/k) . \qquad (38)$$

Thus, it can be seen that there is a scale factor introduced, as well as an expansion of the frequency axis.

Constant Percentage Frequency Error

Constant percentage frequency errors occur when the magnetic tape speed during reproduce differs from the recording speed, or when the frequency axis of the spectral analyzer is improperly calibrated. By analogy to Eq. (37),

$$S^m_{xy}(f) = S_{xy}(kf)$$

where k is a constant (the frequency calibration error).

The cross-correlation function measured with a constant percentage frequency error is

$$R^m_{xy}(\tau) = \int_{-\infty}^{\infty} S_{xy}(kf)\, e^{j2\pi f\tau}\, df$$

$$= \frac{1}{k} R_{xy}(\tau/k) , \qquad (39)$$

so that the constant percentage frequency type of phase error introduces a scale factor error and a τ axis expansion in the cross-correlation function analysis.

Constant Frequency Offset Error

Constant frequency offset errors can occur in heterodyne portions of the measuring circuit, or in the frequency spectrum analyzer readout. For example, assume that there is a 5 cps offset error. Then the true data at 100, 500, and 2000 cps is plotted at 95, 495, and 1995 cps, respectively. The measured spectral density is

$$\begin{aligned} S^m_{xy}(f) &= S_{xy}(f - f_0) ; \quad f \geq 0 , \\ S^m_{xy}(f) &= S_{xy}(f + f_0) ; \quad f \leq 0 , \end{aligned} \qquad (40)$$

where f_0 is the frequency offset error. This error in the cross-spectral density can be easily corrected if f_0 is known accurately.

When computing the effect of a frequency offset error on cross-correlation analysis, the Fourier transform of the cross spectrum must be separated into two parts, because the positive frequency portion of the cross spectrum is being translated in an opposite direction to the negative portion:

$$R^m_{xy}(\tau) = \int_{-\infty}^{0} S_{xy}(f + f_0)\, e^{j2\pi f\tau}\, df$$

$$+ \int_{0}^{\infty} S_{xy}(f - f_0)\, e^{j2\pi f\tau}\, df ,$$

Let

$$-(f + f_0) = v ; \quad dv = -df ,$$

and

$$f - f_0 = u ; \quad du = df ,$$

then

$$R^m_{xy}(\tau) = -\int_{\infty}^{-f_0} S_{xy}(-v)\, e^{j2\pi(-v-f_0)\tau}\, dv$$

$$+ \int_{-f_0}^{\infty} S_{xy}(u)\, e^{j2\pi(u+f_0)\tau}\, du$$

$$= \int_{-f_0}^{\infty} S_{xy}(-v)\, e^{j2\pi(-v-f_0)\tau}\, dv$$

$$+ \int_{-f_0}^{\infty} S_{xy}(u)\, e^{j2\pi(u+f_0)\tau}\, du ,$$

and since

$$\int_{-f_0}^{0} S_{xy}(-v)\, e^{j2\pi(-v-f_0)\tau}\, dv = 0 ,$$

and

$$\int_{-f_0}^{0} S_{xy}(u)\, e^{j2\pi(u+f_0)\tau}\, du = 0 ,$$

$$R^m_{xy}(\tau) = e^{-j2\pi f_0\tau} \int_0^\infty S_{xy}(-v)\, e^{-j2\pi v\tau}\, dv + e^{j2\pi f_0\tau} \int_0^\infty S_{xy}(u)\, e^{j2\pi u\tau}\, du$$

$$= [\cos 2\pi f_0\tau - j \sin 2\pi f_0\tau] \int_0^\infty [C_{xy}(v) + jQ_{xy}(v)][\cos 2\pi v\tau - j \sin 2\pi v\tau]\, dv + [\cos 2\pi f_0\tau + j \sin 2\pi f_0\tau] \int_0^\infty [C_{xy}(u) - jQ_{xy}(u)][\cos 2\pi u\tau + j \sin 2\pi u\tau]\, du .$$

Inspection of the above equation reveals that the two terms are complex conjugates of the form $A^* + A$ or $(a - jb) + (a + jb)$. Therefore, the measured cross-correlation function is equal to twice the real part of either term.

$$R^m_{xy}(\tau) = 2\,\mathrm{Re}\,[A]$$

$$= [2 \cos 2\pi f_0\tau] \int_0^\infty [C_{xy}(u) \cos 2\pi u\tau + Q_{xy}(u) \sin 2\pi u\tau]\, du - [2 \sin 2\pi f_0\tau] \int_0^\infty [C_{xy}(u) \sin 2\pi u\tau - Q_{xy}(u) \cos 2\pi u\tau]\, du$$

$$= R_{xy}(\tau) \cos 2\pi f_0\tau - [2 \sin 2\pi f_0\tau] \int_0^\infty \times [C_{xy}(u) \sin 2\pi u\tau - Q_{xy}(u) \cos 2\pi u\tau]\, du. \quad (41)$$

From Eq. (41), it can be seen that the effect of a constant frequency offset error on the cross-correlation analysis is to introduce a cosine multiplication of the true correlation function plus a bias error.

Constant Phase Shift Error

Next consider the case where the measured signal $y(t)$ is shifted by a constant number of degrees with respect to the measured signal $x(t)$. This error most frequently occurs in the phase mismatch of cross-spectral density analyzers. From Eqs. (6) and (8),

$$y^m_{f,B}(t) = y_{f,B}(t + \phi_0/2\pi f) ,$$

where $y_{f,B}(t)$ = the data signal passed through a bandpass filter of bandwidth B and center frequency f.

The cospectrum can be defined as

$$C_{xy}(f) = \lim_{\substack{T\to\infty \\ B\to 0}} \frac{1}{2BT} \int_{-T}^{T} x_{f,B}(t)\, y_{f,B}(t)\, dt , \quad (42)$$

and similarly, the quadspectrum can be defined as

$$Q_{xy}(f) = \lim_{\substack{T\to\infty \\ B\to 0}} \frac{1}{2BT} \int_{-T}^{T} x_{f,B}(t)\, y_{f,B}\left(t + \frac{\pi/2}{2\pi f}\right) dt . \quad (43)$$

The measured cospectrum becomes

$$C^m_{xy}(f) = \lim_{\substack{T\to\infty \\ B\to 0}} \frac{1}{2BT} \int_{-T}^{T} x(t)\, y\left(t + \frac{\phi_0}{2\pi f}\right) dt .$$

Removing the bandwidth limiting process, an estimate of the cospectrum is obtained.

$$\hat{C}^m_{xy}(f) = \lim_{T\to\infty} \frac{1}{2BT} \int_{-T}^{T} x(t)\, y\left(t + \frac{\phi_0}{2\pi f}\right) dt = \frac{1}{B}\left[R_{xy,f,B}\left(\frac{\phi_0}{2\pi f}\right)\right] , \quad (44)$$

where $R_{xy,f,B}(\phi_0/2\pi f)$ = the cross-correlation evaluated at $\tau = \phi_0/2\pi f$, obtained when both $x(t)$ and $y(t)$ are passed through narrow bandpass filters of bandwidth B and center frequency f.

Similarly, an estimate of the measured quadspectrum is obtained:

$$\hat{Q}^m_{xy}(f) = \frac{1}{B}\left[R_{xy,f,B}\left(\frac{\phi_0 + \frac{\pi}{2}}{2\pi f}\right)\right]. \qquad (45)$$

The true phase factor is

$$\phi_{xy}(f) = \tan^{-1}\frac{Q_{xy}(f)}{C_{xy}(f)},$$

and the measured phase factor is

$$\phi^m_{xy}(f) = \tan^{-1}\frac{Q^m_{xy}(f)}{C^m_{xy}(f)}$$

$$= \tan^{-1}\left\{\frac{\frac{1}{B}\left[R_{xy,f,B}\left(\frac{\phi_0 + \frac{\pi}{2}}{2\pi f}\right)\right]}{\frac{1}{B}\left[R_{xy,f,B}\left(\frac{\phi_0}{2\pi f}\right)\right]}\right\}$$

$$= \tan^{-1}\left\{\frac{R_{xy,f,B}\left(\frac{\phi_0 + \frac{\pi}{2}}{2\pi f}\right)}{R_{xy,f,B}\left(\frac{\phi_0}{2\pi f}\right)}\right\}. \qquad (46)$$

To evaluate Eq. (46), it is necessary to assume some specific form for the correlation function. Assume that single-tuned filters are used to compute the cross spectrum and to simplify the calculations assume that $y(t) = x(t)$. Then, from Ref. 3,

$$R_{xy,f,B}(\tau) = R_{x,f,B}(\tau) = R_x(0)e^{-b|\tau|}\cos 2\pi f_0\tau, \qquad (47)$$

where

$2b$ = the half power bandwidth of the filter,

f_0 = the center frequency of the filter,

$$\phi^m_{xy}(f_0) = \tan^{-1}\left\{\frac{e^{-b\left|(\phi_0+\pi/2)/2\pi f_0\right|}\cos\left[(2\pi f_0)\left(\frac{\phi_0 + \frac{\pi}{2}}{2\pi f_0}\right)\right]}{e^{-b\left|\phi_0/2\pi f_0\right|}\cos\left[(2\pi f_0)\left(\frac{\phi_0}{2\pi f_0}\right)\right]}\right\}$$

$$= \tan^{-1}\left\{\left[e^{-b/\left|(1/4f_0)\right|}\right]\left[-\tan\phi_0\right]\right\}.$$

The "q" of the filter is $f_0/2b$, hence

$$\phi^m_{xy}(f_0) = \tan^{-1}\left\{\left[e^{-|1/8q|}\right][\tan(-\phi_0)]\right\},$$

and if $q > 1$, as is the normal case,

$$\phi^m_{xy}(f_0) = -\phi_0.$$

As expected, the phase factor is in error by an amount ϕ_0. [$\phi_{xy}(f_0)$ should have been zero, since we assumed $y(t) = x(t)$.]

Now the effect of a constant phase error on the magnitude of the cross-spectral density will be determined.

$$\left|S^m_{xy}(f)\right| = \left\{\left[C^m_{xy,f,B}(f)\right]^2 + \left[Q^m_{xy,f,B}(f)\right]^2\right\}^{1/2},$$

$$\left|S^m_{xy}(f)\right| = \left\{\left[\frac{1}{B}R_{xy,f,B}\left(\frac{\phi_0}{2\pi f}\right)\right]^2 + \left[\frac{1}{B}R_{xy,f,B}\left(\frac{\phi_0 + \frac{\pi}{2}}{2\pi f}\right)\right]^2\right\}^{1/2}.$$

Assume, as before, that $x(t) = y(t)$ and the analysis filters are of the single-tuned variety.

$$\left|S^m_{xy}(f)\right| = \frac{R^2_{x,f,B}(0)}{B^2}\left\{\left[e^{-b|\phi_0/2\pi f|}\cos 2\pi f\left(\frac{\phi_0}{2\pi f}\right)\right]^2 + \left[e^{-b\left|\frac{\phi_0+\frac{\pi}{2}}{2\pi f}\right|}\cos 2\pi f\left(\frac{\phi_0}{2\pi f}\right)\right]^2\right\}^{1/2}$$

$$= \frac{R^2_{x,f,B}(0)}{B^2}\left\{\left[e^{-|\phi_0/4\pi q|}\cos\phi_0\right]^2 + \left[e^{-|\phi_0+\frac{\pi}{2}/4\pi q|}\cos\left(\phi_0 + \frac{\pi}{2}\right)\right]^2\right\}^{1/2}.$$

If $\phi_0 < \pi/2$ and $q > 1$,

$$\left|S^m_{xy}(f)\right| = \left\{\frac{R^2_{x,f,B}(0)}{B^2}\left[\cos^2\phi_0 + \sin^2\phi_0\right]\right\}^{1/2}$$

$$= \frac{R_{x,f,B}(0)}{B}.$$

Therefore,

$$\left|S^m_{xy}(f)\right| = \left|S_{xy}(f)\right|. \qquad (48)$$

Thus, as one would intuitively expect, a constant phase error does not cause an inaccuracy in the magnitude of the cross spectrum. The measured co- and quadspectra are:

$$C^m_{xy}(f) = \left| S^m_{xy}(f) \right| \cos \phi^m_{xy}(f)$$

$$= C_{xy}(f) \left[\frac{\cos \phi^m_{xy}(f)}{\cos \phi_{xy}(f)} \right] \qquad (49)$$

$$Q^m_{xy}(f) = \left| S^m_{xy}(f) \right| \sin \phi^m_{xy}(f)$$

$$= Q_{xy}(f) \left[\frac{\sin \phi^m_{xy}(f)}{\sin \phi_{xy}(f)} \right] . \qquad (50)$$

The inaccuracy in the cross-correlation function can be found by transforming the cross spectrum. The transform must be divided into two parts at f equal to zero, since the constant phase error causes the phase factor for positive frequencies to be translated in the opposite direction to the phase factor for negative frequencies. This can be seen from the symmetry properties of the cross spectrum (5).

$$C_{xy}(-f) = C_{xy}(f) , \qquad (51)$$

$$Q_{xy}(-f) = -Q_{xy}(f) . \qquad (52)$$

Since

$$\phi(f) = \tan^{-1} \frac{Q_{xy}(f)}{C_{xy}(f)} ,$$

$$\phi_{xy}(-f) = -\phi_{xy}(f) . \qquad (53)$$

Let the measured phase factor at positive frequencies be:

$$\phi^m_{xy}(f) = \phi_{xy}(f) + \phi_0 ; \qquad (54)$$

then the phase factor at negative frequencies is:

$$\phi^m_{xy}(f) = \phi_{xy}(f) - \phi_0 , \qquad (55)$$

and the cross spectrum can be written

$$S^m_{xy}(f) = |S_{xy}(f)| \, e^{j\phi_{xy}(f)+\phi_0} ; \quad f \geq 0 \qquad (56a)$$

$$= |S_{xy}(f)| \, e^{j\phi_{xy}(f)-\phi_0} ; \quad f \leq 0, \qquad (56b)$$

or

$$S^m_{xy}(f) = e^{j\phi_0} S_{xy}(f) ; \quad f \geq 0 \qquad (57a)$$

$$S^m_{xy}(f) = e^{-j\phi_0} S_{xy}(f) ; \quad f \leq 0 . \qquad (57b)$$

The measured cross-correlation function is written as follows:

$$R^m_{xy}(\tau) = e^{j\phi_0} \int_0^\infty S_{xy}(f) \, e^{j2\pi f\tau} \, df$$

$$+ e^{-j\phi_0} \int_{-\infty}^0 S_{xy}(f) \, e^{j2\pi f\tau} \, df .$$

Let $u = -f$ in the second integral, and $du = -df$, then

$$R^m_{xy}(\tau) = e^{j\phi_0} \int_0^\infty S_{xy}(f) \, e^{j2\pi f\tau} \, df$$

$$- e^{-j\phi_0} \int_\infty^0 S_{xy}(-u) \, e^{-j2\pi u\tau} \, du$$

$$= e^{j\phi_0} \int_0^\infty S_{xy}(f) \, e^{j2\pi f\tau} \, df$$

$$+ e^{-j\phi_0} \int_0^\infty S_{xy}(-u) \, e^{-j2\pi u\tau} \, du$$

$$= A + A^* ,$$

where A^* = the complex conjugate of A. Therefore,

$$R^m_{xy}(\tau) = 2 \, \mathrm{Re} \left[e^{j\phi_0} \int_0^\infty S_{xy}(f) \, e^{j2\pi f\tau} \, df \right]$$

$$= 2 \, \mathrm{Re} \left[(\cos \phi_0 + j \sin \phi_0) \int_0^\infty \left(C_{xy}(f) \right. \right.$$

$$\left. \left. - jQ_{xy}(f)(\cos 2\pi f\tau + j \sin 2\pi f\tau) \, df \right) \right]$$

$$= \cos \phi_0 R_{xy}(\tau) - 2 \sin \phi_0 \int_0^\infty$$

$$\times \left[C_{xy}(f) \sin 2\pi f\tau - Q_{xy}(f) \cos 2\pi f\tau \right] df . \qquad (58)$$

It can be seen that the constant phase error causes the measured cross-correlation function to be equal to the true value multiplied by a

cosine term plus a bias error. Notice that this result is very similar to that in Eq. (41).

Frequency Dependent Phase Errors

A general expression can be obtained for the inaccuracies caused by frequency dependent phase errors. For cross-spectral measurements

$$S^m_{xy}(f) = S_{xy}(f)\, e^{-j\phi_0(f)}, \qquad (59)$$

where $\phi_0(f)$ = the frequency dependent phase error.

For the cross-correlation measurements,

$$R^m_{xy}(\tau) = \int_0^\infty S_{xy}(f)\, e^{j2\pi f\tau} \times e^{j\phi_0(f)}\, df + \int_{-\infty}^0 S_{xy}(f)\, e^{j2\pi f\tau}\, e^{j\phi_0(f)}\, df .$$

Let $u = -f$, $du = -df$ in the second integral,

$$R^m_{xy}(f) = \int_0^\infty S_{xy}(f)\, e^{j2\pi f\tau} \times e^{j\phi_0(f)}\, df - \int_{-\infty}^0 S_{xy}(-u)\, e^{-j2\pi u\tau} \times e^{-j\phi_0(-u)}\, du$$

$$= \int_0^\infty S_{xy}(f)\, e^{j[2\pi f\tau+\phi_0(f)]}\, df + \int_0^\infty S_{xy}(-u)\, e^{-j[2\pi u\tau-\phi_0(-u)]}\, du$$

$$= A + A^*$$

$$= 2\,\mathrm{Re}\left[\int_0^\infty S_{xy}(f) e^{j[2\pi f\tau+\phi_0(f)]}\, df\right]. \qquad (60)$$

As an example, consider the case where the $y(t)$ signal is passed through an RC lowpass filter, while the $x(t)$ signal is not:

$$x^m(t) = x(t),$$

$$y^m(t) = y(t)\, A(f)\, e^{j\phi_0(f)},$$

$$A(f) = \frac{1}{\sqrt{1 + (2\pi fRC)^2}}, \qquad (61)$$

$$\theta(f) = -\tan^{-1}[2\pi fRC]. \qquad (62)$$

From Eq. (59),

$$S^m_{xy}(\tau) \approx S_{xy}(f)\, e^{-j[\tan^{-1}(2\pi fRC)]}, \qquad (63)$$

if f is restricted to a range where $A(f) \approx 1$.

To compute the inaccuracy in the cross-correlation function, let $A(f)$ be restricted as follows:

$$1.0 \geq A(f) \geq 0.98 .$$

From Eq. (61), we find the highest permissible frequency, f_h,

$$f_h = \frac{0.2}{2\pi RC},$$

and from Eq. (62), the maximum phase shift is found to be

$$\theta_{max} = \theta(f_h) = -0.2 .$$

From Eq. (60),

$$R^m_{xy}(\tau) \approx 2\,\mathrm{Re}\left[\int_0^\infty S_{xy}(f) e^{j[2\pi f\tau - \tan^{-1}(2\pi fRC)]}\, df\right].$$

The arc tan can be expanded as follows:

$$\tan^{-1}x = x - \frac{x^3}{3} + \frac{x^5}{5} - \frac{x^7}{7} \ldots,$$

and since for the highest frequency of operation,

$$\tan^{-1}(0.2) = 0.2 - \frac{(0.2)^3}{3} + \frac{(0.2)^5}{5} - \frac{(0.2)^7}{7} \ldots \approx 0.2,$$

we can write

$$-\tan^{-1}(2\pi fRC) \approx -2\pi fRC .$$

Therefore,

$$R^m_{xy}(\tau) \approx 2\,\mathrm{Re}\left[\int_0^\infty S_{xy}(f)\, e^{j2\pi f(\tau - RC)}\, df\right] \approx R_{xy}(\tau - RC),$$

which is the same result as for a constant time delay type of phase error. This is to be expected, since the maximum frequency was restricted to a range in which $\theta(f)$ is linear.

Dynamic Phase Errors

The most severe dynamic phase errors in the measurement system occur in the magnetic tape recording process. These errors are caused by the nonuniform velocity of the tape and motion of one tape track relative to another. Dynamic skew, differential flutter, and differential head stack vibration are sources of this relative motion (6). This error is commonly called dynamic Interchannel Time Delay Error (ITDE). The measured values of $x(t)$ and $y(t)$ are:

$$x^m(t) = x[t + g(t)] , \tag{64}$$

$$y^m(t) = y[t + h(t)] . \tag{65}$$

The estimate of the measured cross-correlation function then becomes

$$\hat{R}^m_{xy}(\tau) = \frac{1}{2T} \int_{-T}^{T} x[t + g(t)]\ y[t + \tau + h(t + \tau)]\ dt . \tag{66}$$

Following the development for the effects of dynamic phase errors on autocorrelation analyses, $x[t + g(t)]$ and $y(t + \tau + h(t + \tau))$ are approximated by the first two terms of a Taylor series.

$$x[t + g(t)] \approx x(t) + g(t)\ \dot{x}(t) ,$$

$$y[t + \tau + h(t + \tau)] \approx y(t + \tau) + h(t + \tau)\ \dot{y}(t + \tau) ,$$

$$\hat{R}^m_{xy}(\tau) \approx \frac{1}{2T} \int_{-T}^{T} [x(t) + g(t)\ \dot{x}(t)]\ [y(t + \tau) + h(t + \tau)\ \dot{y}(t + \tau)]\ dt$$

$$\approx \frac{1}{2T} \int_{-T}^{T} [x(t)]\ [y(t + \tau)]\ dt + \frac{1}{2T} \int_{-T}^{T} g(t)\ \dot{x}(t)\ y(t + \tau)\ dt + \frac{1}{2T} \int_{-T}^{T} h(t + \tau)\ x(t)\ \dot{y}(t + \tau)\ dt + \frac{1}{2T} \int_{-T}^{T} g(t)\ h(t + \tau)\ \dot{x}(t)\ \dot{y}(t + \tau)\ dt .$$

Since $x(t)$ and $y(t)$ are independent of $g(t)$ and $h(t)$, and all four are stationary,

$$E\left[\hat{R}^m_{xy}(\tau)\right] \approx R_{xy}(\tau) - R''_{xy}(\tau)\ R_{gh}(\tau) . \tag{67}$$

(As shown previously, the middle two terms vanish for the dynamic phase error functions typical of magnetic tape recorders.) Thus, the measured cross-correlation function is equal to the true cross-correlation function plus a bias term. This bias term is the product of the second derivative of the cross-correlation function of the data and the cross-correlation function of the dynamic phase error signals.

The effect of these dynamic phase errors on cross-spectral density analyses can be determined by taking the Fourier transform of the measured cross-correlation function:

$$S^m_{xy}(f) = \int_{-\infty}^{\infty} R^m_{xy}(\tau)\ e^{-j2\pi f\tau}\ d\tau$$

$$\approx \int_{-\infty}^{\infty} \left[R_{xy}(\tau) - R''_{xy}(\tau)\ R_{gh}(\tau)\right] e^{-j2\pi f\tau}\ d\tau$$

$$\approx S_{xy}(f) - \int_{-\infty}^{\infty} R''_{xy}(\tau)\ R_{gh}(\tau)\ e^{-j2\pi f\tau}\ d\tau . \tag{68}$$

This measured cross-spectrum is then equal to the true cross spectrum, plus a bias error that also depends on the second derivative of the cross-correlation function of the data and the cross-correlation function of the dynamic phase errors.

ACKNOWLEDGMENT

The author sincerely expresses his gratitude to Mr. George P. Thrall and Mr. Loren D. Enochson for the contributions they made to this paper, and to the Unsteady Aerodynamics Branch of the Marshall Space Flight Center of the National Aeronautics and Space Administration for their support of this work.

REFERENCES

1. R. D. Kelly, "Transducers for Sonic Fatigue Measurements," AFFDL-TR-64-171, Feb. 1965

2. D. Middleton, An Introduction to Statistical Communication Theory (McGraw-Hill, New York), 1960

3. J. S. Bendat, Principles and Applications of Random Noise Theory (John Wiley and Sons, Inc., New York), 1958

4. G. L. Davies, Magnetic Tape Instrumentation (McGraw-Hill, New York), 1961

5. J. S. Bendat, L. D. Enochson, and A. G. Piersol, "Analytical Study of Vibration Data Reduction Methods," prepared for NASA-MFSC, Sept. 1963

6. R. D. Kelly, "Systems for the Collection and Analysis of Dynamic Data," AFFDL-TR-65-94, May 1965

* * *

UTILIZATION OF A DIGITAL COMPUTER FOR ON-LINE ACQUISITION AND ANALYSIS OF ACOUSTIC AND VIBRATION DATA

Daniel J. Bozich
Wyle Laboratories Research Staff
Huntsville, Alabama

An analysis requirement of unprecedented magnitude results from the large numbers of transducers needed to measure an increasing number of experimental variables during flight environment measurement and laboratory environment simulation test programs. An analog/digital data system was developed to acquire either random or sinusoidal sweep test data from a large number of data channels within the real-time duration of the test, and to store these data on digital magnetic tape for later analysis and reduction. Techniques were also developed and programmed in conjunction with this system, for acquiring and analyzing random data or sinusoidal sweep data. The unique technique developed for the acquisition and analysis of sinusoidal sweep (or step) data preserves the response amplitude and relative phase angle characteristics of each channel in a way such that a variety of interchannel relationships can be established accurately. Input and transfer functions throughout the force generating system and the vehicle structural system can be obtained easily and interrelated, even though the data are taken at different times. This technique is summarized. Examples of input force amplitudes vs frequency, and force-to-acceleration transfer function amplitudes vs frequency, obtained from the sinusoidal sweep analysis computer program, are included. Wherever possible, analog analyses are included for comparison. Examples of these same functions condensed into one-third octave band average values of their mean square amplitudes are also presented.

INTRODUCTION

Reliability testing of present and future aerospace vehicles is complicated by the increase in their size and complexity and the accompanying increase in the dynamic environments of these vehicles. Further complications are presented by concurrent increases in reliability requirements, which result in higher densities of measurement points and higher accuracy limitations on dynamic response data. Unfortunately, the attainment of a high degree of reliability usually results in an overdesigned and overweighted vehicle. Space missions, which are becoming exceedingly complex and lengthy, impose stringent requirements on weight-limited aerospace vehicle systems and structures. Consequently, flight environment measurement programs and laboratory environment simulation programs of unprecedented magnitudes are required to ensure mission success.

The extensive nature of these test programs, which involve large numbers of transducers to measure an increasing number of experimental variables, results in data analysis requirements of formidable proportions. Conventional analog analysis techniques prove excessively cumbersome, time-consuming, and expensive for this task. Therefore, a unique, high-speed, hybrid analog/digital data acquisition and analysis system was developed, which could handle the necessary volumes of data, as well as provide an extensive repertoire of analysis methods and techniques to cover the broad spectrum of dynamic environmental data forms. This system can be utilized to acquire and analyze both flight environmental data and laboratory test data, including:

1. Fluctuating or steady-state pressure data.
2. Structural vibration or acceleration data.

3. Dynamic strain data.

4. Dynamic force data.

These may be acquired from wide-band random excitation, sinusoidal sweep (or step) excitation, or sinusoidal resonance dwell excitation.

Laboratory simulation of these environments, which is accomplished by combinations of acoustic, mechanical, and aerodynamic excitation facilities, is used to experimentally test vehicles, vehicle structural components, and equipment. Microphones, accelerometers, strain gauges, and force gauges are the transducers used to provide dynamic data of excitation and response level measurements during actual vehicle flights, and during tests which simulate flight environments. In general, mechanical excitation sources are localized forces acting at fixed points on the structure, while acoustic and aerodynamic excitation sources produce pressure disturbances over large areas of the structure. These sources may couple with various structural elements of the vehicle in such a way as to alter the effectiveness of the excitation sources, or produce apparent secondary sources within the structure. Thus, the effect of interaction between two or more sources or corresponding responses is a basic characteristic of the experimental results.

A growing interest in the joint properties between two measurement points has arisen from increased vehicle size and the necessity to evaluate the relationships between relatively remote sections of large vehicles. Knowledge of the dynamic relationships between measurement points greatly enhances the evaluation of vehicle performance and reliability.

A reasonably detailed description of an acoustic field and/or the vibration of a structure can be obtained from an analysis of random response data. A statistical description of the amplitude characteristics of the vibration data is obtained from a determination of the amplitude probability density function. An evaluation of the autocorrelation function yields a statistical description of the time correlation characteristics of the data. A statistical description of the frequency composition of the random data is determined by the power spectral density function. Furthermore, if data are obtained from two or more vibration responses simultaneously, several joint properties can be evaluated. These joint properties include: (a) joint amplitude probability density functions, (b) crosscorrelation functions, (c) cross-power spectral density functions, and (d) several transfer functions. All of this information can be used to describe the vibration characteristics of a structure excited by random forces within statistical accuracies.

On the other hand, a detailed description of structural vibration can be obtained from sinusoidal response data. The response amplitude can be accurately determined at the sinusoidal excitation frequency. And, if the data from two or more vibration responses are obtained simultaneously, then the relative amplitude and relative phase angle relationships between each pair of measurement points can be obtained. Joint relationships which can be obtained include: (a) transmissibilities, (b) force-to-acceleration input and transfer functions, (c) acceleration-to-acceleration input and transfer functions, (d) input and transfer impedance functions, and (e) spatial correlation functions. These joint properties are obtained with deterministic accuracies, rather than with statistical accuracies.

An analog to digital data system requires a minimum of two synchronized (simultaneous sampling) analog-to-digital conversion channels to satisfy the above requirements. Three factors need to be considered in the design of a general purpose hybrid analog/digital data system, in addition to the normal system hardware and software (programs) requirements. These factors relate the system to the three primary data processing tasks which the system must be able to handle:

1. The first factor to be considered involves the basic problem of acquiring a large number of data channels on-line within the real time duration of the test while, at the same time, preserving the amplitude and phase characteristics of each data signal and the interchannel relationships among the entire collection of data signals. These data must be stored for later retrieval, analysis, and reduction.

2. Retrieval of the data and the required analysis of the data, to obtain the desired basic raw information about each data channel and about certain of its interchannel (joint) relationships with the other data channels, comprise the second factor.

3. The most important application of the system is the evaluation and reduction of the large mass of basic raw information obtained from the test response data. This library of detailed information must be evaluated, compared, manipulated, and condensed into several presentation forms for engineering and management review. Empirical correlation (1) of the excitation environment and detailed

structural parameters with the vibration response of the structural system provides a method for evaluating and effectively condensing the test results, for example.

The use of an analog/digital data system will relieve the engineering staff of the redundant, inadequate, and sometimes erroneous, task of performing data reduction by hand. A considerable saving in decision reaction time is thus obtained.

ANALOG/DIGITAL DATA SYSTEM

The analog to digital data system is capable of acquiring test data in real-time directly on-line to a CDC 3200 computer system which formats and records the data on digital magnetic tape. The system is capable of acquiring (in real-time) sinusoidal and random signals in the frequency range from dc to 10,000 cps, nominally, and, with somewhat decreasing accuracy, up to 25,000 cps. Analysis of the data can be carried out by several methods to examine spectral, amplitude, or statistical properties, with the results presented in graphical or tabular form.

The analog/digital data system comprises two distinct subsystems (following the conventional analog instrumentation) (a) the analog to digital data conversion system, and (b) the digital computer system. Both systems are required for data acquisition; however, only the digital computer system is needed for data analysis and data presentation (plotting and/or printing).

These two systems and their operations during data acquisition and analysis will be described in more detail in this section.

Data Conversion System

The data conversion system is used on-line to convert analog signals received during a test from two channels at a time to two twelve-bit binary words, which are passed on to the CDC 3200 computer system. Six units comprise the data conversion system, as shown in Fig. 1. With the following units, the system can sample up to 128 data channels, or 64 pairs of data channels, in specified addressable/sequential modes:

1. 128-channel patch panel.
2. 64-channel multiplexer A.
3. 64-channel multiplexer B.
4. Analog-to-digital converter A.
5. Analog-to-digital converter B.
6. Control and interface logic.

Characteristics of the analog signals acceptable to the system are:

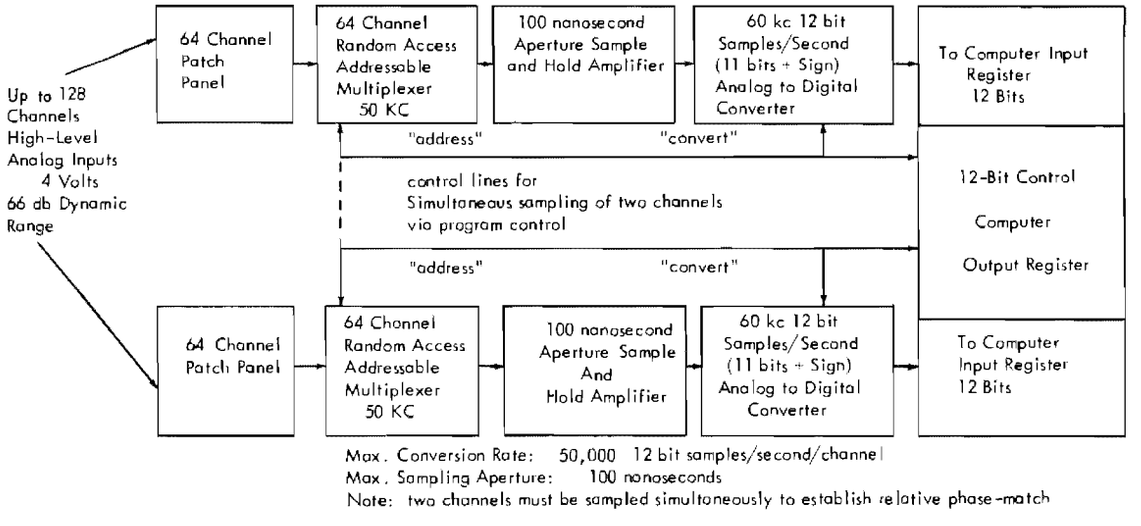

Fig. 1. Schematic of on-line analog to digital dual channel data conversion system

1. Signal input level ±1 volt with peaks up to ±3 volts.

2. Source resistance less than 1000 ohms.

3. Frequency range up to 10,000 cps (nominally) or up to 25,000 cps with reduced accuracy (sharp low-pass cutoff at 25,000 cps).

Digital Computer System

A Control Data Corporation CDC 3200 digital computer comprises the basic system for controlling the on-line real-time data acquisition operation, storing the acquired digital data, analyzing the data subsequent to the test, and presenting the results in printed and/or graphical form. The initial system configuration shown in Fig. 2 has the following components:

1. Magnetic core storage module with 16,384 24-bit words and a memory cycle time of 1.25 μsec per 24-bit word.

2. Central processing unit with two 12-bit input/output communication channels.

3. Console and input/output typewriter.

4. Four digital magnetic tape recorders, each of which has a maximum transfer rate of 60,000 6-bit characters per sec (15,000 words per sec).

5. High speed card reader, which reads 1200 80-column punched cards per minute.

6. High speed line printer, which prints 1000 132-column lines per minute.

7. Calcomp incremental X-Y plotter, which plots up to 300 points per sec, 0.01 in. apart in both the X- and Y-directions.

8. Data conversion system with 24-bit input/output communication channel.

This system is capable of being expanded to include:

1. Up to 32,768 words of magnetic core storage.

2. Floating point hardware.

3. Up to eight input/output communication channels.

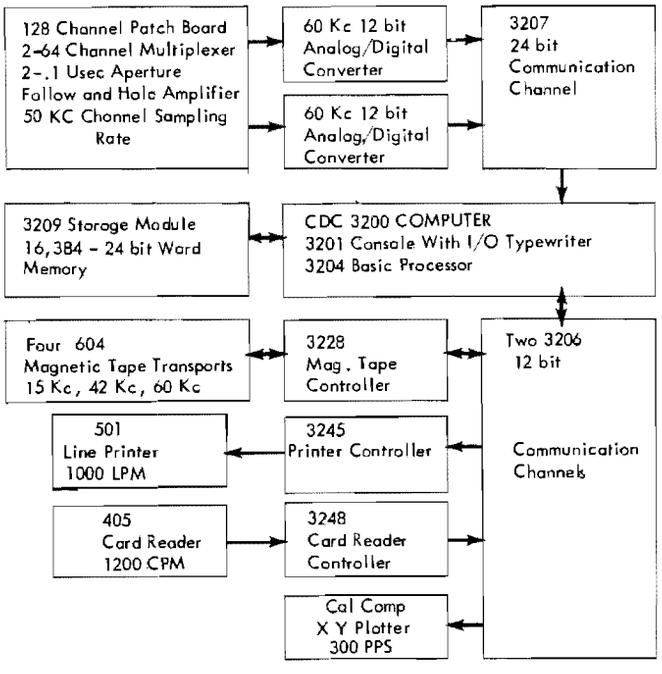

Fig. 2. Analog digital data system

4. Up to sixty-four digital magnetic tape recorders with speeds of 60,000, 83,400, 120,000, or 240,000 characters per sec.

5. Several types of mass-memory units.

6. High-speed oscilloscope/35 mm camera plotter at speeds up to 30 frames per sec.

7. Data conversion systems with 24-bit sampling rates (2-12-bit systems) up to 250,000 samples per sec and even up to 1,000,000 samples per sec; however, this rate requires special equipment and handling.

Some of the outstanding features of the system for data handling are:

1. True high-speed buffering capability.

2. Extremely fast 24-bit fixed point arithmetic (2.5 μsec 24-bit add; 12 μsec 24-bit multiply; 12 μsec 24-bit divide) with 48-bit arithmetic also.

3. Extremely fast and reliable digital magnetic tape recorders with forward and backward read capability.

4. Basic 24-bit word size and ease of interfacing 24-bit communication channel.

Data Acquisition — General Operation

Accuracy in obtaining the statistical transfer relationships between any two measured structural responses requires that two data channels be sampled simultaneously to avoid interchannel phase mismatch errors. The analog to digital subsystem was designed to preserve this accuracy. Also, analog data which has been previously recorded on analog tape channels can be played back to the system and subsequently sampled and analyzed accordingly.

However, as indicated above, any interchannel phase mismatch, which might exist as a result of record and playback instrumentation, will introduce an inherent error in the joint relationships between each subject channel pair.

Therefore, the key operation in digitizing and storing the analog test data is principally one of precise timing and control. The computer program, which has complete control over the entire process, generates the necessary timing and control binary signal codes and transmits them to particular data system components in time to initiate that component's responsible function within the overall operation.

The major components of this data acquisition system are: (a) the analog signal source transducer, (b) analog signal conditioning instrumentation, (c) analog sample multiplexer, (d) analog sample and hold amplifier, (e) analog sample-to-digital sample converter, (f) digital computer communication channel, with digital sample input register and analog system controller, (g) digital computer system with digital sample core memory storage buffers, and (h) digital magnetic tape recording transports for digital sample storage and transport controller. The operation of each of these components is discussed, in detail, in the following.

The analog signal source transducer generates a time-varying electrical signal in response to a mechanical disturbance imposed upon the transducer. This electrical analog signal is sent through a signal conditioning instrumentation channel, which scales the signal amplitude to within a specified amplitude limit.

Each source transducer's analog signal channel is connected to a multichannel multiplexer which, on command from the computer, selects an input analog signal channel and takes a time sample of the analog signal amplitude by switching itself on and then off. This relatively short analog sample is, in turn, sampled by the very narrow time aperture of the sample-and-hold amplifier. It is this analog sample (pulse) which is to be converted to digital binary form.

The analog sample pulse is held by the sample-and-hold amplifier until the analog-to-digital converter has converted it by successive approximation to a digital sample consisting of its sign and absolute magnitude in binary format. The digital binary sample is then assembled in parallel on an input register in the digital computer's communication channel.

A patch panel is provided with 130 dual-wired jacks for patching analog input signals and start/stop control signals into the system. Two jacks are provided for each channel for flexibility in patching in the analog input signal lines. All signal jacks are wired as short circuits when not in use.

The multiplexers are Texas Instruments, Inc., Model 845E03, with 64 differential* input

*Field change from delivered single-ended input channels to avoid grounding problems.

channels each (expandable to 160). They are solid-state time-division multiplexers offering accurate, high-speed bipolar switching. Accuracy is ±0.02 percent of full scale, at the maximum 50,000 channels per sec sampling rate. The units are programmable in either addressable or sequential modes. The two sixty-four channel addressable-sequential multiplexers provide the ability to select predetermined channel pairs, thus providing the capability to analyze up to 128 single channels, and to analyze up to 64 × 64 two-channel relationships among these 128 channels. The two selected channels are then sampled and converted to digital form (11 binary bits + sign) simultaneously until the desired record length is obtained. This process is completed in a period of time of one to five minutes for a 64-channel system, the exact time being a function of the bandwidth.

For low sinusoidal frequencies or random inputs with a low cut-off frequency, advantage can be taken of the fact that the required data sampling rate is low and, therefore, many channel pairs can be sequentially sampled within the same period. Figure 3 illustrates the relation between maximum signal frequency per channel, number of channels, and desired number of samples per cycle for the maximum 50,000 channels per sec rate. The channel sampling rate of the multiplexers means that any subgroup of channels from one to sixty-four can be sequentially sampled at a rate of 50,000 samples per sec by repeated successive switching between the channels of the subgroup. Figure 4 illustrates the importance of source resistance on percentage of channel crosstalk relative to the full scale input level. Figure 5 shows the importance of source resistance on the multiplexer settling time (the time for the sampled output to reach within ±10 percent of its final value).

Two Texas Instrument, Inc., Model 846-DIA-03D high speed analog-to-digital converters are used in the system. The analog-to-digital converters have built-in sample-and-hold amplifiers. The maximum overall conversion rate per channel is 60,000 12-bit samples per sec with an accuracy of ±0.05 percent of full scale at this rate. The converters are successive approximation, feedback voltage encoders, utilizing a built-in precision reference, and an integral sample-and-hold circuit with a 100 nanosecond aperture. Figure 6 contains an illustration of the error due to aperture time as a function of signal frequency. Thus, the analog to digital converters are capable of digitizing the analog samples received from the multiplexers at the rate of 60,000 conversions per sec with an amplitude resolution of one part in 2048 to within 0.1 percent (66 db dynamic range).

The control unit interfaces the data conversion system to the CDC 3200 computer

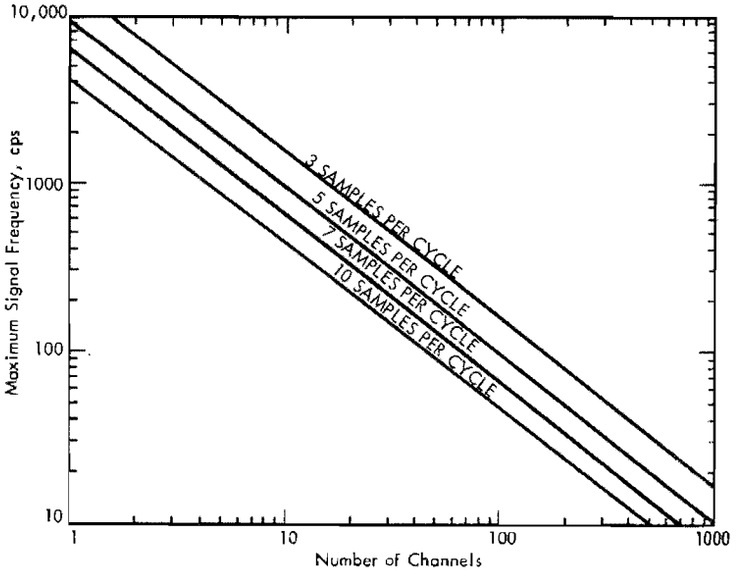

Fig. 3. Relation between maximum signal frequency per channel, number of channels, and desired number of samples per cycle (shown for a multiplexer channel switching rate of 50,000 samples per sec)

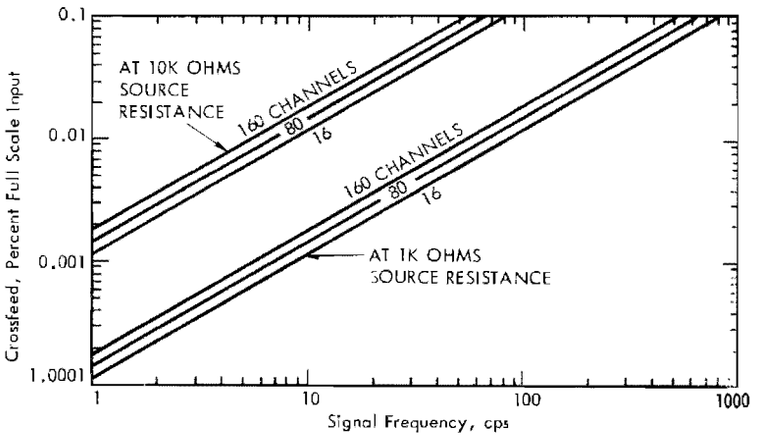

Fig. 4. The effect of source resistance on multiplexer channel crosstalk

system's 24-bit input/output communication channel. The computer treats the data conversion system as a peripheral device with input and output capabilities. The control unit controls the operation and timing of the multiplexers and converters, as well as the transfer of the digitized data.

The data conversion system operates as a dual channel analog-to-digital conversion system. Two analog signals (available from the patch panel via the multiplexers) are digitized simultaneously into two 12-bit binary words, assembled into a 24-bit word and transferred to the computer input/output channel.

The analog-to-digital system controller, which keeps precise timing control of all the above processes, signals the computer central processor that the input register of the communication channel is loaded with a digital sample, and either awaits further instructions, or automatically returns to repeat the sampling process in accordance with a predetermined sampling rate. The computer's central processor transfers the sample from the input register to a location within an allocated core memory buffer block upon receipt of the signal from the controller. The entire sampling procedure is repeated, filling the core memory buffer block locations sequentially until the buffer block is

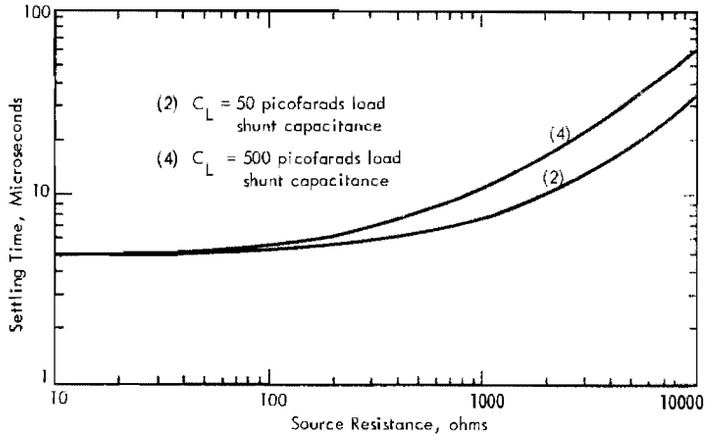

Fig. 5. The effect of source resistance on multiplexer settling time (shown for two values of load capacitance)

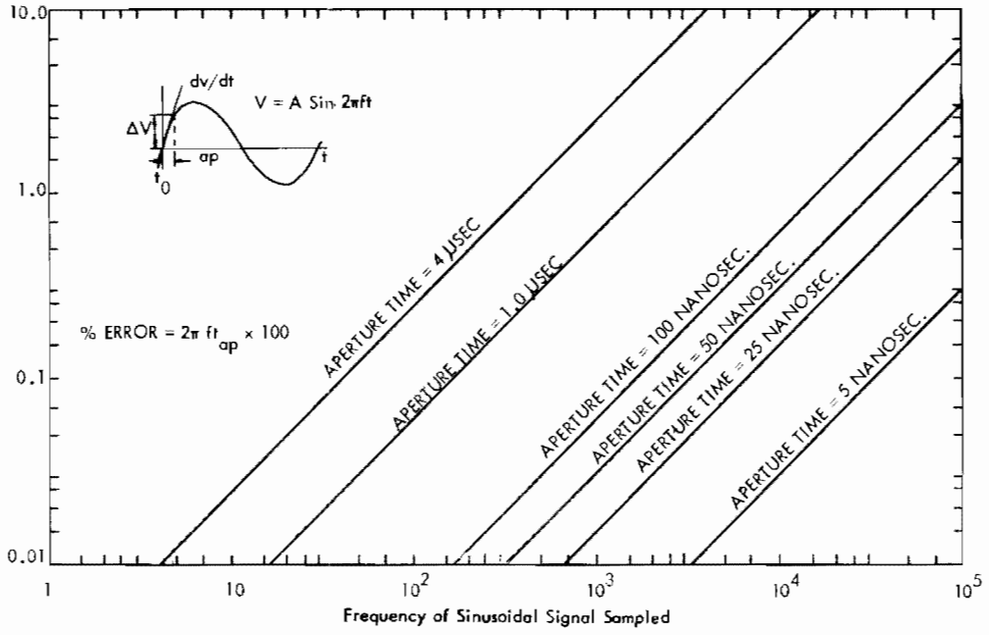

Fig. 6. Maximum error due to aperture time as a function of sample data frequency

full. At this time, the operation is transferred to core memory locations in a second buffer block without interrupting the flow of sampled data. At the same time, the magnetic tape transport controller is instructed to sequentially transfer the entire first buffer block onto digital magnetic tape, for storage with proper identifications added to the transferred data records where needed for later retrieval. This "flip-flop" procedure is repeated for the two buffer blocks until all of the desired data have been recorded.

Once all of the data desired have been recorded on digital magnetic tape, the test may cease. The data are now ready for retrieval, analysis, and reduction.

Data Analysis Capabilities (Summary)

In the analysis of random data, the experimenter must choose the desired frequency range, filter bandwidth, and statistical accuracy. These choices affect the sampling rate, number of time lags, and total number of samples required. These parameters, in turn, determine the recording and analysis time required per channel. The random data analysis capabilities of the computer facility are summarized in Table 1. The quantities which are presently available from the random data analysis computer program include: (a) sample mean value, (b) sample variance, (c) estimated autocorrelation function, and (d) estimated spectral density function. Additional functions which will be available from the analysis program in the near future include: (a) amplitude probability density function, (b) amplitude probability distribution function, (c) skewness and kurtosis of the data sample (d) estimated crosscorrelation function, (e) estimated cross-spectral density function, and (f) joint probability density function.

The analysis of sinusoidal sweep data requires the experimenter to choose the maximum expected response amplitude dynamic magnification factor Q, the desired frequency range, and the resolution accuracy requirement. These choices affect the sweep rate and data sampling requirement. Table 1 summarizes the sine sweep data analysis capabilities of the computer facility. The sinusoidal sweep data analysis program includes computation of the following quantities: (a) frequency of source signal, (b) amplitude of source and response signals, (c) relative phase between any pair of selected signals, and (d) transmissibility (or transfer function amplitude) between any pair of selected signals. The analysis method automatically rejects harmonic response signals.

TABLE 1
Data Analysis Capability

Random Noise	Available 1 April 1966	Present Capability	Example
Frequency range	0 - 10,000 cps	5 - 2000 cps	5 - 500 cps
Number of data points/channel	Unlimited	9000	9000
Maximum number of lags	Relatively unlimited	1000	250
Minimum filter bandwidth	Variable	Variable	10 cps
Number of degrees of freedom	Variable	Variable	72
Number of channels	192	128	60
Data input	Analog or digital	Analog	Analog
Data output	Digital magnetic tape, X-Y plotter and/or line printer	Digital magnetic tape, X-Y plotter and/or line printer	X-Y plotter
Data acquisition time	Variable	Variable	Approx. 1 min
Sine Sweep			
Frequency range	0 - 10,000 cps	5 - 4000 cps	5 - 500 cps
Minimum number of data points between -3 db points on resonance curves with Q = 50	5	5	5
Sweep rate	Variable	Variable	One octave/min
Number of channels	192	64	64
Data input	Analog or digital	Analog	Analog
Data output	Digital magnetic tape, X-Y plotter and/or line printer	Digital magnetic tape, X-Y plotter and/or line printer	X-Y plotter
Data acquisition time	Variable	Variable	Approx. 12 min

Sampling Accuracy of the Data Conversion System (2)

The conversion of an analog signal into digital form involves quantization. Each quantum or increment represents the smallest change between two successive analog input values that produces a change in the digital output. The process of quantizing an analog input voltage is shown in Fig. 7, where the "best fit" is obtained by using eleven equal increments (the 12th increment being greater by more than one-half an increment). Thus, if no other errors are present, the digital output does not vary from the actual analog input by more than one-half of the quantization level. This level may be referred to as the analog value of the least significant bit of the analog-to-digital converter.

For example, in an analog-to-digital converter with 11-bit accuracy and a full-scale analog input voltage of ±2.048 v, the inaccuracy due to the quantization error of one-half the least significant bit (LSB) is found from the following equation for the analog value of one digital bit (or count):

$$V_c = \frac{V_F}{2^n - 1} = \frac{2.048 \text{ volts}}{2047} = 1.0005 \text{ mv}, \quad (1)$$

to be

$$\frac{1}{2} V_c = 0.50025 \text{ mv},$$

where

V_F = full scale input voltage,

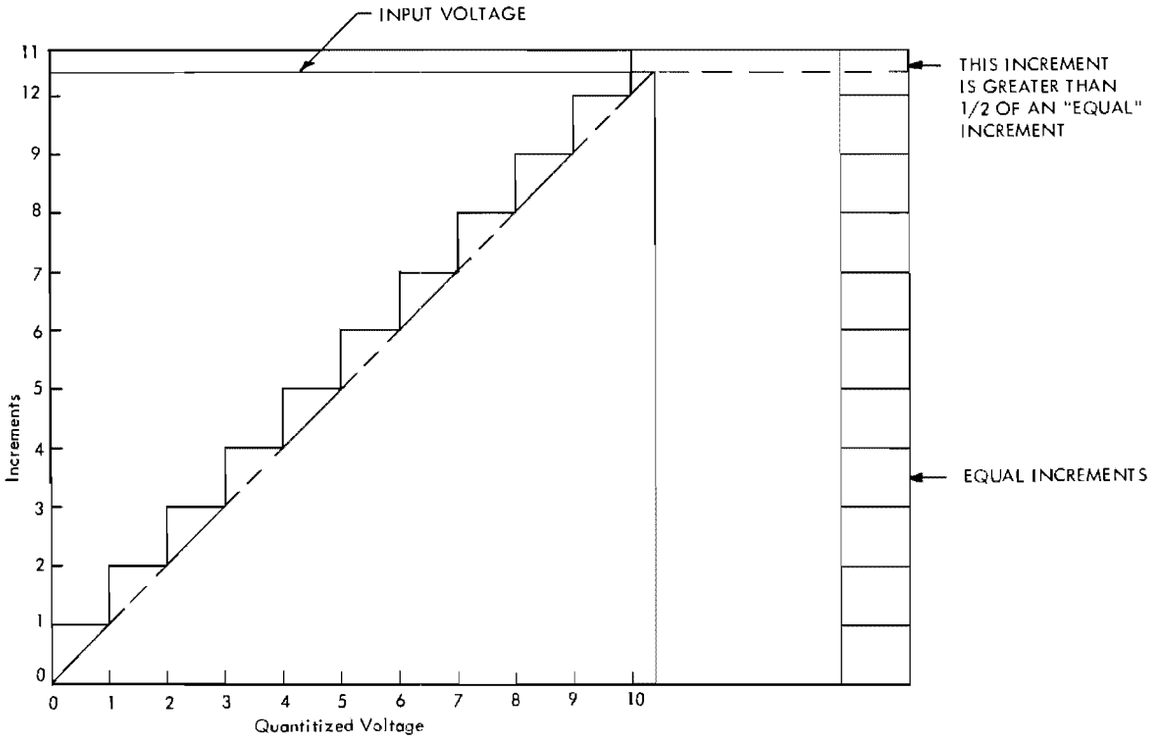

Fig. 7. Quantized voltage and best fit of equal increments

V_c = analog value of 1 count, and

n = number of bits of resolution.

This inaccuracy is independent of the actual value of the input signal, and represents a full scale accuracy of 0.50025 mv/2.048 v or 0.025 percent of full scale. Figure 8 contains a graph of the normalized error (mv/v) due to quantization level (one-half LSB) vs the number of bits of resolution.

Analog-to-digital converters have an associated "window" or aperture time, which produces an additional error. An aperture time comprises a time-lag uncertainty and a disconnect-time uncertainty, both caused by switch-control jitter and finite switch-operating time. The effect of aperture time produces an amplitude error for a given time, during which the measurement is taken, or, alternatively, a time error in measuring a given amplitude. Figure 9 illustrates the effect of the uncertainties that comprise the aperture time.

Aperture time and error due to quantization level are interrelated for rapidly varying analog input voltages. The one-half least significant bit error due to quantization level prescribes a maximum rate of change of input voltage to a given analog-to-digital converter. For example, consider the previously-cited example with the 11-bit converter, which has a 100 nanosecond aperture time limit. Then the maximum rate-of-change of the analog input voltage for a one-half least significant bit quantization level of 0.50025 millivolts is from Fig. 10, 0.50025 mv/100 nanoseconds = 5.0025 mv/μsec. Figure 10 illustrates this example.

The maximum voltage error ΔV due to aperture time t_{ap} occurs on a sine wave as it passes through zero volts. The maximum relative voltage error $\Delta V/V_F$, due to aperture time t_{ap}, is a function of frequency f, and is given by the equation:

$$\frac{\Delta V}{V_F} = 2\pi f \, t_{ap} . \qquad (2)$$

Data error $\Delta V/V_F$ is shown graphically in Fig. 6 for t_{ap} = 100 nanoseconds. The maximum rate of change of input voltage for a full scale input voltage is a function of the frequency of the sinusoidal signal

$$\frac{\Delta V}{V_F \, t_{ap}} = 2\pi f . \qquad (3)$$

Equation (3) is shown graphically in Fig. 11.

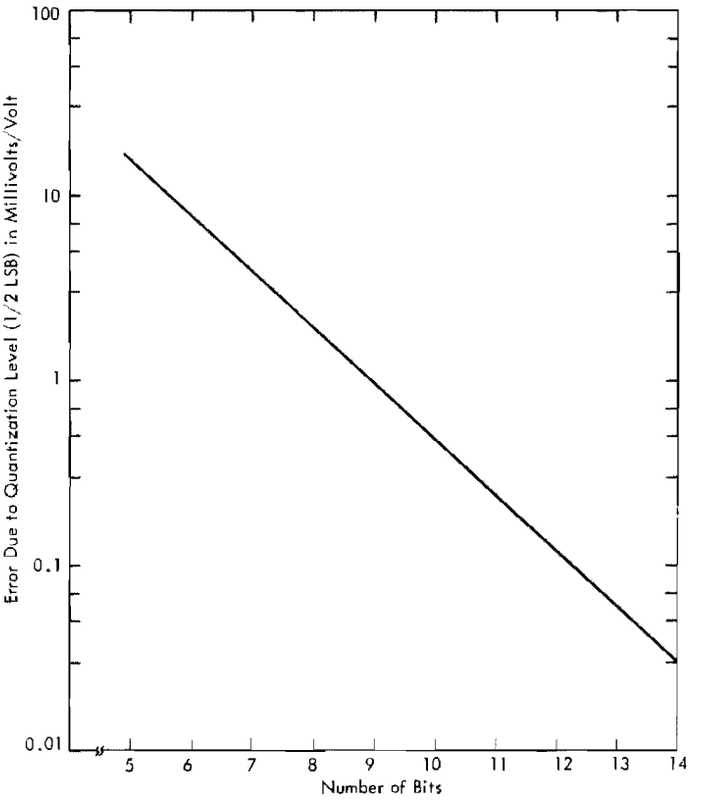

Fig. 8. Normalized error due to quantization level (one-half LSB) in millivolts vs number of bits resolution

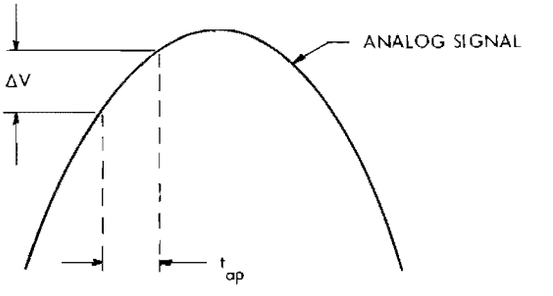

Fig. 9. Illustrating the effects of aperture time

t_{ap} = Aperture Time

ΔV = Amplitude Uncertainty (Possible Voltage Error)

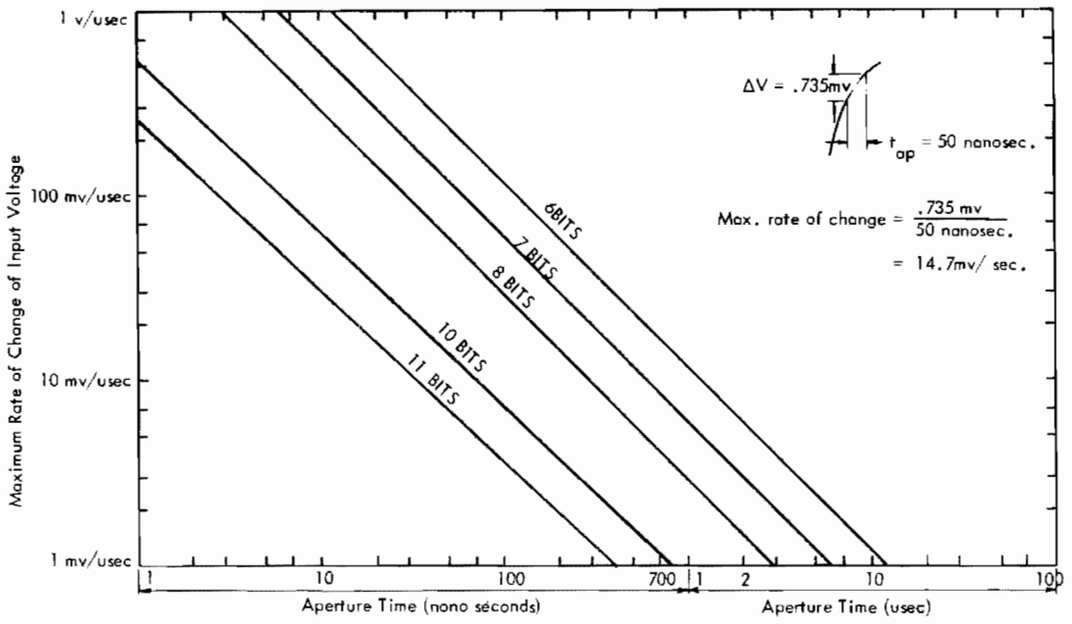

Fig. 10. Maximum rate of change of input voltage with respect to time to remain within the quantization level of one-half LSB vs aperture time. Full scale input voltage = 0.5 v.

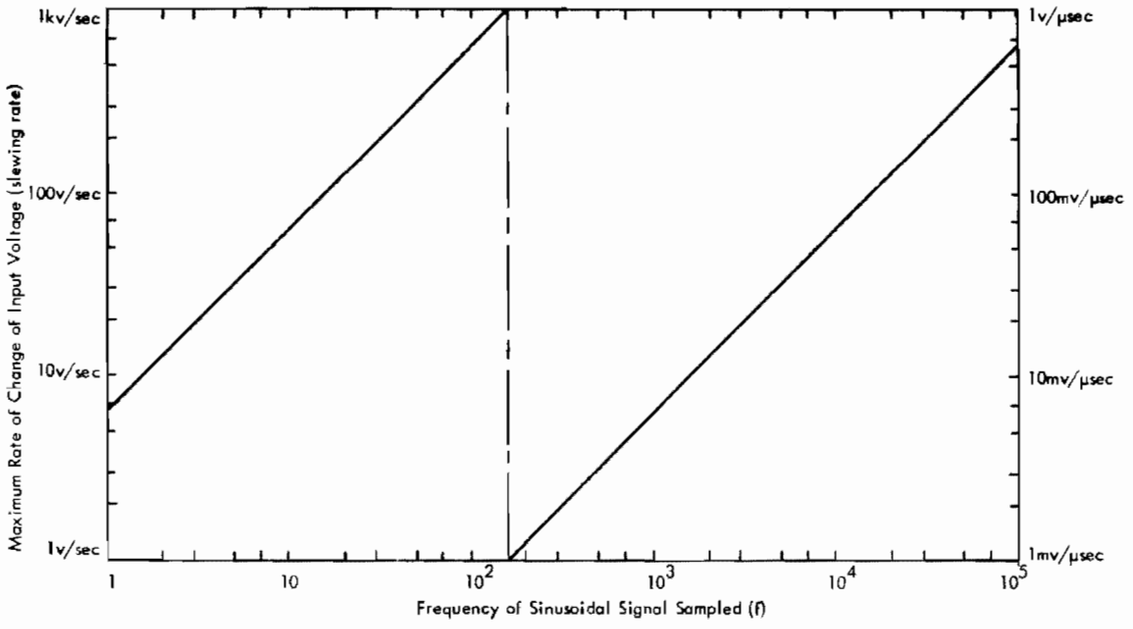

Fig. 11. Maximum rate of change of input voltage with relation to time as a function of frequency of sinusoidal signal sampled $\Delta V / t_{ap} = 2\pi f$

ACQUISITION OF RESPONSE DATA FROM SYSTEMS EXCITED BY SINUSOIDAL FREQUENCY SWEEP FORCES OR DISCRETE FREQUENCY STEP FORCES

The following discussion outlines the parameters and requirements involved in the on-line real-time acquisition of multiple channels of response data from a system undergoing either sinusoidal frequency sweep force excitation at a constant octave-band frequency sweep rate, or discrete sinusoidal force excitation at a constant octave-band frequency step rate.

Time Variation of Frequency

Sinusoidal sweep tests are generally conducted so that the time required to sweep through one octave is a constant. Let t_1 denote the time to sweep through an octave. Then, if the sweep test begins ($t = 0$) at the frequency f_0, the variation of frequency with time t for a constant octave-band sweep rate is shown graphically in Fig. 12. Figure 12 shows that t_1 is the time required to sweep from f_0 to $2f_0$, from $2f_0$ to $4f_0$, and from $4f_0$ to $8f_0$, etc.

The curve in Fig. 12 is given by the equation

$$\frac{f}{f_0} = 2^{t/t_1}, \qquad t \geq 0. \tag{4}$$

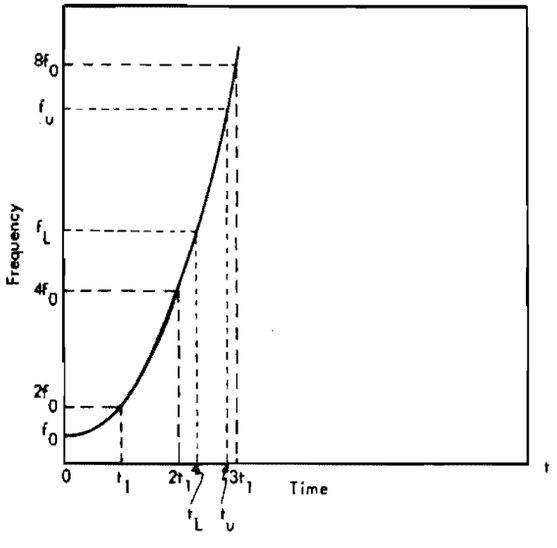

Fig. 12. Variation of frequency with time for a constant octave-band sweep rate

Sweep rates are generally specified in units of octaves per min; thus, if S denotes the sweep rate in octaves per min, and if time t is measured in seconds, then the relationship between S and t_1 is

$$St_1 = 60. \tag{5}$$

Substituting Eq. (5) for t_1 in Eq. (4) results in the following equation relating frequency with time:

$$\frac{f}{f_0} = 2^{St/60}. \tag{6}$$

Consider two arbitrary frequencies f_L and f_u, where $f_L < f_u$. The time in seconds required to sweep through the band of frequencies between f_L and f_u is found easily from the application of Eq. (6) as follows:

$$\frac{f_u/f_0}{f_u/f_0} = \frac{2^{St_u/60}}{2^{St_L/60}},$$

or

$$\frac{f_u}{f_L} = 2^{S(t_u - t_L)/60}, \tag{7}$$

Taking the natural logarithm of both sides of Eq. (7), and rearranging, gives the following expression for the time to sweep from f_L to f_u:

$$t_u - t_L = \frac{60}{S} \times \frac{\ell n\,(f_u/f_L)}{\ell n\,2}. \tag{8}$$

The relationship between the frequencies f_L and f_u and the times t_L and t_u are graphically depicted in Fig. 12.

If a step oscillator (frequency synthesizer) is used, rather than a sweep oscillator, to furnish the excitation control signal, then each discrete frequency step has a deterministic frequency f_k; hence, eliminating a slight frequency error. If the sinusoidal stepping rate is kept equal to the sinusoidal sweep rate, then the two methods of sinusoidal excitation can be interchanged. Thus, in the following discussion, wherever a sinusoidal frequency sweep is used or meant, discrete sinusoidal frequency step excitation can be also used, if proper attention is paid to a smooth change between step frequencies.

Time Required to Sweep through a Lightly Damped Resonance

During a sine sweep test of a linear system having a resonance at frequency f_0, the

root-mean-square (rms) response amplitude of the system will vary in a manner similar to that shown in Fig. 13. For convenience, the response amplitude is normalized so that the amplitude at $f = 0$ is unity.* The largest value of the rms response amplitude occurs at the resonance frequency f_0, and is equal to the resonant dynamic magnification factor Q of the system, since the actual resonant amplitude is Q times the static amplitude. The quantity Q is determined by the damping of the system and, in general, is given by the equation

$$Q = 1/2\zeta , \tag{9}$$

where

$\zeta = c/c_c$, system damping ratio,

c = system damping constant, and

c_c = critical system damping constant.

The half-power points indicated in Fig. 13 define the bandwidth Δf of the resonance, where the lower half-power point occurs at the frequency $f_0 - \Delta f/2$, and the upper half-power point occurs at the frequency $f_0 + \Delta f/2$. From elementary vibration theory, the bandwidth Δf of the resonance is related to Q (for $Q > 1$) by the equation

$$\Delta f = f_0/Q . \tag{10}$$

Now, the time τ required to sweep through the resonant bandwidth Δf is obtained from Eq. (8) by setting $\tau = t_u - t_L$, $f_L = f_0 - \Delta f/2$, and $f_0 + \Delta f/2$, so that

$$\frac{S\tau \ln 2}{60} = \ln \frac{f_0 + \Delta f/2}{f_0 - \Delta f/2} . \tag{11}$$

From Eq. (10), however, this expression can be written as

$$\frac{S\tau \ln 2}{60} = \ln \frac{1 + 1/2Q}{1 - 1/2Q} . \tag{12}$$

For most structural systems, the damping is generally very small, and Q will almost always have values which exceed 10, with typical values in the range of 25 to 50. The argument of the logarithm in Eq. (12) is, therefore, very nearly equal to unity, and the left-hand side is nearly equal to zero. Applying the binomial expansion,

*In this sense, the response amplitude spectrum shown in Fig. 13 was obtained by dividing the actual response amplitude by the amplitude obtained from a static loading of the system.

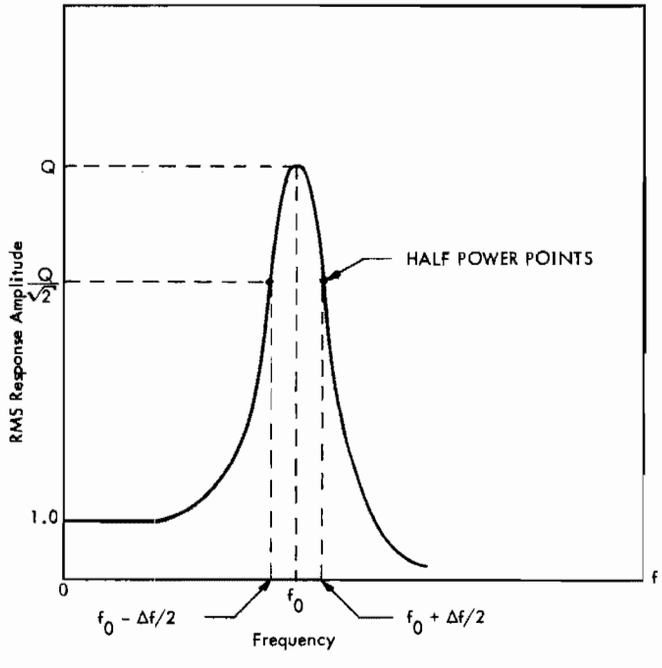

Fig. 13. Lightly damped resonant response peak

$$[1 - 1/2Q]^{-1} \approx 1 + 1/2Q ,$$

gives the approximate expression for Eq. (12),

$$\frac{S\tau \ln 2}{60} \approx \ln [1 + 1/2Q]^2 ,$$

or

$$\frac{S\tau \ln 2}{60} \approx \ln [1 + 1/Q] . \qquad (13)$$

Now, expanding the right-hand side of Eq. (13) in a Maclaurin series about $(1/Q) = 0$ gives

$$\ln [1 + 1/Q] \approx 1/Q .$$

Thus, Eq. (13) reduces to the form

$$\tau = \frac{60}{SQ \ln 2} . \qquad (14)$$

Equation (14) expresses the time τ required to sweep through the bandwidth Δf of a lightly damped resonance at a constant octave-band sweep rate. Note that the time τ decreases as Q increases, or as the damping decreases.

The number of response cycles $\bar{n}$ occurring during the time τ is given by the equation

$$\bar{n} = f_0 \tau ,$$

or

$$\bar{n} = \frac{60 f_0}{SQ \ln 2} . \qquad (15)$$

For example, let the sweep rate S be equal to 0.87 octave per min, and let $Q = 30$. Then, from Eqs. (14) and (15), the following values are obtained:

$$\tau = 3.32 \text{ sec} ,$$

$$\bar{n} = 3.32 f_0 \text{ cycles} .$$

In other words, it takes 3.32 sec to sweep through the resonance above the half-power level, and 3.32 f_0 cycles occur within this time.

The response of a linear system to a sweep frequency input will be nearly identical to its steady-state response, provided the sweep rate is very low. As the sweep rate increases, the frequency f_1 at which the peak amplitude occurs becomes greater, and the amplitude at response decreases. Hence, the bandwidth Δf_1 at the half-power point also increases. These effects are shown in Fig. 14(a) for the peak response of a single degree of freedom system at both its steady-state resonance frequency f_0 and at its sweep response frequency f_1. Figure 14(b) contains curves (3) of (a) the ratio of the peak response amplitudes squared $(y_{1\,max}/y_{0\,max})^2$, (b) the ratio of the half-power bandwidths $(\Delta f_1/\Delta f)$, and (c) the ratio of the frequency separation of the peaks and the bandwidth $(f_1 - f_0)/\Delta f$; all vs the parameter $(df/dt)/(\Delta f)^2$, where df/dt is the time rate of change of the frequency in units of cps/sec.

For the logarithmic sweep rate S, in units of octaves/min, the approximate relation between df/dt and S is given by the equation

$$\frac{df}{dt} \cong 0.0116 Sf . \qquad (16)$$

For example, if the desired range in the square of peak amplitude ratio is

$$1.0 \geq \left(\frac{y_{1\,max}}{y_{0\,max}}\right)^2 > 0.95 ,$$

then from Fig. 14(b), it is seen that

$$\frac{df}{dt} < 0.5 (\Delta f)^2, \text{ cps/sec} ,$$

and therefore, from Eq. (16), the required maximum sweep rate S is

$$S < 43.2 f_0/Q^2 \text{ octaves/min.}$$

Sampling Requirements

The requirements for sampling sinusoidal sweep response data are primarily based upon the maximum expected Q of the system. Once the expected maximum value of Q is chosen, the minimum resonant bandwidth Δf is determined. Now, it is necessary to decide upon the resolution needed to define this narrowest expected response peak and the acceptable error in the measured amplitude. Let $\bar{N}$ denote the number of discrete points required to define a response peak of magnitude Q above the half-power level $Q/\sqrt{2}$. To evaluate the error in measuring the assumed response peak at a frequency f other than the resonance frequency f_0, consider the response of a single degree-of-freedom system to a unit force, as shown in Fig. 15. For a high Q system, the normalized displacement response β is given by the equation

$$\beta = \frac{y}{Q} = \frac{1}{Q\left[(1-\alpha^2)^2 + \frac{\alpha^2}{Q^2}\right]^{1/2}} ,$$

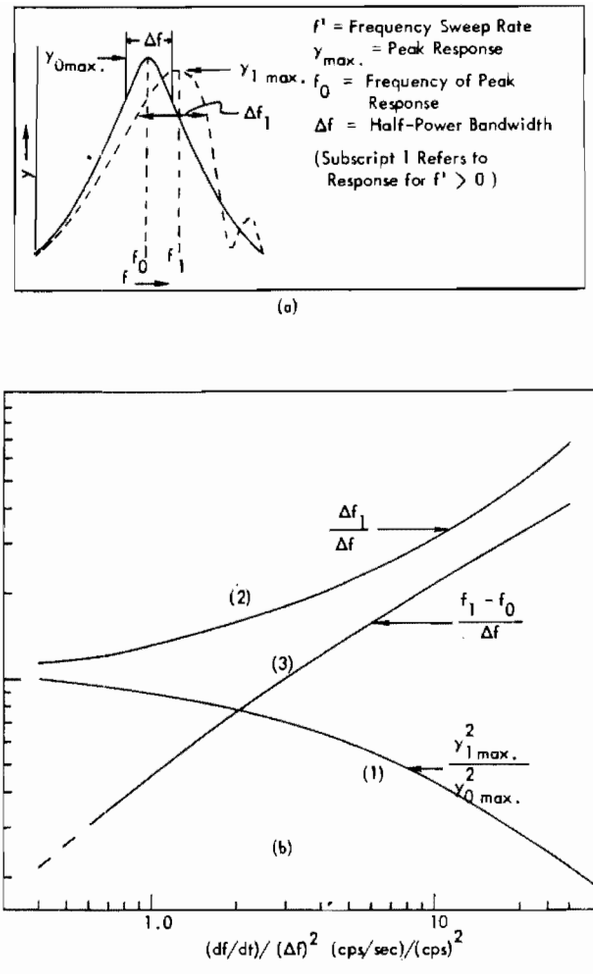

Fig. 14. Effect of frequency sweep rate on response of single-degree-of-freedom system

where y = displacement amplitude and $\alpha = f/f_0$. The amplitude error ϵ at a frequency $f \neq f_0$ is

$$\epsilon = 1 - \beta = 1 - \left[Q^2(1-\alpha^2)^2 + \alpha^2\right]^{-1/2}. \quad (17)$$

Assume, as a worst case, that there are $\bar{N}$ points spaced at a distance $\Delta\alpha/(\bar{N}-1)$ apart (where $\Delta\alpha = 1/Q$) on the response peak above the half-power level $Q/\sqrt{2}$. The error $\bar{\delta}$, of the frequency ratio α with respect to the peak ($\alpha = 1$) is less than or equal to one-half the distance between points; i.e.,

$$\bar{\delta} = \lambda\Delta\alpha/(\bar{N}-1) = \lambda/(\bar{N}-1)Q, \quad (18)$$

where $|\lambda| \leq 1/2$.

Assume that the frequency ratio α is

$$\alpha = 1 - \bar{\delta}. \quad (19)$$

Then, substituting Eq. (19) into Eq. (17) and ignoring $\bar{\delta}^2$ terms,

$$\epsilon = 1 - \left\{Q^2\left[1-(1-2\bar{\delta})\right]^2 + 1 - 2\bar{\delta}\right\}^{-1/2}$$

$$= 1 - \left[4\bar{\delta}^2 Q^2 + 1 - 2\bar{\delta}\right]^{-1/2}$$

$$\cong 1 - \left[\frac{4\lambda^2}{(\bar{N}-1)^2} + 1\right]^{-1/2} = 1 - \left[1 - \frac{1}{2}\frac{4\lambda^2}{(\bar{N}-1)^2} + \ldots\right]$$

$$\epsilon \cong 2\lambda^2/(\bar{N}-1)^2. \quad (20)$$

The maximum amplitude error ϵ_{max} in the peak will occur for $|\lambda| = 1/2$, hence

$$\epsilon_{max} = 1/[2(\bar{N}-1)^2]. \quad (21)$$

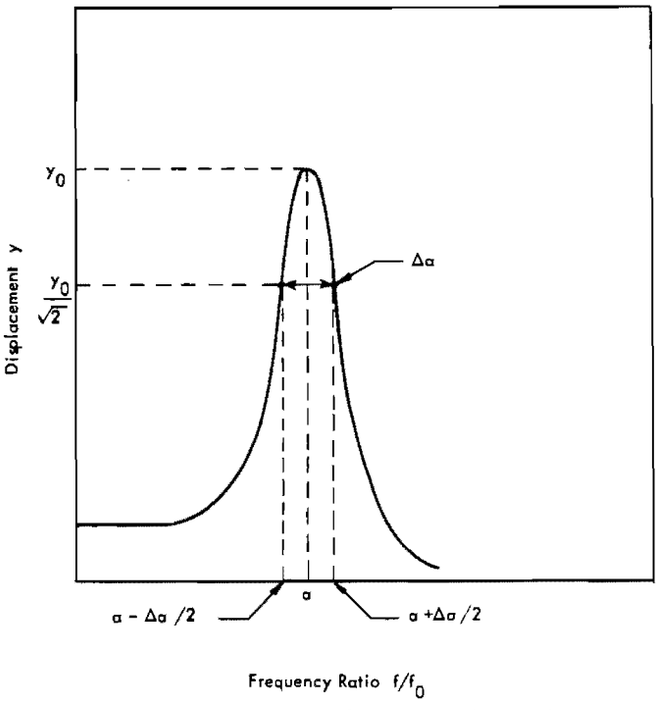

Fig. 15. Response of a lightly damped single degree-of-freedom system

For example, suppose $\bar{N} = 5$ points per $\Delta\alpha$, then $(\bar{N} - 1) = 4$, and

$$\epsilon_{max} = 1/32 ,$$

which is equivalent to about 3 percent of the actual peak value. Thus, for five points the measured peak amplitude is within ±3 percent of the actual peak amplitude. Table 2 contains a few representative examples of $\bar{N}$ and the associated values of ϵ_{max}.

Thus, it is seen from Table 2 that a minimum of three points ($\bar{N} = 3$) above the half-power level $Q/\sqrt{2}$ is required to determine the response peak with any acceptable accuracy (±12.5 percent). Note that a rapid decrease in the maximum error ϵ_{max} is experienced as $\bar{N}$ increases, up to $\bar{N} = 5$. For values of $\bar{N} > 5$, the decrease in ϵ_{max} gets progressively less. Therefore, a good economical choice for $\bar{N}$ is $\bar{N} = 5$.

For a constant octave sweep rate S, the maximum change in frequency within the bandwidth $\Delta f/\bar{N}$ is

$$\delta f = \Delta f/\bar{N} = f_0/\bar{N}Q \text{ cps.} \qquad (22)$$

TABLE 2
Maximum Error Incurred by Measuring Response Amplitude at Frequency Ratio $\alpha \neq 1$.

No. of Points above $Q/\sqrt{2}$, $\bar{N}$	Maximum Error ϵ_{max}	Maximum Error Range (%)
2	1/2	±50
3	1/8	±12.5
4	1/18	± 5.6
5	1/32	± 3.1
6	1/50	± 2.0
7	1/72	± 1.4
8	1/98	± 1.0
9	1/128	± 0.78

The maximum frequency error $\epsilon_{f\,max}$ associated with each of the $\bar{N}$ points at frequency f_0 is given by

$$\epsilon_{f\,max} = \frac{\delta f}{f_0} . \qquad (23)$$

For example, let $\bar{N} = 5$, $f_0 = 100$ cps, $Q = 50$, then

$$\delta f = 0.4 \text{ cps},$$

and

$$\epsilon_{f\,max} = 0.004,$$

or, rather, 0.4 percent of the frequency f_0. Table 3 contains a few representative values of the frequency error $\epsilon_{f\,max}$ for different values of $\bar{N}$ and Q.

TABLE 3
Sine Sweep Frequency Error

No. of Points above $Q/\sqrt{2}$, $\bar{N}$	D.M.F. Q	Maximum Error $\epsilon_{f\,max}$	Maximum Error (%)
3	25	0.0132	1.32
3	50	0.0066	0.66
3	100	0.0033	0.33
5	25	0.008	0.8
5	50	0.004	0.4
5	100	0.002	0.2
7	25	0.00572	0.572
7	50	0.00286	0.286
7	100	0.00143	0.143

The next quantity to be determined is the minimum number of samples H required per cycle at frequency f_k to define the frequency, amplitude, and phase characteristics of the response signals. Associated with the minimum sampling rate H is the minimum number of cycles n required to define the response amplitude at frequency f_k. For example, assume that a minimum value for H for sinusoidal data is around ten samples per cycle. When comparing two sinusoidal signals, the maximum apparent phase difference is 360 degrees, or one cycle, hence, a minimum of two cycles is required to ensure the definition of at least one cycle of both signals relative to the time of occurrence of the first positive maximum of one of the signals.

It is convenient to keep the sampling rate constant over a bandwidth, such as an octave, to improve the efficiency of the multiplexing and sampling process. Now since the frequency is doubled with each octave increase in frequency, it is easily seen, from Fig. 16, that if the minimum sampling rate H occurs at $2f$, then the minimum number of cycles n must occur at f, if the sampling rate is kept constant over the octave from f to $2f$. For example, if $H = 10$ samples per cycle at $2f$ and $n = 2$ cycles at f, then, at f, two cycles are defined with twenty samples per cycle, and at $2f$, four cycles are defined with ten samples per cycle. Thus each response point within the octave is defined by $2Hn = 40$ total samples.

Within a particular octave, the required sampling rate s per data signal is given by the equation

$$s = 2Hf = \text{number of samples per sec per channel}. \qquad (24)$$

If the maximum system sampling rate h is divided by s, then the maximum number of channels $\mathcal{k}$ which can be multiplexed together within the given octave is obtained. Since the sinusoidal sweep rate s is a constant, it is desirable to multiplex the set of $\mathcal{k}$ channels together until the required samples for each of the $\mathcal{k}$ channels are obtained, and then switch to the next set of $\mathcal{k}$ channels, etc., until the total number of data channels has been sampled, in such a way that $2Hn$ samples have been obtained for each data signal within the time increment

$$\Delta\tau = \tau/\bar{N} \text{ sec}, \qquad (25)$$

where $\Delta\tau$ is the time increment required to sweep the bandwidth $\Delta f/\bar{N}$, and τ is given by Eq. (14).

The maximum frequency f_{max} which can be sampled depends upon the maximum system sampling rate h and the specified minimum sampling rate per cycle H.

$$f_{max} = h/H. \qquad (26)$$

For example, if $h = 50{,}000$ samples per sec, and $H = 10$ samples per cycle, then $f_{max} = 5000$ cps. Table 4 contains a chart of the maximum number of channels $\mathcal{k}$ which can be multiplexed together in each octave from 1 cps to 131,172 cps, for a series of system sampling rates h when $H = 10$ samples per cycle at the octave upper frequency f_u.

TABLE 4
The Maximum Number of Channels δ which can be Multiplexed Together for a Few Sampling Rates h at the Octave Upper Frequencies f_u when H = 10 Samples/Cycle

h Samples per sec	Upper Frequency f_u (cps)																	
	1	2	4	8	16	32	64	128	256	512	1024	2048	4096	8192	13684	32768	65536	131172
5120	512	256	128	64	32	16	8	4	2	1								
10240	1024	512	256	128	64	32	16	8	4	2	1							
20480	2048	1024	512	256	128	64	32	16	8	4	2	1						
40960	4096	2048	1024	512	256	128	64	32	16	8	4	2	1					
81920	8192	4096	2048	1024	512	256	128	64	32	16	8	4	2	1				
136840	13684	8192	4096	2048	1024	512	256	128	64	32	16	8	4	2	1			
327680	32768	13684	8192	4096	2048	1024	512	256	128	64	32	16	8	4	2	1		
655360	65536	32768	13684	8192	4096	2048	1024	512	256	128	64	32	16	8	4	2	1	
1311720	131172	65536	32768	16384	8192	4096	2048	1024	512	256	128	64	32	16	8	4	2	1

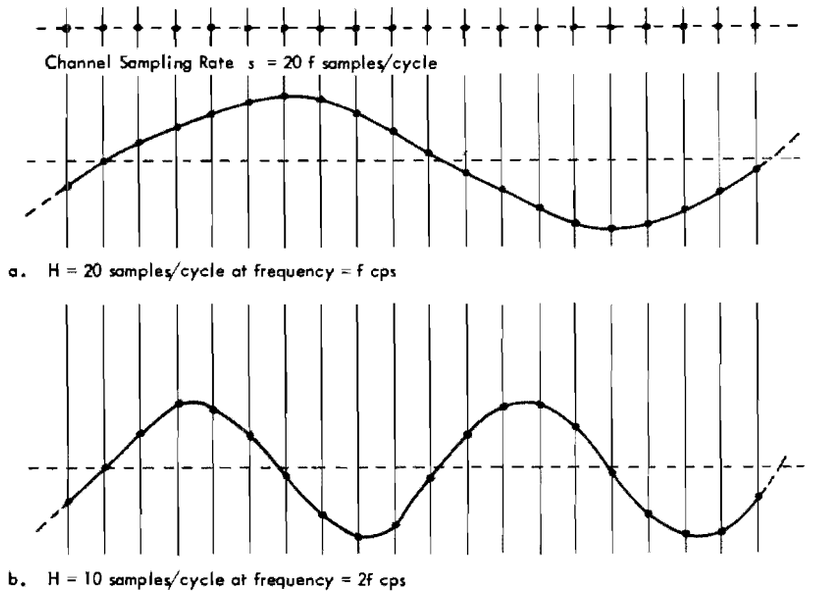

Fig. 16. Schematic illustration of sampling at a constant rate of s samples/sec within the octave f cps → 2f cps

The resolution accuracy can be illustrated with the following numerical example: let

S = 1.175 octaves/min,

Q = 50,

$\bar{N}$ = 5 points above the half-power level,

then

τ = 1.47 sec to sweep through Δf,

$\Delta\tau$ = 0.294 sec per response point,

and

$60/S\Delta\tau$ = 173.9 points per octave.

Thus, it is seen that for this example, there are 173.9 computed response amplitudes per octave and they are 1/173.9 octaves apart. If Q = 100, then there are 347 points per octave, etc.

Reference Signal

All of the requirements which are necessary to acquire sinusoidal response data efficiently have been defined. However, some reliable method is required for preserving the interchannel phase and amplitude relationships between all of the channels, so that the aforementioned multiplexing scheme can be applied efficiently and accurately. A common reference for all of the channels is automatically provided by sampling the actual sweep (or step) oscillator sinusoidal signal simultaneously in parallel with each data channel. Thus, the relative phase angle and amplitude relationship at frequency f_k between each data signal and the reference signal can be evaluated for each set of $2Hn$ samples. These relative values are completely deterministic for both the equally deterministic discrete frequency f_k obtained from a step oscillator, and the assumed discrete frequency f_k obtained from a sweep oscillator.*

Minimum System

A minimum system configuration is defined as one having at least two parallel synchronous analog to digital conversion subsystems, since a reference sample must be obtained with each data sample. Each of the A/D subsystems can then be loaded by a multichannel multiplexer, which can be program-controlled to perform the multiplexing schemes described above. The number of data channels to be acquired, the maximum frequency to be analyzed, and the system Q, combine to define the

*As pointed out previously, this assumption that the frequency is constant has a slight error associated with it; however, the phase and amplitude relationships obtained from each set of $2Hn$ samples are negligibly affected by this error.

maximum system sampling rate h (see Table 4), the required octave-band sweep rate or step rate S, and the system digital magnetic tape recording speed.

For example, if 128 channels were to be analyzed to 5000 cps for an expected Q of, say, 100; then, the minimum system sampling rate h, when $H = 10$ samples per cycle at 5000 cps, is $h = 50{,}000$ 12-bit samples per sec, the sweep rate S is about one-sixth octave per min, and the required magnetic tape recording speed is about 240,000 6-bit characters per sec (this includes tape gapping time, etc.).

ANALYSIS OF SINUSOIDAL SWEEP (OR STEP) RESPONSE DATA

Data Retrieval

Once all of the data have been acquired, the digital data samples are retrieved by a sorting or demultiplexing operation, which separates and arranges the samples into separate channel records. (Note that each sampled data channel, and the particular sampled reference channel which was sampled with it, are identified as a single 24-bit sample for this process.) The first part of the demultiplexing operation is accomplished during the acquisition and recording operation. That is to say, the group of $\mathcal{J}$ channels is sequentially multiplexed until $2Hn$ samples (24-bit sample) are obtained from each channel of the group. Thus, an $\mathcal{J} \times 2Hn$ matrix of data samples is formed as the data are transferred into the computer core buffer block by columns of $\mathcal{J}$ samples, each until the total of $2Hn$ columns are filled. This process is repeated in adjacent matrix blocks of $\mathcal{J} \times 2Hn$ core locations until all channels have been sampled. Now, if the data are transferred into digital magnetic tape records by rows of $2Hn$ samples, then each group of $2Hn$ data samples required to compute a value of response amplitude and phase is isolated for each channel.

The next step in the data retrieval process is to align all of the $2Hn$ data sample records by channels and rerecord these on tape. The data records are also grouped according to octaves. This octave grouping is necessary to obtain the time interval between samples for computing frequency, amplitude, and phase correctly; i.e., if $h = 50{,}000$ samples per sec and $\mathcal{J} = 32$ channels, then the sampling rate per channel s within this octave is 1562.5 samples per sec, and, hence, the samples are 1/562.5 sec apart.

Data Analysis

The objectives of the analysis program are to obtain harmonic distortion-free response amplitudes and phase angles for all values of the frequency f_k, for all channels in such a manner that accurate interchannel transfer function evaluations can be made. The simultaneous sampling of the same reference channel, along with each data channel, furnishes the basic means for the accomplishment of these objectives.

Of course, the reference channel must contain a clean sinusoidal sweep (or step) oscillator signal. If a zero-mean sinusoidal signal of frequency f_k is crosscorrelated with a harmonically distorted sinusoidal signal of the same frequency f_k, then, effectively, the crosscorrelation function is a zero-mean cosine function of frequency f_k, with a maximum amplitude $AR/2$ and a relative phase angle ϕ_{AR} between the reference channel and the data channel, where A is the required amplitude of the data channel and R is the amplitude of the reference channel. Note that the amplitude values and relative phase angle values for all of the channels are obtained relative to the same reference channel. Thus, even though each channel was sampled simultaneously with the reference channel at different times with respect to the other channels, the relations between all possible combinations of channel pairs can be accurately determined. To illustrate this point, consider the vector diagram shown in Fig. 17, which shows that if the vectors between the pairs of points 1 and R, 2 and R, and 3 and R are known, then the vectors between all pair combinations of the points 1, 2, and 3 are determined.

The approximate mean, $\bar{u}$, of the $N = 2Hn$ samples of the reference channel $\bar{r}_i$ is obtained from the following equation:

$$\bar{u} = \frac{1}{N} \sum_{i=1}^{N} \bar{r}_i \,. \tag{27}$$

The approximate mean $\bar{u}$ is then removed from the reference signal $\bar{r}_i$ by subtracting from each sample $\bar{r}_i$

$$R_i = \bar{r}_i - \bar{u} \simeq R \sin (2\pi f_k t_i + \phi_i) \,, \tag{28}$$

which yields the sampled reference sinusoidal signal R_i, with zero mean value and amplitude R.

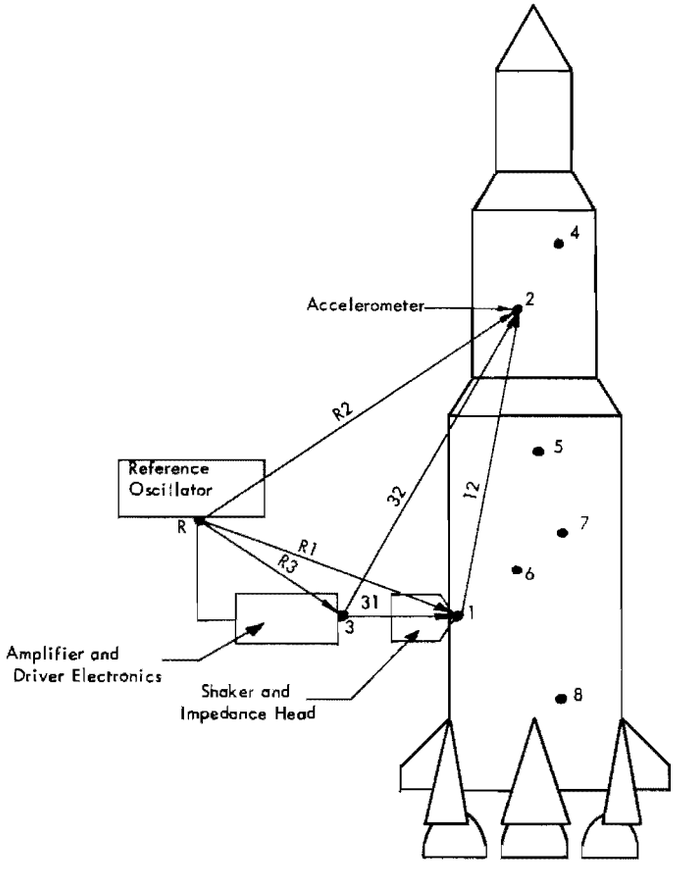

Fig. 17. Schematic of vectors obtainable when vectors R1, R2, and R3 are known

The number of samples per cycle H_k and the frequency f_k need to be determined from the data, hence, three consecutive zero crossings of the samples R_i are interpolated, and the time increment between the first and third zero crossings represents one cycle. Thus, the frequency f_k can be computed and H_k is determined by:

$$H_k = \frac{h}{f_k} \text{ sample/cycle} , \qquad (29)$$

where f_k = the frequency in cycles/sec (cps).

The autocorrelation function $\Gamma(\tau)$ of a sinusoidal signal is defined as

$$\Gamma(\tau) = \frac{1}{T} \int_{-T/2}^{T/2} f(t)\, f(t+\tau)\, dt , \qquad (30)$$

where T is the period of the sinusoidal and τ is a time lag.

Therefore, the sample autocorrelation function $\Gamma_{RR}(r/s)$ (where $r/s = \tau_r$ is the incremental time lag) of the sampled reference signal R_i is

$$\Gamma_{RR}\left(\frac{r}{s}\right) = \frac{1}{H_k} \sum_{i=1}^{H_k} R_i R_{i+r}$$

$$= \frac{R^2}{2} \cos\left(2\pi f_k \frac{r}{s}\right) + (\Delta\bar{u})^2 , \qquad (31)$$

where $r = 0, 1, 2, \ldots, < N - H_k$, and in particular

$$\Gamma_{RR}(0) = \frac{R^2}{2} + (\Delta\bar{u})^2 , \qquad (32)$$

where R is the amplitude of the reference signal and $\Delta\bar{u}$ is any residual positive or negative mean which remains due to the finite length of the data record. Compute $\Gamma_{RR}(r/s)$ until a minimum value is located and interpolated

$$\Gamma_{RR(min)} = \frac{R^2}{2} - (\Delta\bar{u})^2 . \quad (33)$$

Hence,

$$\Gamma_{RR}(0)\Gamma_{RR}(0) - \Gamma_{RR(min)} = R^2 . \quad (34)$$

Thus, the amplitude R of the reference signal is known.

Now, to find the amplitude A of the data signal, it is necessary to first subtract the approximate mean $\bar{u}$ from each sample $\bar{r}_i$ of the reference signal which was sampled with the harmonically distorted data signal A_i, and then compute the crosscorrelation function $\Gamma_{AR}(r/s)$ of the response channel with the almost zero-mean reference signal.

$$\Gamma_{AR}\left(\frac{r}{s}\right) = \frac{1}{H_k}\sum_{i=1}^{H_k} A_i\,(\bar{r}_{i+r} - \bar{u})$$

$$= \frac{AR}{2}\cos\left(2\pi f_k \frac{r}{s} + \phi_{AR}\right) + \bar{a}\Delta\bar{u} , \quad (35)$$

where

$r = 0, 1, 2, \ldots, < N - H_k$,

A = amplitude of the response signal

ϕ_{AR} = relative phase angle between the response signal and the reference signal, and

$\bar{a}$ = sample mean value of the response signal.

Note the harmonic distortion-free sinusoidal crosscorrelation function $\Gamma_{AR}(r/s)$. Again there can be a residual mean value due to the finite sample record length. Hence, evaluating, as in Eqs. (32) and (33), the first minimum and maximum values of $\Gamma_{AR}(r/s)$, and subtracting the minimum value from the maximum value, such as in Eq. (34), the amplitude A of the data signal can be obtained. However, the residual mean $\bar{a}\,\Delta\bar{u}$ is usually so small that it can be neglected.

Figure 18 illustrates the method for obtaining A and ϕ_{AR} for each channel at frequency f_k. These are the basic data needed to obtain the required input and transfer functions $\alpha(f_k)$ and other associated relationships discussed previously.

Computer Programming Techniques

The only special technique required of the computer programs, which was not mentioned previously, is the preparation of data tapes at appropriate points within the data processing procedure.

Sinusoidal sweep (or step) data processing comprises three computer programs:

1. Data acquisition program.

2. Data analysis and reduction programs.

3. General data presentation programs — plotting and printing.

Analysis and reduction of the data to obtain all of the available information require the following scheme of data retrieval, analysis computations, data tape preparations, and plotting options (the analysis of mechanical impedance data is used as an example):

1. Read the acquired data tape, reassemble the data into separate channel pairs, and write a basic raw data tape.

2. Read the basic raw data tape and compute acceleration response amplitudes $|A_{qR}(f_k)|$ (or input force amplitudes $|F_{mR}(f_k)|$) and relative phase angles $\phi_{qR}(f_k)$ (or $\phi_{mR}(f_k)$) for all data channels with respect to the respective reference data channel, at all frequencies f_k. A basic reduced data tape is written containing records of $|A_{qR}(f_k)|$, $\phi_{qR}(f_k)$, and (or $|F_{mR}(f_k)|$, $\phi_{mR}(f_k)$) for all frequencies f_k for all data channels. An option to plot $|A_{qR}|$ and ϕ_{qR} vs f_k can be made at this time.

3. Read the basic reduced data tape and compute the following specified force-to-acceleration transfer function amplitudes and phase angles:

$$|\alpha_{mq}(f_k)| = \frac{|A_{qR}(f_k)|}{|F_{mR}(f_k)|}$$

$$\theta_{mq}(f_k) = [\phi_{mR}(f_k) - \phi_{qR}(f_k)] ;$$

also compute $\Delta f_k = f_{k+1} - f_k$, incremental bandwidth in cps.

A force transfer function tape is written containing records of $|\alpha_{mq}(f_k)|$, $\theta_{mq}(f_k)$,

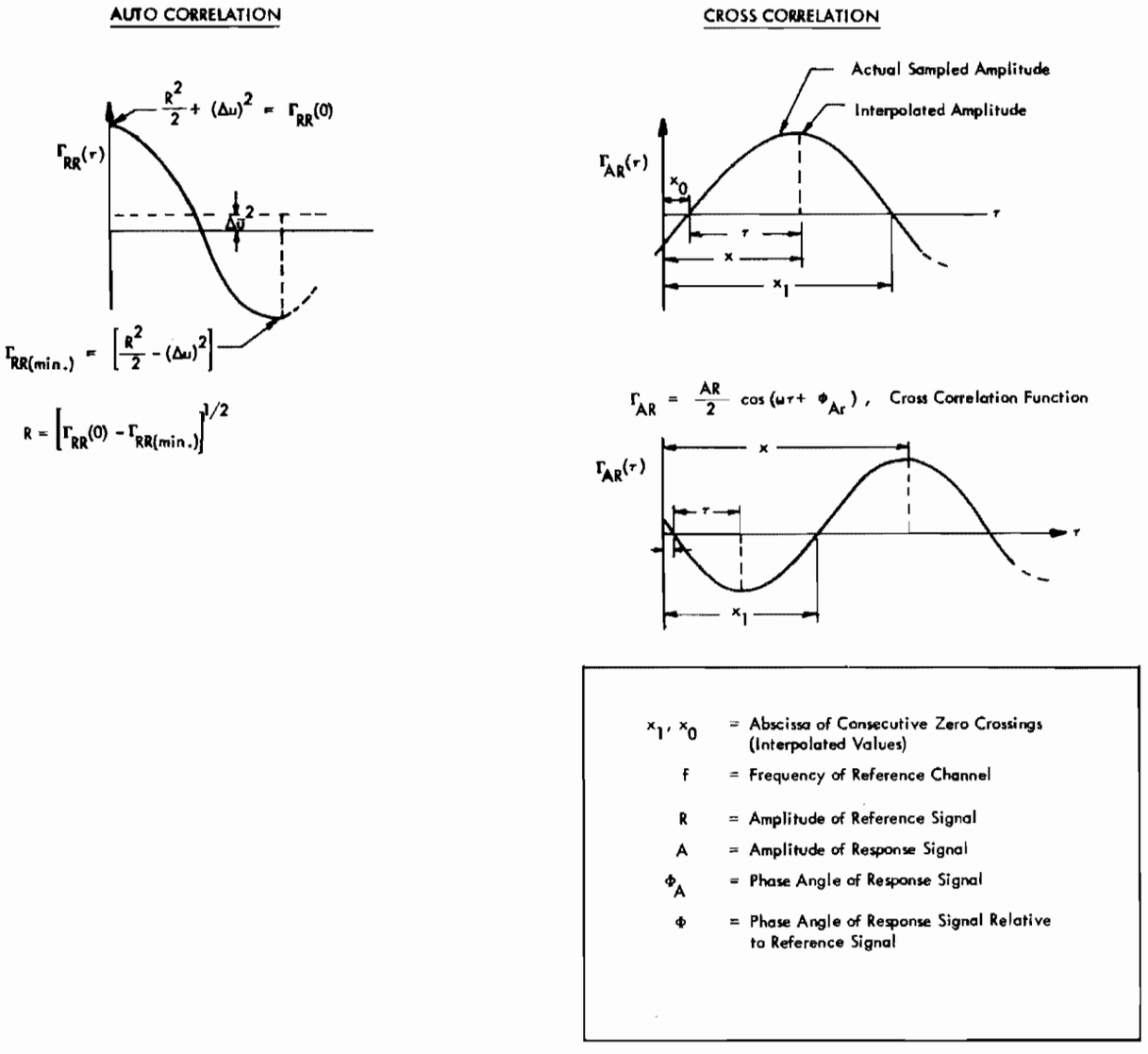

Fig. 18. Calculation of amplitude and phase

Δf_k and f_k for all f_k for all response data channels. An option to plot $|\alpha_{mq}(f_k)|$ and $\theta_{mq}(f_k)$ can be made at this time.

4. Read the force transfer function tape and read from cards the values of f_{u_c}, f_{L_c} and f_c, which describe each of the c bandwidths to be used for obtaining average values of the transfer functions, and compute $\Delta f_c = f_{u_c} - f_{L_c}$, cth bandwidth in cps, and

$$\left\{|\alpha_{mq}(f_c)|^2\right\}_{\Delta f_c} = \frac{1}{\Delta f_c} \sum_{f_k = f_{L_c}}^{f_{u_c}} |\alpha_{mq}(f_k)|^2 \, \Delta f_k .$$

Plot or print a table containing

$$\left\{|\alpha_{mq}(f_c)|\right\}_{\Delta f_c} \text{ vs } f_c .$$

5. Read the force transfer function tape and compute the following specified acceleration-to-acceleration transfer function, amplitudes and phase angles:

$$|\alpha_{q\ell}(f_k)| = \frac{|\alpha_{m\ell}(f_k)|}{|\alpha_{mq}(f_k)|} ,$$

and

$$\theta_{q\ell}(f_k) = \left[\theta_{m\ell}(f_k) - \theta_{mq}(f_k)\right] .$$

An acceleration transfer function tape is written containing records of $|\alpha_{q\ell}(f_k)|$, $\theta_{q\ell}(f_k)$, Δf_k, and f_k for all f_k and all desired data channel pairs q, ℓ. An option to plot $|\alpha_{q\ell}|$ and $\theta_{q\ell}$ vs f_k can be made at this time, or, optionally, the following spatial correlation function $R_k(y_q, y_\ell)$ can be computed and plotted vs f_k,

$$R_k(y_q, y_\ell) = |\alpha_{q\ell}(f_k)| \cos \left[\theta_{q\ell}(f_k)\right] .$$

6. Read the acceleration transfer function tape and the values of f_{u_c}, f_{L_c} and f_c from cards, and then compute the bandwidth averaged values

$$\left\{R_c(y_q, y_\ell)\right\}_{\Delta f_c} = \frac{1}{\Delta f_c} \sum_{f_k = f_{L_c}}^{f_{u_c}} |\alpha_{q\ell}(f_k)| \times \cos \left[\theta_{q\ell}(f_k)\right] \Delta f_k ,$$

where $\Delta f_c = f_{u_c} - f_{L_c}$.

Plot or print tables of

$$\left\{R_c(y_q, y_\ell)\right\}_{\Delta f_c} \text{ vs } f_c .$$

Examples of Experimental Data

The following examples represent actual data taken from experimental measurements of the mechanical impedance of the complex structure of a Saturn I Instrument Unit which is 13 ft in diameter. A point input force was applied at, say, point n through an impedance head, and the input force signal, input acceleration signal, q response acceleration signals, and, of course, the sweep oscillator reference signal were acquired in real-time by the on-line Analog/Digital Data System. After the data were acquired and the particular test ceased, the data were analyzed and the input force, input force-to-acceleration transfer function, and force-to-acceleration transfer functions between input point m and the q response points were determined and plotted vs the frequencies f_k. The maximum Q of the structure was evaluated prior to the test, and was expected to be less than or equal to about 100. Thus, as seen in a previous numerical example, the resolution of the digital plots is about 347 computed points per octave.

Figure 19 contains a digital X-Y plot of the input force amplitude $|F_{mR}(f_k)|$, relative phase angle magnitude $|\phi_{mR}(f_k)|$, and phase angle sign (±) of a point force applied at point m on the structure with respect to the reference sweep oscillator signal $R \sin 2\pi f_k t$. An analog plot of the input force amplitude $|F_{mR}(f_k)|$ is shown in Fig. 20 for comparison. Note the similarity and obviously better resolution of the digital plot. Digital one-third octave band averaged values of the mean-square input force amplitude

$$\left[|F_{mR}(f_c)|\right]^2_{\Delta f}$$

are plotted at the one-third octave band center frequencies f_c in Fig. 21.

Figure 22 contains a digital X-Y plot of the force-to-acceleration transfer function amplitude $|\alpha_{mq}(f_k)|$, relative phase angle magnitude $|\phi_{mq}(f_k)|$, and phase angle sign (±) between force input point m and acceleration response point q on a structure. Digital one-third octave band averaged values of the mean-square, force-to-acceleration, transfer function amplitude $[|\alpha_{mq}(f_c)|]_{\Delta f}$ are plotted at the one-third octave band center frequencies f_c in Fig. 23.

DISCUSSION AND CONCLUSIONS

A unique solution to the data analysis requirements of modern environmental test programs has been described. The key points of the developments contained in this paper are briefly summarized as follows:

1. An analog/digital data system was developed which can acquire either random or sinusoidal sweep test data from a large number of channels within the real time duration of the test and store the data on digital magnetic tape, for later analysis and reduction.

2. A technique for acquiring and analyzing sinusoidal sweep test data in such a way that all possible interchannel relationships can be accurately established is summarized herein. Thus, input and transfer functions throughout the force generating system and the structural system can be obtained and interrelated. This technique also allows the interrelation of data taken at different times and at different points on the structure.

3. A carefully run test program can therefore yield detailed information which can be correlated with respect to the structural

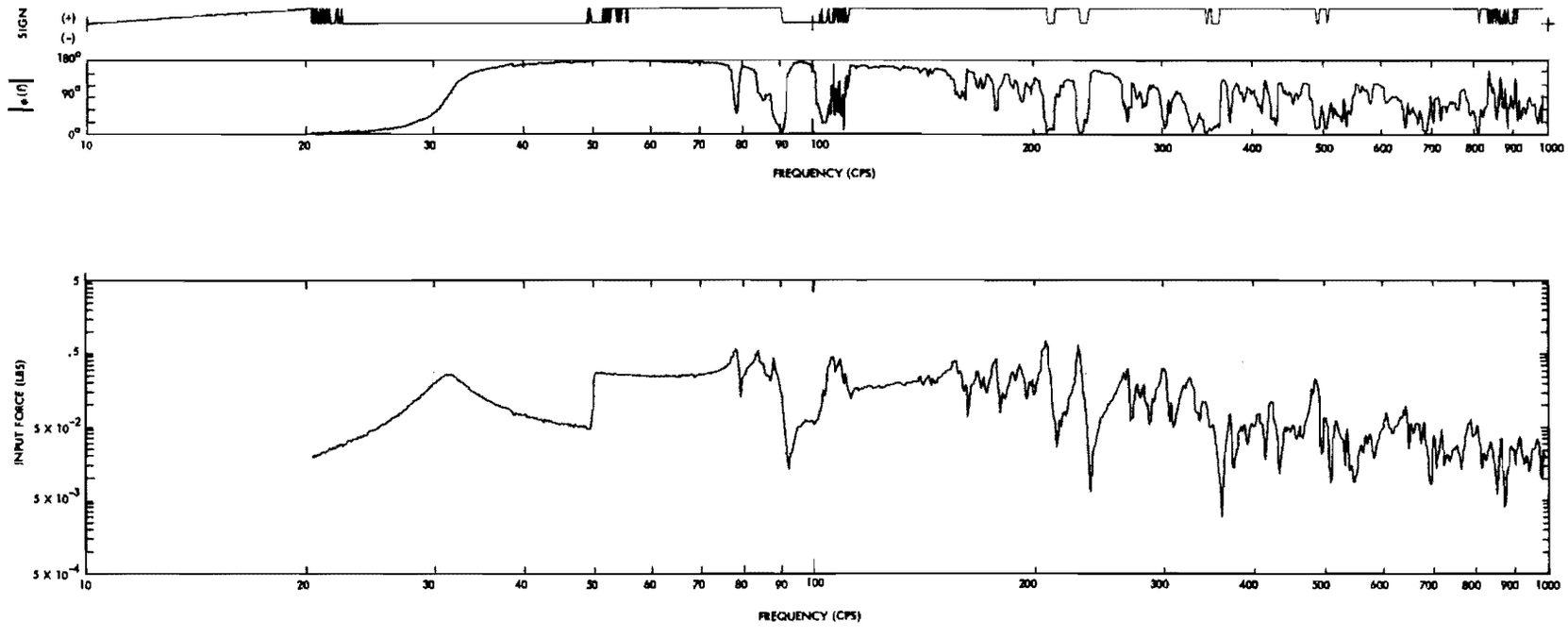

Fig. 19. Input force amplitude and phase angle spectra applied at point No. m

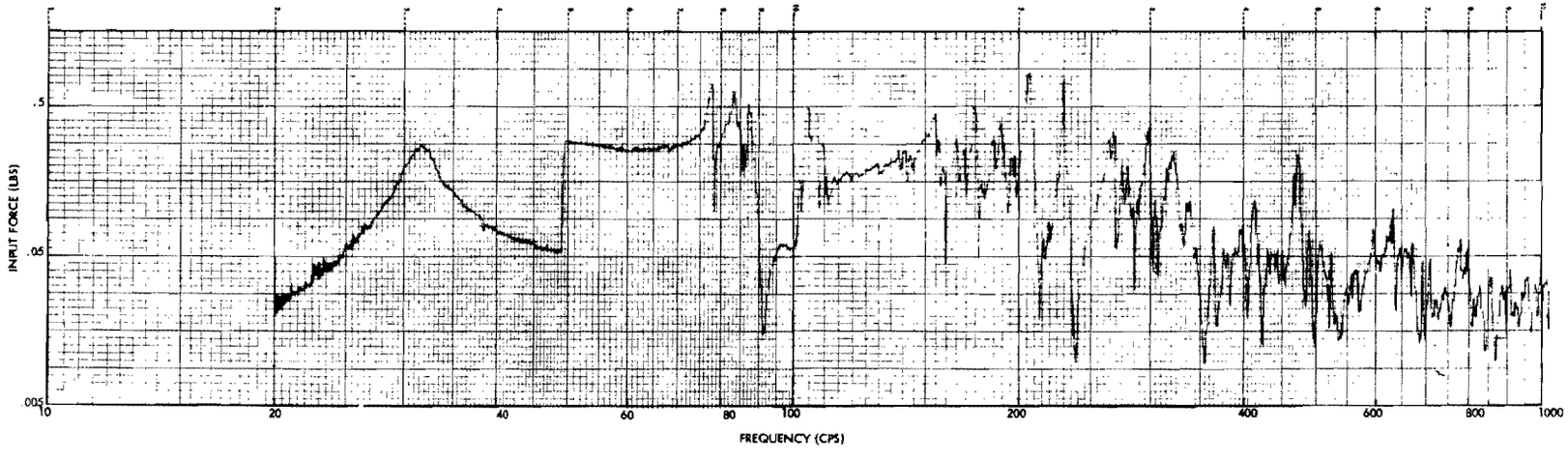

Fig. 20. Input force amplitude and phase angle spectra applied at point No. m (analog)

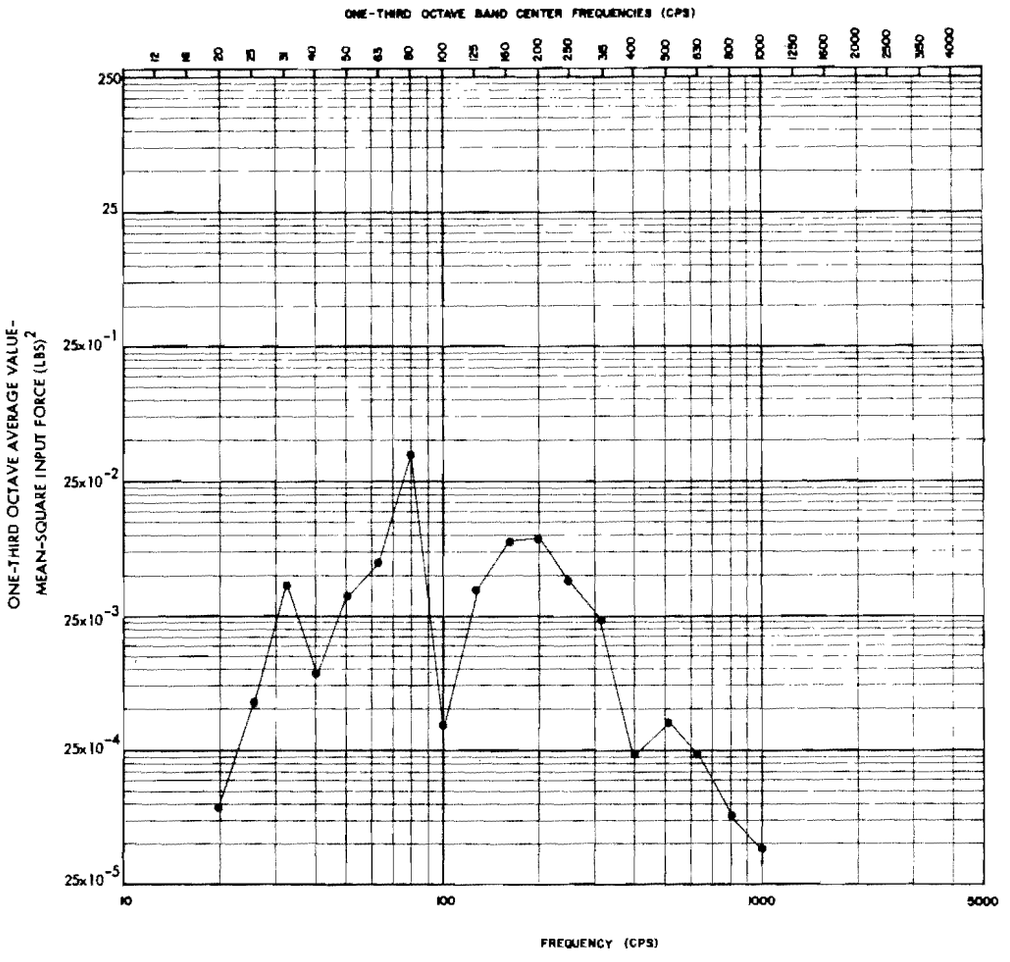

Fig. 21. Mean-square amplitude of the input force, applied at point No. m, averaged over one-third octave bands

configuration, structural parameters and environmental parameters (e.g., mass, stiffness, damping, pressure, etc.). For example, structural mode shapes, force field and response spatial correlations, high acceleration level locations or areas, vibration transfer characteristics of basic structural sections, etc., can be determined at all frequencies at selected frequencies or averaged over specific bands of frequencies.

4. This resultant library of information can be automatically reviewed for pertinent test results and condensed into various report forms for immediate engineering and/or management review, thus effecting a minimum decision-reaction time.

The achievements reported herein represent a major advance in the art of qualification testing. A maximum amount of information can be obtained from a finite amount of data taken during a fixed minimum test duration.

Of course, the ideas presented here are not restricted to environmental testing of structures. These techniques can be equally effective in the areas of underwater and underground acoustic and seismic investigations; e.g., oil and mineral exploration, mapping of terrain and strata, communications, signal source location, recognition, and many others.

ACKNOWLEDGMENTS

The author wishes to acknowledge K. McK. Eldred, R. W. White, and L. C. Sutherland of the Research Staff for their support, discussions, and helpful suggestions during the course of this project; and V. K. McCombs of the Research Staff for the programming assistance which led to successful computer programs.

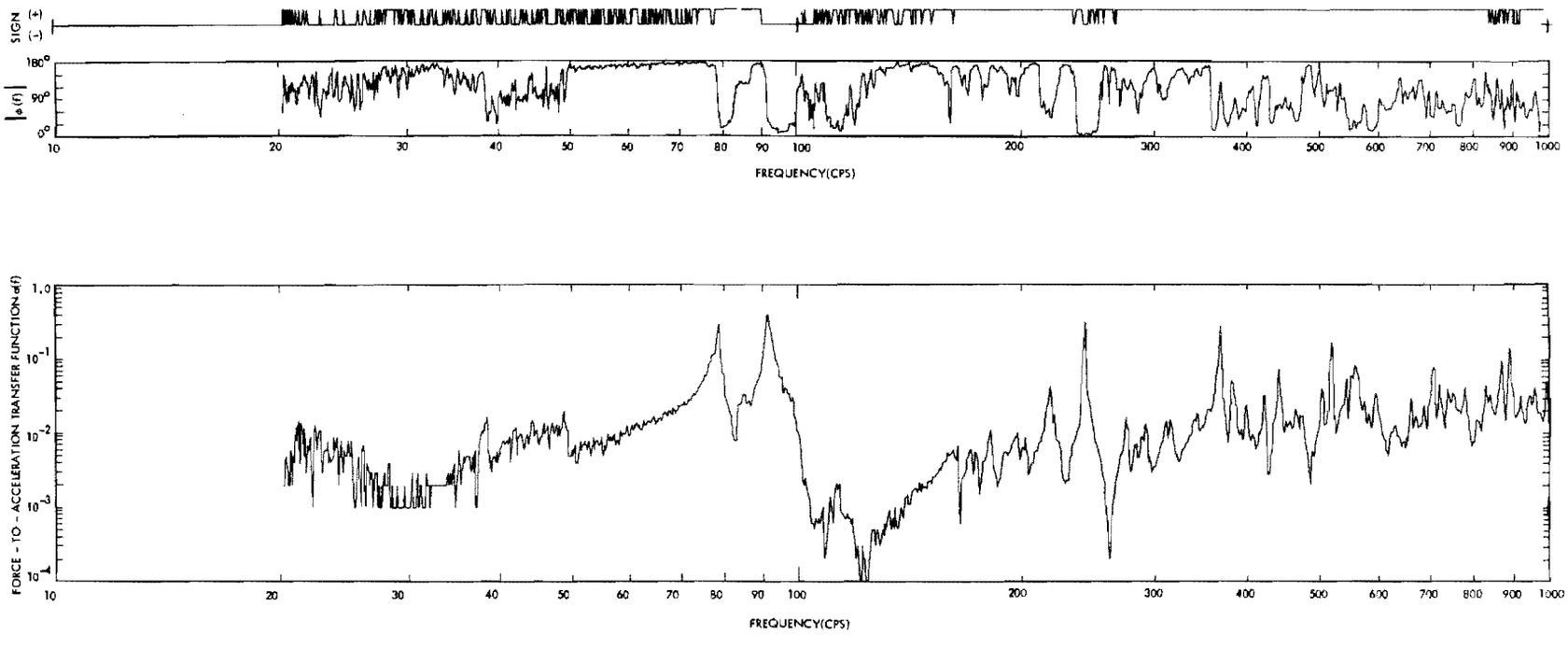

Fig. 22. Force-to-acceleration transfer function amplitude and phase angle spectra between input point No. m and response No. q

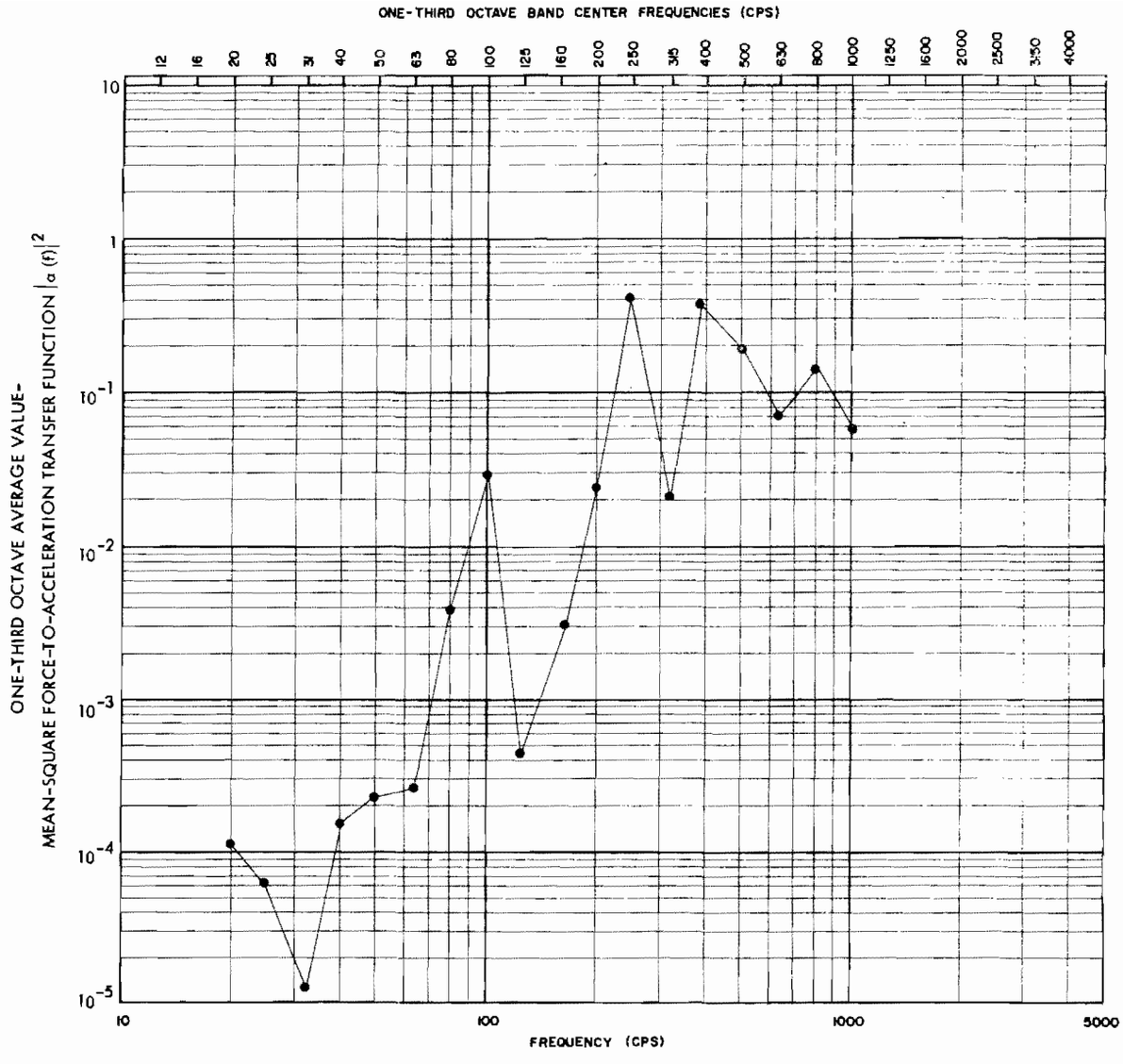

Fig. 23. Mean-square amplitude of the force-to-acceleration transfer function, between input point No. m and response point No. q, averaged over one-third octave bands

REFERENCES

1. R. W. White, D. J. Bozich, and K. McK. Eldred, "Empirical Correlation of Excitation Environment and Structural Parameters with Flight Vehicle Vibration Response," Tech. Rept. AFFDL-TR-64-160, Air Force Systems Command, Wright-Patterson Air Force Base, Ohio, December 1964

2. P. Barr, "Influence of Aperture - Time and Conversion Rate on the Sampling Accuracy of A - D Converters," Digital Products Tech. Bulletin, Issue 2, Raytheon Company, Norwood, Massachusetts, August 1964

3. L. L. Beranek, Acoustic Measurements (John Wiley and Sons, Inc., New York), 1959, pp. 538-540

* * *

A DIGITAL DATA RECORDING SYSTEM FOR STRUCTURAL DYNAMICS RESPONSE TESTING

M. H. Hieken
McDonnell Aircraft Corporation
St. Louis, Missouri

Data generated in the course of structural dynamics response tests is characterized by a broad frequency range and a wide dynamic range. At the McDonnell Laboratories, a Digital Data Recording System has been developed which overcomes the frequency and range problems and permits automated recording and reduction of frequency response data.

The essential elements of the system described in this paper are a wide dynamic range, a high linearity full wave rectifier, and a detector which performs a true integration of the rectified signals. These components are coupled with a scanner to sequentially sample a number of channels and an incremental magnetic tape recorder to store the data in a form suitable for processing by digital computers. In addition to a complete description of the data system, a discussion of the errors in the system is provided.

INTRODUCTION

Structural dynamics response tests (ground vibration tests) are conducted to identify and describe the normal modes of vibration of complete structural assemblies, such as full-scale aircraft, spacecraft, and missiles. The analytical dynamicist relies on accurate experimental descriptions of the dynamic behavior of the structure as a check on calculated values of frequencies, mode shapes, and effective damping.

The initial activity in a complete structural response test is usually a frequency survey of the entire test article. The ultimate product of the frequency survey is a number of frequency response plots which represent thousands of separate data points. Because of the need to review experimental results as quickly as possible following the tests, it was found that manual methods of recording test data, making computations on the tabulated data, and plotting the final curves were not satisfactory.

This paper describes a semiautomatic digital data recording system for structural dynamics response testing. The system permits data to be recorded, computed, and plotted without any manual handling of the data. Features of the data system will be described, and examples of the recorded data will be presented.

DESCRIPTION OF TESTS AND GENERATION OF DATA

The experimental techniques that are followed in conducting structural dynamics response tests have been well documented (1, 2). The first phase of such tests is generally to determine, as a function of frequency, the dynamic response of the test structure to one or more input forces. The usual technique consists of attaching a vibration exciter to a selected point on the structure; varying the excitation frequency while monitoring some input parameter (e.g., force, acceleration, or velocity); and monitoring the signals from response sensing transducers located on the structure under test. Figure 1 illustrates the functions of the various pieces of apparatus used in conducting structural response tests.

Efforts to automate the data handling aspects of response tests have been complicated by two characteristics of the test data. One problem stems from the fact that large structures, such as full scale aircraft and missiles, have fundamental normal mode frequencies which may be as low as 2 to 3 cps frequencies which are well below the low frequency range of conventional ac instruments. From a data-handling point of view, the low frequency signals represent a detection problem. Most ac

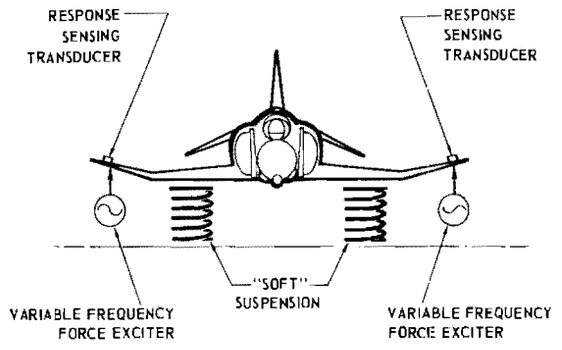

Fig. 1. Basic elements in a structural response test

instruments incorporate resistance-capacitance (RC) circuits to integrate, or smooth the output of a rectifier circuit. This process yields a signal which may be used to indicate the average of the (rectified) signal; the root-mean-square; or the peak value of the ac signal. Conventional voltmeters and vibration meters have this type of detection circuit, and are accordingly limited to frequencies above 5 to 10 cps.

A second factor, which complicates efforts to automate response test data, is the extremely wide dynamic range (range of amplitude) generated in a given test. Wide amplitude variations are characteristic of most structural specimens in which very little response is evident at nonresonant frequencies while amplifications in excess of 50 are not uncommon at excitation frequencies coincident with structural resonances.

During manual data recording procedures, the dynamic range problem is resolved by the simple expedient of range-switching the indicating meter. This approach is feasible for an automatic data system, but would add considerably to the complexity of the system.

The data recording system described in the remainder of this paper has overcome those data characteristics which prevented digital recording of ground vibration testing data prior to the implementation of this system.

CONCEPT OF THE PRESENT SYSTEM

The problem of detecting very low frequency data is essentially a matter of integration time. The problem can be illustrated by considering a low frequency signal which is applied to a detector with an RC integrator, as shown in Fig. 2. The RC integrator circuit must observe the rectified signal for a period which is at least four times greater than the time constant i.e., the product of the resistance times the capacitance of the circuit in order to maintain an acceptable accuracy. Aside from the practical problems of achieving the long time constants required to sense low frequency signals, there are accuracy problems which result from the slow variations of the voltage across the condenser, as described in the appendix. A familiar example of this is the fluctuation of an ac meter needle when a low frequency signal is applied to the meter.

The appearance, several years ago, of instruments which performed a true integration of time varying signals suggested a potential method of detecting the very low frequency signals. The integrating instruments, however, would correctly indicate "zero" as the integrated average for an ac signal. Therefore, it was necessary to perform a full-wave rectification of the ac signals before applying the signals to the integrating detector.

A suitable full-wave rectifier was breadboarded by the McDonnell Laboratories. An integrating digital voltmeter, similar to the one which was incorporated into the final data system, was evaluated in a simulated test operation which included a vibration transducer, the breadboarded rectifier circuit, and the integrating voltmeter.

Results of the early tests were promising. Since the integrating meter used for the tests had a fixed maximum integration time of 1.0 second, the lowest frequency that could be accurately detected was about 2 cps. (A detailed analysis of the errors inherent in the system is presented in the appendix.) The system was found to operate satisfactorily up to 2000 cps, which is well above the frequency band in which structural response tests are normally conducted.

The amplitude accuracy recorded during the original evaluation was somewhat less than had been expected. These errors were found to result from drift and nonlinearities in the full-wave rectifier. Notwithstanding these initial problems, further studies were made to incorporate a full-wave rectifier and integrating detector into a complete data recording system.

DESCRIPTION OF THE DIGITAL DATA RECORDING SYSTEM

The Digital Data Recording System which finally evolved from studies with a rectifier and integrating detector had six major components, as illustrated by the block diagram of Fig. 3.

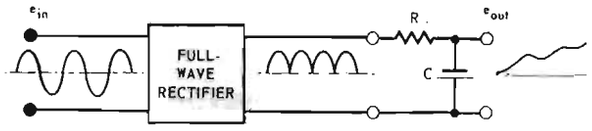

Fig. 2. A detector with an RC integrator

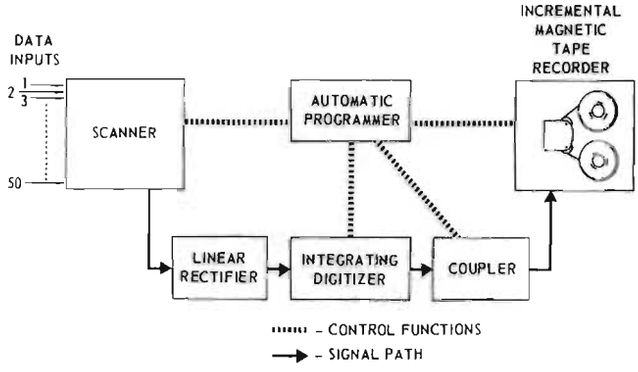

Fig. 3. Block diagram of digital data recording system

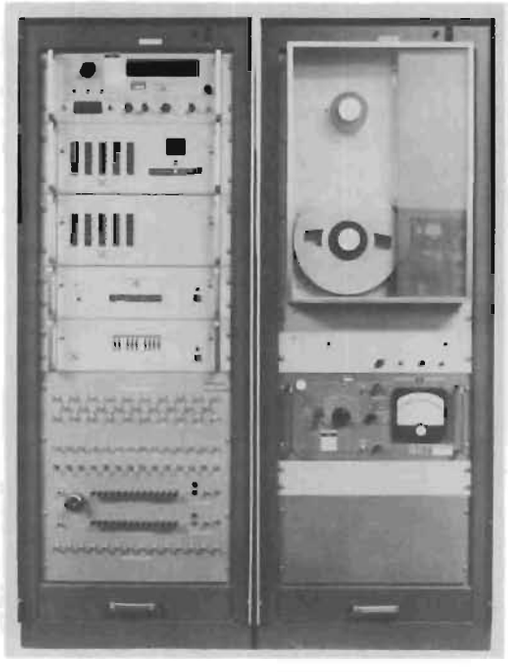

Fig. 4. The digital data recording system

All of these components, with the exception of the linear rectifier developed by the McDonnell Laboratories, are commercially available items (3). The photograph in Fig. 4 shows the physical arrangement of the complete system, conveniently packaged in two 19-in. electronics racks.

Following is a description of the major components of the system.

1. Scanner - The scanner in the digital data system accepts up to fifty 3-wire (signal pair plus ground) inputs. The system operator can select randomly those channels which are to be scanned for a given test by depressing numbered buttons corresponding to each channel. The scanner will then scan sequentially the selected channels when directed to do so by the automatic programmer. During the scanning operation, all three wires of each input signal are scanned. This technique insures maximum rejection of noise throughout the data system. A numerical display in the scanner chassis indicates the channel being scanned.

2. Automatic Programmer - The programming function permits operation of the system in any of several modes. The system can be made to scan the selected data inputs one time or continuously. Initiation of the scan can be accomplished at the data system or remotely. A step mode of operation is also provided to permit a single channel to be observed during system checkout. The programming functions are physically located in the same chassis with the scanner. Another function controlled by the programmer is the time delay from the completion of the switching to a particular channel until

starting the reading of that channel. Four values of time delay, ranging from 30 to 900 ms, can be selected. Another programming feature is the capability to select the function (i.e., voltage or frequency measurement), range, and integration period independently for each channel.

3. Linear Rectifier - The linear rectifier is a wide dynamic range full wave rectifier. Good linearity was achieved in the design of the rectifier by employing a high degree of feedback in the circuit. The use of stable dc operational amplifiers in the rectifier has resulted in the required low drift. Figure 5 shows the linearity of the final circuit employed in the data system. Since the rectifier is direct coupled, the linear performance is achieved from dc to frequencies limited only by the gain-bandwidth characteristics of the operational amplifiers in the rectifier. Since very little gain is required from the rectifier, it is usable to frequencies in excess of 10,000 cps.

4. Integrating Digitizer - The heart of the Digital Data Recording System is the integrating digitizer which performs a true integration of the rectified data signals and converts the integrated average to digital form. The digitizer operates by applying the input analog voltage to a voltage-to-frequency converter. The instrument than "counts" the pulses generated by the voltage-to-frequency converter. Since the integrator operates for a precisely controlled period (1.0, 0.1, or 0.01 seconds), the total count during the sample period is directly proportional to the integral of the applied input voltage. The automatic programmer is coupled to the integrator to control the start, duration, and end of the integration operation. At the end of the integration process, the time average of the input signal is available in binary-coded decimal (BCD) form.

5. Coupler - The coupler prepares the digitized data for recording on the tape recorder. When instructed to do so by the programmer, the coupler briefly stores the following information in parallel form:

1. Identification of the channel being measured, from 01 to 50.

2. The function (voltage or frequency) being measured by the integrating digitizer.

3. The value of the measurement being nade (5 digits).

4. A single range digit indicating the negative power of ten by which the measurement (3, above) is multiplied.

This information is released serially to the incremental magnetic tape recorder. The coupler is also used to select and generate gaps in the magnetic tape.

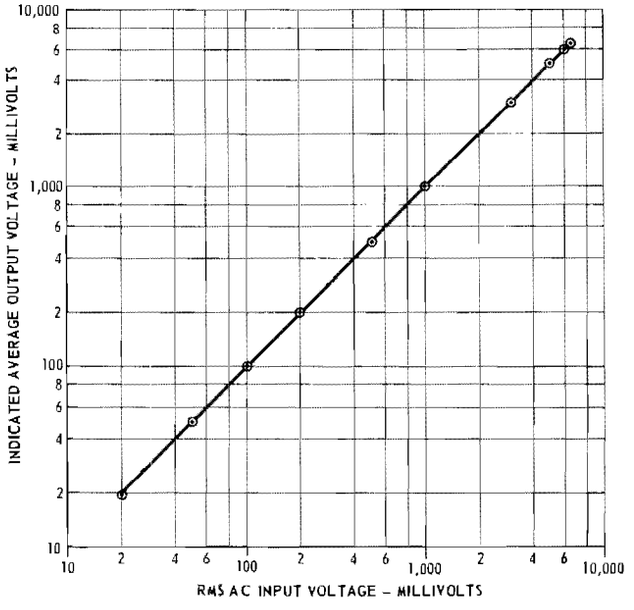

Fig. 5. Linearity characteristics of full wave rectifier

6. Incremental Magnetic Tape Recorder - The tape recorder, whose operation is coordinated by the automatic programmer and coupler, records and permanently stores, in digital form, the data which were temporarily stored in the coupler. The magnetic tape advances in accurately controlled steps of 0.005 in., corresponding to the standard data packing density of 200 bits per in. The 1/2-in. wide tape is recorded on seven tracks whose spacing and electrical characteristics are completely compatible with IBM computer tape transports.

TEST OPERATIONS WITH THE DIGITAL RECORDING SYSTEM

Operation of the digital data recording system is straightforward. Each response transducer is connected to a separate input on the scanner and pushbuttons are depressed to select channels. As indicated earlier, up to 50 transducers can be accommodated at one time. Each channel in the scanner which is being used is then programmed for function, range, integration time, and time delay between scanner switching and start of integrating period. Programming is quickly accomplished by inserting diode pins into a pinboard as shown in Fig. 6.

The output of the scanner is connected to the linear full-wave rectifier. The output of the rectifier is connected to the integrating voltmeter (digitizer). At this point, calibration of the integrating voltmeter is verified by operating the voltmeter in "calibration" function. Then the rectifier is checked by applying a known ac signal through one channel of the scanner and adjusting the rectifier gain and symmetry to obtain the correct (rectified) average indication on the voltmeter.

The coupler is then set to generate the desired tape gaps after each channel, after a selected number of channels, or after each scan. The magnetic tape transport is then loaded, and the system is ready for use.

A special feature of the system is the ability to set in manually, via thumbwheel switches, nine digits of additional information. These digits are used for test identification number, test input frequency, and test force magnitude. During each data scan, the nine digits can be recorded just before the first vibration transducer signal is sampled.

Once the data recording system is set up, the test operations may proceed. The shaker, or shakers, are set at an arbitrary frequency and force level, the input frequency and force are set on the appropriate thumbwheel switches, and the data system "STEP" button is depressed. All of the preselected transducers are scanned, digitized, and recorded. If a one-second integration time has been selected, then approximately

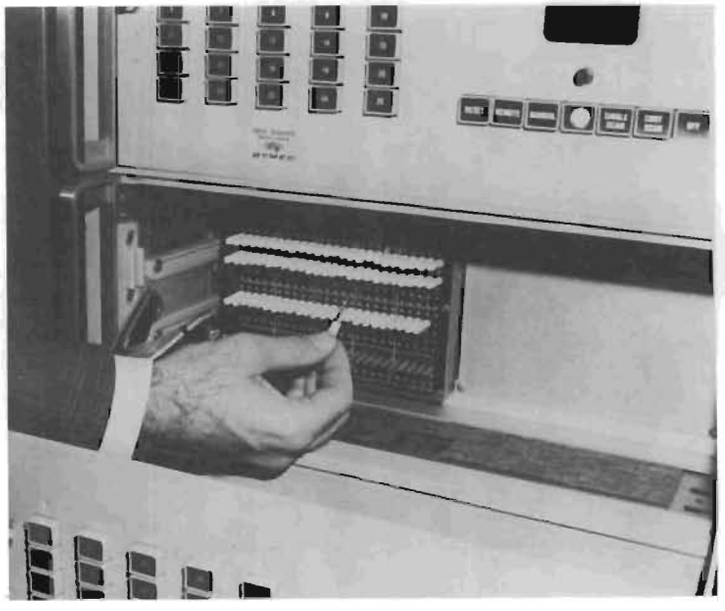

Fig. 6. Pinboard for programming measurement functions

1.1 seconds are required to scan each channel. At the completion of the scan, the test frequency is increased an arbitrary increment, input force is checked, thumbwheel switches set, and the data are scanned again. This procedure is repeated until the frequency band of interest has been surveyed.

DATA PROCESSING OPERATIONS

Data recorded on the magnetic tape are generally processed in two ways: numerical tabulations of the raw data (voltages), and final frequency response plots. Tabulations can be obtained very quickly by the highspeed IBM 1403 Printer. Figure 7 shows the format and information in a data tabulation.

The final frequency response plots take only slightly longer. The flow diagram in Fig. 8 illustrates the several steps—all automated—which are required to convert raw data into final plots. A special IBM 1401 computer program was written to convert the voltage recorded from the transducer into velocity; convert the velocity into double-amplitude displacement; and normalize the amplitude with respect to input force. The computer then scales the normalized response for plotting on semilogarithmic paper. A Benson-Lehner automatic plotter prepares the final plots from the computer output tape. A final plot is shown in Fig. 9.

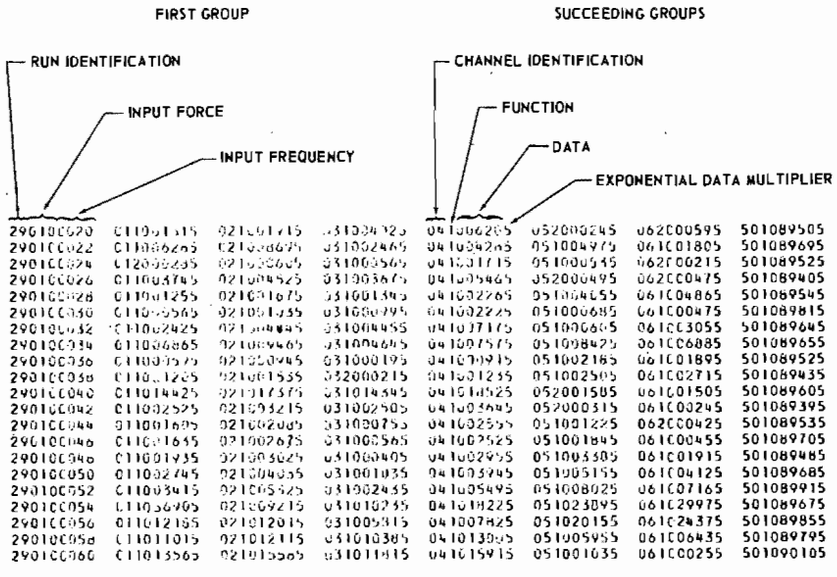

Fig. 7. Typical raw-data print-out

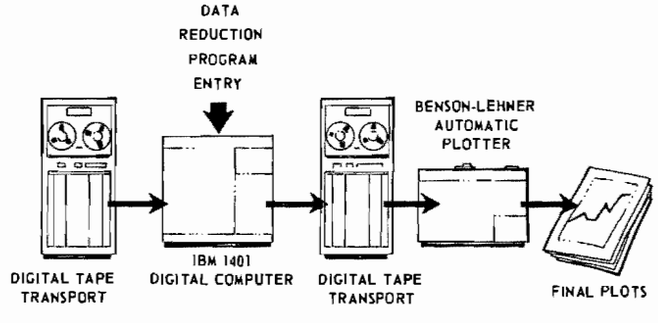

Fig. 8. Flow diagram for processing frequency response data

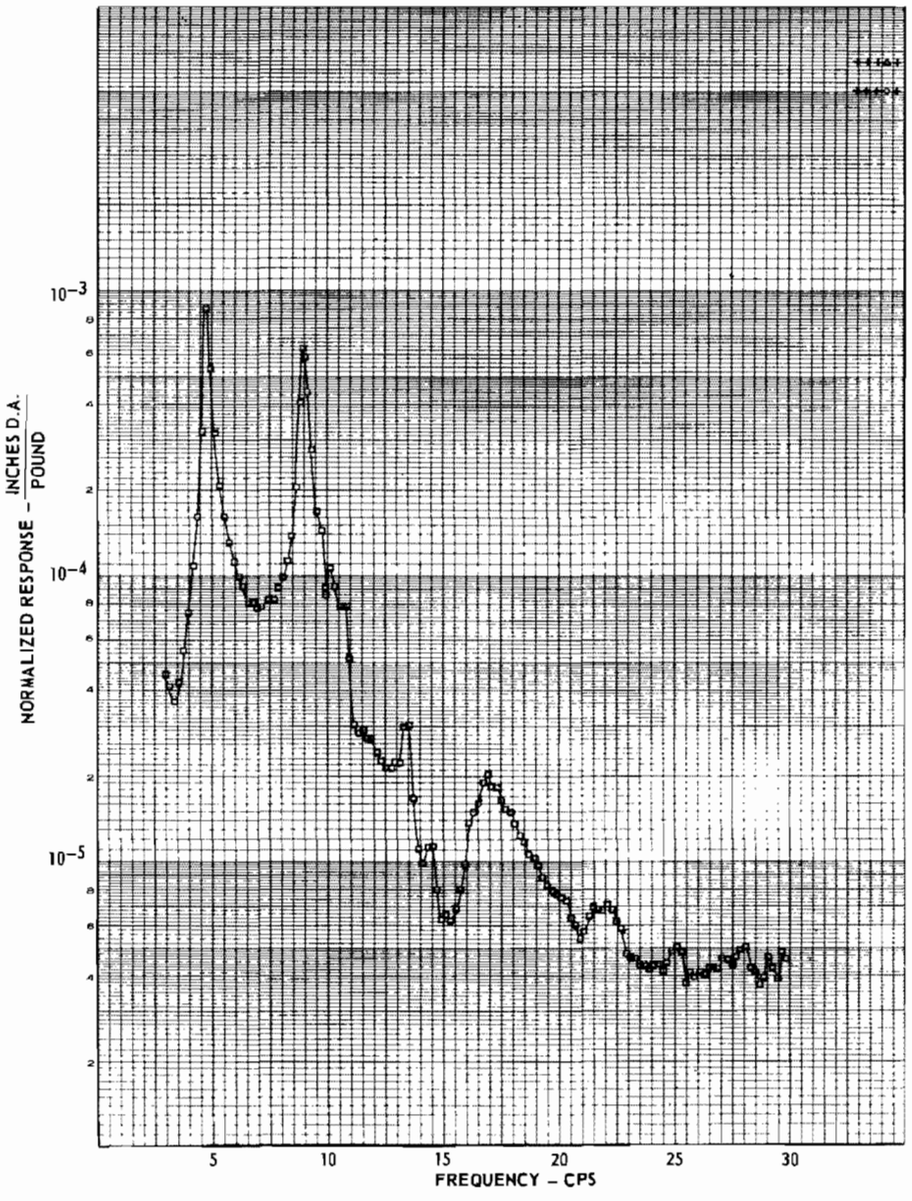

Fig. 9. Final data plot from digital data system

CONCLUSIONS AND AREAS FOR FURTHER STUDY

A Digital Data Recording System has been described which records and processes frequency response data generated in structural dynamics response testing. The system has resulted in substantial savings over previous methods of manual data reduction, while providing increased accuracy and reduced time delay between completion of test and availability of plotted data.

Additional studies are being conducted to use the system on continuous frequency sweep tests and to provide a means for recording mode shape data.

Appendix

ANALYSIS OF ERRORS RESULTING FROM INTEGRATION OF RECTIFIED SINUSOIDAL SIGNALS OVER FINITE TIME PERIODS

The use of a detector which performs a true integration of a rectified sine wave permits the integration errors resulting from a finite integration period to be accurately determined. Consider the output of a full-wave rectifier, which is a series of "half-sine" pulses. The average value of each half-sine is determined from

$$E_{avg} = \frac{1}{\pi} \int_0^{\pi} A_0 \sin \theta \, d\theta , \qquad \text{(A-1)}$$

$$E_{avg} = \frac{2}{\pi} A_0 . \qquad \text{(A-2)}$$

This well known result is obtained whenever an integral number of half-sine pulses is integrated, in which case the result is independent of the starting point of the integration. Errors may result, however, when a non-integral number of half-sine pulses are averaged. The errors will depend not only on the non-integral number of half-sine pulses, but also on the exact point on a pulse at which the integration is initiated. The maximum and minimum integrated values can be calculated for these cases.

The maximum integrated value results when the fractional pulse is integrated near the peak value of the pulse (see Fig. 10). In this case,

$$[E_{avg}]_{max} = \frac{1}{2\theta} \int_{\left[(2n-1)\frac{\pi}{2}-\theta\right]}^{\left[(2n-1)\frac{\pi}{2}+\theta\right]} A_0 \, |\sin \theta| \, d\theta ,$$

$$[E_{avg}]_{max} = \frac{A_0 \sin \theta}{\theta} . \qquad \text{(A-3)}$$

Therefore, the maximum "average" that could be detected would be for integration over very small fractions of a half-sine, where θ approaches zero. Then,

$$\lim_{\theta \to 0} \left(\frac{A_0 \sin \theta}{\theta} \right) = A_0 .$$

It is also apparent that as θ approaches $\pi/2$, we obtain the correct average,

$$E_{avg} = \frac{A_0 \sin \frac{\pi}{2}}{\frac{\pi}{2}} = \frac{2A_0}{\pi} .$$

Following a similar argument, the minimum value of detected average is obtained by integrating the fractional pulses near their zero

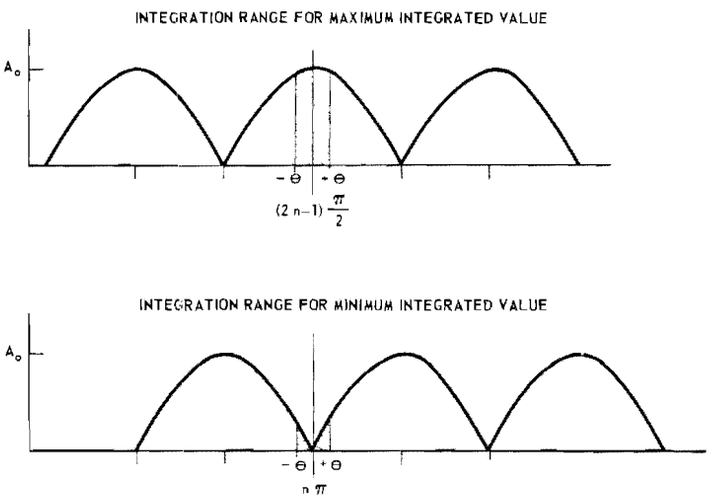

Fig. 10. Integration range for calculation of errors

value, as shown in Fig. 10. For integral values of n,

$$[E_{avg}]_{min} = \frac{1}{2\theta} \int_{n\pi - \theta}^{n\pi + \theta} A_0 \, |\sin \theta| \, d\theta ,$$

$$[E_{avg}]_{min} = A_0 \left(\frac{1 - \cos \theta}{\theta} \right) . \qquad \text{(A-4)}$$

The limiting case as θ approaches zero is

$$\lim_{\theta \to 0} A_0 \left(\frac{1 - \cos \theta}{\theta} \right) = 0 .$$

As θ approaches $\pi/2$,

$$E_{avg} = A_0 \left(\frac{1 - \cos \frac{\pi}{2}}{\frac{\pi}{2}} \right) = \frac{2A_0}{\pi} .$$

The values obtained by averaging over a nonintegral number of half-sine waves, normalized so that the true average is unity, are shown in Fig. 11. The upper and lower curves represent the worst possible errors (maximum and minimum) which could be obtained. As the sampled number of half-sines increases, the error rapidly diminishes.

It is interesting to compare the known error of the present system with the variations in readings which might be obtained with conventional RC integration of the output of a full-wave rectifier. Considering the circuit of Fig. 2, note that the full-wave rectified signal can be represented by its Fourier series equivalent (4):

$$E(\omega t) = A_0 \left(\frac{2}{\pi} - \frac{4}{\pi} \sum_{n=1}^{\infty} \frac{1}{4n^2 - 1} \cos 2n\omega t \right) . \qquad \text{(A-5)}$$

A study of the response of the RC integrating circuit may be made by summing the response to the steady component plus the response to the alternating components. Since the alternating components fall off rapidly with n, only the first ac component (n = 1) will be considered. Assuming a very low source impedance for the full-wave rectifier and a time constant of 0.25 second for the RC integrator, the response of the integrating circuit to the steady-state component of the rectified signal is:

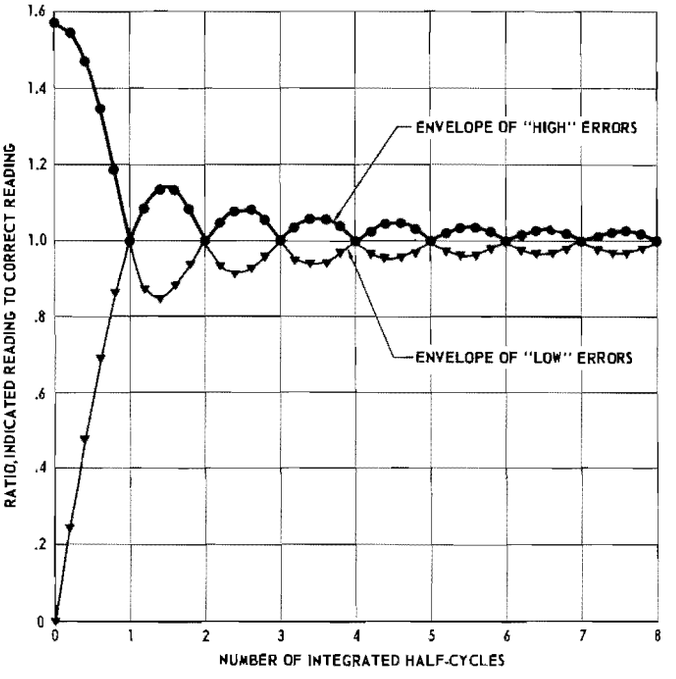

Fig. 11. Range of errors resulting from true integration of rectifier output

$$E_{s.s.} = \frac{2A_0}{\pi}\left(1 - e^{-\frac{t}{RC}}\right), \qquad \text{(A-6)}$$

where RC is the integrator time constant.

The response of the RC circuit to any arbitrary cosine wave of amplitude A, and angular frequency ω is:

$$E_{ac} = \frac{A_0}{\sqrt{1 + R^2C^2\omega^2}}\left[\sin(\omega t + \phi) - e^{-\frac{t}{RC}}\sin\theta\right], \qquad \text{(A-7)}$$

where $\phi = \arctan(1/RC\omega)$.

Therefore, to determine the response of the RC circuit to the first alternating component of the rectified sine wave, it is necessary only to correct the amplitude of the alternating component according to Eq. (A-5). For an applied signal of 2 cps, the first alternating component in the Fourier series is

$$-\frac{4A_0}{3\pi}\cos 8\pi t .$$

This is the component applied to the RC circuit.

From Eq. (A-7), the response of the RC circuit to this applied signal is:

$$E_{f_1} = -\frac{4A_0}{3\pi}\frac{1}{\sqrt{1 + (0.25)^2(8\pi)^2}} \times \left[\sin(8\pi t + \phi) - e^{-\frac{t}{0.25}}\sin\phi\right].$$

Since $\phi = 9.1°$ and $\sin\theta = 0.16$, the response to the first ac component reduces to:

$$E_{f_1} = A_0\left[-0.067\sin(8\pi t + 9.1°) + 0.017\, e^{-\frac{t}{0.25}}\right]. \qquad \text{(A-8)}$$

Finally, the complete response of the RC circuit to the dc component and the first ac component of the rectified sine wave is:

$$E_{RC} = A_0\left[\frac{2}{\pi}\left(1 - e^{-\frac{t}{0.25}}\right) - 0.067\sin(8\pi t + 9.1°) + 0.017\, e^{-\frac{t}{0.25}}\right]. \qquad \text{(A-9)}$$

These three components have been normalized so that the true average is unity, and the results are plotted in Fig. 12. It is interesting to note that the steady component increases exponentially to approach its final value of $2/\pi\,(A_0)$. The alternating component, however, continues to fluctuate about the steady

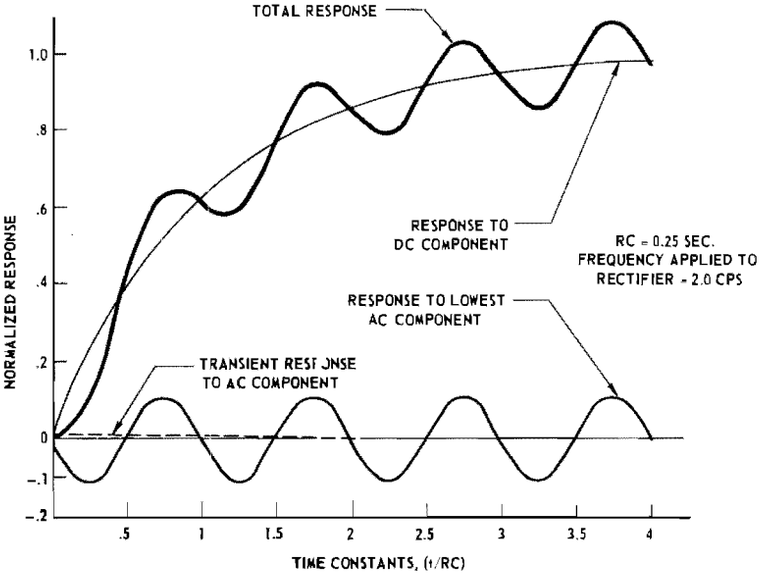

Fig. 12. Response of an RC integrator to a rectified sine wave

component at approximately 10 percent of the true average.

Although the time constant of the RC circuit and the frequency of the applied signal were arbitrarily chosen, the resulting 10 percent error is probably a representative error. If it were desired to decrease this error, an increased RC time constant would be required and this would result in a correspondingly longer time for the dc component of the rectified signal to reach its final value. The detector which performs a true integration of the rectified sine wave is therefore considered to offer the best compromise between reading speed and minimum error.

REFERENCES

1. R. C. Lewis and D. L. Wrisley, "A System for the Excitation of Pure Natural Modes of Complex Structures," J. Aeronautical Sci., 17, No. 11, November, 1950

2. R. H. Scanlan and R. Rosenbaum, Introduction to the Study of Aircraft Vibration and Flutter, (The Macmillan Co., New York) 1951

3. "Training Manual on the DY-2010 Series of Digital Data Acquisition Systems," DYMEC Division of Hewlett-Packard Co., Palo Alto, California, 1963

4. R. Legros and A. V. J. Martin, Transform Calculus for Electrical Engineers, (Prentice-Hall, Inc., Englewood Cliffs, New Jersey) 1961

* * *

COMPARISON OF ANALOG AND DIGITAL METHODS FOR VIBRATION ANALYSIS

William K. Shilling III
AF Flight Dynamics Laboratory
Wright-Patterson AFB, Ohio

The results of comparisons of the analog analyzers at the Air Force Dynamics Laboratory Sonic Fatigue Facility with theoretical results and digital computer analyses are reported. These comparisons provide a method for determining the accuracy of analysis and establish advantages or limitations of analog and digital procedures for various types of statistical analysis. Differences between the three methods of analysis, analog, digital, and theoretical, are determined and analyzed. Methods for reducing some of these differences are suggested and illustrations of improvements are presented. The applicability of analog and digital techniques to the analysis of various kinds of data is discussed and time requirements are compared. The statistical accuracy of the analysis is investigated. Accuracy is compared with results reported in the literature and in the case of the auto-correlation analyzer, an empirical expression for statistical accuracy is determined.

INTRODUCTION

Three functions predominate in providing the statistical information required for modern vibration analysis. These are power spectral density, autocorrelation, and amplitude probability density functions. At the Research and Technology Division (RTD) Sonic Fatigue Facility the vibration is induced in structure by high intensity noise. Analysis of the resulting vibration data is performed by both analog and digital data analysis methods.

The RTD Sonic Fatigue Facility, which is presently nearing completion, will provide the capability to conduct exploratory and advanced development on acoustic problems of flight vehicles such as sonic fatigue of structures and to perform acoustic proof testing of flight vehicle components. This facility will produce a controlled high intensity acoustic environment quite similar to those encountered in service conditions. Sirens, which produce the intense noise, will generate high intensity sounds ranging from a single frequency to a close approximation of broadband noise.

The RTD Sonic Fatigue Facility (formerly the Aeronautical Systems Division (ASD) Sonic Fatigue Facility) was described in detail in a paper presented at the 30th Symposium on Shock and Vibration in 1961 (1). This facility is now almost ready for full operation. The small test chamber of the facility has been in operation for the past year.

The facility instrumentation system provides for 72 continuous data channels or 342 time shared data channels. Individual channels are automatically attenuated, identified, and recorded on FM tape. Quick look monitoring and editing equipment is used to bring the raw data samples down to manageable size. The basic analog analysis equipment, to be described in more detail later, consists of a power spectral density analyzer, a correlation analyzer, and an amplitude probability density analyzer. An IBM 7094 digital computer is available nearby for digital processing of data. This computer is available on either an open shop basis or combined with the services of a programmer.

The purpose of this paper is to illustrate the two basic types of data analysis available at the Sonic Fatigue Facility and to show how each will provide the three major functions required from the raw data.

ANALYSIS FUNCTIONS

The autocorrelation function is the average product of a signal with itself at a later time. This function is often used to determine whether the response of a highly resonant system is responding to a periodic excitation or to a wide

band excitation. The autocorrelation function of a periodic signal oscillates at the same frequency as the signal in question. However, the autocorrelation function of a narrow band random response decays to zero after a sufficient delay. Another use for this function is to separate a periodic signal from noise which may mask it completely. The portion of the autocorrelation function representing the noise decays rapidly to zero, but the portion representing the periodic signal continues to oscillate at the frequency of the hidden periodic signal. The autocorrelation function for a function of time is

$$R(\tau) = \lim_{T\to\infty} \frac{1}{2T} \int_{-T}^{T} f(t)\ f(t+\tau)\, dt .$$

The analog analyzer approximates this expression by performing

$$R(\tau) \approx \frac{1}{2T} \int_{-T}^{T} f(t)\ f(t+\tau)\, dt .$$

The power spectral density of a random signal is essentially the contribution of each infinitesimally narrow band of component frequencies to the mean square value of the signal. The mean square value of the signal is found from the power spectral density function by summing the values of the function for each infinitesimal band of frequencies. The value of the autocorrelation function at zero time delay also gives the mean square value of the signal. The power spectral density is related to the autocorrelation function by the expression

$$G(f) = \int_{-\infty}^{\infty} R(\tau)\ e^{-j2\pi f\tau}\, d\tau .$$

The mean square signal value is given by

$$R(0) = \int_{-\infty}^{\infty} G(f)\, df .$$

The power spectral density function is useful in structural vibration and fatigue analysis because the power spectral density of the vibration response of a structure is equal to the product of the power spectral density of the excitation and the square of the absolute value of the frequency response function of the structure. Whenever any two of these functions are known the third can be determined.

The amplitude probability density function provides a measure of the time that a signal spends in a narrow amplitude range. The probability density, as estimated by the analyzer, is given by $p(y) \approx (1/T)(\Delta t/\Delta y)$. In this expression, Δt is the total time spent by the signal in the amplitude region y to $y + \Delta y$ during the time T that the signal is observed. This information is extremely useful in fatigue testing because it indicates the amount of time various stress levels are present in a structure. This function can provide insight into considerations such as whether a few cycles of high stress levels are more damaging than many cycles of much lower stress levels.

ANALYSIS EQUIPMENT

Analog

The autocorrelation analyzer is a special purpose analog analyzer developed for the Air Force RTD Sonic Fatigue Facility. It is an elaborate piece of equipment capable of many modes of operation. It can be programmed to operate automatically from punched tape instructions and to display its output on charts and punched cards. The performance of this equipment, however, will be based on its use as an autocorrelation analyzer with RC averaging of the lagged product.

For autocorrelation, only one input to the analyzer shown in the block diagram, Fig. 1, is used. Actually, the analyzer can also serve as a cross correlator by providing different inputs for both fixed and variable delay. Variable delay is produced by a rotating magnetic drum. Fixed delay, provided by a delay line, is needed only to generate negative τ for cross correlation. Negative τ provides no new information for the autocorrelation function since it is an even function.

In brief, the analyzer performs the following functions. The input signals modulate a high frequency carrier, are delayed, demodulated, then multiplied. The multiplied output is either integrated by a true integrator, or passed through an RC averaging circuit. The integration circuit is designed to be used with a tape loop input, where a pulse obtained from the tape splice is used to reset the integration circuit to prevent saturation of the operational amplifiers. When a continuous input is used, an RC averaging circuit provides an approximate integration. The averaging circuit was used throughout the tests conducted for this paper. The total range of delay available in the analyzer is from -10 ms to +50 ms.

The power spectral density analyzer approximates the true power spectral density by narrow

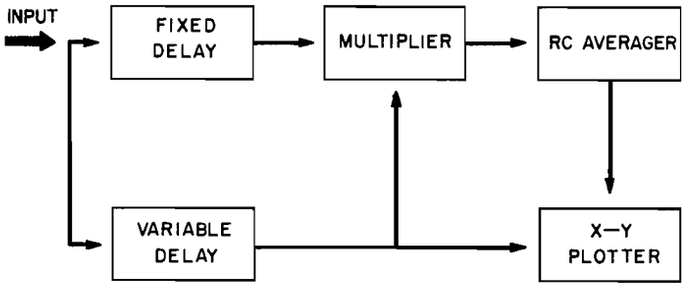

Fig. 1. Block diagram of the autocorrelation analyzer

band filtering. The block diagram of the power spectral density analyzer is shown in Fig. 2. The input signal is modulated and then filtered through a narrow band filter. The mean square output of this filter is plotted against the frequency being filtered. Filter bandwidths are selected from available values of 1, 5, 10, and 100 cps. Outputs of these filters are normalized for bandwidth in order to provide an estimate of power spectral density. The mean square is determined by means of squaring amplifier whose output is placed through an integrator which averages over the length of signal available. The output of this analyzer appears on an X-Y plot with the power spectral density in decibels as the ordinate and frequency as the abscissa.

The amplitude probability density analyzer, shown in Fig. 3, slowly sweeps an amplitude window over the entire range of amplitudes covered by the input signal. The input is first normalized to one volt rms. One volt is then equivalent to one standard deviation (σ). The analyzer can sweep from -6.25 volts to +6.25 volts which is sufficient for almost all signals encountered in practice. When the input signal is in the amplitude window, a gate circuit allows pulses from a generator to be counted. The number of pulses counted at each amplitude position, divided by the total number generated, provides an estimate of the probability density.

The estimated probability density function is plotted continuously on an X-Y plotter as the amplitude window sweeps the maximum amplitude range. The width of the amplitude window was determined by shorting the input and manually sweeping the window through zero volts. The window is 0.1 volts in width.

Digital

The only specific items of equipment required at the Sonic Fatigue Facility for digital data analysis are an analog to digital converter, and a digital tape transport. This equipment provides a means to digitize samples of raw data and record the digitized samples on magnetic tape.

The tape is delivered to the digital computer complex where it is reprocessed to be compatible with SYSTRAN (2). SYSTRAN is a multipurpose program which was developed to provide the analysis capability of a 14-channel FM magnetic tape and light-galvanometer data acquisition system used for Biomechanics Research in the Aerospace Medical Laboratories

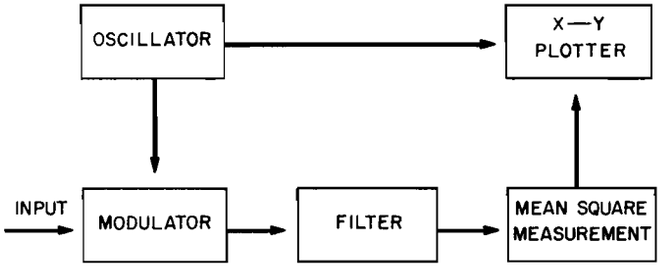

Fig. 2. Block diagram of the power spectral density analyzer

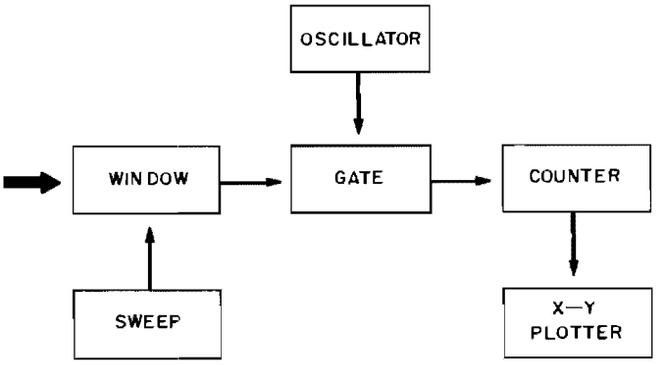

Fig. 3. Block diagram of the amplitude probability density analyzer

at Wright-Patterson AFB, Ohio. It includes subroutines for most of the common tools of frequency domain analysis of linear systems. It provided the power spectral density, autocorrelation, and probability density functions for the digital analysis portion of this paper.

The A-D converter can sample data at rates of 208, 417, 834, 1667, 3333, and 6667 samples per second. To provide even higher effective sampling rates, the input analog tape transport can be reduced in speed by a factor of 10:1. Digital data samples are arranged on the digital tape in a format compatible with the IBM 7094. All necessary identification is recorded at the beginning of each data record.

SELECTION OF TEST SIGNALS AND THEORETICAL ANALYSIS

Several periodic waves will be chosen for test signals. Periodic test signals which are readily available and can be analyzed easily are sine waves, square waves, and triangular waves. These shall be used for calibration purposes for the analyzers.

A sine wave can be expressed as a function of time in the following manner:

$$f(t) = A \sin (2\pi f t + \theta).$$

The autocorrelation function for this wave is found to be $R(\tau) = (A^2/2) \cos 2\pi f \tau$, where τ represents the time delay. The amplitude probability density function for the sine wave can be shown to be $p(y) = 1/A\pi \sqrt{1 - (y/A)^2}$. The power spectral density for a sine wave is a delta function at the sinusoidal frequency.

Upon calculating the autocorrelation function for a square wave one obtains a triangular wave with a maximum value equal to the mean squared value of the square wave. This triangular wave has the same period as the input square wave. The amplitude probability density function for a square wave is given by two vertical lines, one at the maximum, and one at the minimum amplitude.

The triangular wave with peak amplitudes A spends equal time in equal amplitude increments. The amplitude probability density function is therefore a rectangle with height $1/2A$ with width $2A$.

The most commonly used random test signal is Gaussian noise. Good approximations to Gaussian noise are readily available from electronic noise generators. Gaussian noise is defined by the amplitude probability density function

$$p(y) = \frac{1}{\sqrt{2\pi}\,\sigma} e^{-\frac{1}{2}\left(\frac{y-m}{\sigma}\right)^2},$$

where m is the mean and σ the standard deviation.

Another random signal amenable to analysis which also provides a good test signal is the random telegraph signal. The random telegraph signal has a positive amplitude of $A/2$ and negative amplitude of $-A/2$ with a random period. It has an autocorrelation function given by

$$\frac{A^2}{4} e^{-2a|\tau|}.$$

The power spectral density is found from the Fourier Transform of the autocorrelation function. The power spectral density is

$$G(f) = (A^2/2)(a/a^2 + \pi^2 f^2),$$

where a equals the average number of zero crossings per unit time of the random telegraph signal.

The above two signals were also chosen for calibration and comparison purposes. Other signals which are often encountered in the analysis of acoustic test data are broadband siren data and signals contaminated by 60 cycle or other electrical noise.

Periodic and broadband signals comprised the basic test program for the various analysis techniques. The signals were used, however, to determine different properties of the three functions.

For correlation analysis, outputs were compared to theoretical calculations for various values of time delay, τ. It was necessary to see how errors behaved as τ became quite large. Power spectral density analysis was tested to determine accuracy as a function of frequency. Probability density analysis produced a function of amplitude and was tested accordingly.

Sine waves were used as a test signal for each of the three analysis functions. This signal provided a means to check τ accuracy experimentally for correlation measurements and to determine how large a τ the analysis could provide. For a power spectrum analysis the sine wave could be used to determine filter transfer function of the analog analyzer and illustrate the problems arising from finite sample lengths in the digital program. The sine wave amplitude density analysis, however, becomes infinite in theory so it could not be followed completely in this analysis. The degree of approximation can be readily determined.

Triangular waves work well for theoretical analysis of probability density. This wave shape provides a constant value of probability density over its entire amplitude range. This wave is appropriate for determining stability of the analyzer.

The random telegraph wave provides a transition from the completely predictable wave such as sine, square, or triangle to the completely unpredictable broadband Gaussian type signal. In the random telegraph wave, there are only two choices of amplitude, but the period of one cycle can be of any value. This wave form has been encountered in some of the newer acoustic noise generators.

The broadband noise obtained from an electronic noise generator is close to Gaussian, as are many naturally occurring phenomena. Gaussian noise has a well known probability density function and can be used as a test signal to determine the performance of the probability density analyzer. The autocorrelation and power spectral density functions are known for a broadband Gaussian signal, which can be used as a test signal for these analyzers.

Data samples for the digital analysis were limited to a random signal, a sine wave, and a combination of the two. Digital test signals were either generated by the computer or taken from a random number table. The test signals used for the analog analyzers, with the exception of the random telegraph signals, are also combinations of the same types of signals used for digital analysis.

RESULTS AND COMPARISON

The analog, digital, and theoretical results are compared in Figs. 4 through 24. These figures include input signals such as sinusoids,

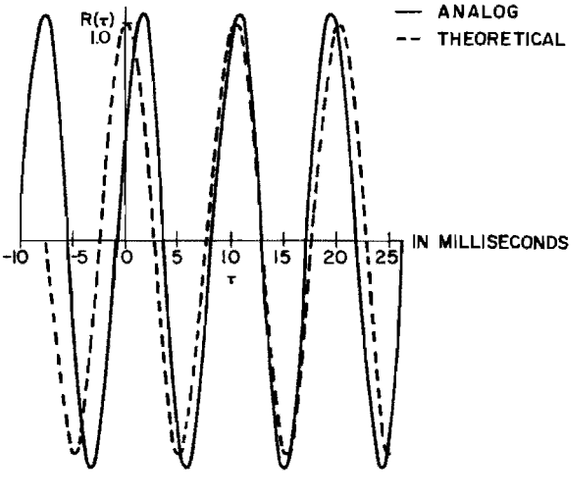

Fig. 4. Autocorrelation analyzer output for a 100 cps sine wave

noise, and combinations of these two for both the analog and digital systems. In addition square waves, triangular waves, and random telegraph signals were used in the analog analyzers. These figures also include the result of clipping sinusoidal input signals to show how each of the three types of analysis can indicate the presence of clipping.

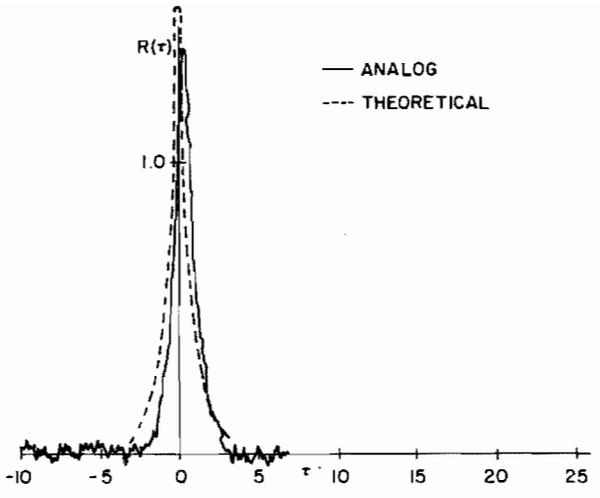

Fig. 5. Autocorrelation analyzer output for a random telegraph signal

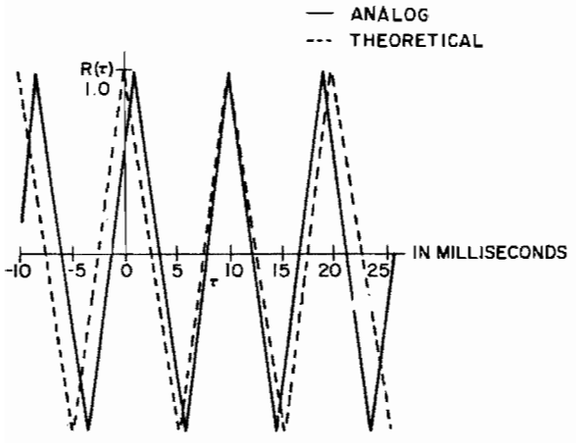

Fig. 6. Autocorrelation analyzer output for a 100 cps square wave

Autocorrelation

The autocorrelation analyzer was found to have a delay which introduced an error in the time delay τ axis as shown in Figs. 4, 5, and 6. To correct this, a 1000 cps sine wave was used to provide one ms markers on the τ axis. Amplitude calibration was performed in two ways. The mean squared value was first measured separately, then this value was assigned to the maximum value obtained by the autocorrelation function. This maximum value also established the zero point on the τ axis. The other approach to amplitude calibration involved a consideration of the statistical error.

The analyzed data exhibited a variation of the maximum amplitude of the autocorrelation function with sweep rate and time constant. In each case, when the time constant or sweep rate exceeds a certain value, the maximum amplitude drops rapidly from the predicted value. Bendat, Enochson, and Piersol (3) give expressions for statistical error and sweep rate as follows:

$$\text{Statistical error } e = \frac{1}{\sqrt{BK}}$$

$$\text{Sweep rate} < \frac{1}{16\,BK}$$

where

B = noise bandwidth of signal, and

K = time constant of analyzer in seconds.

To see if the analyzer followed these equations, narrow band noise signals of noise bandwidth B were introduced at varying sweep rates and time constants. In all cases the maximum amplitude became less than that allowed by the statistical accuracy expression at a much lower sweep rate than indicated above.

In all these cases, a factor of 4.7 times the indicated time constant would place the amplitude in the range predicted by Ref. (3). The Sonic Fatigue Facility analyzer is calibrated

to sweep in increments of ms/min so that allowable sweep rate becomes:

$$\text{Sweep rate} < \frac{6 \times 10^4}{4.7\,(16BK)} \frac{ms}{min}$$

$$= \frac{800}{BK} \frac{ms}{min} .$$

This expression has been compared with other data to see how well it holds. In all cases checked, it has proved to be conservative. The factor 4.7 apparently represents a machine time constant in excess of that indicated on the analyzer controls for averaging the lagged product.

After one becomes used to observing the output of analog analyzers, the digital results, in some cases, do not appear to be an analysis of the same input. With proper interpretation it can be shown that the results are what should be expected for the specific input to the particular analysis system.

The first input to the digital autocorrelation program was a 1.0 volt peak sinusoid. The theoretical autocorrelation function is a cosine wave. The output, instead, was the decaying cosine wave shown in Fig. 7. A decaying cosine wave is what should be expected, though, for a sine wave of finite length d has the autocorrelation function

$$R(\tau) = \begin{cases} \frac{A^2}{2} \cos 2\pi f\tau \left(1 - \frac{|\tau|}{d}\right) & |\tau| \leq d \\ 0 & |\tau| > d \end{cases}$$

where

A = amplitude of sine wave, and

d = sample length in seconds.

If it is desired to consider the autocorrelation function of an infinitely long sine wave, a correction term to compensate for the linear decay would have to be included in the digital program.

The number of τ values available to define the autocorrelation function is limited to 100 in Systran. If it is desired to obtain the power spectral density by transforming the entire non-zero portion of the autocorrelation function the increments between the 100 specific values of τ must be chosen large enough to cover the complete data record.

One of the prime uses of autocorrelation analysis is to separate a periodic signal from random noise. Fig. 8 illustrates how the analog analyzer could detect a 50 mv rms signal buried in one volt rms random noise from a continuous sample. The digital computer was used to detect a 500 mv rms signal in similar noise using a sample length of 0.1 second. This is shown in Fig. 9.

Clipping of the sinusoidal input is shown in Fig. 10. Both the analog and digital systems show the rapid drop in peak correlation and the increasing linearity of the more severely clipped signals.

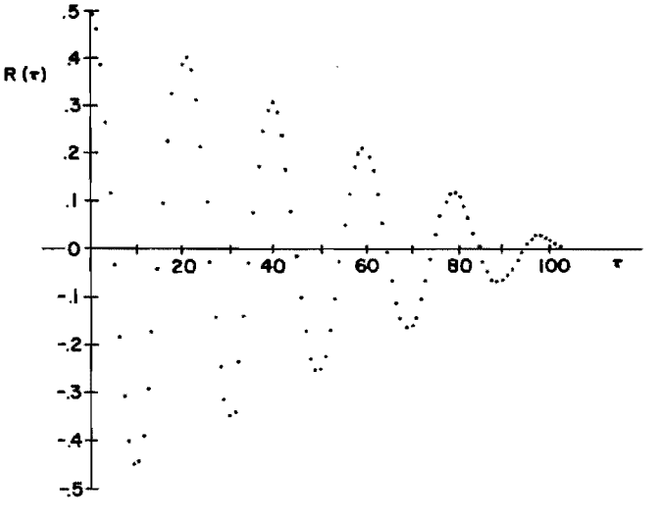

Fig. 7. Digital autocorrelation function for a bounded 50 cps sine wave

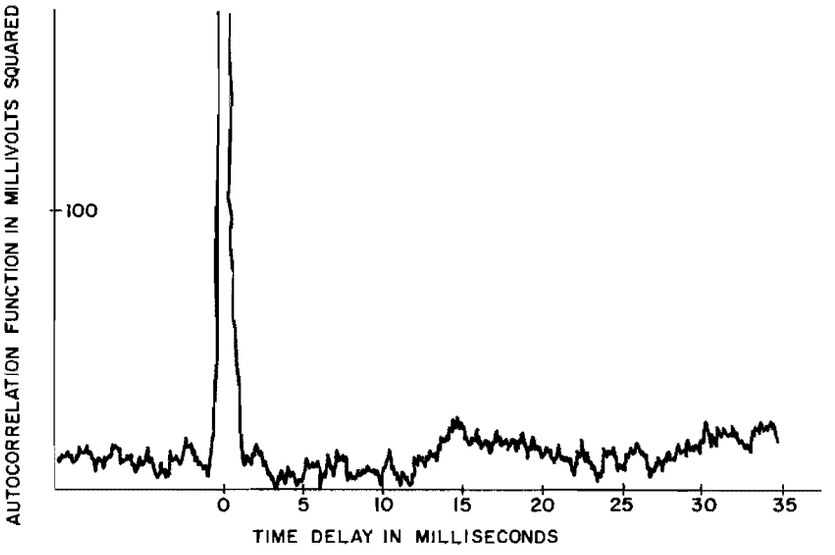

Fig. 8. Analog autocorrelation function for 1 volt rms random noise plus 50 mv 60 cps sine wave

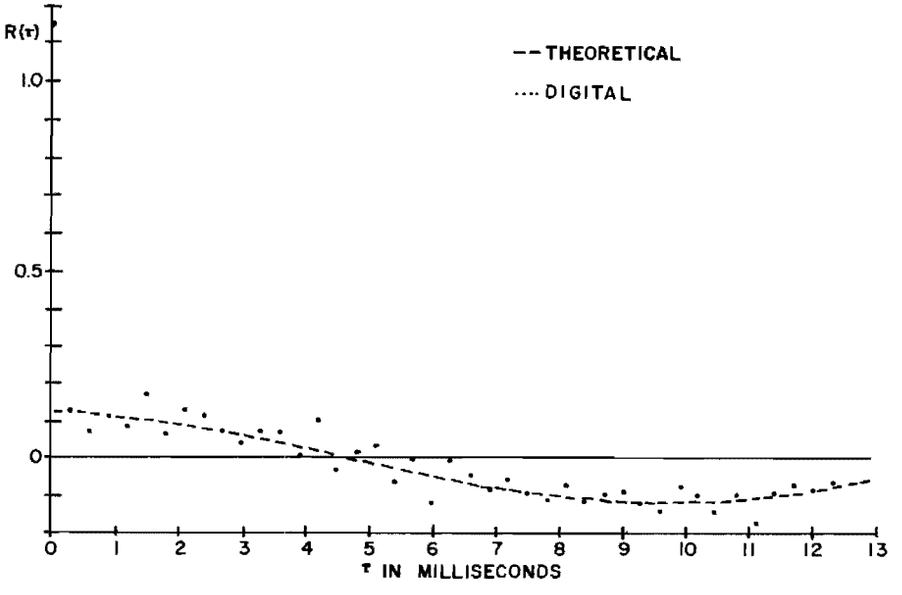

Fig. 9. Digital autocorrelation function for 1 volt rms random noise plus 500 mv 50 cps sine wave

Power Spectral Density

The analog power spectral density analyzer analyzes the input signal one bandwidth at a time. It integrates the output of this bandwidth for a fixed period of time. There are basically two sources of errors. One, statistical amplitude errors due to a finite integration time and two, frequency errors due to faulty readout when the analyzer moves the plotter from one bandwidth to the next. Since the analyzer plots only one point per bandwidth, frequency errors can usually be corrected by counting points from a known frequency.

In general, the statistical error e tends to follow the equation $e = 1/\sqrt{BK}$. Figure 11 shows larger errors at the low frequency end of the analysis of a random telegraph signal where a 1 cps filter was used. As a 5 cps

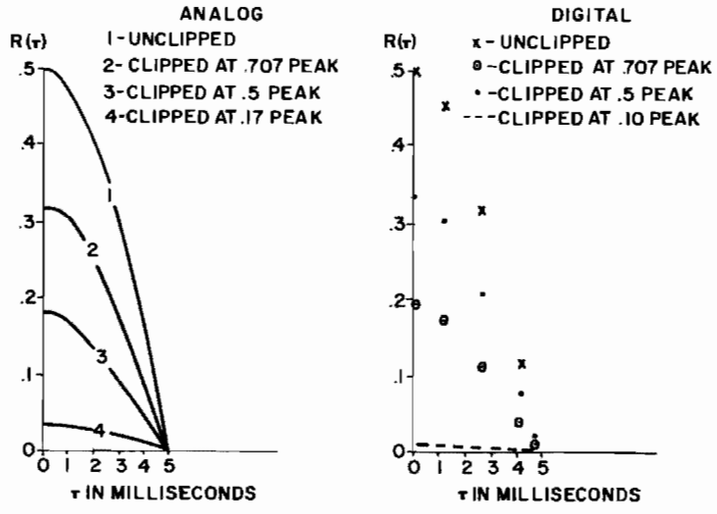

Fig. 10. Autocorrelation function for clipped sine waves

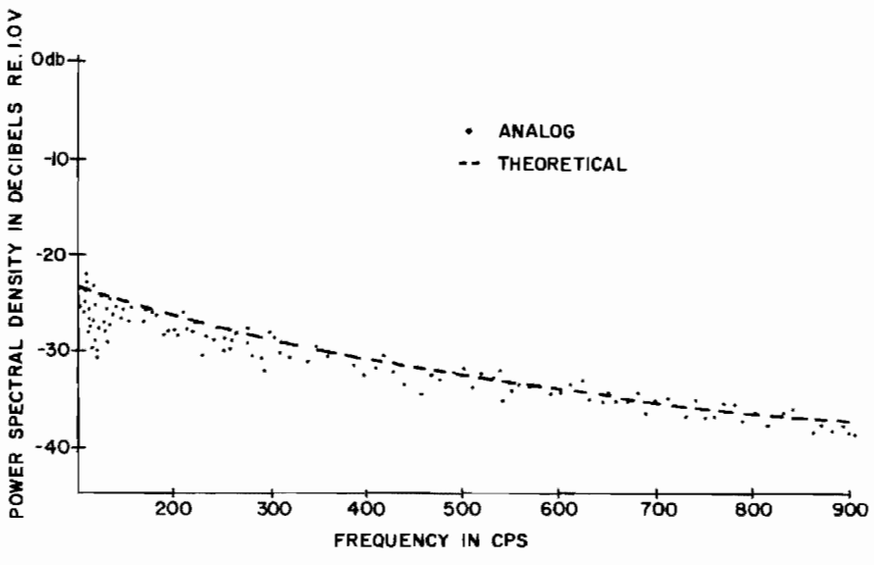

Fig. 11. Analog power spectral density for a random telegraph signal with 565 zero crossings per second

and then a 10 cps filter is switched into operation the error is seen to decrease. Figure 12 shows the analysis of a random telegraph signal where a 1 cps filter was used for the entire plot. In this case, it was necessary to increase the time constant of the mean square measurement circuit to 20 seconds in order to keep the error to a reasonable level. A time constant of 3 seconds was used to obtain the power spectral density shown in Fig. 11.

As can be seen from Figs. 11 and 12, the power spectral density given by the analyzer was quite close to that predicted. The slopes of the analyzer curves obviously fall along the slopes of the theoretical curves.

The digital system produces the power spectral density by performing the Fourier Transform of the autocorrelation function. If the true autocorrelation could be provided, the power spectral density should agree with the theoretical calculation. In the digital calculation of an autocorrelation function for a broadband random signal, the autocorrelation has the form $R(0)[1-(N/d)|\tau|]$ for $|\tau| \leq (d/N)$ and approximately

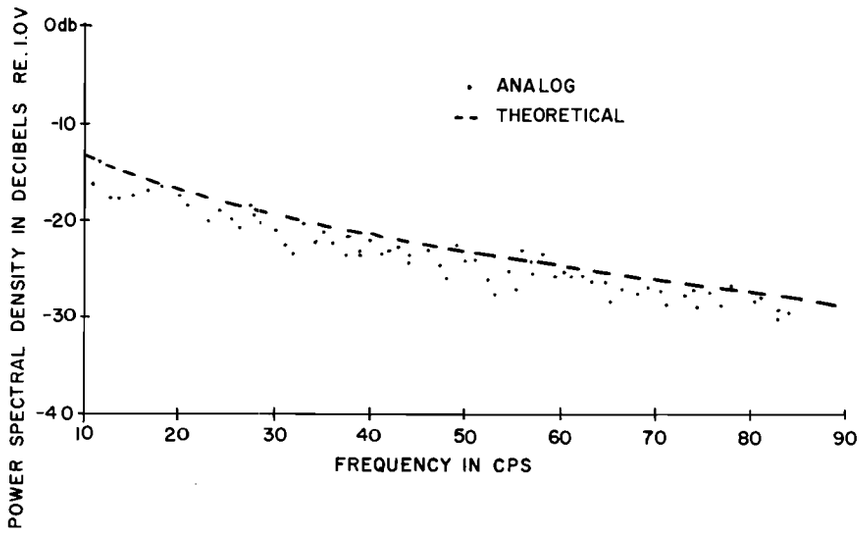

Fig. 12. Analog power spectral density for a random telegraph signal with 25 zero crossings per second

zero thereafter for increasing τ. (d = length of data record and N = number of digital samples). This means that the power spectrum will always be proportional to $(\sin \pi fk/\pi fk)^2$ which is the Fourier Transform of an expression of the form $[1 - (1/k)|\tau|]$. If a narrow band at the lower frequency end of the spectrum is observed it does appear to be the expected flat spectrum. Similarly, a finite length sine wave record will have a power spectral density of the same general form centered about the input frequency, rather than the theoretical delta function at the sinusoidal frequency. This results from the autocorrelation function being of finite length and decaying to zero as τ approaches the record length d. As a longer data record is used, holding the sampling rate constant, the digital power spectral density would be expected to become increasingly narrow.

The use of the digital computer for this analysis forces one into a careful consideration

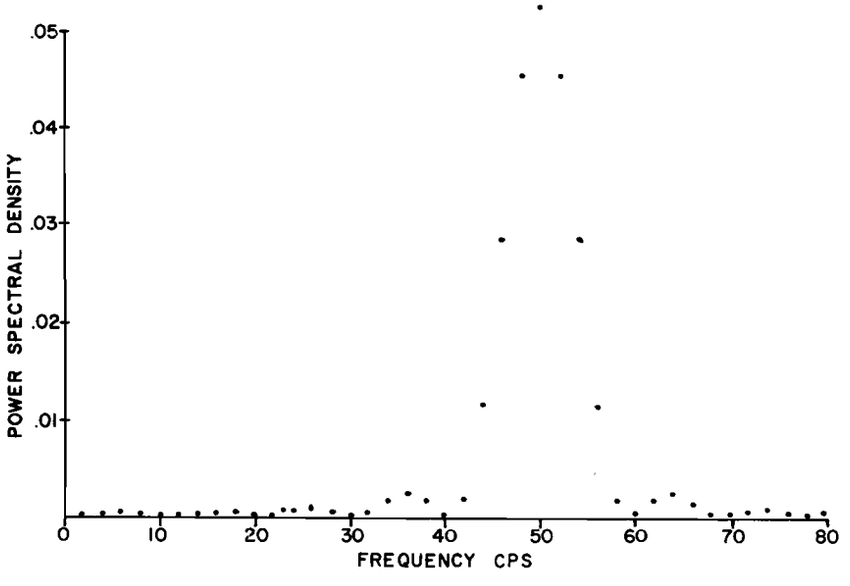

Fig. 13. Digital power spectral density of a bounded 50 cps sine wave

of the mathematics involved. Analytically, the expression for the power spectral density of the bounded sine wave shown in Fig. 13 can be found to be:

$$G(f) = \frac{A^2}{4} d \left[\frac{\sin^2\pi(f + f_0)d}{\pi^2(f - f_0)^2 d^2} + \frac{\sin^2\pi(f - f_0)d}{\pi^2(f - f_0)^2 d^2} \right],$$

where d = sample length of input.

This expression exhibits the proper characteristics in the limit for a sine wave. It illustrates why the absolute maximum at the sinusoidal frequency is not the only maximum. To obtain the above expression, it is necessary that one carefully chooses the range of τ in Systran so the PSD is obtained by the Fourier Transform of the entire autocorrelation function. Although the absolute maximum occurs at the same frequency, the spacing of the resulting maxima can be quite different, and the magnitude changes if the entire autocorrelation function is not transformed.

To obtain a better estimate of the true power spectral density, a spectral window must be used. The use of spectral windows which compensate for the effects of finite record length are described by Blackman and Tukey (4). Systran provides for nine different window options to improve the estimate of the power spectrum. Figure 14 shows how the third harmonic of the sine wave clipped at 0.1 volt is accentuated and the small fluctuations near the fundamental are suppressed when the spectral window $0.54 + 0.46 \cos(\pi\tau/\tau_{max})$ is used. This is the well known "hamming" window. In Systran, this is window option number 5.

The analog analyzer in Fig. 15 indicates the presence of the higher harmonics due to clipping more clearly than the digital analysis. This is due in part to the decibel scale used by the analog analyzer. Digital analysis is inherently limited because of the presence of secondary maxima which tend to obscure the higher harmonics generated by clipping.

Periodic signals can be distinguished in noise as shown in Figs. 16 and 17. Here, as for autocorrelation analysis, a much shorter sample with a correspondingly higher periodic signal is used in the digital analysis.

Amplitude Probability Density

The output of the analog device is quite sensitive to time constants and the instantaneous fluctuations of a random signal. Too long a

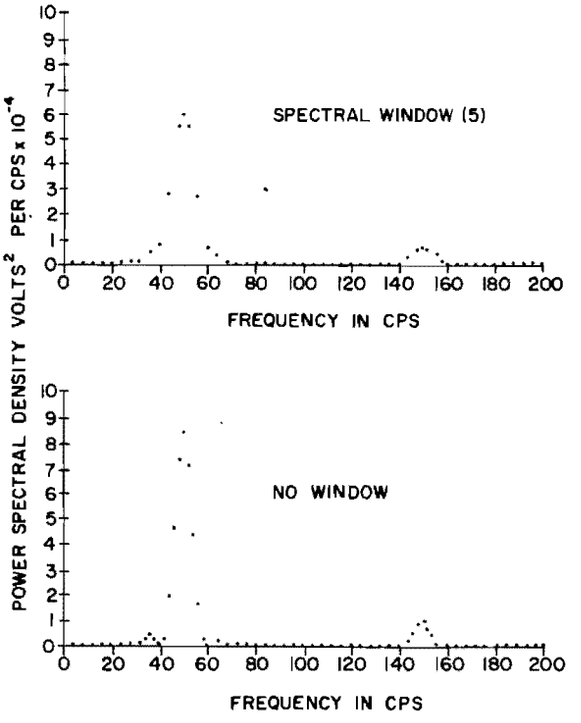

Fig. 14. Digital power spectral density of a bounded 50 cps sine wave clipped at 0.1 peak value

time constant smooths a Gaussian signal beautifully, but will cause the distribution function to be shifted along the σ axis. It also rounds sharp edges found in the analysis of periodic signals, such as sine waves and triangular waves. Figures 18 and 19 show the output of the probability density analyzer for a sine wave and for broadband noise before the time constants were reduced. Figures 20 and 21 show the output with the time constants reduced by a factor of 10:1. Note that the Gaussian curve is not as smooth, but the skew of the previous analysis has been almost eliminated.

The digital program suffers from no such problems. There, the major problem is choosing the amplitude increments in such a manner that enough points are available in each amplitude density function. The short sample length used in the digital analysis for this paper, Fig. 22, showed a bias on the positive amplitude side since it contained more positive half cycles than negative half cycles.

Tests in separation of periodic signals from noise indicate that probability density is not the function to use to separate signal from noise. Autocorrelation or power spectral density can separate a signal hidden in noise

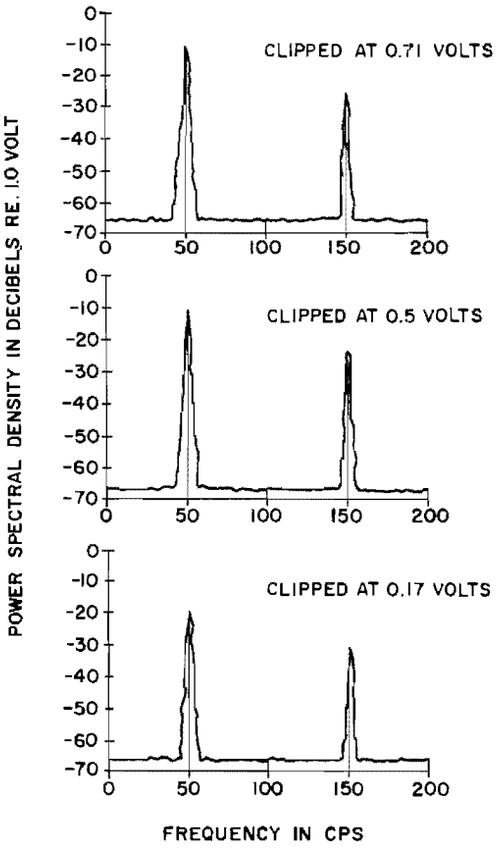

Fig. 15. Analog power spectral density of clipped 50 cps sine wave

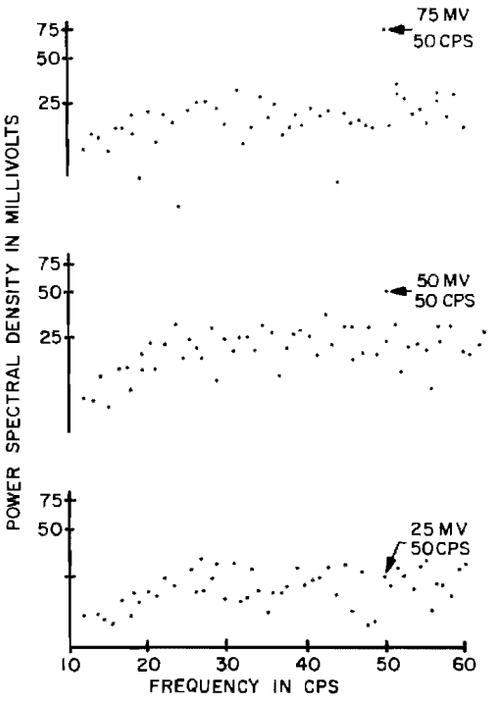

Fig. 16. Analog power spectral density functions for 1 volt random noise plus 50 cps sine wave

that is from 2 to 20 times less than the noise. For a periodic signal to show up in amplitude probability density, it must be larger than the noise signal.

Probability density is a good indication of clipping for a sinusoidal signal. Figures 23 and 24 show how both the analog and digital systems indicate changes due to clipping.

Time Requirements

The time for a computer run to provide a complete autocorrelation function, power spectral

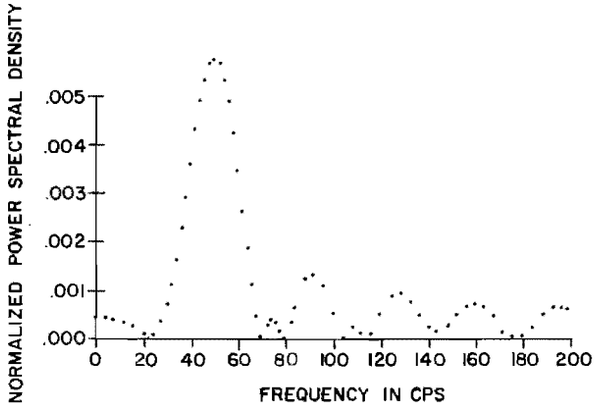

Fig. 17. Digital power spectral density for 1 volt random noise plus 500 mv 50 cps sine wave

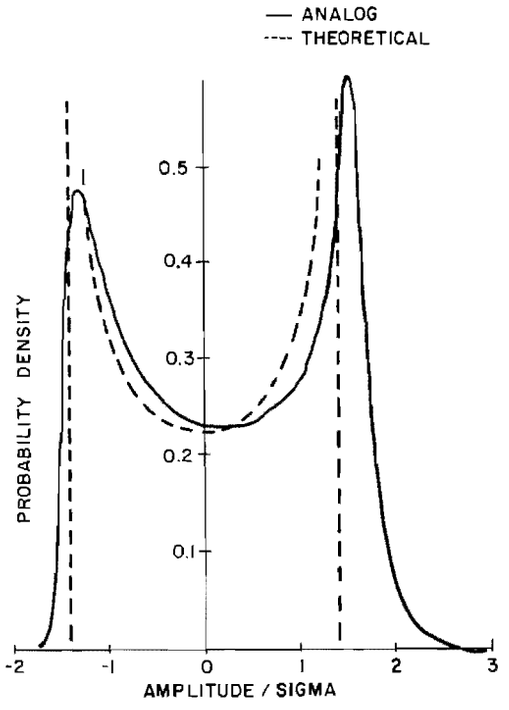

Fig. 18. Probability density analyzer output for 1 volt rms sine wave

density function, and probability density function has varied so far from 4 minutes and 5 seconds to 6 minutes and 43 seconds depending on which storage locations are available to the computer on that run.

The data samples used for digital computation in this paper were 0.1 second in length. These can be increased without changing the analysis time appreciably. Two-thirds of the analysis times quoted above was required for loading the Systran program into the computer. The actual analysis required only one-third of the time, thus considerably more analysis could be accomplished for each separate loading without increasing the overall time by a great amount.

The analog analyzers generally are operated for longer times on one analysis; the minimum sample length being one second. The correlation analyzer will operate between 6 minutes and 10 hours to cover a τ range of 60 ms. The amplitude probability density analyzer requires from 1 to 25 minutes for a single plot. The power spectral density analyzer can also run for hours if a narrow band analysis is required over its full 10,000 cps range for a several second sample length.

The relatively shorter digital times are a little misleading for our particular operation. First the analog tape must be converted to digital in the A-D converter. Then the tape must be run again at the computer facility where it is converted from 200 bits/in. in a continuous tape to 800 bits/in. broken up into data blocks compatible with the IBM 7094. It is then run through a program to put it in a form suitable for analysis by Systran. Needless to say, any saving in analysis time can easily be lost in this re-recording process.

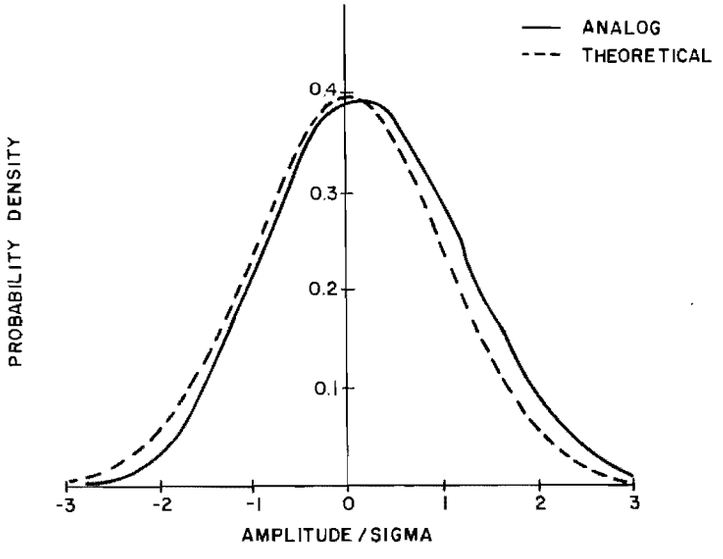

Fig. 19. Probability density analyzer output for 1 volt rms random noise

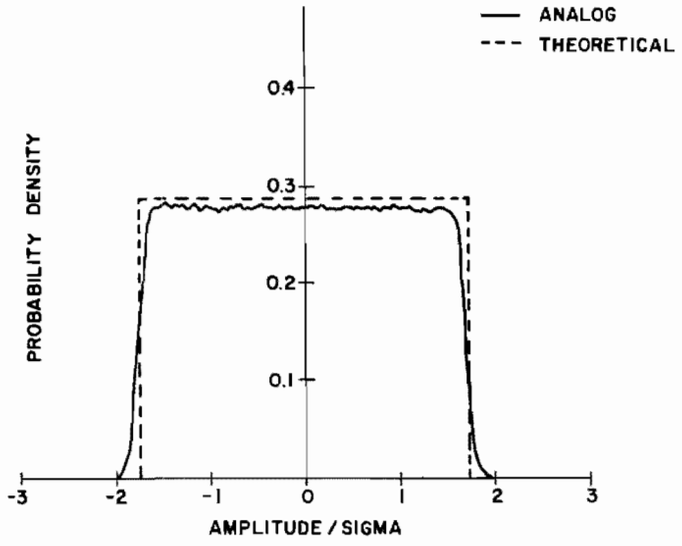

Fig. 20. Probability density analyzer for 1 volt rms triangular wave (modified time constant)

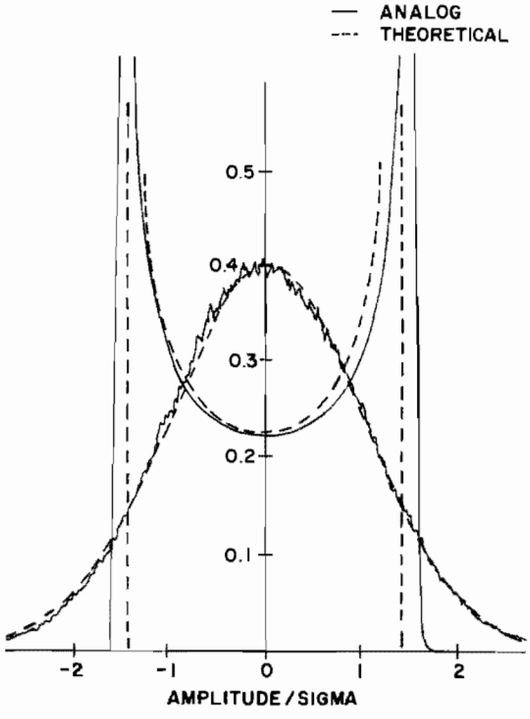

Fig. 21. Analog probability density after modification of time constant

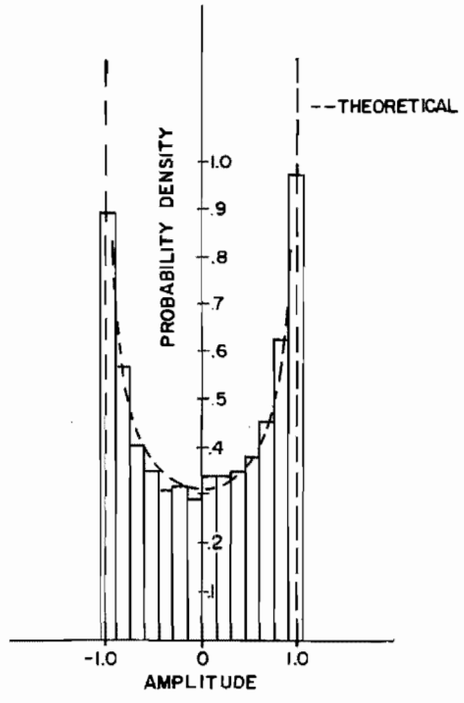

Fig. 22. Digital amplitude probability density for 1 volt peak bounded sine wave

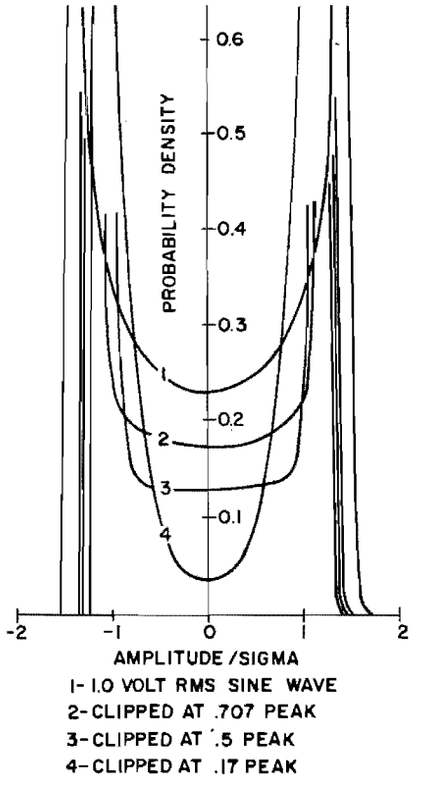

Fig. 23. Analog amplitude probability density for clipped sine waves

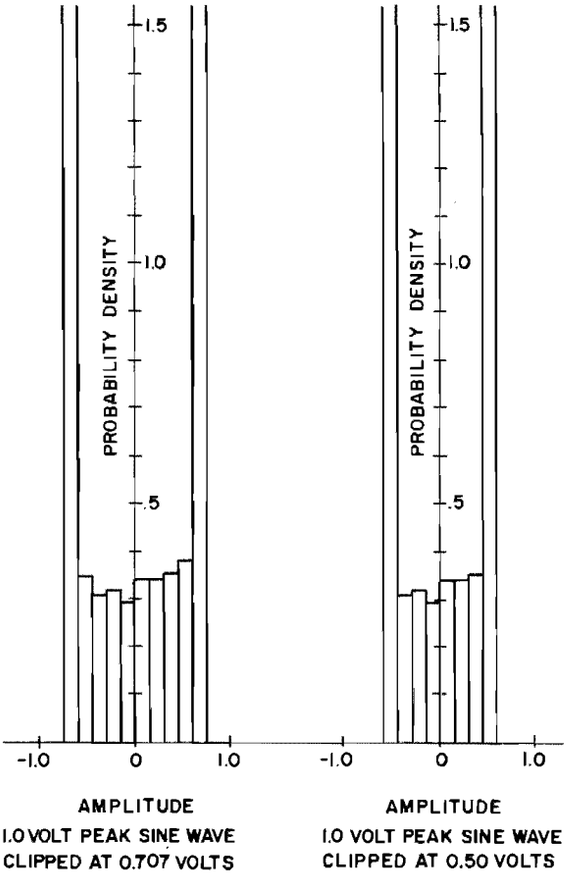

Fig. 24. Digital amplitude probability density for clipped sine waves

CONCLUSIONS

Autocorrelation functions compared favorably. In the digital case, finite sample lengths had to be taken into account. The power spectral density could be more easily interpreted from analog analysis, but shorter digital samples could be analyzed more quickly. The amplitude probability densities compared quite well.

An inherent limitation of the digital processing system is the requirement of three tape runs before getting on the computer. These include digitizing, repacking and blocking, then decoding.

The digital analysis system is more flexible; it is not restricted solely to power spectral density, correlation, or amplitude probability density.

Both methods will provide adequate analysis of selected samples of data. At the Sonic Fatigue Facility, analog methods are used for the bulk of the analysis of routine test data which include many hours of noise recorded on tape. Digital methods are used for special purpose analysis where there are not such great quantities of data.

As far as choosing between the two methods, it seems to depend on whether one would rather work with electronic equipment or would rather delve into the equations describing the functions. In many cases it was found that trying to interpret the digital results forced us into a greater understanding of the mathematics involved in the analysis.

REFERENCES

1. A. W. Kolb and O. R. Rogers, Shock Vibration and Associated Environments Bulletin No. 30, Part V:37 (1962)

2. D. J. La Jeunesse, E. B. Weis, Jr., T. J. Hogan, Jr., "SYSTRAN (Systems Analysis Translator): A Digital Computer Program," AMRL-TR-65-133 July 1965

3. J. S. Bendat, L. D. Enochson, and A. G. Piersol, "Analytical Study of Vibration Data Reduction Methods," Technical Products Company Report prepared for NASA, MSFC, Sept. 1963.

4. R. B. Blackman and J. W. Tukey, The Measurement of Power Spectra (Dover Publications, Inc. New York) 1958

* * *

AUTOMATIC REAL-TIME VIBRATION SPECTRUM ANALYZER SYSTEM USING DELAY LINE TIME COMPRESSION TECHNIQUES

John L. Fryling
Gulton Industries, Inc.
Trenton, New Jersey

An automatic hybrid analog/digital system designed for on-line processing and analysis of vibration and acoustic data signals is described. The system uses time compression techniques to assist in real-time operation. Data can be analyzed for frequency spectrum on both an amplitude and power basis, cross power spectra, autocorrelation, and crosscorrelation. The system provides analog outputs for oscilloscope display and digital outputs in IBM compatible format.

Time compression is provided by two sets of recirculating delay line circuits. Time compression allows the use of a high i-f, fast sweeping, wide bandwidth, heterodyne spectrum analyzer for spectral analysis. Time delays for auto- and cross-correlation are generated by inserting extra delay in one set of delay lines, allowing one data channel to precess in time with respect to the other.

The vibration and acoustic analysis system provides spectrum analysis and time correlation for signals between 0.01 and 20,000 cps. Signals above 5 kc are heterodyned down to frequencies below 5 kc.

The system has been completed and delivered to NASA, Michoud, Louisiana.

INTRODUCTION

With the advent of the larger rocket test programs related to the Apollo Program, there has been increased incentive to fully automate vibration spectrum analysis. The first approach taken by NASA personnel to implement such automation has been to derive complete programs for performing spectrum analysis and other related statistical functions on the newer, large-scale, general-purpose digital computers. All such programs essentially have involved calculation of the autocorrelation function, and then the frequency transform of the autocorrelation function, to derive the amplitude or power spectrum. Such autocorrelation analysis on a digital computer results in a series of multiplications for each tau increment. In turn, the tau resolution determines the bandwidth resolution. For data frequencies to 3,000 cps, computer time required for spectrum analysis has proven to be somewhat costly.

Consequently, NASA, while using the complete digital programs for some spectral analysis work and other more complex calculations such as cross power spectral analysis, etc., has decided that another approach—at least for quick look—may have merit for reducing the computer load and resulting analysis expense. The technique chosen requires first the use of time compression techniques to increase data frequency, then derives spectral information using rapidly swept analog filtering techniques at high intermediate frequencies. The autocorrelation computation and transform calculations in the digital computer are eliminated.

In this hybrid scheme the data are first digitized, then translated upward in frequency via delay line recirculating loops which actually circulate the digitized data. Data words are contained in one-microsecond time slots. The data are then reconverted from a digital to an analog signal. The analog data are then increased in frequency anywhere from 50 to 50,000 times, depending upon the data frequency range chosen by the operator. Because of this frequency transformation, spectrum analysis can proceed at a very fast rate using a heterodyne swept filter type spectrum analyzer which sweeps the data in one second with a fairly wide analyzer

filter bandwidth.. However, when this analyzer filter bandwidth is translated downward to the original frequency of the data, it can be shown that a very narrow band resolution results, without the attendant difficulties in conventional analog systems such as long filter buildup times, filter instability, requirements for magnetic tape loops, and the like.

After this high-speed analysis, the analog spectral results are digitized with the same analog-to-digital converter used at the input. This digitized spectral information is now processed through a format buffer. Summation is performed in the buffer to provide accurate long-term averages. Further calculations and readout can be performed with the aid of a digital computer. These calculations might include squaring, averaging, true integration, normalizing over time integration period, flags for over-range and under-range data, and general formatting for future readout via high-speed digital printers.

Such a facility has recently been delivered the central NASA computer facility in Michoud, Louisiana. The analyzer system is designed for compatibility with the existing IBM 7094 and GE 225 computer systems and the Stromberg-Carlson Model 4020 high-speed character printer system. The analyzer system operates from reel-to-reel magnetic tape recorded analog data and its digital magnetic tape output is IBM-compatible.

The system is a two-channel analyzer and has capabilities for other analysis functions such as cross power spectrum analysis, autocorrelation analysis (in the time domain), and crosscorrelation analysis (in the time domain). The facility can also be used for straightforward analog-to-digital conversion, and computer formatting for complete digital analysis at other NASA computer facilities. In the auto- and cross-correlation modes of analysis, time delay is introduced by allowing different delay line feedback increments to exist between the two data channels, thereby causing one recirculating data signal to precess with respect to the other. Multiplication and integration is performed using analog techniques. Correlation coefficients derived in this manner are then digitized and placed in the format buffer. The correlation function accuracy is enhanced by summation in the format buffer. The basic system block diagram, including auxiliary subsystems is shown in Fig. 1. A photograph of the system delivered to NASA is shown in Fig. 2. The main units in the system are:

1. A Wideband Analog Magnetic Tape Reproducer (Ampex Model FR1400)

2. Wideband FM Discriminators (Data Control Systems Model GFD-8 Units)

3. An SS/FM Ground Station (MSFC 50M 11300 produced by Ortholog Division of Gulton Industries, Inc.)

4. A Timing Discriminator (Data Control Systems Model GFD-5)

5. A Time Decoder and Tape Search Unit (Astrodata Model 6222)

6. A Vibration Analyzer (Gulton Industries, Inc., Ortholog Division Speedup Analyzer)

7. A Real-Time Visual Display (Tektronix Model 564 Oscilloscope)

8. A Digital Format Buffer and Tape Recorder (Gulton Industries, Inc., C-G Electronics Division Format Buffer with Potter Digital Tape Recorder)

9. Patch Panel Provisions (ADC Coaxial Patch Panels and MAC Pre-programmable Patching)

MODES OF OPERATION

The Vibration and Acoustic Analysis System is designed to operate in the following modes:

1. Amplitude spectrum analysis of one or two separate channels simultaneously with output digital recording.

2. Power spectrum analysis of one or two separate channels simultaneously with output digital recording.

3. Cross power (frequency domain crosscorrelation) of two separate channels with output digital recording.

4. Autocorrelation of one channel of information with output digital recording.

5. Time domain crosscorrelation of two separate channels of information with output digital recording.

6. Simultaneous analog-to-digital conversion of two separate signals (selected at the

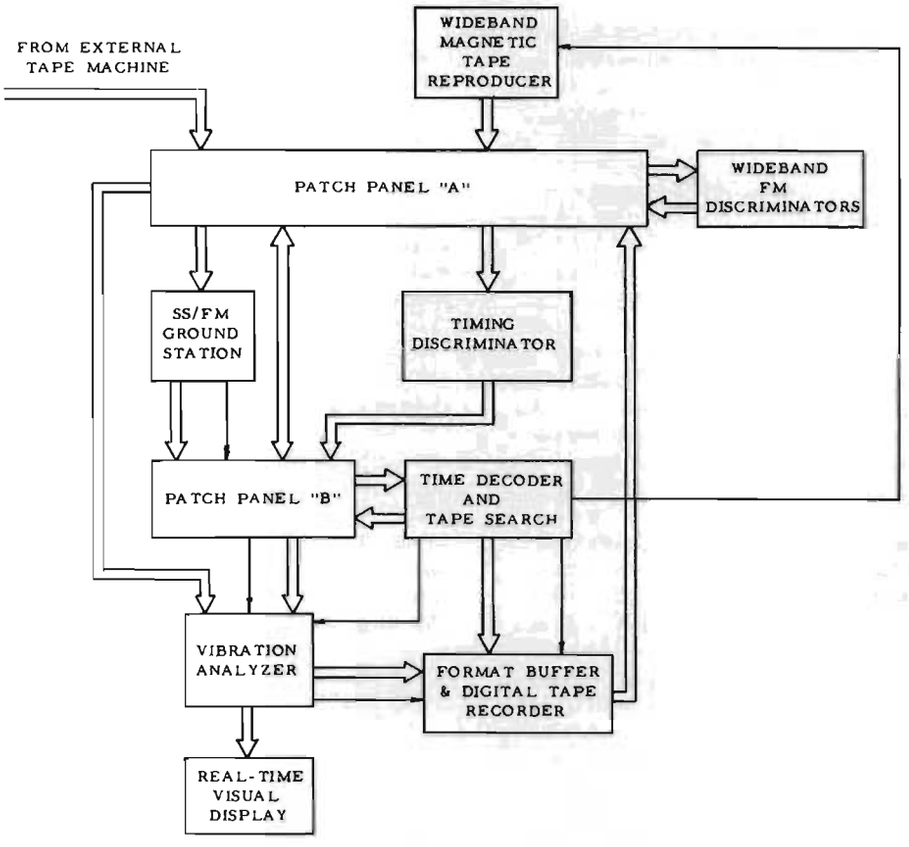

Fig. 1. Basic system block diagram vibration acoustic analysis system NASA, MSFC

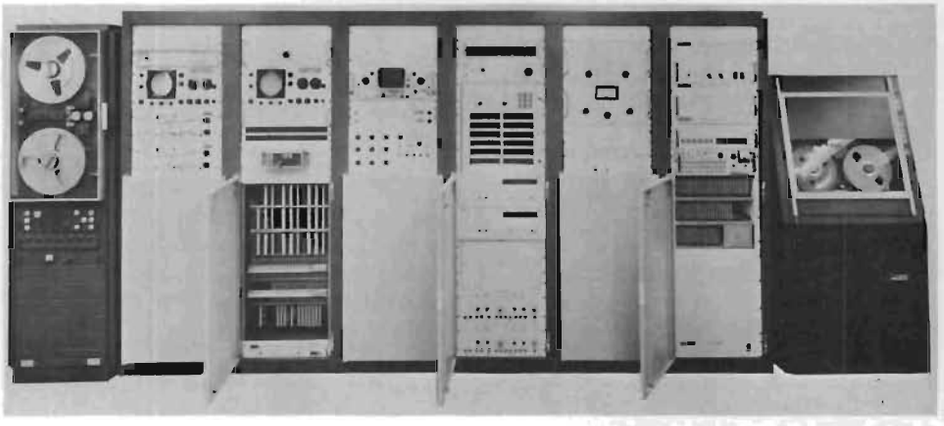

Fig. 2. Automatic real-time vibration spectrum analyzer system

patching facility with subsequent recording in computer format on the output digital tape).

7. Analog-to-digital conversion of a single selected signal with output digital recording.

These modes will be discussed individually in the following paragraphs.

TYPES OF INPUTS TO THE ANALYZER

Possible inputs to the Vibration Analyzer section of the overall system are shown in Fig. 3. While there could be other combinations of inputs, the ones shown in Fig. 3 are those most commonly used.

1. Direct Reproduce Data Signals—Switch positions ② of Fig. 3 show the Vibration Analyzer section driven by two channels of directly reproduced signals from the Ampex FR1400 Reproducer. The maximum frequency which can be analyzed is 20 kc. Low frequency response is limited by the Ampex FR1400 Reproducer to 300 cps at tape speeds of 60 and 120 ips down to 100 cps at 15 ips. Best analysis results are obtained on signals below 5 kc, since signals above this frequency are translated by the analyzer below 5 kc, with accompanying translation errors. This point is further explained in a later section of this paper.

Figure 3 also shows the signal flow of the digital timing signals which are recorded with the data signals. The system, as initially supplied, is capable of operation on AMR B1, B2, D1, and D5 time code formats. Since a universal time code translator (Astrodata Model 6222) is used in the system, other time codes can be used by substituting other translator decoding plugins.

The time code is recorded in FM form. In order to convert this FM signal to a suitable input to the Time Decoder and Tape Search Unit, a Data Control Systems (DCS) Model GFD-5 FM Discriminator is used as the Timing Discriminator. Plugins are provided with the system to demodulate FM timing signals recorded on IRIG Bands 15 (30 kc, ±7-1/2 percent), 17 (52.5 kc, ±7-1/2 percent), and 18 (70 kc, ±7-1/2 percent). If the time code is "directly recorded" on the analog tape, then the Timing Discriminator is not required, and the time code tape track can be patched directly to the input of the Astrodata Model 6222 Time Decoder and Tape Search Unit.

2. Wideband FM Data Signals—Switch positions ③ of Fig. 3 show the Vibration Analyzer inputs from the two Wideband FM Discriminators provided in the system. The Wideband FM Discriminators are Data Control Systems Model GFD-8 FM Discriminators. Plugins provided have center frequencies of 900, 600, 450, 300, and 225 kc. By use of FM, the inputs to the Vibration Analyzer can go to dc, thereby using the full lower frequency range of the Vibration Analyzer down to 0.01 cps.

3. SS/FM Data Signals—Switch positions ① of Fig. 3 show the Vibration Analyzer section driven from two selected outputs of the SS/FM Ground Station. These output are selected at the patching facility. As shown, the SS/FM Ground Station is fed by the output of a Wideband FM Discriminator. However, if the SS/FM signal was recorded directly on the analog tape, the selected tape track would be patched directly into the SS/FM Ground Station at the system patching facility.

PRE-FILTERING, BANDSHIFTING, AND ANALOG-TO-DIGITAL CONVERSION

Before time compression and analysis, data must, in some cases, be frequency translated and then pre-filtered to digital form (see Figs. 4, 5, 6, and 7). Input data are first passed through the Ortholog Frequency Translators or the Rixon Bandshift Modulators and then through the Ortholog Pre-Filters.

The Frequency Translator handles input signals in the following frequency bands: zero to 5 kc, 5 to 8.75 kc, 8.75 to 12.5 kc, 12.5 to 16.25 kc, and 16.25 to 20 kc. The respective output frequencies are zero to 5 kc on the zero to 5 kc range, and 1.25 to 5 kc on all other input ranges. Since the Vibration Analyzer has an upper analysis frequency limit of 5 kc, this frequency translation enables higher frequency signals than 5 kc to be analyzed, even though the basic analog-to-digital conversion rate is limited to 20 kc.

The Rixon Bandshift Modulator accepts input signals up to 5 kc and provides as an output a bandshifted 140 cycle segment of the input. Its output signal range is between 10 and 150 cps, regardless of the frequency range of the 140 cycle segment of the input data selected. Use of the Rixon Bandshift Modulators permits the Vibration Analyzer to analyze with a resolution of 0.5 cycles throughout the range of 0.5 cps to 5 kc.

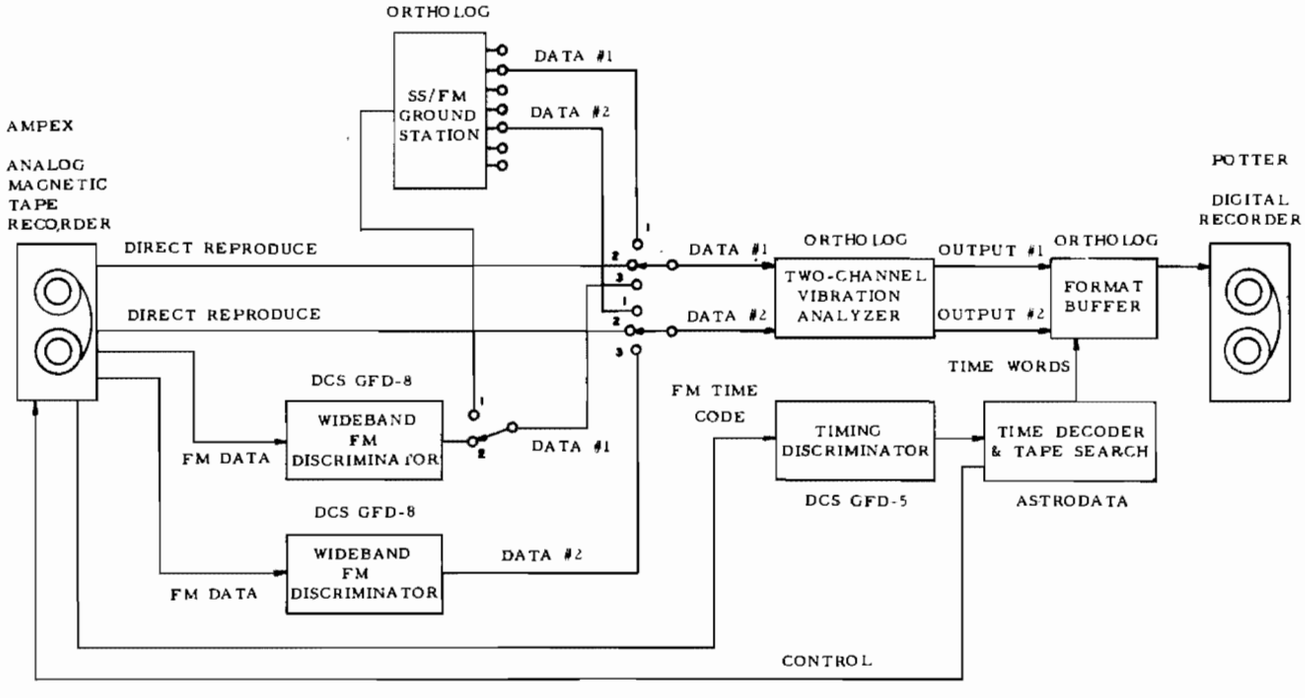

OUTPUT #1 CAN BE

(1) ANALOG-TO-DIGITAL CONVERSION OF DATA #1
(2) AMPLITUDE SPECTRUM ANALYSIS OF DATA #1
(3) POWER SPECTRUM ANALYSIS OF DATA #1
(4) REAL COMPONENT OF CROSS POWER SPECTRUM ANALYSIS OF DATA #1 AND DATA #2
(5) TIME CORRELATION ANALYSIS OF DATA #1 AND DATA #2
(6) AUTO CORRELATION ANALYSIS OF DATA #1

OUTPUT #2 CAN BE

(1) ANALOG-TO-DIGITAL CONVERSION OF DATA #2
(2) AMPLITUDE SPECTRUM ANALYSIS OF DATA #2
(3) POWER SPECTRUM ANALYSIS OF DATA #2
(4) IMAGINARY COMPONENT OF CROSS POWER SPECTRUM ANALYSIS OF DATA #1 AND DATA #2
(5) TIME DELAY VALUE FOR TIME CORRELATION ANALYSIS OF DATA #1 AND DATA #2
(6) TIME DELAY VALUE FOR AUTO CORRELATION ANALYSIS OF DATA #1

Fig. 3. Analyzer system input data signals

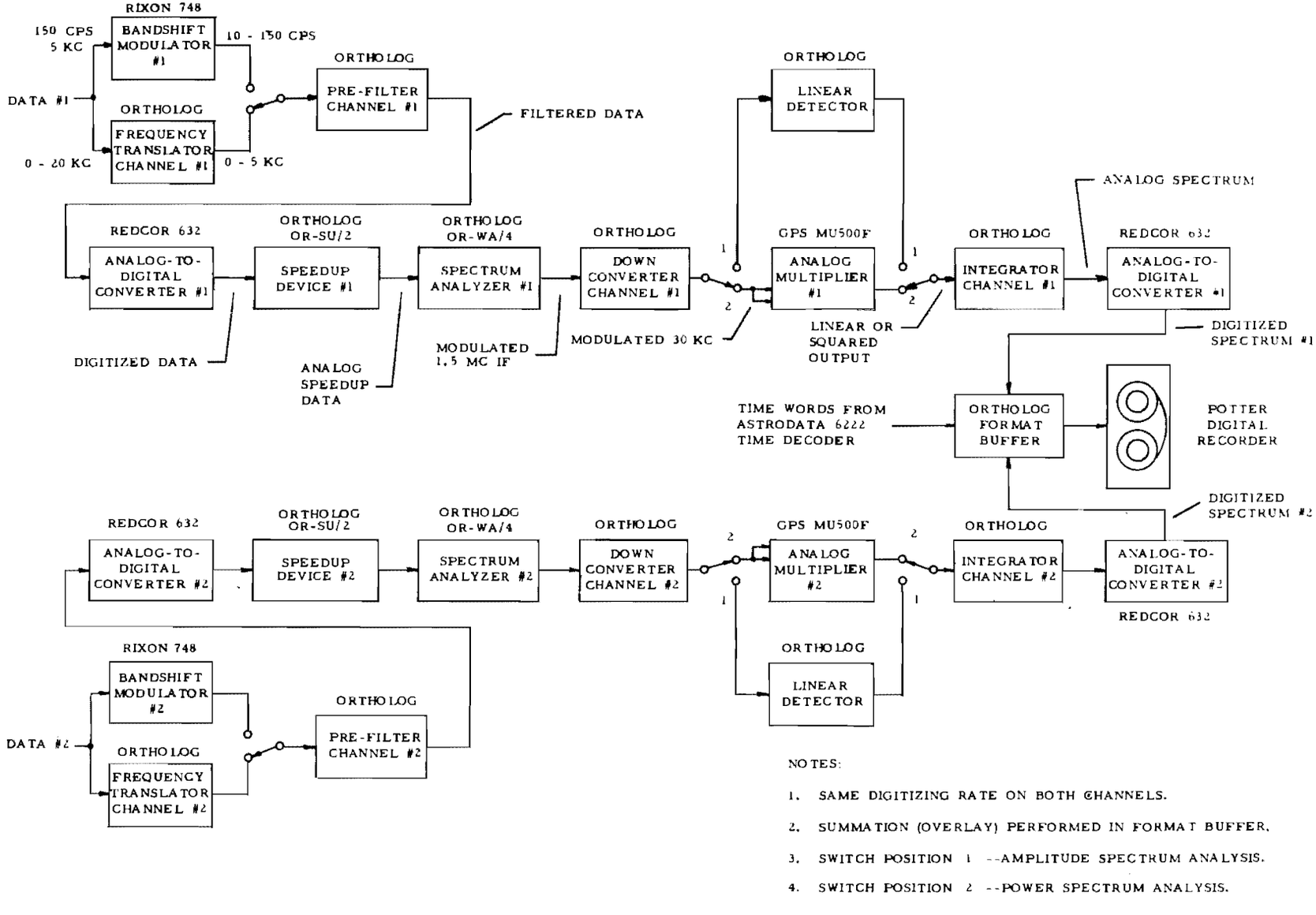

Fig. 4. Signal flow--vibration analyzer amplitude or power spectrum analysis of two data signals

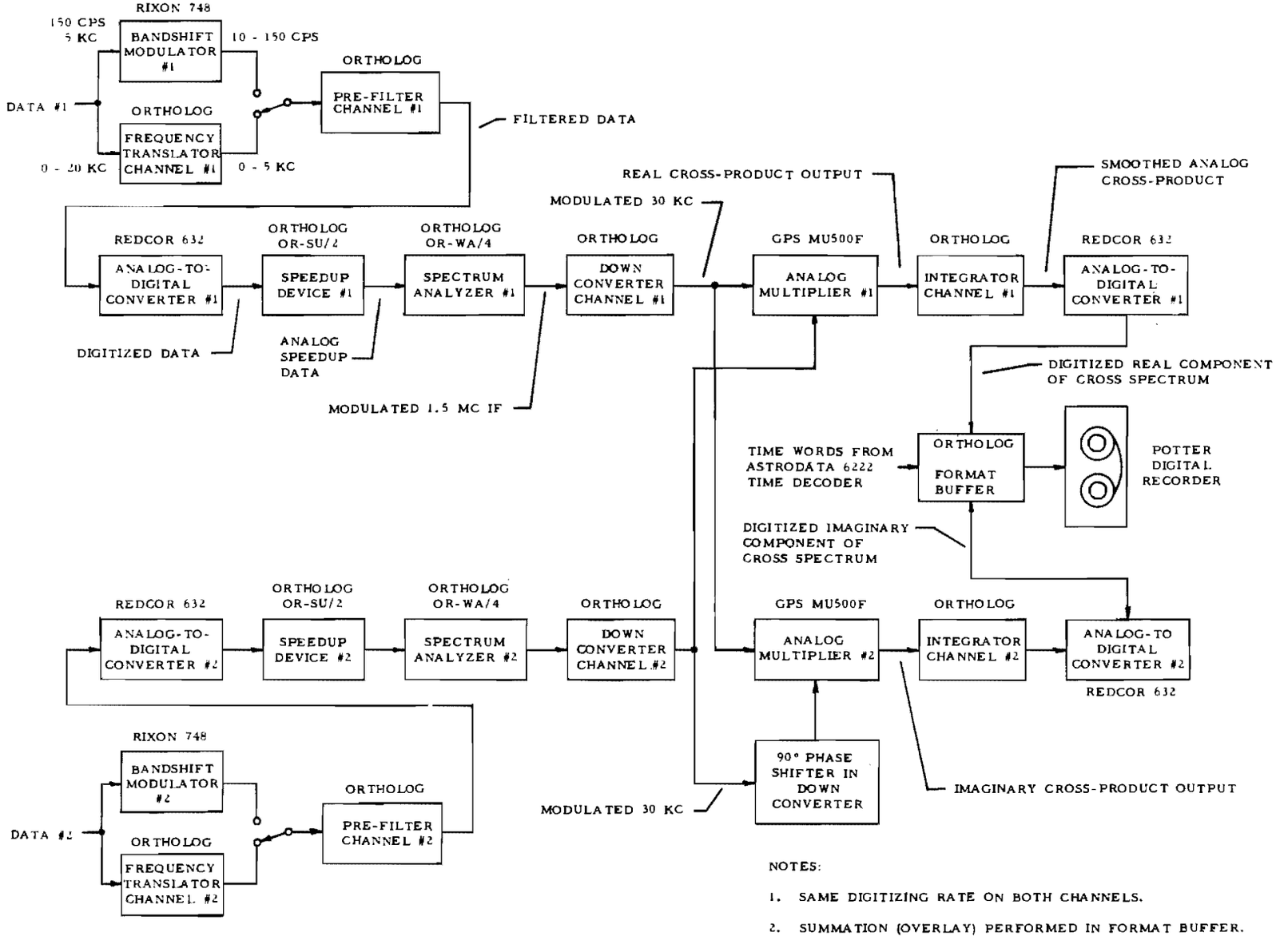

Fig. 5. Signal flow--vibration analyzer cross spectrum analysis of two data signals

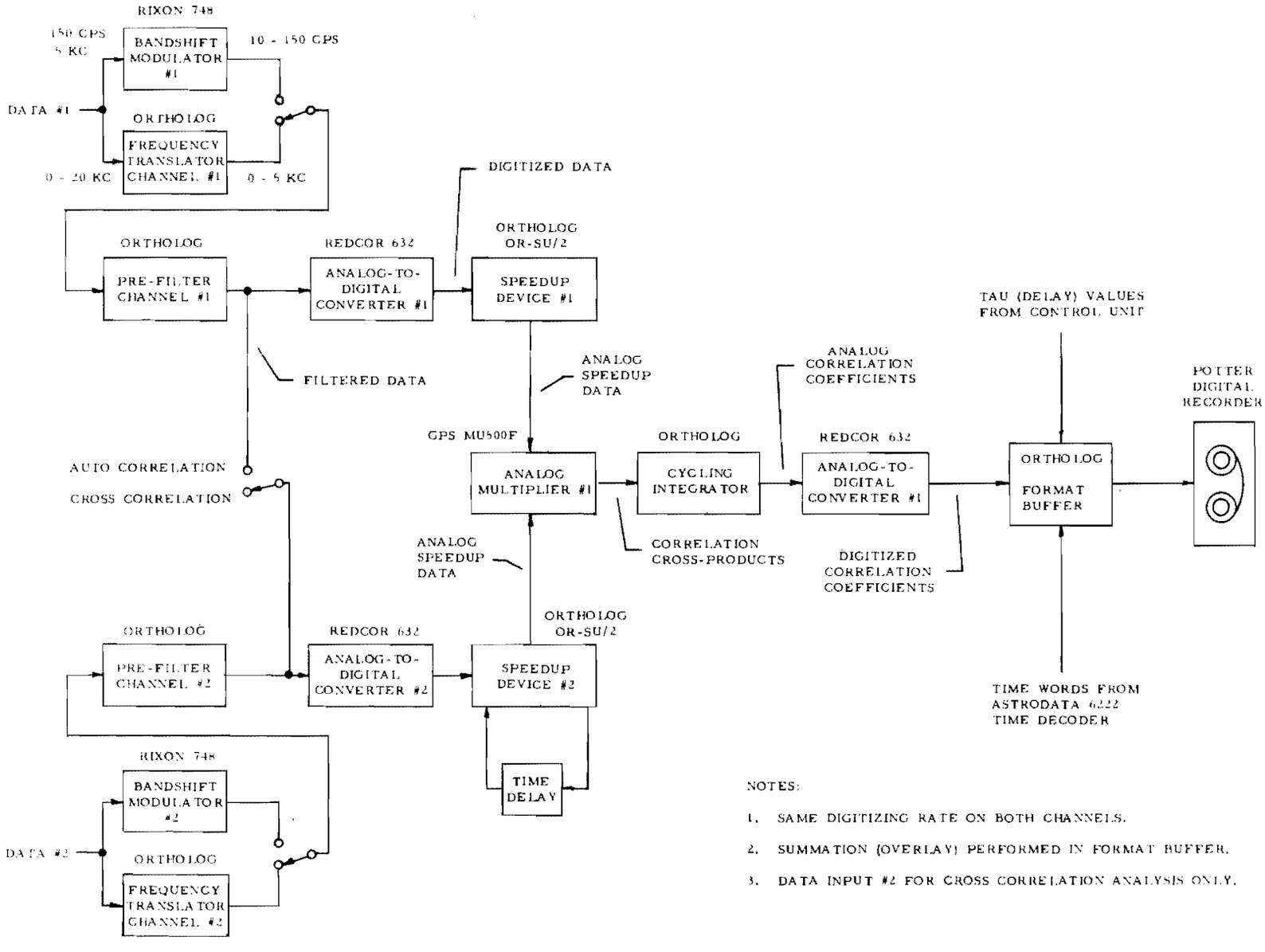

Fig. 6. Signal flow--vibration analyzer auto- and cross-correlation analysis of two data signals

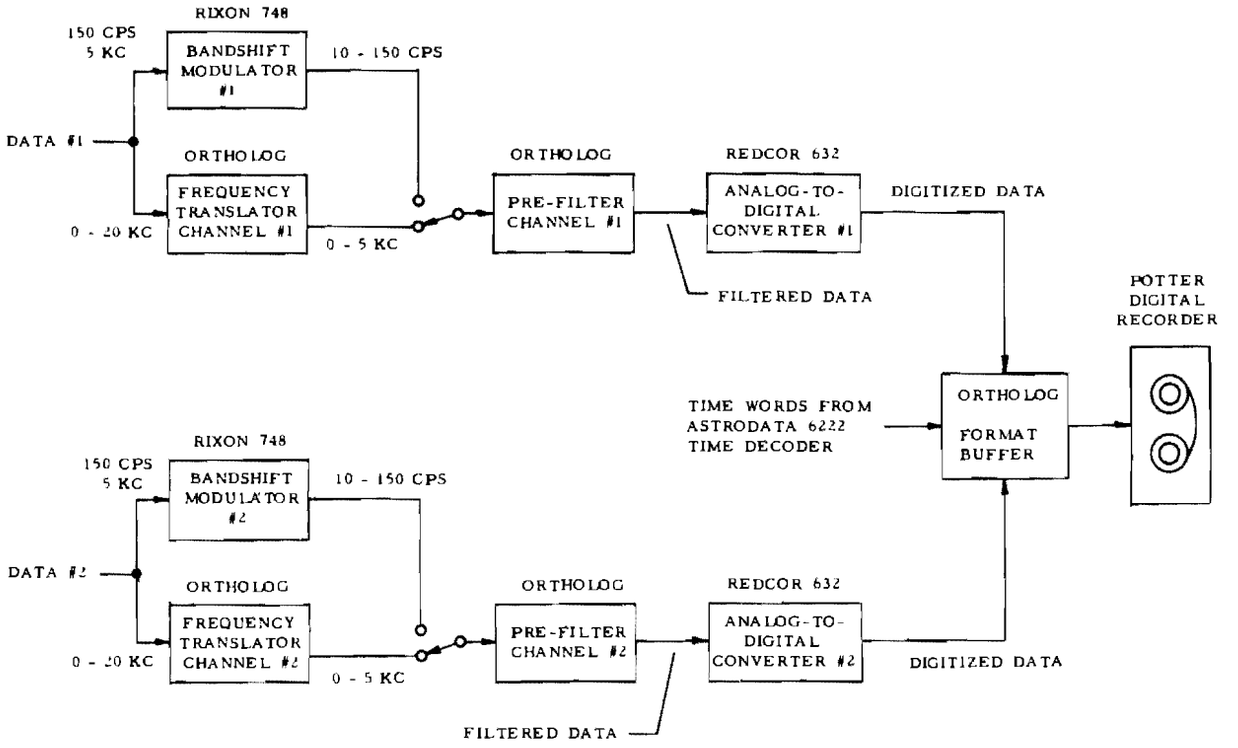

Fig. 7. Signal flow—vibration analyzer analog-to-digital conversion of two data signals

The analog-to-digital conversion rate is selected to be at least four times the highest frequency of interest in the data to be digitized. Hence, when processing data with a high frequency of interest of 5 kc, the 20 kc sample rate is used. If frequencies above 5 kc were present in the signal being digitized, "aliasing" errors would result. To prevent these "aliasing" errors, an Ortholog Pre-Filter precedes the Analog-to-Digital Converter. The Pre-Filter attenuates frequencies above the highest frequency of interest in a given analyzer frequency range. The Pre-Filter ranges are remotely controlled by the Control Unit switch. These ranges are 10 to 5,000; 2 to 1,000; 0.5 to 250; 0.125 to 62.5 and 0.01 to 5 cps.

Conversion from analog to digital form takes place in the Redcor Model 632 Analog-to-Digital Converters. The digital output is an absolute value code of 10 binary bits and a sign bit. The number of analog-to-digital conversions per second is normally established by the settings of the DATA FREQUENCY switches on the Control Unit. These sample rates are 20 kc, 4 kc, 1 kc, 250 cps, and 20 cps, corresponding to upper analysis band frequencies of 5 kc, 1 kc, 250 cps, 62.5 cps and 5 cps, respectively.

It will be noted on Fig. 7 that external signals can be digitized by patching these signals into the Analog-to-Digital Converters. The user must then provide anti-aliasing filtering of his own ahead of the patching.

When two data channels are digitized at the same time, the data appears interspersed on the same digital tape record. The first characters of each record are time words followed by a data word, with subsequent data word order depending on the sample rate ratios of channels No. 1 and No. 2. The maximum sampling rate for one data channel, using the internal sample rate clock in the Vibration Analyzer, is 20 kc. Hence, only one 5 kc data channel can be digitized at a time.

The digitized data words are stored with the time words in the Format Buffer until the Buffer is sufficiently full to create a tape record. Record length is 4092 IBM tape characters corresponding to 682 computer words of 36 bits each.

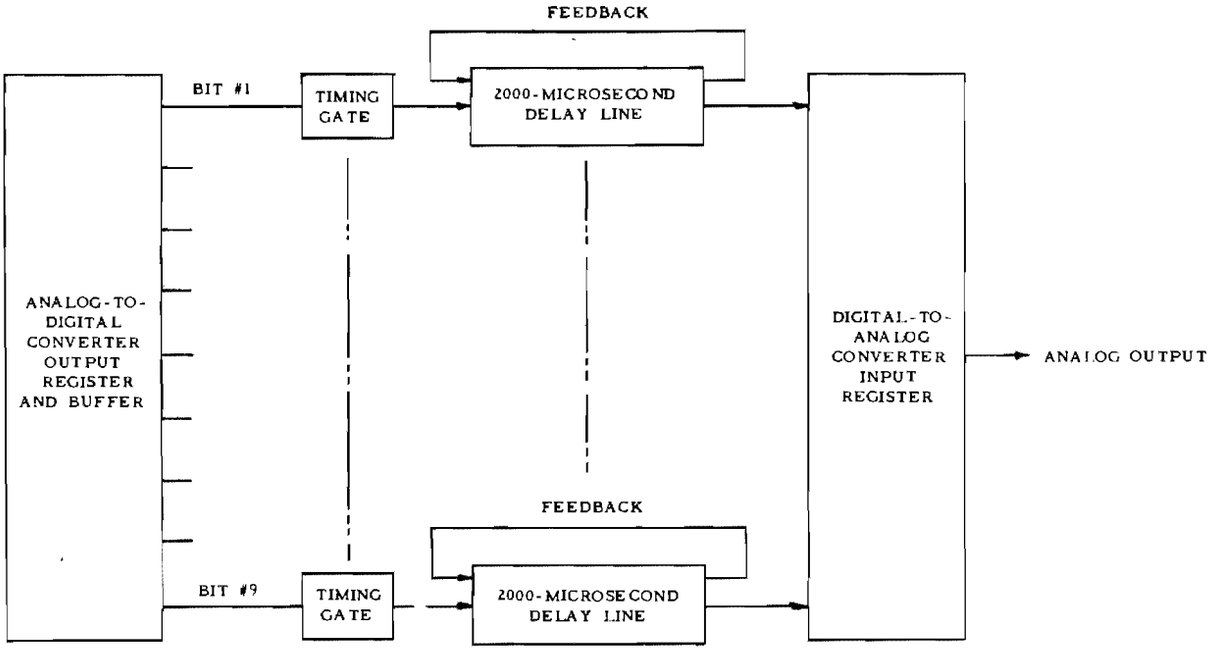

Fig. 8. Basic delay line time compression technique

DESCRIPTION OF HOW DELAY LINES CAN BE USED FOR TIME COMPRESSION

Figure 8 illustrates how a typical 2000-μs delay line as used in the Ortholog system provides time compression of analog data. Digitized samples are inserted in the delay line at rates of 20; 250; 1,000; 4,000; or 20,000 samples per sec. Regardless of the sampling rate, however, it only takes each sample two ms to emerge at the other end of the delay line. Connecting the delay line back upon itself will then result in a sample circulating around the delay line each two ms.

Since the data are in digital form, we assign one-microsecond positions to each pulse. This means, of course, that each pulse has a duration significantly less than one microsecond. Thus, as many as 2000 bits (2000 samples in nine parallel delay lines) can be stored by one channel of the time compression system. Actual circulation of the data, of course, cannot proceed until all time positions in the delay lines have been filled. This fill-up time will vary depending upon the basic analog-to-digital conversion rate of the analyzer system. It is, of course, a simple matter to insert a slight time delay in the feedback loop of some of the delay lines to generate the tau increments for auto- and cross-correlation function analysis.

AMPLITUDE SPECTRUM ANALYSIS MODE

The signal flow for amplitude spectrum analysis of two data channels is shown in Fig. 6. Both data signals to be analyzed are converted at the same sample rate. The mode and rate are selected at the Control Unit.

In the LIN/LOG spectrum analysis mode, 2000 input data signal samples are "time compressed" in the Ortholog Model OR-SU/2 Delay Line Speedup Device to a two ms record length. Two thousand samples recirculated in two ms and reconverted to analog form result in a time compressed data signal with a 250 kc upper frequency limit. The Model OR-WA/4 scans the 250 kc range in one second at a rate of 500 cps per two ms (time for one complete 2000 sample circulation). The analyzer provides analog linear or log detector spectrum outputs (through the Down Converter and Integrator) to be digitized for entry on the digital output tape. The use of 500 cycle bandwidth in the spectrum analyzer provides resolutions ranging from 10 to 0.01 cycles, depending upon the data frequency range being analyzed and, in turn, the particular speedup ratio used.

When it is desired to provide more statistically accurate analysis, successive spectrum analyzer runs can be summed before recording

on the digital output tape. From 1 to 1000 summations are selected in a Control Unit preset counter. The summation is accomplished through use of an adder in the Format Buffer. Two channels of data (500 frequency segments per channel) can be stored and summed in the Format Buffer. Normalization of the summations can be accomplished subsequently in a digital computer.

It is presumed that in many instances in the amplitude spectrum mode and others, control will be handled automatically by the operation of the Astrodata Model 6222 Tape Search. Manual selection of analysis times from the Control Unit is also possible. It would appear, however, that manual selection would be used primarily during setup and initial investigation of certain portions of the analog tape.

When the number of summations selected by the operator is reached, a digital output tape is written. The record length, as in all modes, is 4092 IBM tape characters. The time word at the initial analysis time is written at the beginning of the record, followed by 500 channel No. 1 spectrum analysis summations and 500 channel No. 2 spectrum analysis summations.

POWER SPECTRUM ANALYSIS MODE

The Vibration Analyzer can be used to perform power spectral density analysis of two separate data signals at the same time. Signal flow for this mode of operation is also shown in Fig. 4. The "Square Law" (Power) spectrum analysis mode and rate are selected at the Control Unit.

As in the case of amplitude spectrum analysis, for power spectrum analysis, sampled input data signals are "time compressed" in the Ortholog Model OR-SU/2 Speedup Device to a 2 ms record length which is spectrum analyzed by the Model OR-WA/4 Spectrum Analyzer over 500 frequency intervals, each 500 cycles wide. Each complete analysis takes one second.

The Model OR-WA/4 Spectrum Analyzer is a swept, high frequency heterodyne analyzer which has an i-f centered at 1.5 mc, 500 cycles wide. The modulated i-f data signals are heterodyned down to the 30 kc range and squared in the GPS Model MU500F Analog four Quadrant Multipliers. The squared output of the Analog Multipliers is smoothed in the Ortholog Recycling Integrator to provide a detected output which is digitized and fed into the Format Buffer.

When it is desired to provide more accurate analyses, successive power spectral analysis runs can be summed in the Format Buffer before placement on the digital output tape similar to the amplitude spectrum mode. Again, when the number of summations selected by the operator is reached, a digital output tape is written.

CROSS SPECTRUM ANALYSIS MODE

In the Cross Spectrum Analysis Mode, the Vibration Analyzer is used to compute the "real" and "imaginary" components of the cross spectrum between two input data channels. (Refer to Fig. 5 for signal flow through the Vibration Analyzer.) The spectra of the two data channels are obtained basically as in the amplitude and power spectrum modes above.

To obtain the real component, the spectral outputs of the Down Converters for channels No. 1 and No. 2 are multiplied in a GPS Analog Multiplier. The Multiplier output is integrated, digitized, and entered in the Format Buffer.

The imaginary component of the cross spectrum is obtained by multiplying the output of Down Converter No. 1 with a phase-shifted (90° phase shift) output of Down Converter No. 2. Again, as in obtaining the real component, the Multiplier output is integrated, digitized, and entered in the Format Buffer.

Summation of cross spectrum results can be accomplished in the Format Buffer before placement on the digital output tape. Summations between 1 and 1000 can be selected. The two components of data, real and imaginary, (500 frequency segments per component) can be stored and summed in the Format Buffer. (Normalization of the summations is subsequently accomplished in the digital computer.) Again, when the number of summations selected by the operator is reached, a digital output tape is written. The time word at the initial analysis time is written at the beginning of the record, followed by 500 real and 500 imaginary component cross spectrum summations.

AUTOCORRELATION ANALYSIS MODE

The Vibration Analyzer can be used to compute autocorrelation functions of input data signals. The signal flow for processing autocorrelation functions is shown on Fig. 6. The

auto correlation function of a continuous stationary random process, $x(t)$, is expressed as

$$R(x)(\tau) = \lim_{T\to\infty} \frac{1}{2T} \int_{-T}^{+T} x(t+\tau)\ x(t)\, dt ,$$

where T is the integration time and τ is the time delay introduced in the correlation.

In the speedup process used in the Vibration Analyzer, T in the formula above becomes two ms, which is the length of time required for circulation of the 2000 data samples stored in the Model OR-SU/2 Speedup Devices. The increments of time delay (τ) are selected at the Control Unit. Maximum time delay is one ms or it can be expressed as 1/2 T. Integration is from zero to T. (Referencing actual time delays back to the input data itself before speedup, typically, the 5 cycle data range provides a time delay of 50 seconds over a time period (T) of 100 seconds, which is the time required to fill the Model OR-SU/2 Speedup Devices with 2000 data words.)

It will be noted from Fig. 6 that the time delay (τ) is introduced in Model OR-SU/2 Speedup Device No. 2 while the data are in digital form. Multiplication is performed by analog means in the GPS Model MU500F Analog Multiplier. The final step of integration takes place in the cycling integrator in the Ortholog Integrator unit. Here, two integrators are employed alternately during the two-millisecond integration intervals. The correlation coefficients from the cycling integrator are digitized and placed in the Format Buffer along with their corresponding time delay (τ) values.

In order to compute autocorrelations for input records of as much as one second without loss of data on the 5 kc data frequency range, the Vibration Analyzer digitizes input data to four binary bits. Since only 0.1 sec is required to fill the Model OR-SU/2 Speedup Devices on this data range, computation of correlation coefficients for the 0.1 sec input record cannot exceed 0.1 sec without loss of data. This 0.1 sec restriction sets a limit of 50 on the number of correlation coefficients which can be computed for a given 0.1 sec input record. Typically, 50 coefficients with delay increments of 20 μsec can be computed in 0.1 sec. (Delay increments of 2, 4, 6, 8, 10, and 20 μsec can be selected at the Control Unit.)

Correlation digital readout is possible in two different ways depending on whether or not summation records are desired. The selection is made at the Control Unit. In one case (not summed), groups of coefficients and corresponding tau values are recorded on digital tape, one group after another. For example, assume that a maximum of 50 coefficients are selected at the Control Unit preset coefficient counter. The first correlation coefficient and its delay value are stored in successive locations in the Format Buffer, the second coefficient and its delay value in the next two Buffer memory locations, etc. After the 50th coefficient and its tau (τ) value have been entered into the Buffer, a time word is read into the Buffer, 50 more coefficients and tau values alternately, etc. When the Buffer is full, a digital tape record is written. Computation continues, creating as many digital tape records as required for the analog data record being processed.

In the second mode, summation of the correlation coefficients is accomplished in the Format Buffer. The number of summations is selected at the Control Unit preset summation counter. As many as 1280 summations can be handled. In this operation, as many as 500 correlation coefficients can be summed and stored in the "1st half" of the Format Buffer with corresponding delay values (as many as 500) stored in the higher numbered memory locations. When the desired number of summations is reached, an output digital tape record is written. This tape record has a time word at its beginning followed by successive correlation coefficients and tau values. If less than 500 coefficients are selected, zeros are supplied for those memory locations not used. Record length is 4092 IBM tape characters as in all other modes.

CROSSCORRELATION ANALYSIS MODE

Crosscorrelation of two input signals can also be accomplished as shown in Fig. 6. The crosscorrelation function of two continuous stationary random processes, $x(t)$ and $y(t)$, is expressed as follows:

$$R_{xy}(\tau) = \lim_{T\to\infty} \frac{1}{2T} \int_{-T}^{+T} x(t+\tau)\ y(t)\, dt ,$$

where T is the integration time and τ is the time delay introduced in the correlator.

Signal processing through the Vibration Analyzer is essentially the same as for the autocorrelation mode, except that two input signals are used instead of one. Again, T is two ms in the Model OR-SU/2. Tau increments, maximum time delay, and integration from zero to T are the same as in the autocorrelation mode.

Also, digital readout is the same as for the auto-correlation analysis mode.

POSSIBLE IMPROVEMENTS TO EXISTING SYSTEM

If the analyzer is operating on-line in the spectrum analysis modes of operation, it skips an increasingly large percentage of the data for the higher frequency bands. The following table illustrates the fillup times and the percentage of data skipped for each of the basic frequency bands:

TABLE 1
Fillup Times and Percent of Data Not Sampled

Analysis Band (cps)	Fillup Time (sec.)	Percent of Data Not Sampled	
		(No Updating)	(Updating)
10 - 5000	0.1	91	90
2 - 1000	0.5	67	50
0.5 - 250	2.0	33	0
0.125 - 62.5	8.0	11	0
0.01 - 5	100	1	0

Data skipping on the lower frequency bands, which is of only minor significance, can be completely eliminated by continuous updating through logic circuit timing. For such updating, another column illustrates the percentage of data still being skipped. It should be noted, however, that even updating does not significantly lessen the problem at the higher frequency ranges.

The method of eliminating all data skipping is to employ an intermediate tape storage between the analog-to-digital converter and the input to the delay line time compression system. Such an improvement, of course, would not allow use of the analyzer for complete on-line spectrum analysis. Rather, all data would first be digitized, the digital tape then rewound, and finally 2000-word sample groups read into the analyzer. For the highest frequency range to 5 kc, data would be reduced in approximately 11 times real time and at successively lower ratios for the lower frequency bands. Ortholog Division is currently designing and building a system using such an intermediate tape storage technique for NASA, Kennedy Space Center, Florida.

POTENTIAL IMPROVEMENTS ON FUTURE ANALYZERS OF THIS TYPE

Design of the system described herein was started in June 1964. Since that time, a number of small digital computer main frames with very fast memory cycle times have been introduced. Such computer main frames can be used to accomplish the same time compression techniques provided by a delay line system. Moreover, the digital computer can be used for overall timing, system control, and for other calculations, such as: summation of spectral or correlation coefficients, and normalization of these coefficients.

To provide time compression, such computer main frames read out successive data samples to specially designed external registers and then return the data from these registers to the computer memory. The "Data Break Input/Output" modes of operation for several very inexpensive computer main frames provide this capability. As a result, it is anticipated that future systems of this type will employ digital computer main frames for time compression and control at costs competitive with delay line methods.

Finally, many other speedup ratios, analog-to-digital conversion rates and effective filter bandwidths would be provided in future systems, depending upon flexibility requirements.

ACKNOWLEDGMENTS

Thanks are expressed to Mr. Robert Lavin, Ortholog Chief Systems Engineer, and Mr. Jim Foster, Ortholog System Engineer, for assistance in the preparation of this paper.

* * *

THE ANALOG CROSS SPECTRAL DENSITY ANALYZER SYSTEM*†

R. L. Randall
Atomics International
Canoga Park, California

An analog data analyzer system designed for measuring input-output characteristics of systems under dynamic test is described. This system is designed to handle essentially all types of analog test data recorded on either magnetic tape or strip charts, including random, periodic, or transient signals. Typical measurements that may be performed include: (a) spectral amplitude, (b) power spectral density, (c) transmissibility, (d) cross spectral density (coincident, quadrature, and magnitude), and (e) gain, phase, and coherence (the degree of linear correlation between any two signals at each frequency). Variations in the system permit the detection and analysis of both stationary and nonstationary excitation and response data, and the study of systems with both linear and nonlinear response characteristics. Outputs from the analyzer are recorded as functions of time or frequency in either analog or digital form.

SUMMARY

Problems in handling test data from experimental work in the fields of Reactor Kinetics and Control, Heat Transfer, and Hydraulics and Structural Dynamics have led to the development of a unique spectrum analyzer system capable of computing a wide variety of mathematical and statistical relationships between excitation and response signals from a system or process under dynamic test.

The analyzer system now in operation in the Data Acquisition and Reduction Center at Atomics International is designed to handle essentially all types of dynamic test data, recorded in analog form, including: (a) random, periodic, or transient signals, (b) signals with noise contamination, and (c) signals that represent certain types of nonstationary excitation or response functions, or certain types of nonlinear response functions. Figure 1 is a photograph of most of the equipment included in the analyzer system.

Analyses may be performed on random, periodic, or transient test data over any 3-decade frequency range from below 0.0003 cps to above 100,000 cps. For example, transient test data from a fraction of a millisecond in duration up to several hours in duration may be analyzed. The analyzer system can store and process up to 150,000 cycles of analog information at the highest frequency to be studied. The data are stored on a 14-channel tape loop reproducer. Gating circuitry permits the selection of all or any portion of the data for detailed analysis. Swept periodic or swept random test data may usually be processed directly from a reel-type tape reproducer, thus bypassing the limitations on data sample length imposed by the capacity of a tape loop reproducer.

Typical measurements that may be performed include: (a) spectral amplitude, (b) power spectral density, (c) transmissibility, (d) cross spectral density (coincident, quadrature or magnitude), and (e) gain, phase, and coherence (the degree of linear correlation between any two signals at each frequency). Variations in the system permit the detection and analysis of both stationary and nonstationary excitation or response data, and the study of systems with both linear and nonlinear response characteristics.

Outputs from the analyzer system are presented as functions of time or frequency, and displayed either on analog strip charts or x-y recorders, or recorded on punched paper tape

*Work done under AEC Contract AT(11-1)-GEN-8.
†This paper was not presented at the Symposium.

Fig. 1. The analog cross spectral density analyzer system

for additional manipulation, computation of confidence bands, etc., with a digital computer.

FREQUENCY RESPONSE

Let us consider the problem of measuring the dynamic response characteristics of a system or process exposed to some form of excitation. The system under consideration may be represented schematically as

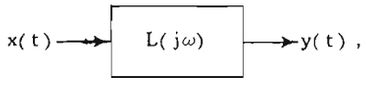

where $x(t)$ is the system driving force and $y(t)$ is the system response. Since any arbitrary driving function can be represented as a sum of sinusoids, the complete dynamic characteristics of a time invariant linear system can be obtained for any excitation function, when one knows the response of a system to an arbitrary sinusoidal driving function of frequency, ω, amplitude, A, and phase ϕ.

For a time invariant linear system, the response to a sinusoid is another sinusoid with the same frequency, ω, but with amplitude multiplied by a gain factor and phase-shifted by a phase factor. For descriptive convenience, these gain and phase factors are represented by $L(j\omega)$, a single complex-valued function of frequency called the transfer function. The basic problem is thus reduced to comparing the frequency components of the input and response functions. This comparison is performed automatically in the cross spectral density analyzer, and is described in the following section.

ANALOG COMPUTATIONS

Time Invariant Linear System

Let us first consider the problem of measuring the dynamic response characteristics of a time invariant linear system excited with a driving force $x(t)$ and with a response $y(t)$. The complex components of $x(t)$ and $y(t)$ in the frequency band $\Delta\omega$, centered about the frequency, ω, are extracted by use of in-phase and quadrature filters with a bandwidth, $\Delta\omega$.

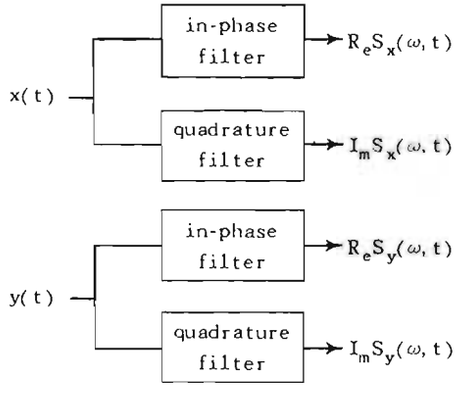

Next, all possible cross products are computed and combined to form $R_eS_{xy}(\omega, t)$ and $I_mS_{xy}(\omega, t)$, where

$$R_eS_{xy}(\omega, t) = R_eS_x(\omega, t)\, R_eS_y(\omega, t) - I_mS_x(\omega, t)\, I_mS_y(\omega, t) ,$$

and

$$I_m S_{xy}(\omega, t) \cong I_m S_x(\omega, t)\ R_e S_y(\omega, t) + R_e S_x(\omega, t)\ I_m S_y(\omega, t) .$$

Next, the average values of these two cross products are computed to form the in-phase and quadrature components of the cross spectral density function, relating $x(t)$ and $y(t)$ at the frequency, ω. Where the true average requires integration over an infinite length of time, in practice one is limited to estimating the average by integrating only over the length of the data sample, T. Thus,

$$R_e S_{xy}(\omega) \cong \frac{1}{T}\int_0^T R_e S_{xy}(\omega, t)\, dt ,$$

and

$$I_m S_{xy}(\omega) \cong \frac{1}{T}\int_0^T I_m S_{xy}(\omega, t)\, dt .$$

The statistical accuracy of this estimate will be defined in a later section.

While computing the cross spectral density function, the analyzer also computes the power spectra of the input and response functions. The filtered components of $x(t)$ and $y(t)$ are simply squared, added, and averaged to compute $S_{xx}(\omega)$ and $S_{yy}(\omega)$, respectively. Thus,

$$S_{xx}(\omega) \cong \frac{1}{T}\int_0^T \left[R_e S_x(\omega, t)^2 + I_m S_x(\omega, t)^2\right] dt ,$$

and

$$S_{yy}(\omega) \cong \frac{1}{T}\int_0^T \left[R_e S_y(\omega, t)^2 + I_m S_y(\omega, t)^2\right] dt .$$

The transfer function relating $x(t)$ and $y(t)$ at frequency ω is then computed by dividing the cross spectral density by the power spectral density of the excitation signal:

$$L(j\omega) = \frac{S_{xy}(j\omega)}{S_{xx}(\omega)} = \frac{R_e S_{xy}(\omega)}{S_{xx}(\omega)} + j\,\frac{I_m S_{xy}(\omega)}{S_{xx}(\omega)} .$$

Next, the real and imaginary components of the transfer function are converted to gain and phase functions, $L(\omega)$ and $\phi(\omega)$, respectively, where

$$L(\omega) = \frac{\left(\left[R_e S_{xy}(\omega)\right]^2 \left[I_m S_{xy}(\omega)\right]^2\right)^{1/2}}{S_{xx}(\omega)}$$

and

$$\phi(\omega) = \tan^{-1}\frac{I_m S_{xy}(\omega)}{R_e S_{xy}(\omega)} .$$

Measurements of the power spectral density, cross spectral density, and gain and phase functions are performed over the desired frequency range by varying the center frequency of the band pass filters and repeating the above computations.

It should be noted at this point that the methods employed to compute the transfer function apply to all types of system driving functions, random, periodic, or transient.

System With Noise Contamination

Noise contamination of dynamic response signals is a common problem which occurs both in the field and in the laboratory. The following summarizes the mathematical concepts involved in the determination of transfer functions from noise-contaminated response signals.

Let $L(j\omega)$ represent the transfer function of a system relating two observed variables, $x(t)$ and $y(t)$.

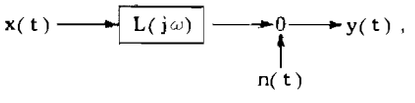

where $y(t)$, the observed response signal, is being affected by $n(t)$, an extraneous disturbance (e.g., instrumentation noise or the response of the system to some unknown driving function).

If $x(t)$ and $n(t)$ are statistically uncorrelated with each other, the transfer function may be determined from the power spectral density of $x(t)$, $S_{xx}(\omega)$, and the cross spectral density relating $x(t)$ and $y(t)$, $S_{xy}(j\omega)$, as if the disturbance $n(t)$ did not exist. Thus, the transfer function is described by

$$L(j\omega) = \frac{S_{xy}(j\omega)}{S_{xx}(\omega)} .$$

The power spectrum of $y(t)$, $S_{yy}(\omega)$, is given by

$$S_{yy}(\omega) = S_{xx}(\omega)\,|L(j\omega)|^2 + S_{nn}(\omega) .$$

If $S_{nn}(\omega)$ is very small compared to $S_{yy}(\omega)$, the magnitude of the transfer function may be determined from the transmissibility ratio $S_{yy}(\omega)/S_{xx}(\omega)$. Thus,

$$|L(j\omega)| \cong \left[\frac{S_{yy}(\omega)}{S_{xx}(\omega)}\right]^{1/2},$$

if

$$S_{nn}(\omega) << S_{xx}(\omega)\ |L(j\omega)|^2 .$$

This transmissibility measurement cannot provide phase response measurements, and if $S_{nn}(\omega)$ is not small compared to $S_{yy}(\omega)$, the transmissibility measurement will not give the true gain response. Thus, cross spectral density techniques should be used whenever extraneous noise is excessive, or phase response information is required. Another advantage of the cross spectral density measurement is that information about the relative power spectral density of an extraneous disturbance can be determined from the product of two measurements, (a) the transfer function obtained in the forward direction using $x(t)$ as the input, and (b) the transfer function measurement obtained in the reverse direction by treating $y(t)$ as the input. This frequency-dependent product is called the coherence function, (1) $R^2(\omega)$, where

$$R^2(\omega) = \frac{|S_{xy}(j\omega)|^2}{S_{xx}(\omega)\ S_{yy}(\omega)} .$$

By use of the above model, $R^2(\omega)$ may be presented in terms of power spectra,

$$R^2(\omega) = \frac{|L(j\omega)|^2\ S_{xx}(\omega)}{S_{yy}(\omega)} = 1 - \frac{S_{nn}(\omega)}{S_{yy}(\omega)} .$$

$R^2(\omega)$ expresses the fraction of the observed system output signal, which is linearly dependent upon the observed input signal. This fraction varies from zero to one, depending on the relative spectral intensity of the two components of the output power spectrum.

The power spectrum of the disturbance $n(t)$ can be computed from the coherence and the output power spectrum,

$$S_{nn}(\omega) = S_{yy}(\omega) \times (1 - R^2(\omega)) .$$

In Ref. 2 it is shown that confidence bands can be computed at each frequency for estimates of gain, $L(\omega)$, phase, $\phi(\omega)$, and the real and imaginary components of the transfer function, $R_eL(j\omega)$ and $I_mL(j\omega)$, respectively. First, a constant, k, is computed for given values of the following: confidence level, c; filter bandwidth, b (in cps); and data sampling time, t (in seconds), where

$$k = \left(\frac{1}{1-c}\right)\left(\frac{1}{bt-1}\right) - 1 .$$

The gain deviation, $\Delta L(\omega)$ and the phase deviation $\Delta\phi(\omega)$ can then be computed from estimates of $S_{xx}(\omega)$, $S_{yy}(\omega)$, $R^2(\omega)$, and $L(\omega)$, where

$$\Delta L(\omega) = \left[k\ \frac{S_{yy}(\omega)}{S_{xx}(\omega)}\ (1 - R^2(\omega))\right]^{1/2},$$

and

$$\Delta\phi(\omega) = \arcsin \frac{\Delta L(\omega)}{L(\omega)} .$$

According to Ref. 2, the probability is equal to or greater than the confidence level, c, so that: (a) the true value of gain lies in the band, $L(\omega) \pm \Delta L(\omega)$, (b) the true value of phase lies in the band, $\phi(\omega) \pm \Delta\phi(\omega)$, (c) the true value of the real part of the transfer function lies in the band, $R_eL(j\omega) \pm \Delta L(\omega)$; and (d) the true value of the imaginary part of the transfer function lies in the band, $I_mL(j\omega) \pm \Delta L(\omega)$.

The method described above for computing the coherence function $R^2(\omega)$ would require a series of four or five multiplication and division operations. While this function may readily be computed off-line (from the punched tape output of the analyzer system) for the purpose of determining confidence bands and the like, a similar but simpler coherence function $R^1(\omega)$ is computed directly by the cross spectral density analyzer system for the purpose of data evaluation.

The filtered components $x(t)$ and $y(t)$ are passed through limiters (circuits that detect polarity changes) to obtain simple binary signals of the form $R_eS_x(\omega,t)/|R_eS_x(\omega,t)|$, etc. Conventional binary logic circuits are then used to obtain all possible cross products. These cross products are then combined and averaged in a manner identical to that described for the computation of the real and imaginary components of the cross spectral density function. However, with the addition of the limiters, these averaged products take the form

$$\frac{R_eS_{xy}(\omega)}{|S_x(\omega)| \times |S_y(\omega)|}$$

and

$$\frac{I_m S_{xy}(\omega)}{|S_x(\omega)| \times |S_y(\omega)|}$$

These averaged products vary linearly with phase, $\phi(\omega)$, and the magnitude of these products, which is obtainable by simply adding their absolute values, is defined as the coherence function $R^1(\omega)$.

$$R^1(\omega) = \left| \frac{R_e S_{xy}(\omega)}{|S_x(\omega)| \times |S_y(\omega)|} \right| + \left| \frac{I_m S_{xy}(\omega)}{|S_x(\omega)| \times |S_y(\omega)|} \right|.$$

As shown in Ref. 3, $R^1(\omega)$ is related to $R^2(\omega)$ by

$$\frac{1}{R^2(\omega)} - 1 = \left(\frac{1}{R^1(\omega)} - 1 \right)^2.$$

While $R^2(\omega)$ represents the fraction of the power spectral density of $y(t)$, which came from the source, $x(t)$, $R^1(\omega)$ represents the fraction of the rms spectral density of $y(t)$, which came from the source, $x(t)$. $R^1(\omega)$ is used primarily to electronically screen data and determine the frequency regions where the data are sufficiently coherent to warrant recording of computed gain and phase estimates. The discrimination level may be set to trigger at any desired level of coherence.

NON-STATIONARY LINEAR SYSTEM

Let us now consider the problem of measuring the dynamic response characteristics of a linear system with nonstationary parameters. If the parameters, are changing slowly compared to the lowest frequency of interest in the system transfer function, a series of transients may be applied to the system, and a transfer function computed for each transient, or each series of transients.

For example, a series of fast-swept sinusoidal perturbations in discharge pressure was introduced in a rocket engine fuel pump during a test firing. The problem was to determine what changes occurred, if any, in the transfer functions relating the inlet and outlet pressures and flow rates as the fuel was consumed and the inlet pressure decreased. All instrumentation signals were contaminated with noise from cavitation effects. The analog cross spectral density analyzer was used to successfully determine all system transfer functions for each fast-swept sinusoidal burst. However, if the system parameters are changing rapidly compared to the frequencies of interest, amplitude or frequency modulation of the system response may occur, which destroys the linear coherence relating the observed excitation and response signals.

If signals are available which represent changes in a parameter suspected of introducing modulation effects, cross spectral analysis between such signals and the absolute value of the response signal may be used to detect and study possible amplitude modulation effects. If the response signal has periodic components, which can be extracted with appropriate filters, these components can be used to drive an FM frequency discriminator, and the frequency variations, if any, can be converted to an analog signal for comparison by cross spectral analysis with the signal representing a suspected source of frequency modulation.

Stationarity comparisons can also be made between the input and response signals of a system suspected of having nonstationary response parameters. One test for stationarity involves passing a given signal through two or more band pass filters in different frequency regions, and comparing their instantaneous absolute values, or instantaneous squared values, with the use of standard cross spectrum analysis techniques. If a signal is stationary, amplitude or intensity variations in one frequency range should not be coherent with amplitude or intensity variations in another frequency range (4). Comparison of the cross spectra and coherence functions obtained from such analyses of input and response signals may be used to detect and study the extent of nonstationary response parameters. Adjustable band pass filters, absolute value circuits, and squaring circuits are included in the analyzer system, for studying stationarity problems and detecting certain types of nonlinear system response characteristics, as described in the following section.

NONLINEAR SYSTEMS

Let us now consider the problem of measuring the response characteristics of a nonlinear system. Two methods of detecting and studying nonlinearities in a system will be described. One involves cross spectrum analysis of response signals with intensity variations of an input signal. A second method involves a measurement of the lowest order nonlinear interactions within a system.

If a system is being driven by one or more random input signals, it may be difficult to detect certain types of nonlinearities by examining time traces, or measuring transfer functions. One method of detecting nonlinear behavior involves comparing response signals with the

instantaneous absolute value, or instantaneous squared value, of the excitation signal. Provisions have been made in the analyzer for computing the coherence function, cross spectrum, etc., between one signal and intensity variations in another signal.

In a nonlinear system or process, each frequency component of the driving signal interacts with every other frequency component of the driving signal. The lowest-order interaction is one involving three different frequency components; two components of the input signal and one sideband component (at either the sum or difference frequency) resulting from their interaction. Two band pass filters are used to select any two frequency components of a given signal. The instantaneous product of the two components is then compared, by use of cross spectrum analysis techniques, with a third frequency component, at a frequency corresponding to the sum of the frequencies of the first two components. A series of such measurements for the different combinations is called the bispectrum (5). The bispectrum is a measure of the lowest order nonlinear interaction within a system where the driving signal is not directly observable. Similar measurements may be obtained between two components of a system input signal and the component in the system response signal at a frequency corresponding to the sum of the frequencies of the first two components. A series of such measurements for the different frequency combinations is called the cross-bispectrum.

SYSTEM DESCRIPTION

The input equipment for the analog cross spectral density analyzer system includes: (a) two FM reel-type tape transports for compressing or expanding the time base of input data for the analyzer; (b) an FM tape loop transport for making selected portions of the input data repetitive; (c) gating circuits to permit selection of all or any portion of the tape loop for detailed analysis; (d) signal conditioning preamplifiers for optimizing the amplitude and bandwidth of input signals; (e) adjustable high pass, low pass, or band pass filters for prewhitening input signals, or selecting certain frequency components in the input data; (f) a delay line for alignment of time-dependent input signals (a form of prewhitening); (g) absolute value and squaring circuits for examining variations in the amplitude or intensity of input signals; (h) FM discriminators for examining phase or frequency variations of selected frequency components of input signals; and (i) multichannel strip chart recorders for visual inspection and comparison of input signals. In some cases, dynamic test signals are recorded originally on strip charts instead of magnetic tape. Chart readers are provided for retrieving test data from analog strip charts, and providing analog voltage signals, which may then be recorded on magnetic tape and processed on the analyzer system.

The basic analyzer includes: (a) four input preamplifiers; (b) two in-phase and two quadrature, or four in-phase, band pass filters with selectable bandwidth and electronically controlled center frequencies (6), (c) frequency tracking oscillator, which controls the center frequency of the filter, and keeps the filters tuned to the fundamental frequency of a swept periodic or swept random input signal; (d) a sweep generator to vary the center frequency of the filters across the desired range of frequencies at a selected rate, (e) filter amplifiers to optimize the level of each filtered component before it is squared, multiplied, etc., (b) absolute value and squaring circuits to detect the amplitude or power of filtered components, (g) analog multipliers for computing cross products of filtered components, (h) summing and difference amplifiers for combining multiplied or squared filter components, (i) smoothing or integrating circuits for computing time averages of selected spectral components, and analog dividers for computing ratios of spectral components, (j) a Nyquist to Bode converter to compute magnitude and phase from real and imaginary cross spectral components, (k) gating circuits to control the integrators for detailed analysis of transients or short samples of data from the tape loop machine, and (l) a coherence computer with gating circuits to electronically screen data and determine the frequency regions where data are sufficiently coherent to warrant recording of computed gain and phase estimates.

Output equipment includes: (a) x-y recorders for plotting spectral components, gain, phase, coherence, etc., as a function of linear or log frequency, (b) chart recorders for plotting spectral components as a function of time, (c) analog to digital converter for recording all outputs of the analyzer in digital form, as functions of time or frequency, on punched paper tape for additional manipulation, computation of confidence bands, etc., with a digital computer, and (d) a digital to analog converter for replotting selected variables from the punched paper tape.

APPLICATIONS

The analyzer system was assembled for applications to test programs associated with the development of SNAP 2, 8, and 10A space nuclear electric power systems. Specific examples

of previous applications are described in the following sections.

Reactor Kinetics and Control

Power spectral density measurements of high frequency fluctuations in reactor power, caused by statistical variations in fission rate, were obtained to determine the average duration of prompt neutron chains (7). This provides measurements of prompt neutron lifetime and subcritical reactivity for various reactor core configurations. These measurements extended from 1 to 100,000 cps, and required development of fast response neutron detection systems and advanced analysis capabilities.

Heat Transfer

Thermal response characteristics of a SNAP 8 reactor core were experimentally determined at various operating conditions, from the response of neutron power and outlet temperature to small random binary perturbations in coolant flow rate (8). This program required development of equipment to measure transfer functions from noise-contaminated instrumentation signals over the frequency range from below 0.0003 cps to above 1 cps. A coherence computer was developed for determining the signal to noise relationships at each frequency.

Hydraulics

Cross spectrum analysis techniques were applied to the problem of measuring localized fluid velocities and flow distribution in hydraulic test models. This was done as part of a program to develop flow controlling devices which optimize transfer of heat energy from fuel to coolant in SNAP reactors. The basic experimental approach involves detecting, recording, and analyzing localized random fluctuations in conductivity of water as it propagates past two or more detection devices. Variations in conductivity are induced by injecting small amounts of salt solution into the stream of water passing the detectors. Analog cross spectral density measurements yield the transient time delay relating signals picked up from two adjacent detectors. The degree of coherence between various detectors yields information on mass flow distribution. (A cross correlation computer, assembled from certain sections of the cross spectral density analyzer, has been used extensively in this application at AI.) (9)

STRUCTURAL DYNAMICS

Measurements of the structural response of SNAP 2, 8, and 10A space nuclear electric power systems to random, swept sinusoidal and transient vibration were performed from tape recordings of accelerometer outputs. Several thousand plots of reduced data were obtained for these projects in the form of time series, amplitude spectra, displacement, transmissibility, coherence, power spectra, cross spectra, gain and phase. These data were used to document the flight qualification of the vehicles tested.

CONCLUSIONS

Applications of the analyzer system have largely involved the measurement of the dynamic response characteristics of various mechanical, electronic, nuclear, thermal, or hydraulic systems or processes. Other applications involve: (a) the study of cause and effect relationships between various random processes, the determination of the source of extraneous disturbances which appear in a system, (b) the determination of the path or flow pattern which some process takes in propagating through a system, and (c) the measurement of the associated transit times. Many other possible applications exist in essentially every field of research and engineering. The field of biomedical research faces problems with noise contamination of response signals, nonstationary excitation and response signals, and nonlinear characteristics of many systems in the human body. Problems in the field of ocean engineering, related to the response characteristics of systems created by ocean waves and currents, also involve noise-contaminated data, nonstationary excitation and response functions, and nonlinear interactions. In the aerospace industry, vehicles to be flown or launched into space must undergo extensive dynamic testing. Large quantities of dynamic test data must be processed for qualifying each component, instrument, engine, payload, etc.

The analog cross spectral density analyzer system is not one instrument, but a group of instrument systems, combined in one facility to form a flexible and comprehensive data processing capability. The ability to handle almost any type of dynamic test data, from both magnetic tape and strip charts, makes this analyzer system applicable to nearly every field of engineering.

REFERENCES

1. N. R. Goodman et al, "Frequency Response from Stationary Noise: Two Case Histories," Technometrics 3: 245-268 (1961)

2. N. R. Goodman, "Simultaneous Confidence Bands for Matrix Frequency Response Functions and Related Results," Rocketdyne Research Memorandum RM 972-351, (1963)

3. R. L. Randall, "Coherence Measurements," NAA-SR-TDR-9841, (April 1965)

4. N. R. Goodman, "Statistical Tests for Stationarity Within the Framework of Harmonizable Processes," Rocketdyne Research Report RM 972-351, (1965)

5. Gordon J. F. MacDonald, "The Bispectra of Atmospheric Pressure Records," In Proceedings of the IBM Scientific Computing Symposium on Statistics (October 1963), (Edited and published by International Business Machines)

6. A. G. Ratz, "A Transfer Function Computer Using Random Functions," Bulletin 0-30A, Gulton Industries, Inc., Trenton, New Jersey, (1964)

7. R. L. Randall, and C. W. Griffin, "Application of Power Spectra to Reactor System Analysis," Symposium on Noise Analysis in Nuclear Systems, AEC-TID-7674, R. E. Uhrig (June 1964)

8. P. J. Pekrul, "Dynamic Measurements of SNAP 8ER Feedback Coefficients," presented at the winter meeting of the American Nuclear Society, Washington, D. C., (November 1964)

9. G. R. Grayban, P. J. Pekrul, and R. L. Randall, "Development of Noise Analysis Techniques for Measuring Reactor Core Velocities," NAA-SR-11193, (October 1965)

* * *

TRANSIENT DATA DISTORTION COMPENSATION*

John D. Favour
The Boeing Company
Seattle, Washington

This paper discusses a technique capable of removing frequency-dependent distortion from transient data. The instrumentation system transfer function is determined by dividing the Fourier integral transform of the output by the Fourier integral transform of a known input. The system inverse transfer function is then developed and applied to any output signal to remove distortion. Three test efforts were conducted to prove the feasibility of the technique. Distorted outputs with measurable errors in excess of sixty percent were reconstructed with errors of less than two percent. The mathematical method and limitations of the technique are defined. The design of a recommended calibration pulse generator is presented.

INTRODUCTION

The purpose of a data acquisition system, or generalized instrumentation system, is to provide a calibrated analog record of a desired phenomenon. The calibration must involve both amplitude and time correlation.

The accurate measurement of high-speed transient phenomena can be difficult, not only in technical terms, but also in terms of the availability of adequate data-acquisition equipment. When equipment with inadequate frequency response is used, the output record contains distortion both in amplitude and time correlation (Fig. 1). Distortion in transient data is very difficult to recognize by visual inspection. Often it is not recognized at all. When it is recognized, the test has already been run. At this point, the normal procedure is to discard the distorted data and make the necessary changes to rerun the test to obtain more accurate data. This procedure requires replacing the instrumentation equipment with more sophisticated equipment, or injecting an on-line compensator as suggested in Ref. (1).

A more desirable procedure involves the development of a "complex compensation factor," which is applied to the existing data to remove all distortion. This procedure can reconstruct distorted data, prevent costly retesting and be applied to future tests without replacing existing equipment. This procedure is described below.

*This paper was not presented at the Symposium.

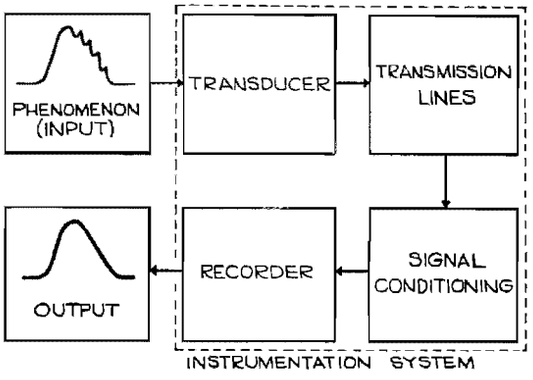

Fig. 1. Inadequate instrumentation system

If a known transient calibration signal* is applied to the input of an instrumentation system, a distorted output signal or record results. By comparing mathematically the known input with the resultant output, the "transfer function" of the system can be determined. This transfer function describes the dynamic relationship between the input and output of the system.

The "complex compensation factor" can be realized by developing another transfer function which is the inverse of the original system transfer function. Multiplying the Fourier integral transform of any distorted output signal by

*Certain requirements are made of the input calibration transient signal. See "Limitations" following.

the inverse transfer function results in a "reconstructed" output, without distortion,* once it is integrated back to the time domain. See Fig. 2.

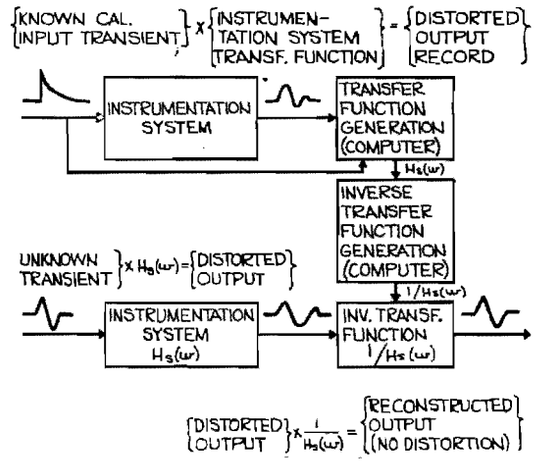

Fig. 2. Description of technique

TESTING

The following paragraphs describe the application of this compensation technique to three separate tests. These tests provided insight into the problems of practical application, as well as information concerning the techniques boundary conditions.

Simulated System Tests

Three separate tests were performed on a simulated instrumentation system. The system was simulated by an SKL Model 302 filter, bandpassed from 8.5 to 40 kc for the first test and from 20 to 200 cps for the second and third tests. (See Fig. 3.) The filter roll-off slopes were 18 db/octave. The transient pulses were generated by an Exact Model 250 pulse generator.

The general procedure was identical for all three tests. An electrically-generated calibration pulse and a test pulse were sequentially applied to the SKL filter. Polaroid photographs of the input and output waveforms were obtained. The photographic records were manually reduced to digital form. This digital information was given to the computer. The computer developed the system inverse transfer function

*Within limits. See "Limitations" following.

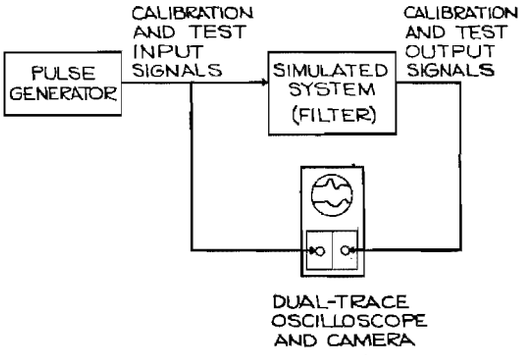

Fig. 3. Diagram of simulated tests

from the Fourier transforms of the calibration input and output pulses. The Fourier transform of the test output pulse was then multiplied by the inverse transfer function, integrated back to the time domain, and compared to the test input pulse.

Reproductions of the three sets of pulses obtained during the testing are shown in Figs. 4, 5, and 6. The figures show the input test pulse superimposed upon the numerically reconstructed test pulse. A qualitative indication of the effectiveness of this technique can be seen by comparing the test output and reconstructed output with the input test pulse; for example, although the output test pulse of Fig. 4 bears no visual relationship to the original test input, the reconstructed pulse reproduces the original rise time and pulse duration very closely. The output pulse of Fig. 6 shows a pulse duration approximately 50 percent greater than the input pulse. The error in the reconstructed pulse is barely detectable.

Connector Dynamic Load Test

Members of one test group indicated concern over distortion in some test data. They were interested in the dynamic load required to separate two halves of a connector (see Fig. 7). Two sets of mating pins were wired to provide a continuity indication of separation. The separation was indicated as occurring during the initial tension pulse. This did not seem reasonable.

A brief investigation indicated that the trouble was in the load cell. It was a 500-lb ring-type load cell. (The resonant frequency of the cell itself was known to be quite low, approximately 300 cps.) The first requirement was to calibrate dynamically the instrumentation system. This was achieved by suspending

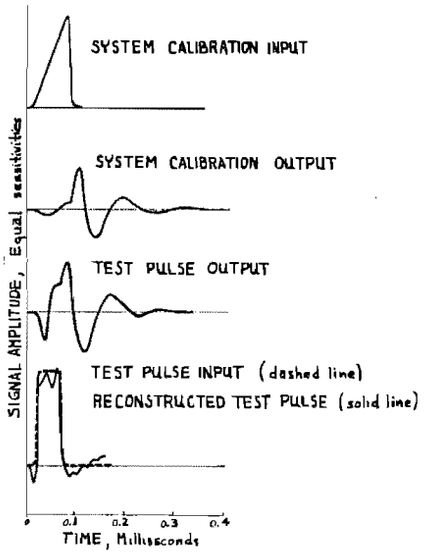

Fig. 4. Results of first simulated test

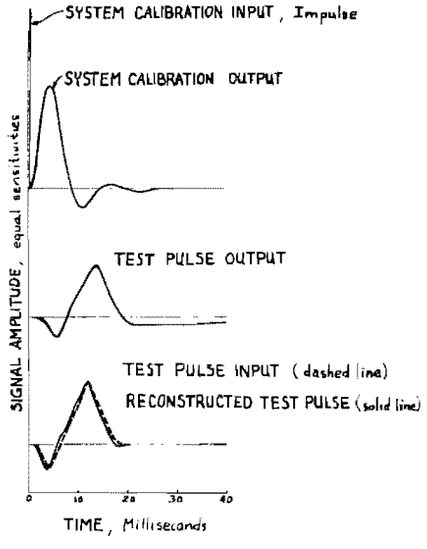

Fig. 5. Results of second simulated test

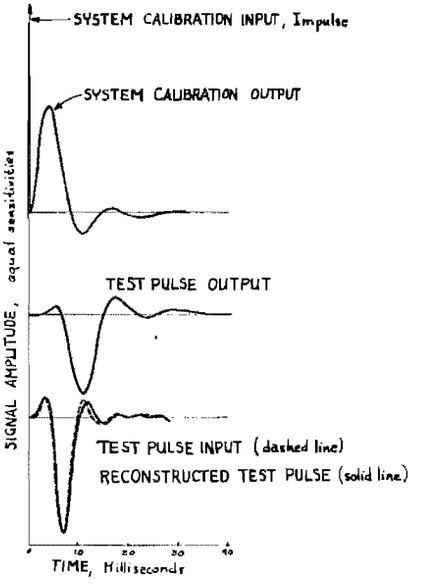

Fig. 6. Results of third simulated test

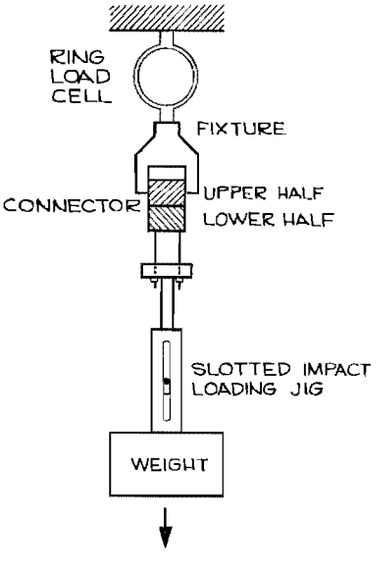

Fig. 7. Diagram of connector load test

144 lb of dead weight from the load cell, fixture, and upper half of the connector, via piano wire, and then by cutting the wire to release the weight (see Fig. 8). This process produced a negative-going, step input force function in the system.

Because the input transient failed to meet a boundary condition (see "Limitations" following), the computer was not used to describe the system transfer function.* The load cell was known to be the limiting factor in this system, and it is known to have a response described as:

*It is not necessary to use transient pulses and the computer to calibrate the system. Any technique capable of describing the system transfer function adequately may be substituted.

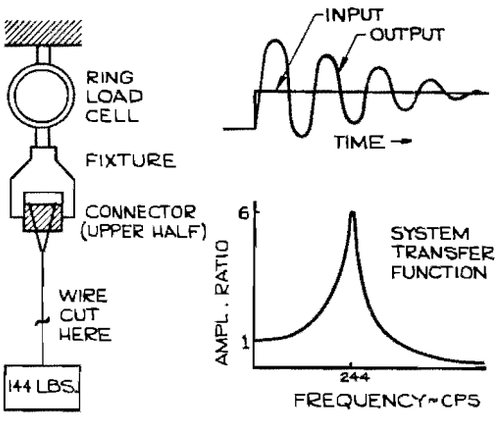

Fig. 8. Instrumentation dynamic calibration

$$H_s(\omega) = \frac{K}{\left\{\left[1 - \left(\frac{\omega}{\omega_0}\right)^2\right]^2 + \left(2B\,\frac{\omega}{\omega_0}\right)^2\right\}^{1/2}}, \qquad (1)$$

where

ω_0 = resonant frequency (radians/sec.),

ω = frequency (a variable),

B = damping ratio, and

K = constant.

Analysis of the output record using standard technique, or measuring logarithmic decrement and oscillation frequency, indicated these values for the above parameters:

ω_0 = 1530 rad/sec (244 cps),

B = 0.075, and

K = 192 lb/in. (galvanometer defl.).

The data from a previous test, which were believed to be distorted, were then reduced and given to the computer along with the transfer function description of Eq. (1). The results are illustrated in Fig. 9.

The peak load was of primary interest in this test. The reconstruction indicated that it was 10 percent lower than originally recorded. It should also be noted that a significant time shift existed between the distorted output and the reconstruction. This means that there could be no reasonable time correlation between the distorted data and the separation indications. Time correlation is reasonable between the reconstructed pulse and separation. After the initial tension load pulse, a compression load is indicated. This is due to a spring-loading device within the connector which assists separation, once it is initiated.

Accelerometer Shock Test

Two accelerometers were mounted, back to back, in a shock calibration anvil in such a way that both transducers would experience identical shock pulses. One accelerometer was a piezoelectric type and was used as a standard. The other accelerometer, a strain gage type, was used as a limiting factor in an instrumentation system which would produce distortion. The purpose of this test was to remove distortion from the strain gage accelerometer output, as it was not designed for this type of measurement, and to compare the reconstructed output with the standard.

The entire instrumentation system, for both channels, is illustrated in Fig. 10. Both accelerometers were first calibrated on an electromagnetic vibrator at several discrete sinusoidal frequencies. This calibration provided the

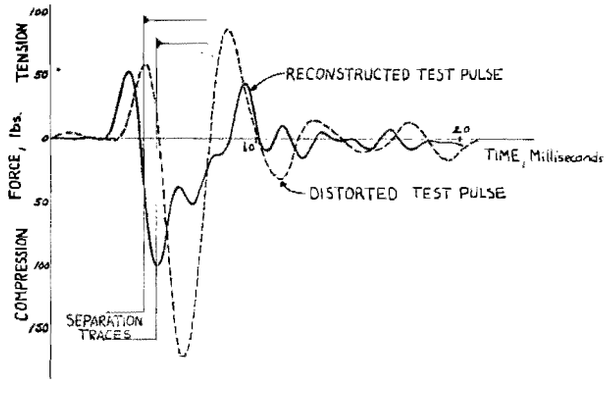

Fig. 9. Results of connector load test

transfer function characteristics of both transducers (see Fig. 11). With the transducers mounted on the anvil, the anvil was suspended in air, by string, and restricted to swing in only one plane. The hammer was similarly suspended within the same plane, so that it would impact the anvil when deflected from its stable position and released. Foam rubber padding was used as an impacting medium. Since only the dynamic calibration of the transducers has been performed, the dynamic calibration of the individual channels of the instrumentation system following the transducers, had to be performed. This was accomplished by applying a single square pulse to each channel at the input of the first amplifier. The pulse amplitude was 25.5 mv, with a 10-μsec pulse duration. The responses of each channel were recorded on an FM magnetic tape at 60 ips. Again, refer to Fig. 10.

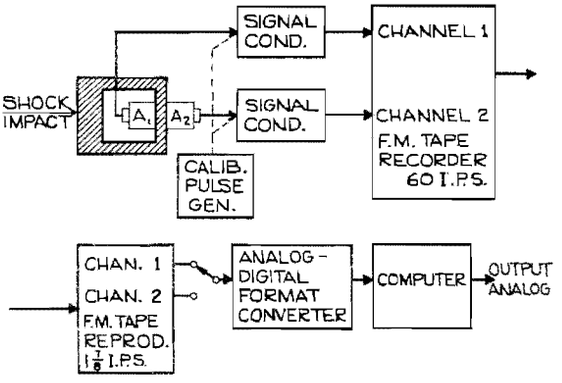

Fig. 10. Instrumentation for accelerometer shock test

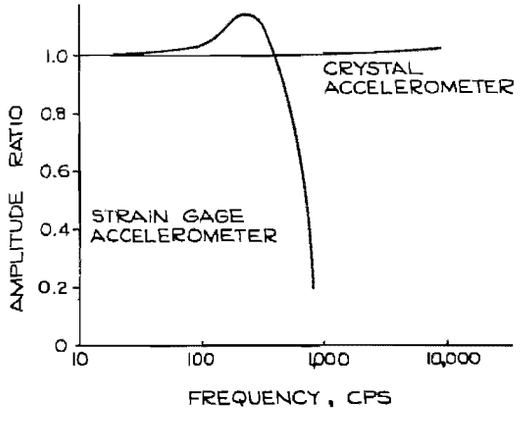

Fig. 11. Accelerometer transfer functions

Following calibration, the shock pulse was created by allowing the hammer to impact the anvil. The signals from both transducers were recorded on the FM magnetic tape at 60 ips. The magnetic tape recording was played back at 1-7/8 ips and the pulses, both calibration and test, were digitized for computer application. The proper time sampling interval was programmed into the computer to accommodate the tape speed change. The computer generated the instrumentation system (excluding transducers) inverse transfer functions from the calibration pulses. The inverse transfer function of the transducer was computed from the transfer function derived from transducer calibration. The reconstructed shock pulse was realized by integrating the complex product of the Fourier transform of the output pulse, and the inverse transfer function of the transducer and instrumentation system, back to the time domain.

The standard pulse was processed in the same manner to eliminate any distortion which might have occurred within the instrumentation system. The results are illustrated in Fig. 12.

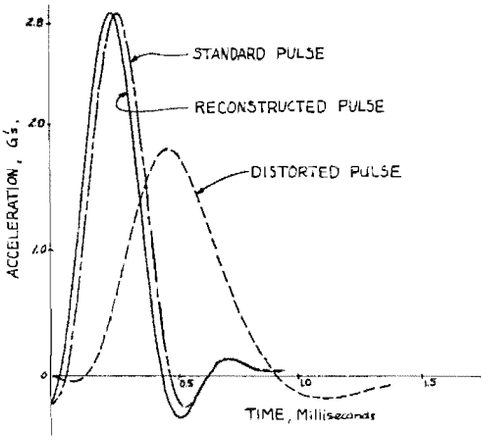

Fig. 12. Results of acceleration shock test

Three criteria were chosen by which to evaluate the results: (a) peak amplitude, (b) pulse duration (time between zero crossing), and, (c) real time correlation of initial zone crossing and peak, with respect to standard pulse. The standard pulse has a peak amplitude of 2.88 g's and a pulse duration of 430 μsec. The distorted output pulse had a peak amplitude of 1.80 g's. This was an error of 37.5 percent. The pulse duration was 730 μsec, or an error of 70 percent. For time correlation, the initial

zero crossing lagged the standard by 84 μsec and the peak lagged by 210 μsec. The reconstructed pulse had an amplitude of 2.88 g's or no error. The pulse duration was 430 μsec, or no error. For time correlation, the initial zero crossing and peak both led the standard by 30 μsec.

MATHEMATICAL METHOD AND LIMITATIONS

Mathematics

For a linear system, the output is related to the input by Eq. (2)

$$H_o(j\omega) = H_i(j\omega)\, H_s(j\omega)\,, \tag{2}$$

where

$H_o(j\omega)$ = the Fourier integral transform of the output,

$H_i(j\omega)$ = the Fourier integral transform of the input, and

$H_s(j\omega)$ = the system transfer function.

Since the above parameters are functions in the frequency domain, the following should be recognized as the Fourier integral transform:

$$F(j\omega) = \int_{-\infty}^{\infty} f(t)\, e^{-j\omega t}\, dt \tag{3a}$$

and, inversely:

$$f(t) = \frac{1}{2\pi} \int_{-\infty}^{\infty} F(j\omega)\, e^{j\omega t}\, d\omega\,. \tag{3b}$$

Dynamic calibration of the system is accomplished by taking the ratio of the Fourier integral transforms of the known input and output transients, as

$$H_s(j\omega) = \frac{H_{oc}(j\omega)}{H_{ic}(j\omega)} = \frac{\int_{-\infty}^{\infty} h_{oc}(t)\, e^{-j\omega t}\, dt}{\int_{-\infty}^{\infty} h_{ic}(t)\, e^{-j\omega t}\, dt}\,, \tag{4}$$

where

$h_{oc}(t)$ = output calibration transient and

$h_{ic}(t)$ = input calibration transient.

The system inverse transfer function is computed simply as $1/H_s(j\omega)$. To reconstruct a test input transient, $h_i(t)$, from the test output transient, $h_o(t)$, the following multiplication is performed:

$$H_o(j\omega) \times \frac{1}{H_s(j\omega)} = H_i(j\omega)\,. \tag{5}$$

The product is integrated back to the time domain, by Eq. (3b), as:

$$h_i(t) = \frac{1}{2\pi} \int_{-\infty}^{\infty} H_i(j\omega)\, e^{j\omega t}\, d\omega\,. \tag{6}$$

Limitations

Mathematics — The limits of integration,* 0 and T, must encompass the complete transient such that $h(t) = 0$ for $t < 0$ and $t > T$. Then

$$H(j\omega) = \int_{0}^{T} h(t)\, e^{-j\omega t}\, dt \tag{7}$$

is mathematically rigorous.

The limits of integration,† ω_{min} and ω_{max}, must encompass the complete frequency spectrum of the transient such that $H(j\omega) = 0$ for $\omega \le \omega_{min}$ and $\omega \ge \omega_{max}$. Then

$$h(t) = \frac{1}{2\pi} \int_{\omega_{min}}^{\omega_{max}} H(j\omega)\, e^{j\omega t}\, d\omega \tag{8}$$

is mathematically rigorous.

Sampling — All time functions are defined by discrete samples. Therefore, to assure an accurate representation of $H(j\omega)$ in the range ω_{min} to ω_{max}, the sampling rate must satisfy the inequality,

$$\Delta t < \frac{\pi}{2\omega_m}\,,$$

where ω_m is the highest frequency component, in rad/sec, of the time function.

*The limits 0 and T are substituted for $-\infty$ and ∞ in Eq. (3a), since $h(t) = 0$ for $t < 0$ and $t > T$.

†The limits ω_{min} and ω_{max} are substituted for $-\infty$ and ∞ in Eq. (3b) since $H(j\omega) = 0$ for $\omega \le \omega_{min}$ and $\omega \ge \omega_{max}$.

Each Fourier integral transform is defined at discrete frequencies for the range ω_{min} to ω_{max}. To assure the accurate reconstruction of a transient, the resolution of $H(j\omega)$ must satisfy the inequality $\Delta\omega \leq (\pi/T)$, where T is the length of the transient in time. This also says that $\omega_{min} \geq \Delta\omega$.

System

$$|H_s(j\omega)| \geq (0.1)\ |H_{sf}(j\omega)| \quad \text{for } \omega_{min} \leq \omega \leq \omega_{max}.$$

$H_{sf}(j\omega)$ = the system gain at the normal, usable, "flat" frequency range.

$\omega_m \leq$ the frequency where

$$H_s(j\omega) = (0.1)\ H_{sf}(j\omega).$$

System noise is negligible.

Calibration — The input calibration pulse $h_{ic}(t)$ must represent significantly all frequencies in the range ω_{min} to ω_{max}. If $H_{ic}(j\omega) \to 0$, then, by Eq. (4), $H_s(j\omega) \to \infty$.

$h_{oc}(t) = 0$ for $t < 0$ and $t > T$, and must be sampled in such a way that $\Delta t \leq (\pi/2\omega_m)$.

CALIBRATION PULSE GENERATOR

Requirements

A list of the requirements placed upon a pulse generator by this technique follows:

1. The calibration pulse must completely saturate the instrumentation system with respect to frequency content.

2. The calibration pulse must be equal to zero before initiation ($t = 0$) and, after completion, ($t = T_{max}$).

3. The calibration pulse generator must be highly repeatable.

4. The calibration pulse generator must be portable, of simple design and construction, and insensitive to common environmental changes.

Description

The generator and pulse are described in Fig. 13. The pulse is generated from a simple RC decay of a charged capacitor. The pulse is initiated by opening a common household, mercury (silent type) toggle switch. This eliminates contact bounce.

The generated pulse is described as:

$$f_c(t) = -\,U(t)\,\frac{E_B R_2}{R_1 + R_2}\,e^{-\frac{t}{(R_1+R_2)C}}. \qquad (9)$$

The Fourier integral transform of the pulse is:

$$H_c(j\omega) = \left[\frac{E_B R_2}{R_1 + R_2}\right]\left[\frac{1}{\frac{1}{(R_1 + R_2)C} + j\omega}\right], \qquad (10)$$

and is described in Fig. 13.

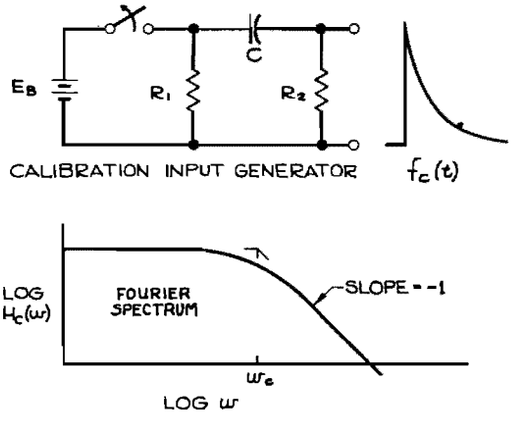

Fig. 13. Recommended calibration pulse generator

CONCLUSIONS

This technique has been proven feasible and highly economical. Its boundary conditions and limitations are well defined; test results have shown the technique to be accurate. The digital computer makes the technique practical and further application will increase its value.

ACKNOWLEDGMENT

The success of this investigation was made possible only through the help and suggestions of D. R. Harting and J. P. Dempsey. The computer programming was handled by F. Efta and T. C. Wilfong of our Applied Mathematics Department.

REFERENCES

1. F. F. Liu and T. W. Berwin, Rev. Sci. Instr. 29:1 (1958)

2. M. Schwartz, Information, Transmission, Modulation and Noise (McGraw-Hill, New York), 1959

3. R. W. Lawler, B. R. Wilson and T. C. Wilfong, "FXFORM Fourier Transform of IBM 7090," Aero-Space Div. Engineering Operations Dept., Boeing, Ref. No. AS1312, August 1962

4. R. W. Lawler, B. R. Wilson and T. C. Wilfong, "IXFORM Inverse Fourier Transform for IBM 7090," Aero-Space Div. Engineering Operations Dept., Boeing, Ref. No. AS1313, August 1962

* * *

DISTRIBUTION

Aberdeen Proving Ground, Md.
- Att: Ballistic Research Lab. 1
- Att: Development & Proof Services 1
- Att: Physical Test Lab. 1

Air Defense Command, Ent AFB
- Att: Deputy for Civil Engineering 1
- Att: ADIRP 1

Air Force Academy, Colo.
- Att: Dept. Mech. DFME (UNCLASSIFIED) 1

Air Force Packaging Evaluation Agency, Brookley AFB
- Att: MOSPR 1
- Att: MONE 1

Air Proving Ground Center, Eglin AFB
- Att: PGTRI, Technical Library 1

Air Force Headquarters, DC
- Att: Operations Analysis Off., Off. Vice Chief of Staff, Library 2
- Att: AFDRD-GW 1

Air Force Logistics Command, W-PAFB
- Att: Mr. G. P. Civille, MCTEP 1

Air Force Missile Development Center, Holloman AFB
- Att: RRRT/Miss R. Porter 1
- Att: MDS/Dr. M. G. Jaenke 1
- Att: MDLR/Mr. H. J. Dunbar 1
- Att: MDSGS/Mr. G. R. Moser 1
- Att: MDSTE/Mr. J. M. Mapes 1

Air Force Missile Test Center, Patrick AFB
- Att: MT LLL-3 (Classified Material) 2
- Att: MU-135, Technical Library (UNCLASSIFIED) 1

Air Force Office of Scientific Research, DC
- Att: Library (UNCLASSIFIED) 1

Air Force Regional Civil Engineer
- Att: North Atlantic Region, AFRCE-NA-A 1
- Att: South Atlantic Region, AFRCE-SA-E 1

Air Force Rocket Propulsion Lab., Calif.
- Att: Mr. A. J. Davies (RPFDE) 1
- Att: Mr. R. A. Silver 1

Air Force Systems Command, Andrews AFB
- Att: Technical Library 2

Air Force Weapons Laboratory, Kirtland AFB
- Att: Development Test Division 1
- Att: Dr. W. E. Fisher, WLRS 1
- Att: SWOI 631-276 1

Army Air Defense Center, Ft. Bliss
- Att: Technical Library 1

Army Chemical Center, Maryland
- Att: Library 1

Army Electronics Materiel Agency, Phila. 1

Army Electronics Command, Ft. Monmouth
- Att: AMSEL-RD-ADT 1
- Att: AMSEL-RD-PEE 1
- Att: AMSEL-RD-PRT 1
- Att: AMSEL-RD-G 1
- Att: AMSEL-RD-GTF 1
- Att: Mr. J. J. Oliveri 1

Army Engineer District, New York
- Att: NANGD 1

Army Engineer R&D Laboratories, Ft. Belvoir
- Att: Package Development Branch 1
- Att: Mr. A. Carolla 1
- Att: Director of Research 1
- Att: Chief, Spec. Proj. Branch 4

Army Engineer Waterways Experiment Station, Vicksburg
- Att: Mr. J. M. Strange 1

Army Materials Research Agency, Watertown
- Att: Dr. Reinier Beeuwkes, Jr. 2

Army Materiel Command, DC
- Att: AMCRD-RS-CM 1

Army Materiel Command, Redstone Arsenal
- Att: Technical Library 4

Army Missile Command, Redstone Arsenal
- Att: AMSMI-RB 1
- Att: AMSMI-RG 1
- Att: AMSMI-RL 1
- Att: AMSMI-RS 1
- Att: AMSMI-RT 1
- Att: AMSMI-RTR, Mr. J. M. Taylor 1
- Att: AMSMI-RSM, Mr. E. J. Wheelahan 1

Army Mobility Command, Centerline
- Att: Mr. Otto Renius 1

Army Natick Laboratories, Mass.
- Att: Technical Library 2
- Att: Mr. W. B. Brierly 1
- Att: Chief, Container Div. 1

Army, Office Chief of Engineers, DC
Att: ENGMC-EM 2

Army, Office Chief of Research & Development, DC
Att: Scientific & Technical Information Div. 1

Army, Office Chief of Transportation, DC
Att: Director of Transportation Engineering 1

Army Ordnance Ammunition Command, Joliet
Att: ORDLY-T 1
Att: NNSC/A 1

Army Staff Group, DC
Att: Mr. J. Valler (UNCLASSIFIED) 1

Army Tank-Automotive Center, Warren
Att: SMOTA-RRS, Tech. Library 1
Att: SMOTA-RCE.3, Mr. D. J. Hackenbruch 1
Att: SMOTA-RRC 1

Army Transportation Engineering Agency, Ft. Eustis
Att: Library 1
Att: Mr. L. J. Pursifull 1

Army Transportation Research Command, Ft. Eustis
Att: Dr. R. L. Echols, Physical Sci. Res. Group 1

Arnold Engineering Development Center, Arnold AFS
Att: AEOIM 1

Atomic Energy Commission, Oak Ridge
Att: Office of Technical Information 6

Atomic Energy Commission, DC
Att: Library 1

Aviation Supply Office, Philadelphia
Att: Code TEP-1 1

Ballistic Systems Division, USAF, Norton AFB
Att: Technical Data Division 3

Boston Naval Shipyard, Mass.
Att: Library 1

Bureau of Medicine & Surgery, USN, DC
Att: Research Division 1

Bureau of Naval Weapons, USN, DC
Att: DLI-3 2
Att: FWAA, Mr. C. H. Barr 1
Att: RREN-5 5
Att: RRMA 1
Att: RAAE-2 1
Att: RM-3 2
Att: RM-2 1
Att: RSSH 2
Att: FWAE 1
Att: RREN-8 1

Bureau of Naval Weapons Rep., E. Hartford 2

Bureau of Naval Weapons Rep., Pomona
Att: Chief Engineer 1
Att: Metrology Dept. Code 60 1

Bureau of Naval Weapons Rep., Sunnyvale 1

Bureau of Ships, USN, DC
Att: Code 423 20

Bureau of Supplies & Accounts, USN, DC
Att: Library 1

Bureau of Yards & Docks, USN, DC
Att: Code D-440 1
Att: Code D-220 1
Att: Code D-220 (UNCLASSIFIED) 6

Coast Guard Headquarters, DC 1

David Taylor Model Basin, UERD, Portsmouth
Att: Code 281A 1

David Taylor Model Basin, DC
Att: Library 3
Att: Mr. Harry Rich 1
Att: Code 591L, Mr. J. A. Luistro 1
Att: Contract Res. Administrator 1

Defense Atomic Support Agency, DC
Att: Technical Director 1
Att: Weapons Development Division 1
Att: Mr. John G. Lewis 1

Defense Atomic Support Agency, Livermore
Att: Administrative Officer 1

Defense Documentation Center, Va. 100

Defense Intelligence Agency, Va.
Att: DIAAP-1K2 1

District Public Works Office, 14th Naval District 1

Electronic Systems Division, L. G. Hanscom Field
Att: ESTI 1

Electronics Supply Office, USN, Great Lakes 1

Erie Army Depot, Ohio
Att: Chief, Materiel Testing Div. 1

Federal Aviation Agency, DC
Att: Emergency Readiness Div., Off. Plans & Requirements 2
Att: Chief, Tech. Processing Br., Library Serv. Div. (UNCLASSIFIED) 1

Forest Products Laboratory, Dept. of Agriculture, Madison
Att: Mr. Robert Stern (UNCLASSIFIED) 1

Frankford Arsenal, Philadelphia
Att: Library Branch, CC 0270/40 1
Att: Mr. David Askin, CC 1730/230 1

Harry Diamond Laboratories, DC
Att: Chief, Lab. 700 1
Att: Chief, Branch 850 1
Att: Technical Information Officer 2

Inspector of Naval Material, San Francisco 1

Library of Congress, DC (UNCLASSIFIED) 2

Long Beach Naval Shipyard, Calif.
Att: Code 240 1

Mare Island Naval Shipyard, Vallejo
Att: Library 1

Marine Corps Equipment Board, Quantico 1

Marine Corps Headquarters, DC
Att: Research & Development Section 1
Att: Code AO4E 1

Maxwell AFB, Alabama
Att: Air University Library 1

NASA, Ames Research Center, Moffett Field
Att: Tech. Management Office N203-5 1

NASA, Flight Research Center, Edwards
Att: Library 1

NASA, Goddard Space Flight Center, Greenbelt
Att: Code 320, Mr. J. C. New 1
Att: Code 623.3, Mr. G. Hinshelwood 1
Att: Code 321.2, Mr. K. M. Carr 1
Att: Code 321.2, Mr. F. Lindner 1
Att: Dr. Elias Klein 1
Att: Mr. W. R. Forlifer 1
Att: Library 1

NASA, Langley Research Center, Hampton
Att: Library 2
Att: Mr. S. A. Clevenson 1
Att: Mr. D. J. Martin 1

NASA, Lewis Research Center, Cleveland
Att: Library 2

NASA, Manned Spacecraft Center, Houston
Att: Technical Library 1

NASA, Marshall Space Flight Center, Huntsville
Att: Mr. J. H. Farrow, M-P&VE-ST 1
Att: Mr. R. M. Hunt, M-P&VE-S 1
Att: Mr. R. E. Jewell, R-P&VE-SVR 1
Att: AMSMI-RBLD 1

NASA, Michoud Operations, New Orleans
Att: Mr. H. L. Williams, QR (UNCLASSIFIED) 1

NASA, Scientific & Technical Info. Facility, Bethesda
Att: NASA Representative 1

NASA, Headquarters, DC
Att: Mr. D. Michel, RV-2 1

National Bureau of Standards, DC
Att: Mr. B. L. Wilson 1
Att: Mr. S. Edelman, Mech. Div. 1

National Security Agency, DC
Att: Engineering 1

Naval Air Development Center, Johnsville
Att: Mr. E. R. Mullen 1
Att: Aeronautical Instruments Lab. 1
Att: NADC Library 2

Naval Air Engineering Center, Philadelphia
Att: Library 1

Naval Air Test Center, Patuxent River
Att: Electronics Test Div. 1
Att: VTOL/STOL Branch 1
Att: Instrumentation Br., Flight Test Div. 1

Naval Ammunition Depot, Crane
Att: Code 3540 1
Att: Code 3400 1

Naval Ammunition Depot, Portsmouth
Att: Mr. Jerome Smith, Code QALE 1

Naval Ammunition Depot, Red Bank
Att: Chief Engineer 1

Naval Ammunition Depot (Oahu)
Att: Weapons Technical Library 1

Naval Applied Science Laboratory, Brooklyn
Att: Library 3

Naval Attache, Navy No. 100, NY
Att: Logistics Division 1

Naval Avionics Facility, Indianapolis
Att: MAL Library 1

Naval Civil Engineering Lab., Pt. Hueneme
Att: Library 2

Naval Construction Battalion Center, Pt. Hueneme
Att: Civil Engineer Corps Officers 1

Naval Medical Field Research Lab., Camp Lejeune 1

Naval Mine Engineering Facility, Yorktown
Att: Library 1

Naval Missile Center, Pt. Mugu
Att: Library, N-03022 1
Att: Env. Div., N314 2

Naval Operations, Office of Chief, DC
Att: Op 31 1
Att: Op 34 1
Att: Op 75 1
Att: Op 07T6, Mr. T. Soo-Hoo 1
Att: Op 725 1

Naval Ordnance Laboratory, Corona
Att: Code 234, Technical Library 1
Att: Code 56, Sys. Eval. Division 1

Naval Ordnance Laboratory, Silver Spring
Att: Technical Director 1
Att: Library 3
Att: Environmental Simulation Div. 6
Att: Mr. George Stathopoulos 1

Naval Ordnance Plant, Forest Park
Att: Mr. R. E. Seely, Div. 5600 1

Naval Ordnance Test Station, China Lake
Att: Technical Library 1
Att: Code 3023 1
Att: Code 3073 1
Att: Code 4062 2
Att: Code 4533 1
Att: Code 5516 1

Naval Ordnance Test Station, Pasadena
Att: P8087 3
Att: P8092 1
Att: P8073 1
Att: P80962 1

Naval Postgraduate School, Monterey
Att: Library 1

Naval Propellant Plant, Indian Head
Att: Library 1

Naval Radiological Defense Lab., San Francisco
Att: Library 3

Naval Research Laboratory, DC
Att: Code 6250 1
Att: Code 6260 1
Att: Code 6201 1
Att: Code 6020 2
Att: Code 2027 2

Naval Security Engineering Facility, DC
Att: R&D Branch 1

Naval Supply R&D Facility, Bayonne
Att: Library 1

Naval Torpedo Station, Keyport
Att: QEL, Technical Library 1

Naval Training Device Center, Pt. Washington
Att: Technical Library 1

Naval Underwater Ordnance Station, Newport
Att: Technical Documents Library 1

Naval Underwater Weapons Systems Engrg. Center, Newport
Att: Library 1

Naval Weapons Evaluation Facility, Albuquerque
Att: Library, Code 42 1

Naval Weapons Laboratory, Dahlgren
Att: Technical Library 1

Navy Electronics Laboratory, San Diego
Att: Library 1
Att: Code 3360 1

Navy Marine Engineering Laboratory, Annapolis
Att: Library 1

Navy Mine Defense Laboratory, Panama City
Att: Library 1

Navy ROTC and Administrative Unit, Cambridge 1

Navy Underwater Sound Laboratory, New London
Att: Technical Director 1
Att: Mr. J. G. Powell, Engrg. & Eval. Div. 1

Navy Underwater Sound Reference Lab., Orlando
Att: Mr. J. M. Taylor, Code 120 1

Norfolk Naval Shipyard, Portsmouth
Att: Design Superintendent 1

Norton AFB, Off. of Inspector General
Att: AFIMS-2-A 1

Office Director of Defense R&E, DC
Att: Technical Library 3
Att: Mr. Melvin Bell 1
Att: Mr. W. M. Carlson 1

Office of Naval Material, DC 1

Office of Naval Research, DC
Att: Code 439 6
Att: Code 104 1

Office of Naval Research Branch Office, Boston 1

Office of Naval Research Branch Office, Pasadena 1

Office of Naval Research Branch Office, San Francisco 1

Ogden Air Materiel Area, Hill AFB
Att: Service Engineering Dept., OONEOO 1

Oklahoma City Air Materiel Area, Tinker AFB
Att: Engineering Division 1

Pearl Harbor Naval Shipyard
Att: Shipyard Tech. Library, Code 246P 1

Philadelphia Naval Shipyard, Pa.
Att: Ship Design Section 1
Att: Naval Boiler & Turbine Lab. 1

Picatinny Arsenal, Dover
Att: Library SMUPA-VA6 1
Att: SMUPA-VP7, Mr. R. G. Leonardi 1
Att: SMUPA-T, Mr. R. J. Klem 1
Att: SMUPA-D, Mr. E. Newstead 1
Att: SMUPA-VP3, Mr. A. H. Landrok 1

Portsmouth Naval Shipyard, NH
Att: Code 246 1
Att: Mr. E. C. Taylor 1

Puget Sound Naval Shipyard, Bremerton
Att: Code 275 1
Att: Material Laboratories 1
Att: Code 242, Mr. K. G. Johnson 1
Att: Code 281 1

Randolph AFB, School of Aviation Medicine, Texas 1

Rome Air Development Center, Griffiss AFB
Att: Mr. Dana Benson, RASSM 1

6511th Test Group (Parachute), USAF, El Centro
Att: Mr. E. C. Myers, Tech. Director 1

6570th Aerospace Medical Research Labs., W-PAFB
Att: MRMAE 1
Att: Mr. R. G. Powell, MRBAE 1

San Francisco Naval Shipyard, Calif.
Att: Design Division 1

Savanna Ordnance Depot, Illinois
Att: OASMS 1

Sheppard AFB, Texas
Att: Dept. of Missile Training 1

Special Projects Office, USN, DC
Att: SP Technical Library 1

Strategic Air Command, Offutt AFB
Att: Operations Analysis Office 1

Supervisor of Shipbuilding, USN, Camden
Att: Code 299 2

Tobyhanna Army Depot, Pa.
Att: SMC Packaging and Storage Center 1

Watervliet Arsenal, New York
Att: ORDBF-RR 2

White Sands Missile Range, New Mexico
Att: STEWS-AMTED-E 2

Wright-Patterson AFB, Dayton
Att: AFFDL (FDFE, E. H. Schell) 1
Att: AFFDL (FDFE, C. W. Gerhardt) 1
Att: AFFDL (FDD, H. A. Magrath) 1
Att: AFFDL (FDDS, C. A. Golueke) 1
Att: AFML (MAMD, J. P. Henderson) 1
Att: SEG (SEFSD, R. F. Wilkus) 1

Yuma Proving Ground, Arizona
Att: Library 1